# Atmospheric Pressure Chemical Vapour Deposition of Tin Sulfide Films on Glass

A Thesis Presented to the
University of London
in Partial Fulfillment of the Requirements
for the Degree of
Doctor of Philosophy

**Louise Susan Price**

Department of Chemistry,
University College London,
Christopher Ingold
Laboratories,
20 Gordon Street,
London, WC1H 0AJ


December 2001

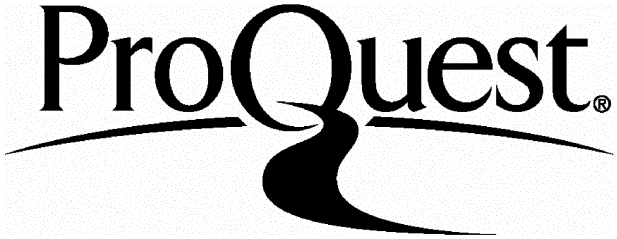

# Abstract

This thesis investigates the formation of films of tin sulfides on glass by the chemical vapour deposition process. Two methods were used. These were atmospheric pressure chemical vapour deposition with either thermal delivery or aerosol delivery. The primary system investigated was the reaction of tin tetrahalides with hydrogen sulfide. This was found to form all three binary phases of tin sulfide, in high purity. The factor which had highest influence on the phase deposited was the deposition temperature. In general, it was found that below 450 °C tin(IV) sulfide was formed, above 550 °C tin(II) sulfide was formed and at intermediate temperatures mixed valent tin(II) tin(IV) trisulfide was formed.

Single source precursors to tin sulfides were also investigated. These included tin thiolates and tin dithiocarbamates. The tin thiolates studied were tin(IV) thiolate, tin(IV) $\eta^2$-ethane 1,2-dithiolate and tin(IV) 2,2,2-trifluoroethane thiolate. The tin(II) thiolate [$Sn(SCPh_3)_2$] was also studied, but no film could be formed. The only homoleptic dithiocarbamate studied was [$Sn(S_2CNEt_2)_4$], although a large number of alkyl tin dithiocarbamates were investigated. These were [$R_3Sn(S_2CNR'_2)$] R=Me, $^n$Bu; R'=Me, Et and asymmetric dithiocarbamate precursors [$Me_3SnS_2CNMeBu$] and [$BuSn(S_2CNMeBu)_3$]. In almost all cases addition of hydrogen sulfide was necessary to make tin sulfide films. This was because, as mass spectrometry showed to be the case for [$Sn(SPh)_4$], two thiolate groups may be lost as an RSSR moiety. A small number of reactions were successful in forming tin sulfide without $H_2S$. Tin(IV) $\eta^2$-ethane 1,2-dithiolate was the most successful single source precursor, and this was attributed to the inability to lose an RSSR entity.

Some precursors were investigated with a view to forming tin oxide sulfide and tin sulfide selenide. To make tin oxide sulfide, tin tetrachloride, hydrogen sulfide and water were reacted together. Subsequently, single source precursors [$Cl_2Sn(SCH_2C(O)OMe)_2$] and [$^tBu_2\overline{Sn(-OCH_2CH_2S)}$] were investigated. To form tin sulfide selenides [$Sn(SPh)_4$] and [$Sn(SePh)_4$] were reacted together. Ligand exchange formed [$Sn(SPh)_n(SePh)_{4-n}$] (n=0-4) with all compounds in the statistical ratio. This was then investigated by CVD.

Visual inspection, Raman microscopy and EDAX were used to investigate all films produced. The morphology of each film was observed by SEM, and particles were of the order 0.5 - 5 μm in dimension. A number were also examined by X-ray diffraction and X-ray Photoelectron Spectroscopy. Band gaps were measured for some of the films.

# Acknowledgements

I would like to thank Professor Ivan Parkin for his supervision of my Ph.D. I would also like to thank Dr. Kieran Molloy and Dr. Tom Hibbert of the University of Bath, who collaborated with us on this work. Dr. Tom Hibbert synthesised and analysed many of the precursors used in the thesis. Mr. Dave Knapp, Mr. Joe Nolan and Mr. Dave Morphett designed and built the CVD rig used in this work. They also maintained it during the whole of my Ph.D. Dr. Marianne Odlyha carried out the DSC and TGA measurements on many of the compounds. Mr. Kevin Reeves helped with EDAX and SEM.

People within the same research group also helped with much of the work. Mr. Shane O'Neill and Mr. Mark Field carried out much of the XPS. Dr. Steve Firth, Miss Amanda Hardy and Miss Katherine Brown helped with the Raman. Other people who helped in various ways were Dr. Graham Shaw, Dr. Gareth Elwin, Mr. Chris Dinnage, Dr. Daniel Morrison, Mr. Warren Cross, Miss Catherine Lipton, Dr. Dickon Champion, Miss Louise Affleck, and Mr. Marco Aguas.

Finally, I would like to thank my parents who made it possible for me to do a Ph.D., and my best friend Susanne Campbell for all her support during the past year.

**Contents**

**List of Figures and Tables**

**Chapter 1**



**Chapter 2**

**Chapter 3**

**Chapter 4**



**Chapter 5**

**Chapter 8**

# Chapter 1
# Introduction

In modern society, the use of new materials is continually expanding. In some cases, materials are developed for specific purposes, for example, development of polytetrafluoroethene for use as a container for highly reactive materials such as $UF_6$ and HF.[1] In other cases, materials are developed and uses defined based on the properties of the material.

One area of expanding interest in recent times is that of semiconducting materials for microelectronic applications. Some materials, which have been known for many years, are finding new applications as semiconductors; tin sulfide is an example of this.[2]

At the start of the last century, it was observed that particle size plays an important role in the properties of a semiconductor. With this in mind, many people are interested in nanoparticulate materials or the deposition of thin films. These both have considerably different electronic properties from bulk materials due to electron confinement, in three dimensions in the case of nanoparticulate materials and in one direction in the case of thin films.[3] These are termed "mean-free-path" or "size" effects.

Many different routes are used in depositing thin films. They have varying success and differing advantages and disadvantages. Chemical vapour deposition (CVD) is used in industry for the deposition of thin films. Low pressure CVD is used to deposit semiconductors, as control is much greater.[4] On the other hand, commercial coating of glass employs atmospheric pressure CVD, as coverage is sufficiently even for uniform optical properties and deposition is very fast.[5]

This work concerns the deposition of the semiconducting material, tin sulfide, onto glass substrates *via* atmospheric pressure chemical vapour deposition. In this chapter, the background to the work will be discussed. Properties, uses and preparative routes to all forms of tin sulfide will be reported. Semiconductors in general will be discussed along with specific consideration to tin sulfide and related materials. Recent routes to film deposition will be compared, highlighting the advantages of chemical vapour deposition over other routes.

# 1.1 General description and structure of tin sulfides

## 1.1.1 The phases of tin sulfide

Many forms of tin sulfide have been observed. Those reported include tin(II) sulfide, tin(IV) sulfide, mixed valent compounds such as $Sn_2S_3$,[6] intercalation compounds based on the binary phases[7] and framework compounds modelled around various organic molecules.[6] The phase diagram of tin and sulfur has been produced many times.[8,9,10] There is conflicting evidence over which phases of tin sulfide may be formed. Karakhanova *et al.*[8] formed all tin-sulfur phases with 40-62 at. % sulfur by direct heating of the elements in sealed ampoules. They determined the existence of SnS, $Sn_2S_3$, $Sn_3S_4$ and $SnS_2$. Melting points, a polymorphous change for SnS and the existence of a eutectic between SnS and $Sn_3S_4$ were reported.

Another study of tin sulfides was carried out three years later.[9] This was a further attempt to determine which phases were stable in which regions of the phase diagram. Gerasimov[11] had reported the existence of $Sn_4S_5$ as an intermediate in the thermal decomposition of SnS to $SnS_2$. Attempts to produce this phase by heating tin and sulfur of a 4:5 ratio in sealed ampoules produced only Sn, $Sn_{1-x}S$ and $Sn_2S_3$.[9] In that study, it was shown that SnS is only stoichiometric when in the presence of excess tin. Otherwise, the sub-stoichiometric phase, $Sn_{1-x}S$, is formed. The other metastable compound, $Sn_3S_4$, which had been reported previously by some groups,[8,12] caused problems in this work. The elements were heated together in stoichiometric quantities for many hours in sealed silica ampoules, and analysed by X-ray diffraction at elevated temperatures or after quenching. It was found that at temperatures up to 800 °C, no phases other than $Sn_{1-x}S$, $Sn_2S_3$, liquid sulfur and liquid tin-sulfur phases were formed from a 3:4 elemental ratio of tin and sulfur.[9]

The most recently published phase diagram, which is a review of all the relevant data in the past, concluded that there are only three discrete phases containing exclusively tin and sulfur.[10] $Sn_3S_4$ and $Sn_4S_5$ were described as metastable phases and not included in the phase diagram. This is reproduced in Figure 1.1. All three phases exhibit more than one allotrope, however the α-phase is stable to above 600 °C in all cases. β-SnS

dissolves excess sulfur in small amounts up to 50.5 at. % sulfur. β-$SnS_2$, on the other hand, may be slightly tin-rich. $Sn_2S_3$ forms three high temperature phases, which are all capable of including excess tin and excess sulfur. The congruent melting points of SnS and $SnS_2$ are given as 880 and 865 °C respectively. The peritectic melting point of $Sn_2S_3$ is 760 °C.

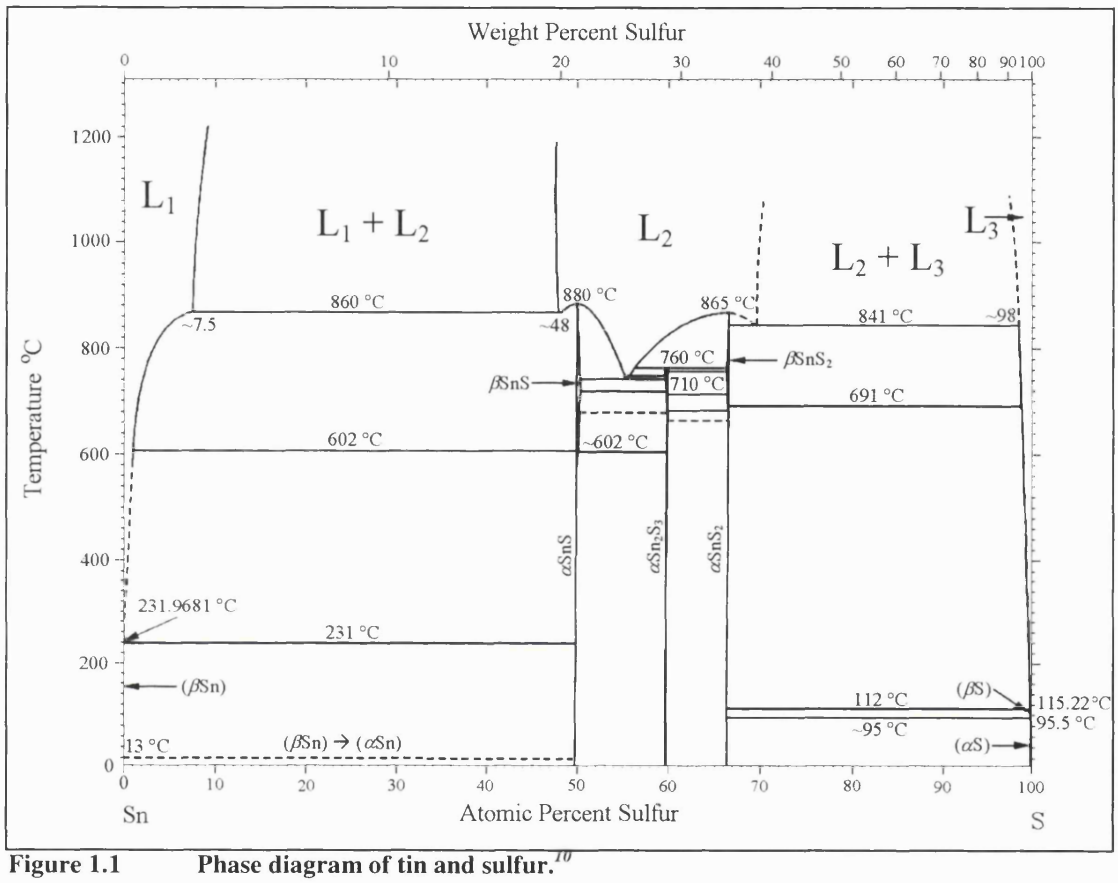


**Figure 1.1 Phase diagram of tin and sulfur.**[10]

Extensive studies using Mössbauer[13] found only two tin resonance absorptions. The $^{119}Sn$ Mössbauer of mixed valent compounds such as $Sn_2S_3$ and $Sn_3S_4$ showed only two lines indicating Sn(II) and Sn(IV) environments corresponding exactly to those observed in SnS and $SnS_2$. As will be shown in section 1.1.2, mixed valent $Sn_2S_3$ has two tin environments, which are almost identical to tin environments in tin(II) sulfide and tin(IV) sulfide.

## 1.1.2 Structure of tin sulfides

Tin(II) and tin(IV) sulfides exhibit layer structures, whereas mixed valent tin(II) tin(IV) trisulfide forms a ribbon structure.[6]

Tin(II) sulfide is orthorhombic, with tin-sulfur double layers.[14] It takes a deformed rock-salt structure and is isostructural with germanium sulfide, although near the melting point it adopts the tellurium iodide structure.[15] Of the group IV-VI compounds, only GeS, GeSe, SnS and SnSe adopt an orthorhombic structure.[16] SnTe and all lead compounds crystallise in the more symmetric rock salt structure.[16] In tin(II) sulfide six sulfur atoms surround each tin atom in a highly distorted octahedron.[14] Three short tin-sulfur bonds (*ca.* 2.6 Å) are formed within the layer, and longer bonds are formed to the sulfur atoms of the next layer approximately 3.3 Å distant. The sulfur-tin-sulfur angles within the layer deviate from the perfect octahedral values. This deformation causes the tin(II) lone pair to be stereochemically active.[14]

The space group of tin monosulfide is *Pnma* and the unit cell parameters were determined as $a$ = 11.180(6), $b$ = 3.982(2), $c$ = 4.329(3) Å.[14] The unit cell contains two tin sulfur double layers as described above. SnS is shown schematically in Figure 1.2.

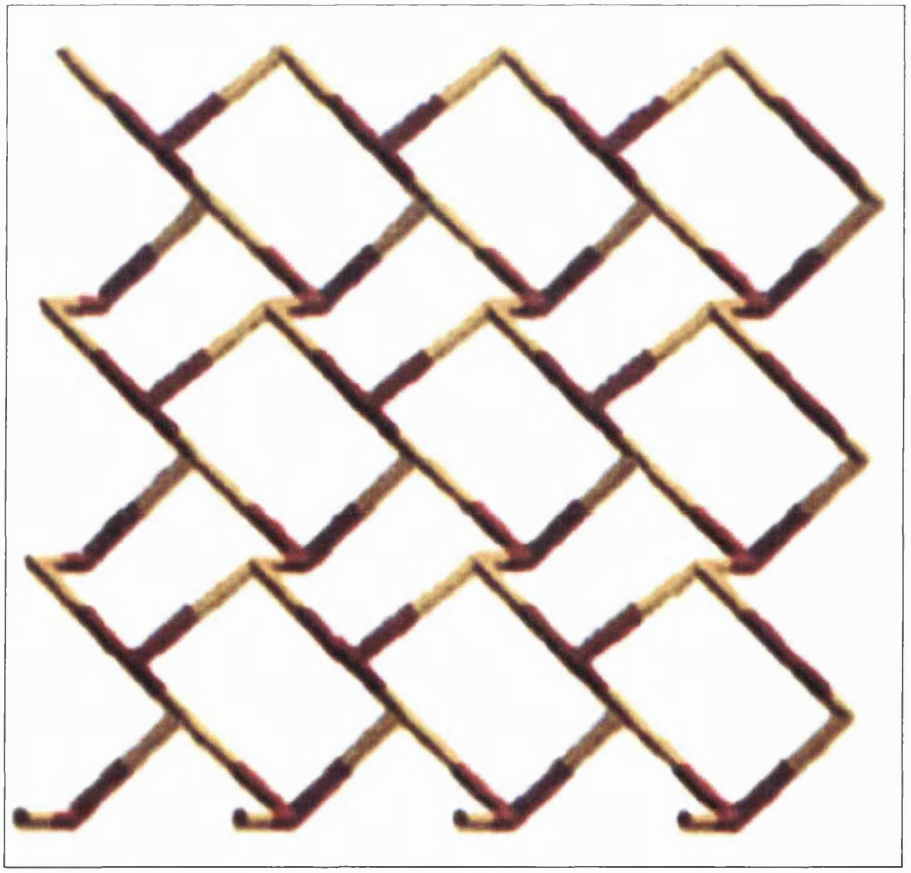

**Figure 1.2 Schematic representation of the layered structure of tin(II) sulfide.[6] (Tin is shown in red and sulfur in yellow).**

Tin(IV) sulfide also has a layered structure. It is hexagonal and isostructural with $CdI_2$.[17] Sulfur-tin-sulfur sandwich layers form the basis of the structure. Within the layer, six sulfur atoms surround each tin atom in an approximately octahedral arrangement, with three atoms above and three below the plane of the tin atoms. The tin-sulfur distances are approximately 2.5 Å. Between layers weak tin-sulfur and sulfur-sulfur van der Waals interactions occur. A schematic representation of tin(IV) sulfide is given in Figure 1.3.

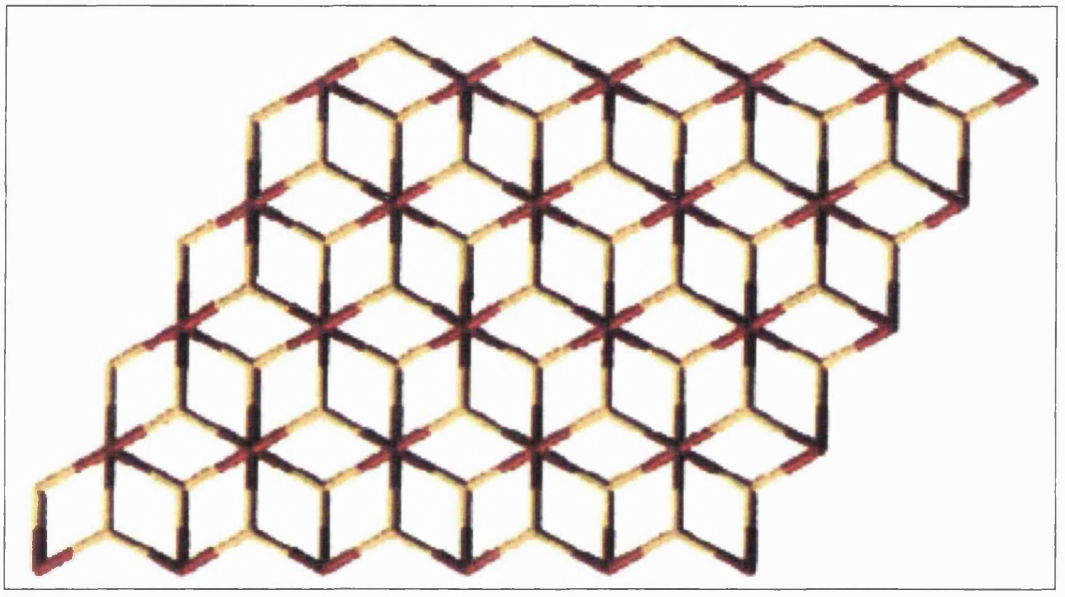

**Figure 1.3 Schematic representation of tin(IV) sulfide layer.[6] (Tin is shown in red and sulfur in yellow).**

The layer structure of tin disulfide gives it the ability to form many polytypes. Over 70 have been observed[6] although the most common are 2H ($P\bar{3}m1$), 4H (P3m1) and 18R ($R\bar{3}m$).[18] Polytypism results from variation in the order of stacking the same structural unit. In the case of tin sulfide, hexagonal layers described in the last paragraph form the basic building blocks, which can then be stacked in many different ways. Within the layer, $a$ = 3.6470(8) Å while the minimum $c$-distance is $c_{2H}$ = 5.8990(5) Å.[18] Other polytypes have their $c$-parameter as a multiple of this minimum. In almost all cases, the repeat unit consists of two sandwich layers. This effect alters the unit cell of the material, and so changes the X-ray diffraction pattern. Most other properties of the material are unaffected by this though.

Tin(II) tin(IV) trisulfide has a similar local order to both tin sulfides previously discussed. Overall, it exhibits a ribbon- type structure.[19] One tin atom is found in

the centre of the ribbon and is six coordinate, whereas the other, on the edge of the ribbon, is three coordinate. All sulfur atoms are three coordinate. Tin(IV)-sulfur distances are *ca.* 2.5 Å and tin(II)-sulfur bond lengths are *ca.* 2.7 Å.[6]

Tin sesquisulfide ($Sn_2S_3$) is orthorhombic and exhibits the *Pnma* space group.[19] Unit cell parameters are found to be $a$ = 8.878(2), $b$ = 3.751(1), $c$ = 14.020(3) Å. Figure 1.4 shows mixed valent tin sulfide in a schematic representation.

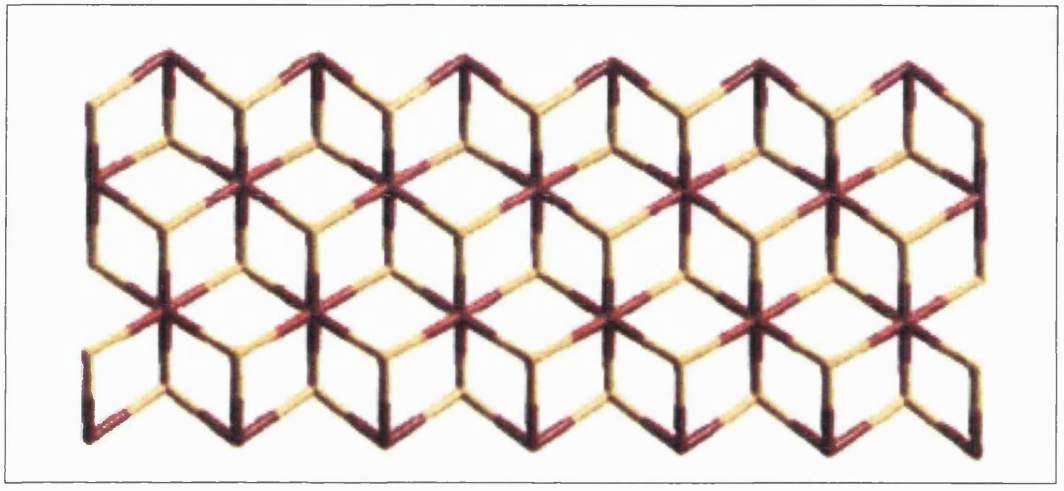

**Figure 1.4 Schematic view of the ribbon structure of tin(II) tin(IV) trisulfide.[6] (Tin is shown in red and sulfur in yellow).**

Very little data is available for the other phases of tin sulfide. $Sn_3S_4$ is described as tetragonal with $a$ = 7.553, $c$ = 8.383 Å.[12] Lattice constants of $a$ = 7.473(1) and $c$ = 33.064(1) have also been recorded.[8] The longer $c$-distance in this case is due to vacancies in the lattice. No x-ray diffraction data is available for $Sn_4S_5$. The lack of information supports previous observations that these phases are not stable at normal temperature and pressure.

### 1.1.3 Visual appearance of tin sulfides

Tin monosulfide forms dark grey crystals or a black amorphous powder.[20] It is also known as herzenbergite, after the German mineralogist, R. Herzenberg, who first reported it.[6]

Tin disulfide is observed as yellow hexagonal crystals.[21] This bright yellow colour

gives it its other name – "mosaic gold"[22] – although this term also applies to the alloy of 65.3 % copper, 34.7 % zinc.[20] Historically, tin disulfide has been used as pigment for gilding and bronzing.[20] The mineral name of tin disulfide is berndtite. A second type of crystal has been observed for tin(IV) sulfide, which is shiny silver in colour.[23]

Tin sesquisulfide is also known as ottemannite after J. Ottemann – the German mineralogist who discovered it.[6] It is brown.

# 1.2 Synthesis and applications of tin sulfides

## 1.2.1 General historical methods

Tin(IV) sulfide was first prepared in the laboratory approximately 230 years ago.[24] "Aurum Mosaicum," as it was known in 1771, was prepared by heating a tin amalgam with sulfur and ammonium chloride. The Aurum Mosaicum sublimed from this combination. Mercury only sufficed to activate the tin, and ammonium chloride served only to prevent melting of sulfur. Various recipes were proposed, with and without use of mercury and ammonium chloride, and purity of the product was determined by colour and taste. Aurum Mosaicum is of a shining golden colour when pure, and has no taste. The highest yield came from combining 12 ounces of tin with 7 ounces of sulfur, which are stoichiometric amounts for the formation of tin(IV) sulfide. Woulfe's calculations determined that 1 $^{7}/_{10}$ ounces of Aurum Mosaicum contained 1 ounce of tin. This is equivalent to 59 % Sn by mass, whereas $SnS_2$ contains 65 % tin by mass. These values are very close, considering the accuracy to which it was possible to work in 1771.

Aurum Mosaicum was used as a vermifuge, but Woulfe surmised that as compounds of metals and sulfur were inactive, this did little good. He concluded that, as other scientists had found Aurum Mosaicum to have a "rough taste", it was tin chloride impurity which was responsible for the anthelmintic effects. A further use proposed by Woulfe was in fireworks. His reasoning was that since tin reacts violently with nitre, a tin sulfide would do so to a greater degree.

Woulfe also investigated the combination of tin and sulfur by fusion. Heating tin and sulfur together at temperatures that were not quite red hot yielded a shining flaky brittle substance, known as "sulfurated tin." The quantities used by Woulfe amounted to there being a four-fold excess of sulfur contained in this reaction. On heating Aurum Mosaicum, mass was lost and the appearance became more like that of sulfurated tin. Further heating led to more sulfur loss and the appearance being even more like that of sulfurated tin. It is likely that in the direct formation of sulfurated tin some sulfur was lost, and that this compound was similar to tin(II) sulfide. On the melting points, Woulfe noted that Aurum Mosaicum melts more readily than sulfurated tin, as it contains more sulfur. The melting points of tin(II) and tin(IV) sulfides have since been reported across a wide range, although tin(IV) sulfide does melt *ca.* 15 ° below tin(II) sulfide.[10]

Since that first description of the syntheses of tin sulfides, many alternative routes have been developed. These have had varying degrees of success, and many differences in properties have been recorded.

### 1.2.2 Bulk syntheses of tin sulfides

All tin sulfides have been made as bulk compounds by direct reaction of stoichiometric quantities of the elements in sealed ampoules at elevated temperatures.[8,9] This method is used as a general technique for formation of metal sulfides.[26] Reaction of elemental tin and sulfur in liquid ammonia at room temperature yielded tin sulfide.[27] This was found to be a mixture of 60 % SnS, 35 % $SnS_2$ and 5 % unreacted tin metal. All products were X-ray amorphous, however heating affords only tin(II) sulfide. Metathesis provides a further pathway to tin sulfides.[28] Tin(IV) iodide and lithium sulfide were ground together and sealed in an ampoule, sonicated for 10 min and heated, wrapped in glass wool, at 550 °C for 5 hours. Washing with methanol, water or dilute hydrochloric acid removed lithium iodide, tin metal and unreacted $SnI_4$. The resulting product was shown to contain only tin and sulfur by EDAX. The driving force of the reaction is the high enthalpy of formation of lithium iodide.[28]

Single crystals of SnS were prepared for X-ray diffraction studies by sublimation at

900 °C in an evacuated quartz ampoule.[14] The Bridgman technique has also been applied to the formation of tin(II) sulfide crystals.[29]

Molecular precursors, such as $[(R_3Sn)_2E]$, $[(R_2SnE)_3]$, $[R_2Sn(ER)_2]$ or $[R_3SnER]$ (R=Ph, Bz; E=S, Se,), have been used to produce tin(II) sulfide.[30] The benzyl compounds, prepared from benzyl tin chloride and $Na_2E$ in THF, decompose below 450 °C to form tin chalcogenide and dibenzyl. In the case of the linear precursors, SnE and tin metal were formed as would be expected from the precursor stoichiometry, whereas the cyclic precursors yielded only tin chalcogenide. Mixtures of sulfide and selenide precursors afforded $SnS_xSe_{1-x}$ when pyrolysed in appropriate ratios. In the analogous reactions with phenyl precursors, which occur above 300 °C, biphenyl was not observed and the mechanism was thought to go *via* the cyclic $[(Ph_2SnE)_3]$.

Deposition from solution is another route by which tin(II) sulfide has been prepared. A general method for the precipitation of metal sulfides is available.[26] This involves the reaction in aqueous solution of metal cations with $H_2S$ or $(NH_2)_2S$. MnS, $Fe_9S_8$, CoS, $Co_9S_8$, NiS, CuS, ZnS, CdS, HgS, PbS and SnS have all been prepared by this method. A more commonly used method is passing $H_2S$ gas through a solution of $SnCl_2$ in hydrochloric acid.[31] This yields a yellow powder.

Single crystals of $SnS_2$, suitable for X-ray diffraction, have been grown by the chemical transport method.[32] This produced yellow platelets up to 0.2 mm thick and 3 – 4 mm across. At temperatures below 600 °C the 2H polytype of tin sulfide was formed. 4H $SnS_2$ was produced above 800 °C, and 18R $SnS_2$ was formed between these temperatures. Alternative routes to single crystals are physical vapour transport[33] or chemical vapour transport using iodine as the transport medium.[34,35] In addition, $SnS_2$ has been prepared by reaction of $SnCl_2$ with $Na_2S$ followed by treatment with sulfur and ammonium chloride at high temperatures.[36]

Nanocrystalline β-$SnS_2$ has been prepared by a solvent-thermal method using $SnCl_4$ and anhydrous $Na_2S$ in toluene at 150 °C.[37] Particles of *ca.* 12 nm were formed. Tubular crystals of β-$SnS_2$ have also been formed.[38] These are (001) tubes formed by curling round a (001) sheet of β-$SnS_2$.

As already mentioned, tin sesquisulfide may be prepared by heating tin and sulfur in a sealed, evacuated tube.[8,9,12] A combination of 54 at. % sulfur and 46 at. % tin heated in a quartz ampoule to 720 °C over 24 hr, yielded needle-shaped crystals of sufficient quality to perform X-ray diffraction.[19] Alternatively, thermal annealing of the binary sulfides, namely tin(II) sulfide and tin(IV) sulfide, at 500 °C led to crystals of diameter 1 – 2 mm and many mm long.[39] Mixed metal sulfides containing tin(II) or tin(IV) have also been prepared by this method.

### 1.2.3 Film deposition of tin sulfides

Many methods have been employed in tin sulfide thin film deposition, however perhaps the simplest is to form the sulfide by another means and thermally evaporate it onto a substrate. This method was used by many groups.[40,41] Badachhape *et al.*[31] went one stage further in the deposition of thin films. They prepared tin(II) sulfide by passing $H_2S$ through a solution of $SnCl_2$ in hydrochloric acid as described above, and then evaporated it onto rock salt or collodion (cellulose nitrate) substrates. These substrates were then dissolved away in water, leaving a single crystal of tin sulfide. As these crystals were grown epitaxially on another crystal, they did not necessarily conform to the usual orthorhombic structure of tin(II) sulfide. On the (100) plane of sodium chloride, hexagonal SnS was deposited with $a$ = 3.63, $c$ = 6.00 Å at 200 – 250 °C. At temperatures of 300 – 350 °C cubic SnS was observed with $a$ = 5.16 Å. These structures did not revert to orthorhombic even on cooling.[31]

Tin(IV) sulfide has also been evaporated onto substrates in order to produce thin films.[42] Amorphous films were the result, and at temperatures 21 °C < T < 70 °C the optical band gap was 1.05 ± 0.1 eV. Increasing the deposition temperature to T < 336 °C, the optical band gap increased to 1.93 eV due to a polycrystalline state being formed.

In some cases, tin sulfide films have been deposited directly from solution. Chemical baths of a variety of compositions were used to this effect. A general method for the deposition of metal sulfide films exists.[43] This involves use of an acidic medium containing $Na_2S_2O_3$ as sulfur source, and has been used in the deposition of I-VI, II-VI,

IV-VI and IV-VI films. Pertaining specifically to tin sulfide, a bath containing $Sn^{4+}$ salt solution, $Na_2S_2O_3$ and EDTA in acidic aqueous solution has been used to deposit $SnS_2$ onto various substrates.[43] These films were of a polycrystalline nature, exhibited n-type conductivity with a band gap of 2.2 eV. A further solution reaction is that of $SnCl_2.2H_2O$, thioacetamide, triethanolamine and aqueous ammonia in acetone, which was used to deposit SnS onto glass slides supported vertically on the walls of the beakers.[45] This could be carried out at room temperature, but raising the temperature to 75 °C increased the rate of deposition. Excess triethanolamine was found to prohibit film growth, and excess ammonia led to incorporation of hydroxide in the films. Films of many thicknesses and a correspondingly wide range of reflection and transmission colours were deposited in this manner. A related solution of $SnCl_2$, triethanolamine, ammonia and thioacetamide in glacial acetic acid and water also yielded SnS.[46] Glass slides were placed vertically in the solution, which went brown on addition of the thioacetamide, and a brown film was deposited on both sides of the glass. X-ray diffraction revealed that the films were amorphous, however heating powder scraped from the films to 400 °C led to a powder which analysed as tin(II) sulfide.

A further solution deposition method involved dipping glass slides alternately in cold $Na_2S$ and hot $SnCl_2$ solutions of equal concentration.[47] In this reaction, the pH of the $SnCl_2$ solution was important in determining the quality of the final films. At $pH < 3$ films were not particularly adherent, whereas at $pH > 3$ a transparent red-brown film was deposited on both surfaces of the substrate. At $pH \approx 7$ dissolved $SnCl_2$ is partially hydrolysed, impeding deposition and slowing the rate of film formation. Films were of good quality and uniform thickness, as determined by their interference patterns. The films were analysed by X-ray diffraction, which showed preferential growth in the [013] direction. Small opaque crystals were formed, which were surrounded by a transparent brown phase of amorphous SnS. Higher pH of the $SnCl_2$ solution during deposition led to more crystalline materials being formed; ultimately, at pH = 12 no amorphous SnS is seen. Heating these films of SnS changed conductivity from p-type to n-type and increased it over one order of magnitude. Heating for longer periods resulted in partial disproportionation of SnS to $SnS_2$ and Sn. Annealing for a short time followed by subsequent deposition from the bath led to an n-p homojunction, whereas longer annealing followed by subsequent deposition from the bath led to an n-p heterojunction of n-$SnS_2$/p-SnS. Annealing SnS in air resulted in white $SnO_2$ being formed.[47]

Deposition of tin(IV) sulfide has been achieved from a solution of $SnCl_2$, HOAc, EDTA, ammonia, thioacetamide and hydrazine.[48] Glass slides placed vertically in the solution were coated with tin(IV) sulfide, over 10 – 120 minute periods. An optical band gap of 2.3 eV was recorded for these films and n-type conductivity observed.

Electrodeposition of tin(II) sulfide from a solution containing $SnCl_2$ and thiosulfate anions has been carried out.[49] Electrodeposition has also been used with a non-aqueous solution of $SnCl_2$ and elemental sulfur in ethylene glycol.[50] This was used to deposit onto indium tin oxide glass. An electroless deposition method has been used to deposit tin sulfides onto non-conducting substrates such as glass.[51] This comprised a solution of organic acid, tin(II) salt, sulfur and tin(II) complexing agent (potassium gluconate or tartaric acid) in water. Water and the complexing agent affected the stoichiometry of the film, grey-black $Sn_{1-x}S$, brown $Sn_{2\pm x}S_3$ and $SnS_{2-x}$ all being accessible.

The electrodeposition of tin(IV) sulfide has been studied by cyclic voltametry.[52] It was found that the first anodic peak was associated with deposition of a $SnS_2$ monolayer resulting from the adsorption of $HS^-$ on the electrode surface. More positive potentials led to a second anodic peak related to a tin disulfide film over the entire electrode.

Films of tin(II) sulfide have been deposited on Corning glass and silicon slices by plasma-enhanced chemical vapour deposition.[2] The reagents used were $SnCl_4$ and $H_2S$, and hydrogen was the diluent gas necessary to remove any chlorine radicals formed in the $SnCl_4$ decomposition. X-ray diffraction was used to analyse the resulting films, and it was observed that, at constant plasma power, the lowest substrate temperature (100 °C) gave rise to a film composed of SnS, $SnCl_2$, $SnCl_4$ and sulfur. Increasing substrate temperature led to higher purity in the film, in fact by 200 °C only peaks corresponding to SnS were observed. Preferential growth in the (111) peak was seen at a deposition temperature of 250 °C, however this preferential growth was lost at higher substrate temperatures due to faster nucleation. Plasma power also had an effect on the film composition. At 0.023 $Wcm^{-2}$ only SnS was seen. On increasing the power to 0.040 $Wcm^{-2,}$ some sulfur was seen in the x-ray diffraction pattern due to this power being sufficient to decompose $H_2S$. Higher plasma power led to the removal of this peak, as $SnCl_4$ decomposition is facilitated. Metallorganic chemical vapour deposition has also been used in the deposition of tin(II) sulfide films.[53] Precursors used were tetraethyl tin

and hydrogen sulfide. No characterisation was carried out on the films, although it was assumed that they were tin(II) sulfide because of the reducing hydrogen atmosphere present in the system. Thin films of SnS have been prepared by sulfidization of the surface of a tin metal film.[54] Tin was heated to 100 – 230 °C for > 5 minutes in a hydrogen sulfide atmosphere. This sulfidized the surface, and further heating to 231 – 800 °C allowed sulfidization of tin within the film. The resulting film exhibited good adhesion with few defects.

Spray pyrolysis has also been used to deposit tin(II) sulfide films.[55] Equimolar solutions of tin(II) chloride and n,n-dimethylthiourea were sprayed onto Corning glass substrates at temperatures of 100 – 450 °C.

Van der Waals epitaxy has been used in the study of tin(IV) sulfide films.[56] A variety of single crystal substrates was studied, and growth was observed to be of a two-dimensional layer-by-layer fashion. Tin selenide has also been studied in this manner, and it was found that tin sulfide exhibits a more strictly layer-by-layer growth mechanism, which was attributed to greater surface diffusion rates.[56] Different growth morphologies were observed in the first few monolayers by STM and AFM.[56]

Spray pyrolysis of tin sesquisulfide has been carried out using $SnCl_2$ and n,n-dimethylthiourea.[57] A solution of these two components in a mixture of water and propan-2-ol was used. The substrate was Pyrex glass and dry air used as the carrier gas. Depositions were carried out at a substrate temperature of 320 °C, and X-ray diffraction used to determine the composition of the film. Previous studies had shown that only temperatures below 360 °C afforded $Sn_2S_3$.[58] Higher substrate temperatures (370 – 390 °C) resulted in deposition of SnS films, whereas temperatures in excess of 390 °C yield $SnO_2$.[58]

### 1.2.4 Applications of tin sulfide

The applications of tin sulfide with which we are concerned in this work are mostly related to their electronic and optical properties. As such, they will be discussed in section 1.3, which deals with these aspects.

A further application of tin(IV) sulfide is related to its structure. The isomorphous compound $TiS_2$ is commonly used as a solid state lubricant.[59] Compounds of the formula $M^1_lM^2_mM^3_nS_x$ ($M^1$, $M^2$, $M^3$ = Ti, V, Mn, Fe, Cu, Zn, Mo, W, Sb, Sn, Bi; l, m = 1-5; n = 0-5; x = 2-8) are used as solid lubricants in friction materials.[60] Another group prepared a composite containing aramid fibres, organic binders, organic and/or inorganic fillers, tin(II) and/or tin(IV) sulfide as a lubricant and metals or metal compounds.[61] This compound shows greater crack resistance than a similar compound incorporating $Sb_2S_3$ in place of the tin sulfides. These composites are used in friction materials such as brake and clutch linings.

A tin-based thin film comprising SnS, SnSe or fine particles of tin dispersed in tin oxides, sulfides or selenides has found use as an optical recording medium.[62]

### 1.2.5 Related compounds

Compounds related to tin sulfides have also been prepared by many groups. Sulfides based on $SnS_2$ of the general formula $(Sn_xM_{1-x})S_2$ (M = Ti, Mo, Fe, Cr, Ta, Nb, Mn, Bi, W, Cu; x = 0.5 – 1) have been prepared by combination of tin, metal M and/or metal sulfide and superstoichiometric amounts of sulfur.[63] This was done in the presence of halogenide compounds especially ammonium chloride or tin chloride, in an inert atmosphere. Ternary sulfides based on $Sn_2S_3$ of the form $M^{II}M^{IV}S_3$ ($M^{II}$ = Sn, Pb; $M^{IV}$ = Sn, Ge) have been prepared by heating mixtures of the binary sulfides in sealed ampoules at 500 – 600 °C.[39]

Microporous materials based on tin sulfides have also been widely studied. [TMA-SnS-1] (TMA = trimethylammonium) has been prepared in aqueous media at room temperature.[64] [$C_{16}$TMA-SnS-L1] ($C_{16}$ = cetyl) has been prepared from a system comprising $C_{16}$TMABr (cetyltrimethylammonium bromide), $SnCl_4$ and $Na_2S$ in water.[65] The pH of the reaction mixture was 12. The material exhibited a monoclinic layered structure with a basal spacing of 25.5 Å. An increase of crystallisation time led to transformation to [$C_{16}$TMA-SnS-L], which had a different chemical environment about the tin(IV) although both were tetrahedral. Packing of the $C_{16}TMA^+$ chains was also different. The tin:sulfur ratio in these two phases was 1:2.5. A further phase denoted

[$C_{16}$TMA-SnS-M] has been prepared with a tin:sulfur ratio of 1:2. This compound had octahedral co-ordination about tin. Related compounds [$(Et_4N)_2Sn_3S_7$] and [$(^nPr_4N)_2Sn_4S_9$] have also been prepared.[66] These incorporate $Sn_3S_4$ units linked by sulfide bridges.

# 1.3 Electronic considerations

The principle application of tin(II) sulfide is as a semiconductor. It is also of interest as a heat mirror coating on windows. With these applications in mind, it is useful to have a brief overview of the terms used in discussing semiconductors, photovoltaics and heat mirrors.

## 1.3.1 General description of semiconductors

From the aspect of conductivity, there are five recognised classes of material. These are, in order of decreasing conductivity, superconductors, metals, semimetals, semiconductors and insulators. Metals, and superconductors above their $T_C$, exhibit metallic conductivity. This means that the resistance increases with temperature due to lattice vibrations impeding the motion of electrons. This effect is observed throughout all materials. Semimetals, semiconductors and insulators have decreasing resistivity with temperature. This is because of the band structure of the materials.

### 1.3.1.1 Band theory

In a single atom, there are discreet energy levels. When two or more atoms are brought together, there is a slight perturbation in the energy levels with respect to those in the isolated atom. They are still very similar in energy. If a large number of atoms are brought together, then the energy levels form a continuous band.

Each atomic energy level within an atom may contain only two electrons – one with spin up and the other with spin down. This is the Pauli exclusion principle, which states that no two electrons may have identical sets of quantum numbers associated with them.

This means that if n atoms are brought together in a solid, then the band associated with each level will be capable of containing 2n electrons. Figure 1.5 shows how bands may be filled or empty. Energy is plotted along the x-axis and frequency of states with this energy up the y-axis. The figure depicts which states are filled or empty at absolute zero, however temperature affects occupancy according to the Boltzman distribution. In a material, there will be an energy which has exactly half its states occupied at any temperature. This is called the Fermi-level and is denoted $E_f$.

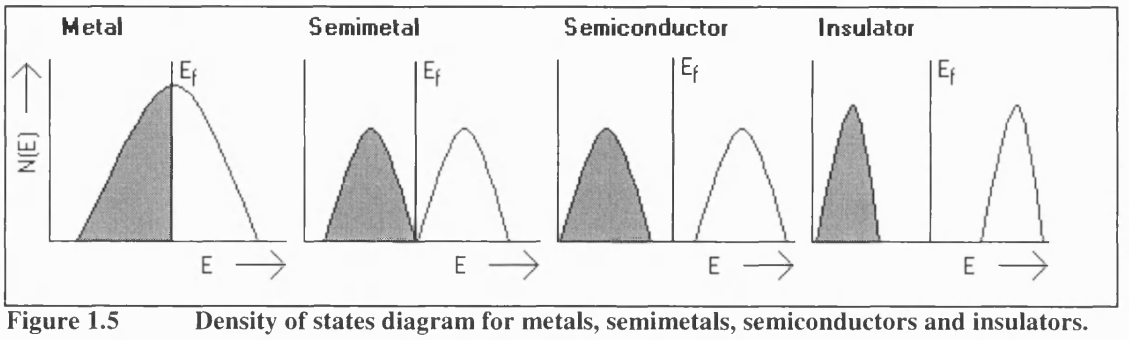


**Figure 1.5** **Density of states diagram for metals, semimetals, semiconductors and insulators.**

In a metal such as sodium, the 3s orbital contains only one electron, and the 3s band of a solid will contain n electrons. Since the band may hold up to 2n electrons it is half full. This is depicted in Figure 1.5. Metallic conduction occurs when a band is partially filled. A metal such as magnesium has two electrons in its 3s orbital, so it would appear that this has a full 3s band and the next band up (3p) would be empty. However, the 3s and 3p bands overlap, allowing electrons to move freely into the 3p orbital. In these cases, the Fermi levels fall within a region of non-zero density of states. This is the strict definition of metallic conduction.

Superconductors behave in an identical manner to metals. The difference is in the resistance at low temperatures. As previously mentioned, atomic vibrations impede electrons flowing through the material. At lower temperatures atoms vibrate less, and conductivity increases. Superconductors are materials whose low-temperature resistance is zero.

Band theory for materials with covalent bonding, such as silicon, needs to be modified according to molecular orbital theory. In silicon, the 3s and 3p orbitals are hybridised to form four $sp^3$ hybrids. These can be shown by symmetry to point toward the corners of a tetrahedron with the atom in the centre. This explains the tetrahedral bonding in

materials such as silicon and diamond.

In molecular orbital theory, when two atoms are brought together, atomic orbitals with the same symmetry, similar energy and similar size can combine. Two atomic orbitals will be transformed into two molecular orbitals – bonding and anti-bonding. In the case of silicon, there are four atomic orbitals on each atom, and two atoms will therefore combine to give four bonding and four anti-bonding orbitals. Consequently, n atoms will provide 2n bonding and 2n anti-bonding orbitals. Each atom provides four electrons, so there are 4n electrons in total. This is sufficient to fill 2n orbitals. In summary from the molecular orbital viewpoint, there will be two bands – bonding and anti-bonding – one of which is filled, and the other, empty. In terms of band theory, these are called the conduction (bonding) and valence (anti-bonding) bands.

It is seen from this, that there is no energy level which has half of its states occupied and half empty. In this case, the Fermi level is found within the region of zero density of states.

The difference in energy between the valence band and conduction band is called the band gap. It is denoted $E_g$. Semimetals differ from semiconductors and insulators in that their band gap is zero. This means that the two bands, although they are separate, touch. The Fermi level is still found in a zero density of states, although the band gap is zero.

The difference between semiconductors and insulators is somewhat more difficult to define. In some cases charge carrier density is used, however this is temperature dependent, allowing insulators to become semiconductors at high temperatures and semiconductors to become insulators at low temperatures. A more universal method is to say that the difference between the two is the energy of the band gap. Semiconductors have $0 < E_g < 4$ eV, while insulators have $E_g \geq 4$ eV.

#### 1.3.1.2 Intrinsic and extrinsic semiconductors

Pure silicon is an elemental semiconductor. Each atom has four electrons and shares one from each of the four atoms to which it is bound. This creates the noble gas configuration of eight valence electrons. When energy is provided and one of these

electrons is promoted to the conduction band, a hole is left behind. Many things can occur as a result of this, one of which is recombination, i.e. the electron dropping back into the hole and releasing energy in the form of electromagnetic radiation or lattice vibrations (phonons). More interesting, however is that the electron and hole may migrate through the silicon.

Movement of the electron is easy to comprehend, and is identical to the mechanism in a metal where the electron may be anywhere in the delocalised band over the whole sample. Focussing on the hole created, a valence electron from a neighbouring atom may move to fill this hole. This can be repeated, with the effect that the hole migrates across the sample. If the silicon is placed in an applied field, the electron in the conduction band will migrate in the opposite direction to the field, and current flows. Any electrons moving into the hole will also be affected by the applied field and move in the direction opposite to it. The effect of this is that the hole is moving in the direction of the field.

In the case of pure silicon, the number of electrons will always be equal to the number of holes. This is called intrinsic conduction. The Fermi level lies in the centre of the band gap in intrinsic semiconductors.

Impurity atoms can lead to there being a large excess of one type of charge carrier over the other, and conduction of this type is said to be extrinsic. If a silicon atom is replaced with an atom of a group V element such as phosphorus, this will have five electrons in its outer shell, and will receive four from neighbouring silicon atoms to which it is bound. This creates a total of nine electrons, which is in excess of the noble gas configuration. The extra electron will readily be accepted into the conduction band. It is called a donor electron and the energy level diagram of this is shown in Figure 1.6. In this case, the majority charge carriers are negatively charged electrons, and the semiconductor is said to be n-type.

At T = 0 K, the donor levels are all filled, and the Fermi level is situated between the donor states and the conduction band. This is shown in Figure 1.6. Increasing the temperature causes electrons to move into the conduction band, leaving empty states in the donor levels, so the Fermi level moves down. At high temperatures intrinsic conduction takes over, and the Fermi level will be found approximately in the centre of

the energy gap as in the intrinsic case.

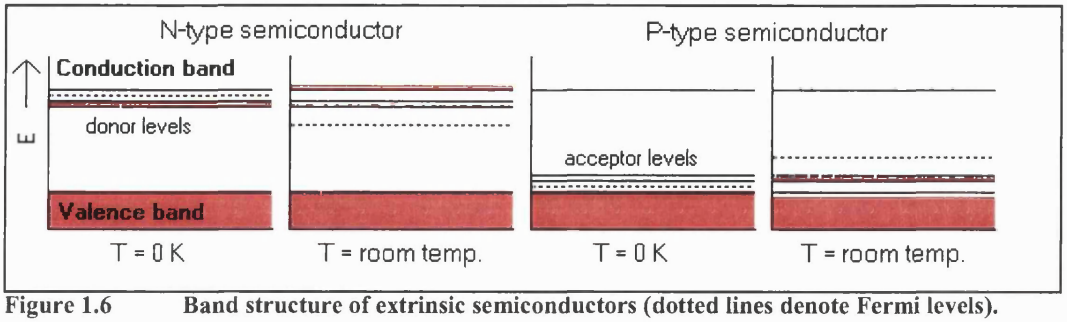


**Figure 1.6 Band structure of extrinsic semiconductors (dotted lines denote Fermi levels).**

The opposite case may apply if a silicon atom is replaced by a group III atom. Now the atom is electron deficient, having only seven electrons in its valence shell. The space remaining may be filled by electrons from neighbouring atoms as in hole migration in pure silicon. Impurity atoms of this type are known as acceptor atoms and give rise to acceptor levels in the energy level diagram as seen in Figure 1.6. The hole, although it is the absence of an electron rather than the presence of something else, is treated as though it was a particle. It behaves in the same manner as a positron and has the symbol $h^+$. Holes are positively charged carriers, and semiconductors of this type, which have positively charged particles as majority carriers, are called p-type.

Now, at T = 0 K, the Fermi level will be found above the valence band and below the acceptor levels. With increasing temperature, it moves towards the centre of the energy gap as shown in Figure 1.6.

In extrinsic semiconductors, donor levels are close to the conduction band (n-type) or acceptor levels are close to the valence band (p-type). Due the proximity of these levels, very little energy is required for all donor levels to be emptied or acceptor levels to be filled. Relatively low temperatures are required for all the extrinsic behaviour of a material to be experienced, however, intrinsic conduction still occurs. This is an exponential growth with respect to temperature, and the overall carrier density of an extrinsic semiconductor as temperature changes is shown in Figure 1.7.

A further modification of this type of semiconductor is one where two dopants are used – one n-type and the other p-type. This is called a compensated semiconductor. It is possible to have a partially compensated semiconductor, where both types of dopant exist, but one is in excess over the other.

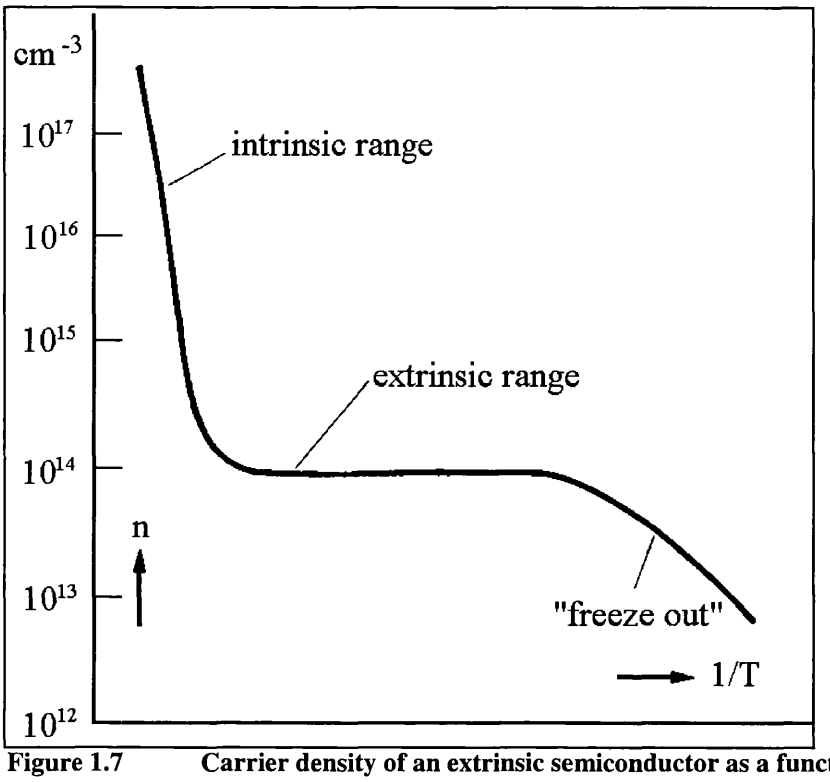


**Figure 1.7** **Carrier density of an extrinsic semiconductor as a function of temperature.**[67]

### 1.3.1.3 Compound semiconductors

Many compounds also exhibit semiconducting properties. Binary compounds of Group III and Group V elements exist with a structure similar to that of silicon. Each atom is surrounded by four atoms of the other element in a tetrahedral arrangement with four covalent bonds. The difference is that three of the bonds contain one electron from each atom, and the fourth is a dative bond with two electrons from the Group V element. As dative bonds and covalent bonds cannot be distinguished, the arrangement of valence electrons is isoelectronic with that in silicon. This is the zincblende structure (ZnS).

Compounds of Group II and Group VI also exhibit semiconducting properties, but the difference in electronegativity of these two groups causes the bonds to be more ionic. This means that their band gaps will be wider than those of III – V semiconductors. Group I – Group VII compounds, such as sodium chloride, are almost fully ionic, and are therefore insulators.

In III-V, II-VI and I-VII semiconductors, it would be expected that they would exhibit intrinsic behaviour. A perfect crystal would, but almost all crystals contain defects, which act in the same way as doping atoms. A compound semiconductor might have a

deficiency of the cationic element, which would lead to there being localised excesses of electrons. This makes the semiconductivity n-type. On the other hand, if there were a deficiency of the anionic element, conductivity would be p-type.

As the band gap of similar materials varies greatly, there is significant interest in making ternary or quaternary compounds in order to tune the band gap to suit a particular purpose. An example of a ternary compound is aluminium gallium arsenide, $Al_xGa_{1-x}As$, and $In_xGa_{1-x}As_{1-y}P_y$ is an example of a III-V quaternary compound.

#### 1.3.1.4 Direct and indirect semiconductors

In order to appreciate the difference between direct and indirect band gap semiconductors, it is necessary to realise that the above models do not describe actual transitions, but the existence of allowed and forbidden states. The full picture is only realised when specific energy levels are studied along with associated transitions.

The simplest way to visualise a solid from the point of view of an electron is as a periodic array of potential energy minima. The model is simplified further, if each minimum is assumed a square-edged well, and only a one-dimensional crystal is considered. This is the Kronig-Penney model[68].

A particle of the size and mass of electron can also be described as a wave. This is quantified in the de Broglie relationship

$$\rho = \frac{h}{\lambda} \qquad 1.1$$

where h is Planck's constant and $\lambda$ is the wavelength of the particle.
Another term that must also be defined is the momentum vector or wave vector, k.

$$k = \frac{2\pi}{\lambda} \qquad 1.2$$

From 1.2 and 1.3 it is seen that the momentum may be written as

$$\rho = k\hbar \qquad 1.3$$

where $\hbar = h/2\pi$

An electron in a vacuum experiences no external forces. Therefore, its energy is

described entirely by its kinetic energy.

$$E = \tfrac{1}{2} mv^2 \qquad 1.4$$

From 1.3 and 1.4 the energy of a free electron in a vacuum becomes

$$E = \frac{k^2 \hbar^2}{2m} \qquad 1.5$$

In a solid, the atomic nuclei exert a force on the electrons. This can be envisaged as a local potential well. Over the whole solid, this is a three dimensional array of potential wells.

For a one-dimensional solid, considering only s-orbitals, the lowest energy occurs when all orbitals are in phase, i.e. $\psi = (s_1 + s_2 + s_3 + s_4 + \ldots)$

The wavelength of this is infinite, so the wave vector is zero. This means that the energy of an electron in this environment would have no kinetic energy term, and only a potential energy term.

Considering the highest energy condition for only s-orbitals, this would have all orbitals out of phase. $\psi = (s_1 - s_2 + s_3 - s_4 + \ldots)$

In this case, there is a nodal plane between all the atoms. This can be depicted as a wave, with wavelength 2a where a is the lattice spacing. All intermediate instances of s-orbital configurations will lead to intermediate energies and intermediate wavelengths.

For $p_z$-orbitals, the lowest energy state, exists when all orbitals are bonding. This occurs when they are *out of phase*, so $\psi = (p_{z1} - p_{z2} + p_{z3} - p_{z4} + \ldots)$.

The wavelength is the same as that for all in phase s-orbitals, 2a, but the nodes are on the atoms rather than between them. When the $p_z$-orbitals are in phase $\psi = (p_{z1} + p_{z2} + p_{z3} + p_{z4} + \ldots)$ they are at their most anti-bonding and highly energetic state. The wavelength is a.

In the case of s-orbitals, energy increases as you progress from all in phase to all out of phase, so it is said to disperse upwards. For $p_z$-orbitals, energy disperses downwards as you progress from all in phase to all out of phase. $P_x$- and $p_y$-orbitals will follow the same trend as s-orbitals, however there will be a difference in energy due to different potentials.

A plot of energy *vs.* wave vector shows where an electron may exist. This is shown in Figure 1.8 for the simple description above. It is usual to plot the wave vector only as high as $\pi/a$, as extending it beyond this range repeats that which is experienced within this range.

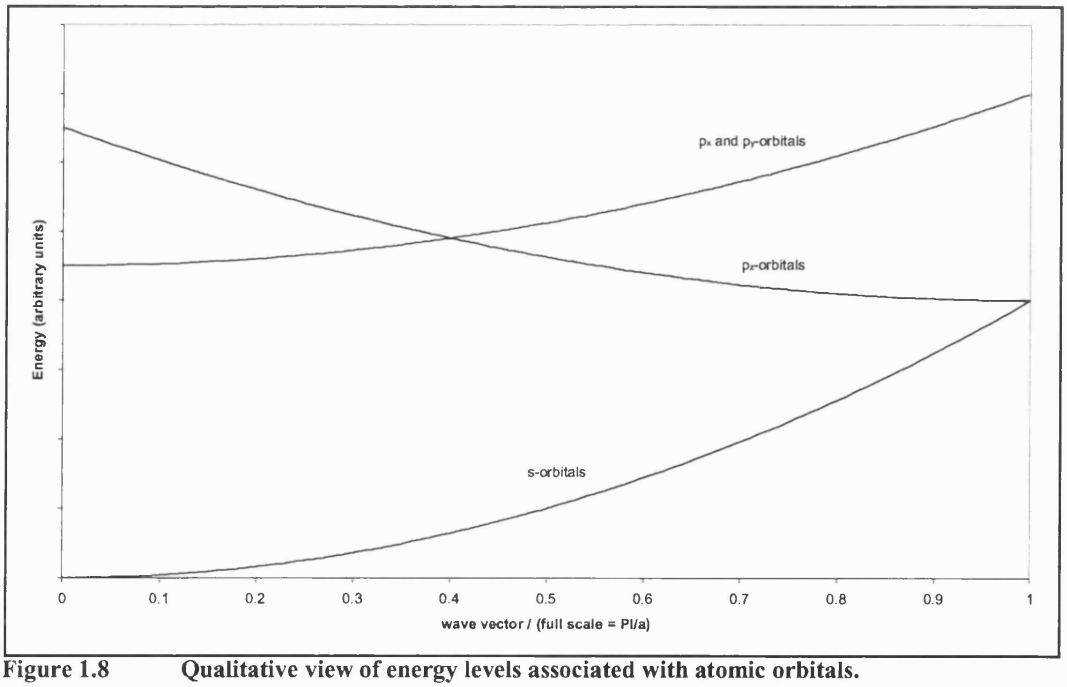


**Figure 1.8 Qualitative view of energy levels associated with atomic orbitals.**

In this description, which is only concerned with the n=2 energy levels, electrons may occupy states at all energies. In a real crystal, some energies may have no states

associated with them, as was demonstrated in the simple band description above. For electrons to transfer from a state below this forbidden gap to one above there must be an increase in energy. The wave vector, as previously seen, is a measure of momentum. As a photon has no mass, in order to obey the law of conservation of momentum, only vertical transitions are allowed on an energy / wave vector diagram.

Some materials, namely narrow band gap III-V and all II-VI semiconductors, have their highest energy state below the gap and their lowest energy state above the gap at the same wave vector. This means that the incidence of a photon can excite the crystal by the minimum amount. These are called direct band gap semiconductors. Group IV and cubic III-V semiconductors do not exhibit this property. Instead, vertical transitions, as caused by photons, excite electrons by more than the minimum energy gap of the crystal. These are called indirect band gap materials. Band structures of these two types of material are seen in Figure 1.9.

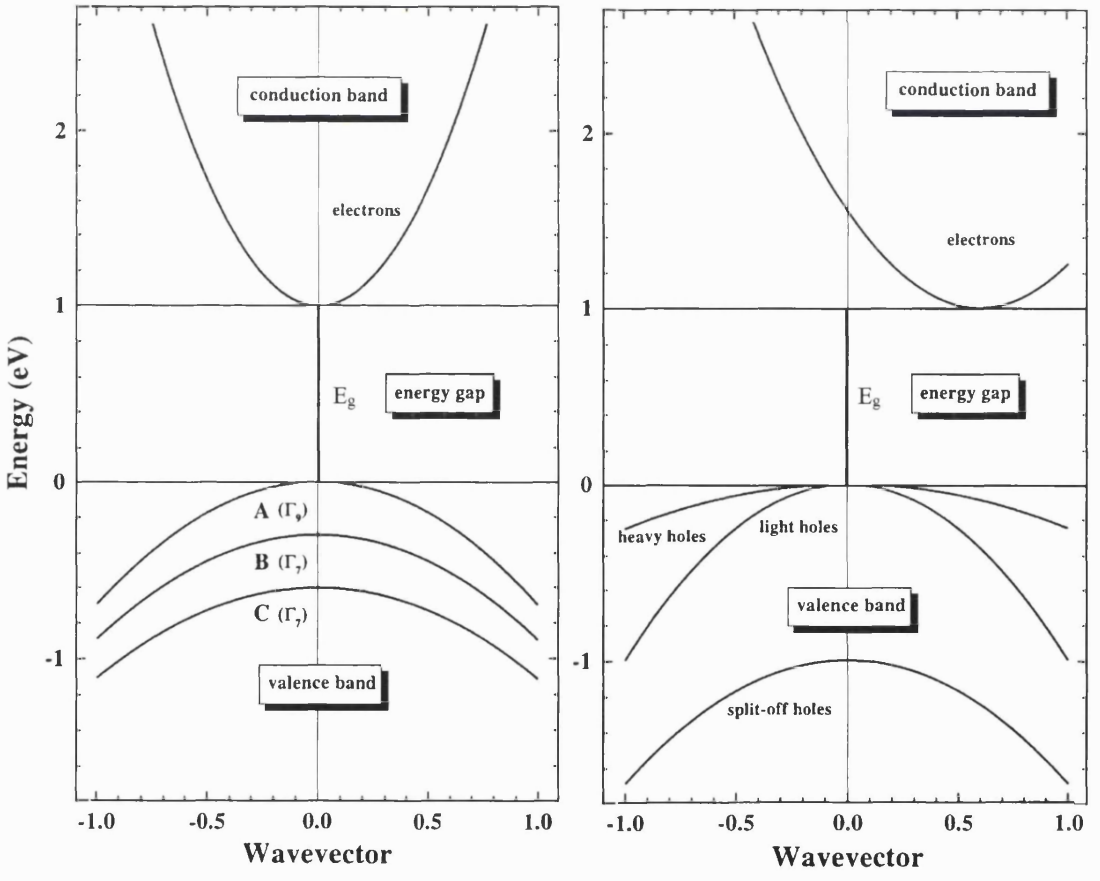


**Figure 1.9 Wave vector vs. energy plot for direct (left) and indirect (right) band gap semiconductors.**[68]

In order to measure the width of the narrowest part of the gap in indirect band gap

materials, forbidden transitions must occur. These involve the action of phonons. When a photon excites an electron, a phonon may also be involved allowing horizontal motion through the energy / wave vector plot. This is shown schematically in Figure 1.10. Phonons may be either created or annihilated in this action.

The optical absorption spectrum of a perfect ideal direct band gap semiconductor, would have no absorption at energies less than the band gap, and 100 % absorption at energies above the band gap. For an indirect band gap semiconductor, energies less than the narrowest path across the gap would have no absorption. Energies above the narrowest vertical transition would have 100 % absorption. In between, absorption tails off from one extreme to the other.

A real example of an indirect band gap semiconductor is germanium. The absorption spectrum of germanium is given in Figure 1.11. This shows the direct transition, with the indirect transition forming a shoulder on it.

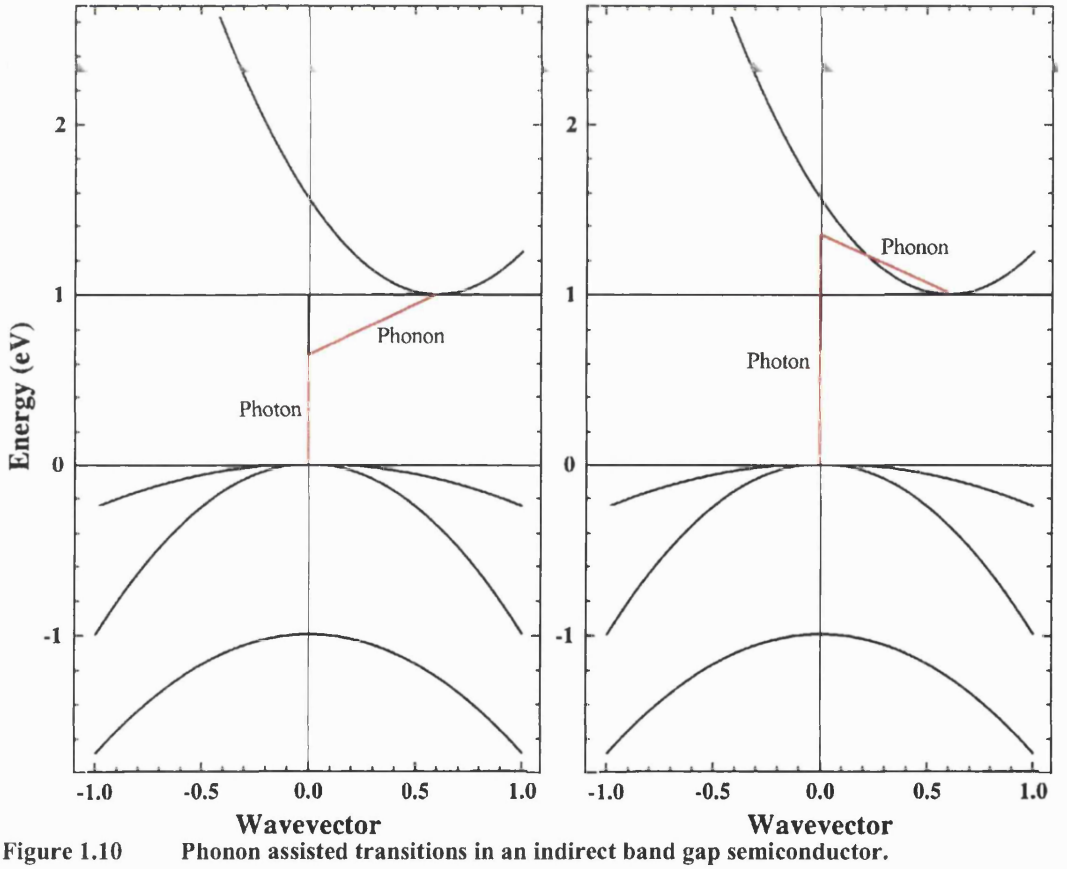


**Figure 1.10** **Phonon assisted transitions in an indirect band gap semiconductor.**

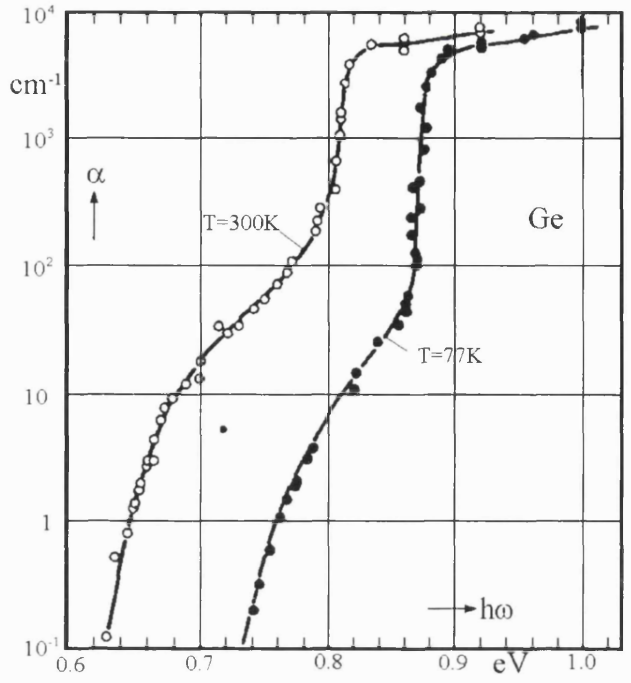


**Figure 1.11 Absorption spectrum of Germanium.**[69]

## 1.3.2 Photovoltaic materials

In today's fast moving world, power consumption is increasingly important. The need for renewable energy sources has become accepted, as fossil fuels are rapidly depleted. Solar cells are an obvious choice, as these devices, fitted to the roofs of most houses, would receive enough sunshine for all the energy requirements of the occupants to be met, provided sufficient storage is available.

Solar cells contain n-p junctions. In an n-p junction, semiconductors of these two types are brought together. As separate materials, the Fermi levels are separate. On contact electrons, which are the majority carriers on the n side of the barrier, migrate into the p-type material due to a concentration gradient. This leaves uncompensated donors and a net positive charge in the n-type material. Conversely, holes on the p side of the barrier migrate toward the n side leaving negatively charged acceptor atoms. The valence and conduction bands bend as this happens, bringing the Fermi levels into line. The system is only at equilibrium when the Fermi levels align, because the Fermi level is equivalent to the chemical potential, which, by definition, is equal throughout a system at equilibrium. The charge flow gives a dipole at the junction, called the space charge region. The interface between these regions is typically < 1000 Å, the exact width

depending on the doping concentration, and may be different on either side of the barrier.

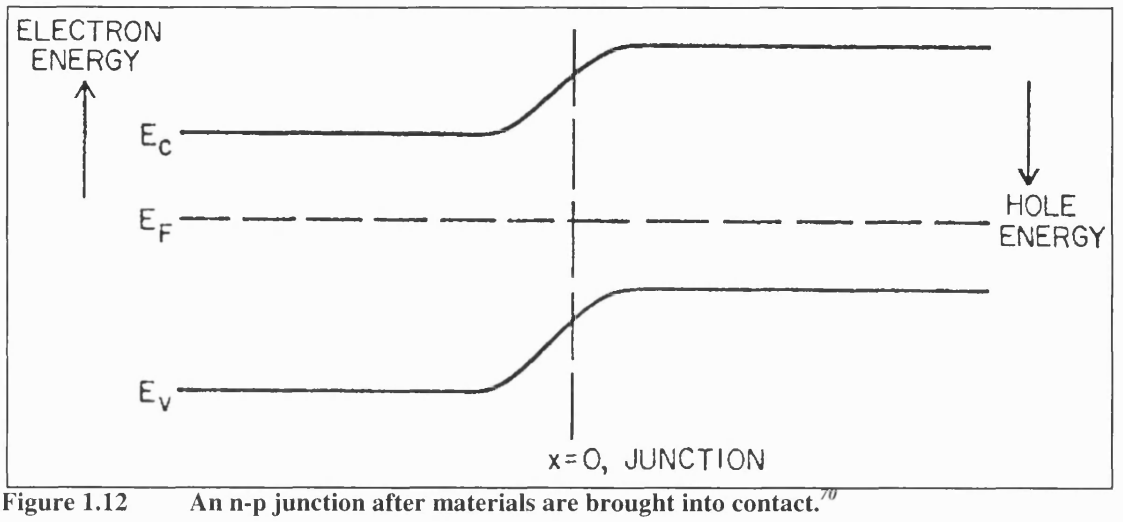


**Figure 1.12 An n-p junction after materials are brought into contact.**[70]

Electron hole pairs can still be created either side of the junction. These have a finite lifetime, and recombination soon occurs unless the charges can be separated. This is done by the electrostatic region at the centre of the junction. Any electrons in the conduction band on the p-side will be attracted to the positively charged region on the n-side of the junction. This makes up the thermal current. At the same time, some electrons on the n-side of the barrier will have sufficient energy to overcome the electrostatic forces. These migrate to the p-side and recombine with holes. This is the recombination current. At equilibrium, they balance.

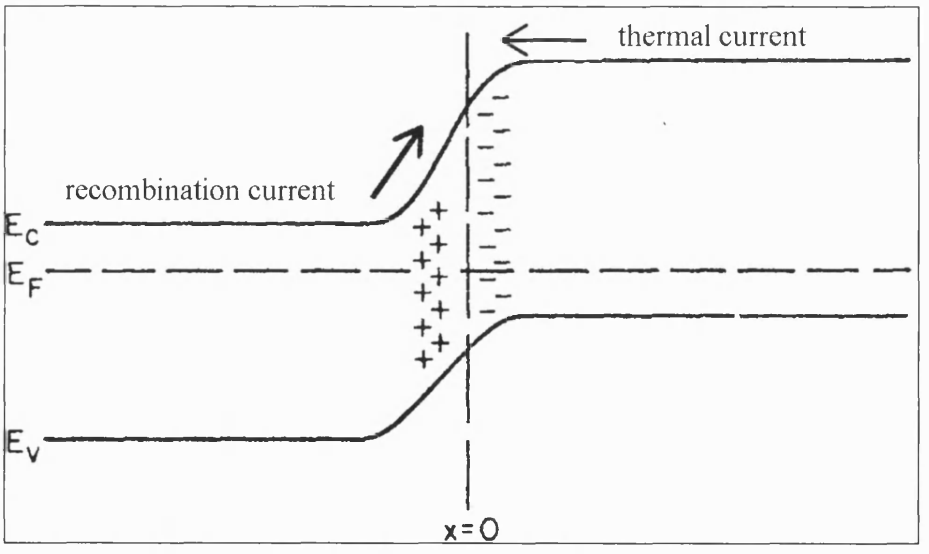


**Figure 1.13 Thermal current and recombination current in an n-p junction.**[70]

Applying a potential difference across the junction causes the bands to bend to a greater or lesser degree. If a negative bias is applied to the n-type material, this increases the levels of bands on this side of the junction. Now electron flow from here to the p-type material is facilitated and current may flow. The junction is said to have forward bias.

Under reverse bias, the n-type material is positively biased with respect to the p-type material. Now the difference in energy between the bands on either side is increased, so electrons are less likely to flow. They will only proceed if the current is high enough.

Recombination of electrons and holes after migration across the junction may be radiative or non-radiative. Radiative transitions, accompanied by the emission of a photon, only occur with direct band gap materials such as gallium arsenide. These are used as light emitting diodes. For indirect band gap materials, this transition is forbidden due to conservation of momentum, and the energy must be lost as lattice vibrations, or heat.

The photovoltaic effect is the reverse of a radiative transition. Incident sunlight causes the number of electron-hole pairs to rise greatly. This leads to an increase in the current due to electrons moving from the p-side to the n-side, due to band bending. Now the carriers are separated prohibiting recombination and excess charge carriers on either side of the material may be collected to do useful work. Charge carrier flow across the junction leads to a decrease in the band bending. Without this decrease, the cell would be at equilibrium and no current could flow. Current will flow as long as the bands are still bent sufficiently for charge separation.

In a solar cell, the n-type material is on top of the p-type material. Short wavelength photons create electron-hole pairs within the n-type material, and longer wavelength photons penetrate into the p-type material creating electron-hole pairs there. Under the p-type material, a contact covers the entire surface. Above the n-type material the contact is in the form of a grid, allowing light to shine on the surface. The surface of the n-type material between the grid may be covered with an anti-reflective coating, to maximise photon absorption.

### 1.3.3 Important considerations for heat mirrors and solar control coatings

In cold countries, the cost of heating buildings is high. Conversely, the cost of cooling buildings in warm climates is high. If it is possible to minimise these costs and energy consumptions, by use of solar energy, that is to our advantage. One way would be using solar cells, but the direct use of sunlight is another.

All objects emit black body radiation depending on their temperature. The sun, which has a surface temperature of 5762 K, emits black body radiation in the visible region of the electromagnetic spectrum. Most objects in the home or workplace are at a temperature of, say, 290 K, and black body radiation of these objects is of infrared wavelengths.

Buildings all have windows, which are transparent to the vast majority of radiation in the visible and infrared regions. If coatings can be applied to windows, then the optical properties may be modified to suit the needs of the particular climate.

In cold climates, little sunshine is seen through most parts of the year. High latitudes receive less sunlight, as it has to pass through a greater thickness of the atmosphere. Windows need to transmit as much of the visible light as possible, so the temperature in a room will rise. They also need to reflect infrared radiation. This is important to keep black body radiation emitted within the room from escaping. The transmittance reflectance spectrum for an ideal heat mirror is shown in Figure 1.14.

In warm climates, plenty of sunshine is available, and the light is very bright. If transmission of visible light through a window is as low as 10 %, there is still sufficient light within the building. Transmission in the infrared must also be minimised to stop heat from the sun entering the building. The major problem is that reducing transmission usually leads to increasing reflection. Outside the buildings, light is very bright, and highly reflective windows could lead to spots almost as bright as the sun itself. This distraction could lead to major road accidents and other such problems, so government legislation in most countries limits the reflective properties of windows in urban areas to 10 %. The ideal solar control coating, therefore cannot have low

transmission unless absorption occurs, so visible transmission of 10 – 50 % is the target. Figure 1.15 shows the transmittance reflectance spectrum of an ideal solar control coating.

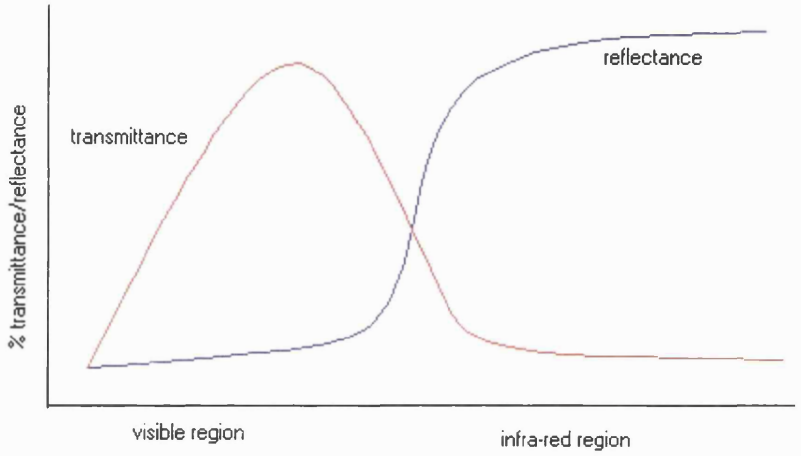


**Figure 1.14 Transmittance reflectance spectrum for an ideal heat mirror.**

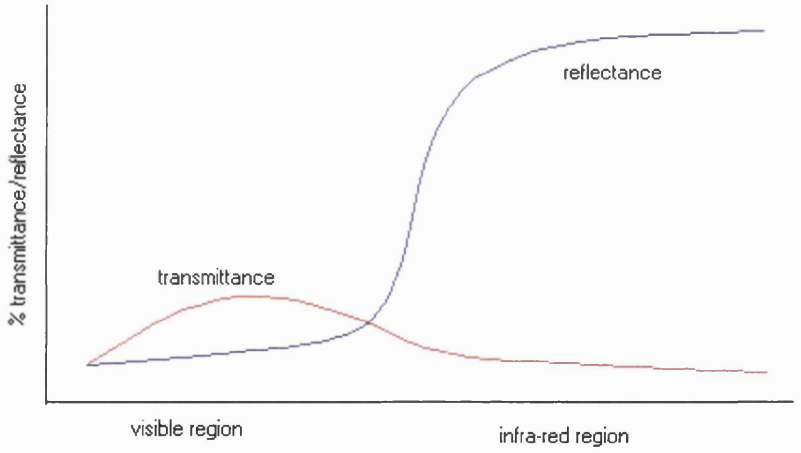


**Figure 1.15 Transmittance reflectance spectrum for an ideal solar control coating.**

## 1.3.4 Electronic and optical description of tin sulfides

Tin(II) sulfide has attracted attention in recent years, as its electronic band gap of 1.3 eV[30] is intermediate between those of silicon (1.2 eV) and gallium arsenide (1.43 eV).[2] This makes it potentially suitable for solar cell applications.[71] The optical band gap of SnS is 1.08 eV,[41] although in some instances band gaps as high as 1.51 eV have been recorded.[46] The conductivity in SnS is p-type with tin vacancies forming acceptor

levels.[47] An excess of tin alters conductivity to n-type.[47] Ortiz *et al.*[2] studied the optical absorbence of SnS and measured an optical energy gap of 1.34 eV (which agrees with most other measurements). Estimating the phonon involved in the transition to have an energy of 0.18 eV, they calculated that the direct band gap of tin(II) sulfide is 1.16 eV. Optical band gaps have also been measured using plane polarised light with the plane of polarisation parallel to the *a*- and *b*-crystallographic directions.[29] It was found that the band gaps are 1.161 ± 0.031 and 1.139 ± 0.015 eV in the *a*- and *b*-directions respectively. A 2-dimensional model of this confirms that the transition is indirect forbidden with optical energy gaps of 1.089 and 1.068 eV in the *a*- and *b*-directions.[72] Phonons involved in these transitions have respective energies of 0.08 and 0.062 eV. A 3-dimensional model agrees that the transition is indirect, but does not determine whether it is allowed or forbidden.[72]

Conductivity measurements on tin(II) sulfide[2] give an electrical conductivity of *ca.* 5 x $10^{-6}$ $\Omega^{-1}cm^{-1}$. The activation energy of this was found to be 0.3 eV, and is associated with acceptor levels due to excess tin in the samples studied.

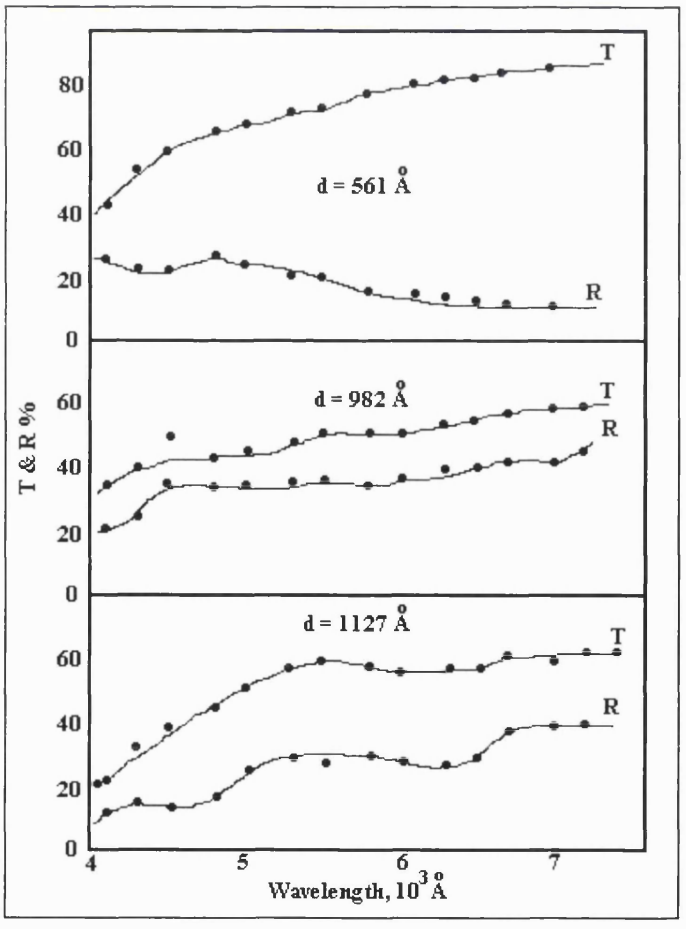


Transmittance and reflectance data have been recorded for tin(II) sulfide films.[40] Spectra of these are shown in Figure 1.16. These films were vacuum-deposited onto glass slides at 100 °C. Films deposited in the same manner at 200 °C were observed to be hexagonal in structure and more reflecting and less transmitting.

**Figure 1.16 Transmittance reflectance spectrum recorded for tin(II) sulfide films of different thicknesses.[40]**

Tin(IV) sulfide is much less interesting from this aspect as its band gap is 2.07 eV.[47] It is an n-type semiconductor. The optical band gap of 2H-$SnS_2$ has been measured as 2.18±0.02 eV.[73] The main phonon associated with this occurs at 0.07 eV, with two others observed at 0.053 and 0.075 eV.[73] An indirect transition assisted by a phonon of energy 0.04 eV has been identified in crystals grown by physical vapour transport.[34] Doped tin sulfide crystals have also been prepared and their electrical conductivity studied.[74] Cu, Au, Be, Zn, Ga, In, Pb, P, Sb, Se, Te and Pt were all investigated as dopents. Impurities had no effect on the structure of the crystals – 2H, 4H and their intergrowths being formed. Values of conductivity depend on the impurity element, although all materials were found to be n-type semiconductors. The exception to this occurs on simultaneous doping of In and Cu, which produces large, perfect $SnS_2$ crystals that exhibit p-type conductivity.[74]

Mixed valent $Sn_2S_3$ is a classical type-I mixed valent compound.[75] As such, it is expected to exhibit insulating properties, however, it is a direct forbidden semiconductor with an electronic band gap of 0.85 eV.[39] The room temperature conductivity is 3 x $10^{-5}$ $\Omega^{-1}cm^{-1}$. The ribbon-structure of $Sn_2S_3$ leads to a large anisotropy in the conductivity. This anisotropy is temperature dependent within the range $3 < \sigma_c/\sigma_a < 10$.[39] Conductivity is n-type and the optical band gap is 0.95 eV[39] for single crystals or 1.16 eV in the case of thin films.[57]

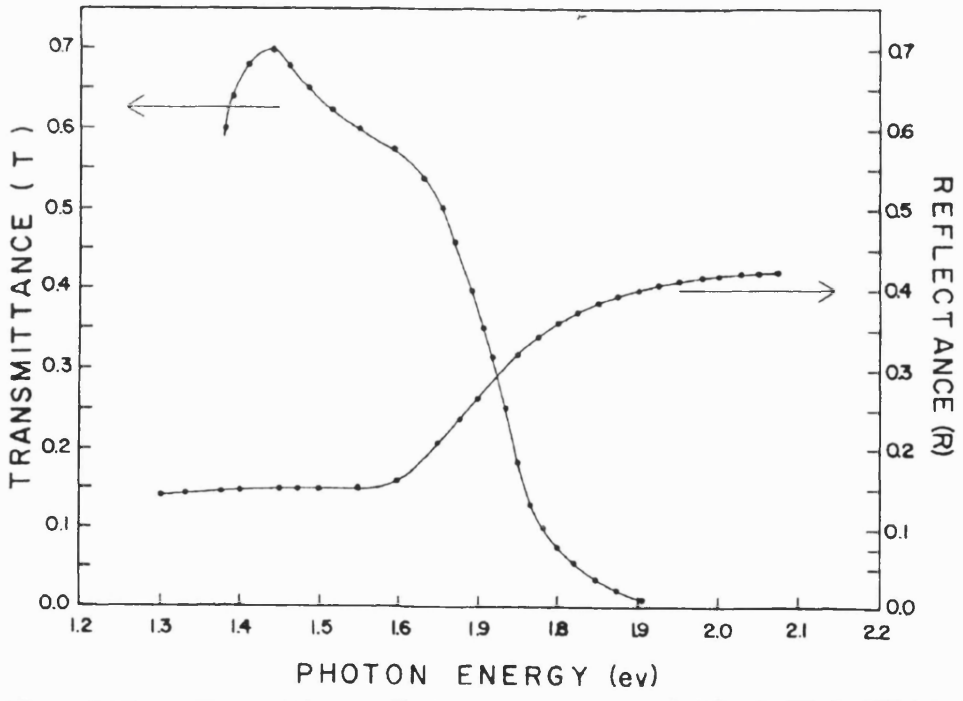


**Figure 1.17 Transmittance reflectance spectrum recorded for tin(II) tin(IV) trisulfide.[57]**

Details of the transmittance and reflectance of films of tin(II) tin(IV) sulfide deposited by spray pyrolysis have been recorded.[57] The spectrum of this is reproduced in Figure 1.17.

# 1.4 Methods of thin film deposition

Thin films, as a loose term, have been known for many, many centuries. Paints and glazes may be defined as thin films. Recently, however, thin films are a specialised technology whereby layers are deposited atom by atom rather than by laying down large particles.

Many methods are used to deposit thin films and these may be split into two categories – physical and chemical deposition. Some of the more widely used methods are outlined in this section, although other methods, such as chemical bath deposition, may be used, as was described in section 1.2.3

## 1.4.1 Chemical vapour deposition

Chemical vapour deposition is an extensive technique. Many factors can be varied, often changing the name of the process, but all of which fall under this broad heading. Main variations are the methods of precursor release and film deposition. The third common variable is the pressure inside the reactor chamber, which can be low (*ca.* $<10^{-3}$ atm.) or atmospheric (*ca.* 0.1 – 1 atm.).

### 1.4.1.1 Methods of precursor release

Precursors of many types are used in chemical vapour deposition. Gas precursors may be admitted to the system directly, but solid and liquid precursors must first be vaporised.

The simplest route to vaporisation of precursors is in a bubbler. The bubbler contains a volatile solid or liquid. It is heated with a hotplate or thermal jacket. An inert gas is

passed through the bubbler and transfers some of the vapour to the reactor. This route is only applicable to materials with high vapour pressures. The gas lines through which the vapour passes must also be heated to stop condensation, which can lead to blockages.

Involatile materials or materials which decompose at low temperatures may also be used, but a non-thermal method of vaporisation is required. In this case, an aerosol of the precursor in a suitable solvent may be formed. Then, when the droplets arrive at the reactor, the high temperature conditions within the reactor lead to evaporation of the solvent and the precursor. Many methods of aerosol formation are used. Two of the most common involve a piezoelectric device or blowing a liquid through a small nozzle into a high pressure gas flow. Aerosol Assisted CVD or Spray Pyrolysis denotes use of these methods to vaporise the precursor.

#### 1.4.1.2 Methods of film deposition

There are many differences in film deposition. The way in which the film relates to the substrate is a key one. Films can be epitaxial or non-epitaxial, and epitaxial films may be grown on like substrates or different substrates. If the substrate is different from the material being deposited, the film need not necessarily exhibit its usual crystal structure. Epitaxial films grown from organometallic precursors can be called organometallic CVD (OMCVD), metallorganic CVD (MOCVD) or Organometallic Vapour Phase Epitaxy (OMVPE).

Film deposition on the substrate usually requires a form of additional energy. This is thermal energy in most cases. The substrate can be heated in many ways, and these determine the design of the reactor. The substrate can be placed inside a quartz tube, and either heated by an element within the tube, or by heating the entire tube from a tube furnace outside. This differentiates cold- and hot-walled reactors. Reactors may be horizontal or vertical and this describes the direction in which gases flow through them. A horizontal low pressure CVD reactor can coat more than one substrate at a time, by mounting them vertically with spacing between. This looks like a toast rack.

In some cases, particularly when the required heat energy is very high, heating is not an effective method of providing energy. Other methods of supplying energy to the

substrate and precursors include photo assistance and plasma assistance.

In the case of photo-assistance, a laser is shone onto the substrate. Two geometries are possible – perpendicular, where the laser is normal to the surface, and parallel, where the laser shines parallel to the substrate. Use of ultra-violet wavelengths allows a large amount of energy to be added to the system with very little heating of the substrate.

Plasma enhanced CVD (PECVD) makes use of electrical energy to promote film growth. Plasmas may be created by high temperatures or electric or magnetic discharges. Those created by heat have local equilibria between ions, electrons and neutral species. Nonequilibrium or "cold" plasmas have electrons and ions that are more energetic than neutral species.

In film deposition, the most common method of plasma formation is using a radio frequency (rf) electric field. The field interacts with free electrons present in the gas. Ions are also affected, but this is negligible because of their much higher mass. The electrons' energies will hardly be affected by elastic collisions, because of the huge difference in mass. Nor will they be affected much by inelastic collisions, unless they have energy sufficient to ionise the atom with which they collide.

When high energy electrons collide with atoms reactive species such as ions or radicals are produced as well as more electrons. These reactive species have lower energy barriers to chemical reactions on the substrate surface or in the gas phase. This means that lower substrate temperatures are required in chemical vapour deposition.

#### 1.4.1.3 Types of precursor

Many precursors may be used for chemical vapour deposition. Differences in precursors can put the reaction into one of two categories – multi-source or single-source.

Where two or precursors are admitted separately, the chemistry of the precursors is less important. The two must react together, and being volatile or gaseous ensures easy transport to the reactor.

In the case of single source precursors to compound materials, the precursor must be a molecule that contains all the elements required in the film, with bonds between them. The other components of the molecule must be weakly bound to the atoms of interest. It is important that there is a facile decomposition route to remove the unwanted parts of the molecule to volatile species and allow them to diffuse away rather than be incorporated into the film.

Precursors to films that are organometallic compounds, give the process the name Organometallic CVD (OMCVD) or Metallorganic CVD (MOCVD).

#### 1.4.1.4 Mechanism of chemical vapour deposition reactions

In the CVD reaction there are a number of steps, all of which are important in the overall reaction, and each of which may be the rate limiting step. They are:

- Transport of precursors to the vicinity of reaction,
- Possible gas phase reactions to yield film-depositing species,
- Adsorption of reactive species onto substrate,
- Diffusion of species over surface to growth sites,
- Reaction to deposit film,
- Desorption of by-products, and
- Transport of by-products away from the vicinity of reaction.

The fifth step has two parts – nucleation and growth. Films of different types are deposited depending on comparative rates of these two processes.

When nucleation occurs at many sites over the surface, small islands are created two-dimensionally. Eventually, these coalesce into a continuous film. This mechanism prevails when atoms of the film bind more strongly to one another than to the substrate. This pathway is usually the one observed in metal film deposition. In an extreme case, nucleation is so hard for aluminium films, that a $TiCl_4$ catalyst is required to assist nucleation.

If atoms are equally strongly bound to one another and to the substrate, or if bonds to the surface are stronger a two-dimensional layer-by-layer growth is observed. This mechanism dominates for homoepitaxial growth. Most heteroepitaxial films also follow

this mechanism.

In some cases with thicker films, initial growth will follow the two-dimensional layer-by-layer mechanism. As the number of layers increases, subsequent layer growth becomes unfavourable and three-dimensional island growth takes over.

Deposition temperature affects the structure of the film. At low temperatures, surface diffusion is low and nucleation high so amorphous films tend to deposit. At high temperatures, surface diffusion is more prolific than nucleation and crystalline single layers can build up. At intermediate temperatures nucleation and diffusion occur at similar rates, so films grow at many different locations over the substrate. This leads to island growth.

## 1.4.2 Physical methods

### 1.4.2.1 Evaporation processes

The simplest of all film growth methods is evaporation. This involves vaporising a pure material, which then deposits on a cooler substrate. The resulting film is generally of higher purity than the original sample.

In order to evaporate a pure sample, one must first be produced. This may be made by a number of techniques. Slowly cooling a sample from the melt is a straightforward way to produce pure crystals. This relies on the fact that impurities tend to be more soluble in the liquid than the solid, so remain in the melt. The Bridgman and Stockbarger technique is an example of this, where a ceramic boat containing the liquid is transported through an oven with a temperature gradient. Across the oven the temperature drops, and as the boat passes through the melting temperature the liquid freezes.

A similar method, but with vertical motion is the Czochralski method. Here, a seed crystal is slowly drawn upwards from a bath of the molten material. As the crystal is moved, it grows from the melt leaving the impurities behind.

In the evaporation process, many methods may be used to vaporise the sample. Thermal heating with tungsten or tantalum wires is often used. In some cases, the material to be evaporated reacts with these metals and a ceramic crucible must be used. The most effective way to completely stop the material from coming into contact with the metal is to contain the material in a quartz boat, which has an inner quartz tube housing the metal spiral.[76] This is required for cadmium sulfide.

Typical evaporation equipment would have a source to substrate distance of *ca.* 10 – 50 cm. In order to ensure that the atoms travel in a straight line from source to substrate, their mean free path must be greater than this distance. A pressure of less than $10^{-5}$ Torr is required to guarantee this.

In the case of evaporating alloys, further complications are involved as one element has a higher vapour pressure than another. This leads to it vaporising from the source at a greater rate, leading to different deposition rates on the substrate and the possibility that it may sublime out of the deposited film. One solution is to use a source material that has a low concentration of the element likely to vaporise faster. This will only work for small variations in vapour pressure of the constituent elements.

A more effective solution in the case of elements with a large difference in vapour pressure is to use multiple sources of the different components. In the case of cadmium sulfide, where sulfur has a higher vapour pressure than cadmium, one source will be cadmium sulfide, and a second sulfur source will be used. The higher flux of the material with high vapour pressure will stop evaporation of it from the deposited film. In addition, the temperature of the substrate must be sufficiently high that materials will react, but too high for the element with the higher vapour pressure to condense alone.

Another method of vaporisation is flash evaporation. This is used for multicomponent alloys where components evaporate at different rates. In this technique, small particles are dropped one at a time onto a very hot surface where they evaporate instantaneously.

Electron bombardment may be used to evaporate the sample. This overcomes the problems of reaction with the crucible, which can be associated with thermal evaporation. One problem associated with electron bombardment is that the energy of impinging electrons may be sufficient to decompose compounds, and this technique is

often used where the target film is a decomposition product of the starting material.

### 1.4.2.2 Molecular beam epitaxy

This technique involves the deposition of an epitaxial film – that is one in which the crystal structure matches that of the substrate exactly. In order to achieve this, the growth rate must be very slow, typically 1 μm/h.

The technique employs an ultra high vacuum, typically 5 x $10^{-11}$ torr. To achieve such a high vacuum takes a long time, so the equipment is maintained under vacuum almost all the time. Elaborate mechanisms have been devised to admit substrates and precursors. Crystals of the highest purity may only be formed if the substrate is completely clean. As etching *in situ* would compromise the vacuum, a number of multi-step procedures have been developed to remove contaminants.

The precursor is often transported to the substrate as a molecular beam. Knudsen cells are used where the precursor is heated by filaments encasing a pyrolytic boron nitride (PBN) crucible. A single Knudsen cell forms a single beam directed at the substrate, however the angular distribution of particles from this is small, so only small samples may be coated. A multiple Knudsen cell, with a number of 1 mm apertures gives a better uniformity of films, due to superposition of many beams.[77]

Some materials, notably arsenic and phosphorus, form tetramers on evaporation. These lead to a large number of defects in resulting film, while deposition from dimers yields higher quality final films. In this case, the element should be dissociated before reaching the substrate by passing through a hot zone after the main reservoir. Typical temperatures are 300 °C within the main reservoir and 900 °C in the hot zone.

Low vapour pressure materials require much harsher conditions in order to achieve vaporisation. Electron beams are used for materials, such as silicon, which fall into this category. To minimise contamination from the metal used as the filament, the thermal electrons are deflected by a magnetic field through 270 ° before impinging on the source.

Multicomponent films may be built up using a number of Knudsen cells. Each

would contain a different material, and computer control shutters are used to switch the molecular beams on and off allowing layer by layer build up.

One advantage of molecular beam epitaxy is that *in situ* characterisation may be carried out due to the ultra high vacuum environment of the system.

### 1.4.2.3 Sputter deposition

In this method, high energy atoms or ions are continually bombarded at a surface, causing atoms from that surface to be ejected. As it is easier to accelerate charged particles, ions are used more often.

The number of atoms ejected from the surface per arriving particle is termed the sputtering yield. This depends on the energy of the incident particles, and their mass relative to the mass of the material being sputtered. Heavier ions will sputter a surface composed of light atoms much more easily than would light ions. The angle of the beam to the surface also affects sputtering yield, which increases as $1/\cos\theta$ where θ is the angle between the beam and the normal direction.

The source ions used to bombard the material are created by accelerating electrons from a hot filament through a gas. The high energy electrons strip electrons from the gas leaving positively charged ions. A continual source of electrons is not necessary to sustain plasma if the pressure is greater than about 20 millitorr. An applied electric field between two electrodes will cause a self-sustaining glow discharge. As positive ions impinge on the cathode, secondary electrons will be emitted maintaining the plasma.

The material to be sputtered is negatively biased, in order to attract the ions to it. Although the energy required to remove a surface atom is usually of the order of 3 – 5 eV, the minimum threshold of the particles coming in to the surface is set to about 20 eV. This is sufficient to dislodge bulk atoms, which then strike surface atoms from below ejecting them. Atoms ejected by this means have higher energies than thermally ejected atoms and are often ionised. Single atoms, diatomics and clusters of atoms are all produced in a sputtering process.

One problem with sputter deposition is that there is a high contamination of the resultant film. This is because any impurity in the sputtered material is also susceptible to sputtering. The resulting film will be of similar stoichiometry to the original sample. One solution to this is to deposit the film over a long distance. The impurity particles will tend to deposit sooner, being more reactive and further away from the source, and a film of higher purity is produced. Another contamination problem is that the sputtering gas may be incorporated into the film. In contrast to intuition, it is found that increasing the pressure of the sputtering gas decreases the amount of absorption into the film.

Incorporation of the sputtering gas into the film is sometimes exploited. This is known as reactive sputtering and is used when high oxidation state oxides are required. Here, use of oxygen as the sputtering gas removes the potential problem of dissociation to lower oxides.

#### 1.4.2.4 Cathodic arc plasma deposition

This technique is an alternative to chemical vapour deposition used in coating cutting tools with hard coatings such as titanium nitride. The setback with chemical vapour deposition is that temperatures in excess of 1000 °C are necessary to deposit these coatings, but this is above the annealing temperatures of the tools. Cathodic arc plasma deposition uses ion bombardment to form the films rather than elevated temperatures.

The source material is the cathode in an arc discharge circuit. Material is eroded in many forms, the most important of which are ions and microdroplets. Approximately 30 – 100 % of the emitted vapour is ionised, and typical kinetic energies are in the region 10 – 100 eV.

High deposition rates are afforded by this method, and films are of high adhesion and density. Alloy compositions are maintained during deposition.

## 1.4.3 Other chemical methods of film deposition

### 1.4.3.1 Sol-gel methods

The sol-gel process describes any process that involves the transition of a solution or sol into a sol-gel. The sol-gel is a rigid, porous mass of solid and solvent-filled pores, which comes about by destabilisation, precipitation or supersaturation. When applied to film deposition, however, the term sol-gel tends to include any coatings formed by dipping, spinning or draining.

A commonly use sol-gel system is one involving alkoxides. When a metal alkoxide and water are combined in a mutual solvent (e.g. ethanol) the alkoxide undergoes hydrolysis. Polymerisation soon occurs, and the system transforms to an alcogel, i.e. a gel formed from an alkoxide rather than from ion-exchange solutions or colloidal sols, which are termed hydrogels. Heat is often applied to accelerate this process. The solvent is removed by evaporation or evacuation.

In coating a sample, coating is carried out at the solution or sol stage and the sol-gel transition occurs while on the substrate. Resulting films are high in purity, homogeneous and achieved at low temperatures. The principle problem is cost of raw materials and difficulty in handling.

# Chapter 2
# Experimental Techniques

# 2.1 Description of the CVD apparatus

## 2.1.1 Design of the rig

The apparatus used for the chemical vapour deposition reactions was purpose-built and based on previous reactors of the same type.

The main reaction chamber was supplied by Pilkington Glass plc. and consisted of a horizontal block of a graphite composite containing 3 Whatman cartridge heaters. Above the block, at a distance of 1 cm, was a glass top plate. At the end of the block was a piece of glass *ca.* 3.5 cm long and of the same thickness as the glass to be coated. Both these measures were to ensure an even flow of gases over the substrate by minimising turbulence. The ends of the reactor were attached with 6 bolts. An unheated exhaust line left the reaction chamber and was vented into the fume cupboard extraction system. At the entrance to the reactor was a brass block. This altered the incoming gas flow from a ½ inch pipe to a thin lamellar flow across the entire width of the reactor. It was easily removed for cleaning, and was prone to blockages as it contained the narrowest flows in the entire reactor. A schematic view of the reactor can be seen in Figure 2.1.

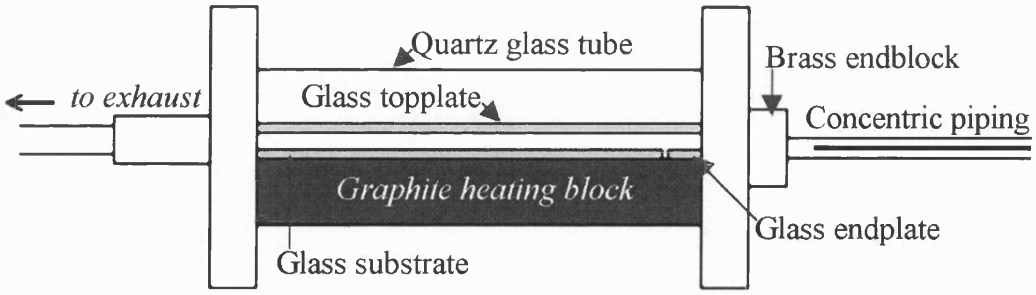


**Figure 2.1 Schematic view of the CVD reactor.**

The bubbler was made up of four parts. The base of the bubbler was machined stainless steel. The lid, inlet and outlet pipes, were also stainless steel. Between these was a metal and rubber O-ring acting as a seal. The lid was held on with a metal collar fastened with a wing nut. A brass cylinder to minimise heat losses surrounded the main chamber of the bubbler.

Five independent gas lines were used in the reactor. These allowed gases to be directed to and away from the reactor with a series of valves. Two lines were used for the introduction of volatile precursors such as tin(IV) chloride. These lines contained heated nitrogen, which could be diverted through the bubblers containing the precursors. The bubblers were heated, using a hotplate, to a temperature at which the vapour pressure above the liquid was sufficiently high for a reasonable amount of carry-over to occur. A third line, containing pure nitrogen, met with these two and allowed further dilution of the precursors. The fourth line was a pure nitrogen line. This met the lines from the bubblers at a four-way valve. The valve directed either the line from the bubblers or the plain line over the reactor and the other through a heated exhaust. The fifth line contained the co-reactant with diluting nitrogen. This could be a gas, as in the case of hydrogen sulfide, or a liquid admitted through the use of a syringe driver, for example, water. This line joined the other lines at a point 21.5 cm from the brass block. The two lines did not meet in a simple T-piece as this proved to cause turbulence and reaction of the precursors before they entered the reactor. Instead, two concentric pipes were used, the inner carrying the gases from the four-way valve and the outer the gases from the fifth line. The inner tube was *ca.* 3 cm shorter than the outer, although a shorter insert was available if necessary. All this is shown in the schematic representation in Figure 2.2.

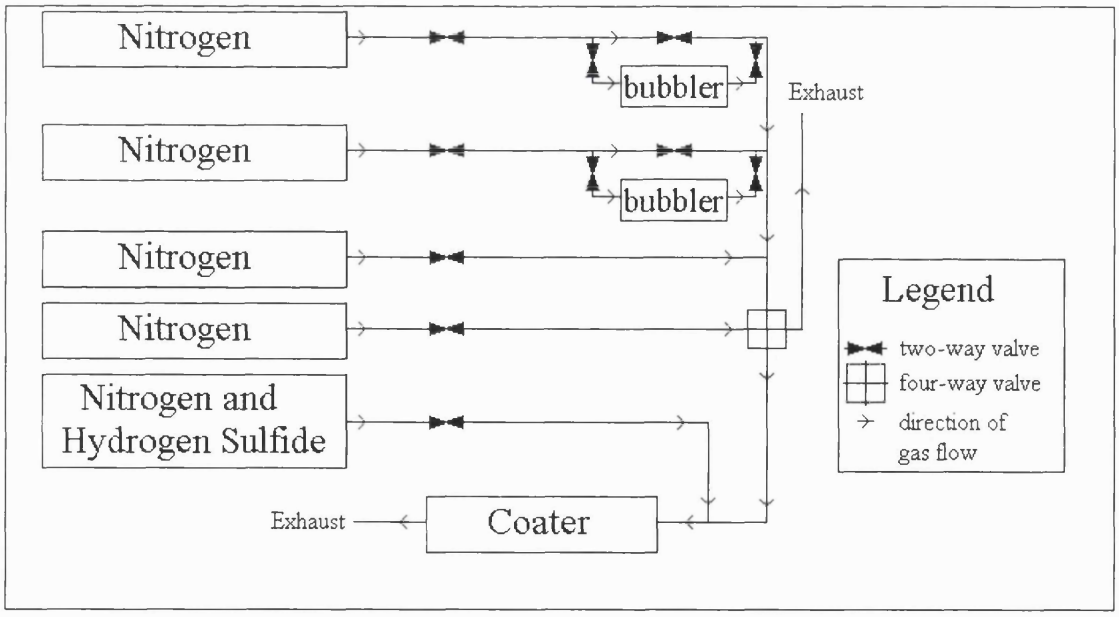


**Figure 2.2** **Schematic view of CVD rig.**

All gas flows were monitored using gravity flow meters. All lines were made of stainless steel, as this was unreactive towards $H_2S$. Lines were heated using Eurotherm

heater controllers. A series of two-way valves were used to shut down various lines, for example if only one bubbler line were to be used, the second line would be closed to prevent cross-contamination from a previous precursor in this line. NUPRO "BK" series valves were used to adjust the flows through the lines. These were situated between the regulator and flow meter for each line. The four-way valve contained a VESPEL® insert. This is a polyimide material manufactured by Du Pont, which does not melt and has no glass transition temperature. It may be used at high temperatures and pressures and causes low wear and friction.

## 2.1.2 Operation of the rig

Loading of the bubbler was required before any reactions could be carried out. In the case of some materials this was simple, but air- and moisture-sensitive reagents required more careful handling. Tin tetrachloride was purchased from Aldrich in Sure Seal bottles. This could be loaded into the bubbler using a syringe. Tin tetrabromide, which is a solid at room temperature, was purchased from Aldrich packaged under nitrogen and was loaded into the bubbler in a glove box. All other reagents used with the bubbler were not air-and moisture sensitive so could be loaded *in situ*.

Three types of glass were provided by Pilkington Glass plc. All were previously coated with a barrier layer to prevent diffusion of atoms from the glass into the films. The three barrier layers provided were carbon-doped silica, tin oxide/silica and pure silica. The glass with pure silica coating was 2.9 mm thick and the other two were 4 mm thick. All glass was cut to 224 x 89 mm and the edges ground before being supplied to UCL. As the glass was produced on a float line, there were tin atoms on the uncoated side. These tin atoms fluoresce, so inspection under an ultra-violet lamp was carried out to determine which side was to be coated. The side to be coated was cleaned by wiping with a paper towel soaked in petroleum spirit 40-60, washing with propan-2-ol and drying in air. Once dry, this was placed in the reactor, pre-coated side up, and the reactor end bolted on and exhaust attached.

A small flow of nitrogen gas was admitted to each line and the line heaters were turned on. For most reactions, each was set to 150 °C. This was sufficient for any precursor or water in the lines not to condense out. The heaters in the graphite block were turned

on. They were set to increase at 12 °C $min^{-1}$. Faster heating could lead to cracking of the glass especially the thinner silica coated glass. The hotplate under the bubbler was also turned on. This was set to a temperature where there would be sufficient volatility of the precursor for carry-over to occur. Volatility of the precursor was estimated from vapour pressure data given in the Handbook of Chemistry and Physics[78] for tin tetrachloride. For tin tetrabromide no vapour pressure values were available, so data from tin tetrachloride were used adjusting for the different melting and boiling points. Vapour pressure curves for these materials are given within Chapter 3, which discusses deposition reactions involving these precursors. For all other materials, a temperature between the melting and boiling points was chosen. Information on these was supplied by Differential Scanning Calorimetry, along with decomposition temperatures of the materials.

When the lines, bubbler and reactor had reached the required temperatures the system was left for at least five minutes to attain thermal equilibrium. The temperatures in the lines were recorded at this point, as some reaction times were too short for all data to be recorded during the reaction. Gas flows were increased in all the lines and hydrogen sulfide, if required, was admitted to the system. Nitrogen was diverted through the bubbler by closing the bypass valve, opening the outlet valve and opening the inlet valve. Flows from the bubbler were directed over the glass by turning the four-way valve. The stopwatch was started at this point. When the required time had elapsed, the four-way valve was turned directing the vapours away from the reactor and out through the exhaust. Then operating the valves in the reverse of the previous order closed the bubbler. Hydrogen sulfide was turned off and nitrogen flows in all other lines were reduced to a minimum. The heaters in all lines were turned off and the bubbler and reactor were allowed to cool.

When the glass in the reactor had cooled sufficiently to allow handling, it was removed from the reactor. A visual inspection was carried out and the film tested for adhesion. The film was cut into smaller pieces for various analyses to be carried out and stored in sample tubes or small bags.

## 2.1.3 Modification of the rig to allow aerosol delivery

The bubbler method of delivery is only suitable for precursors that are reasonably volatile at temperatures below 200 °C. Also, the precursors must not decompose in the bubbler, as the decomposition products are invariably involatile. Some precursors such as the homoleptic thiolates fall into this category – decomposition occurs at lower temperatures than boiling. In the case of these materials an alternative method of delivery is required. The solution used in this thesis was aerosol delivery. The way in which this works is described in section 1.4.1.1.

The section of the rig where the two precursors meet is easily removed for cleaning. This was removed and replaced with a section of stainless steel, to which a round-bottomed flask could be attached. The pipes to and from the flask were flexible PTFE. The bottom of the flask was modified by the glass-blowers so the glass was thinner. This was because ultrasonic waves would not pass through glass of normal thickness. A clamp stand held the flask in place above a PIFCOHEALTH Ultrasonic Humidifier product no. 1077. This setup is shown in Figure 2.3.

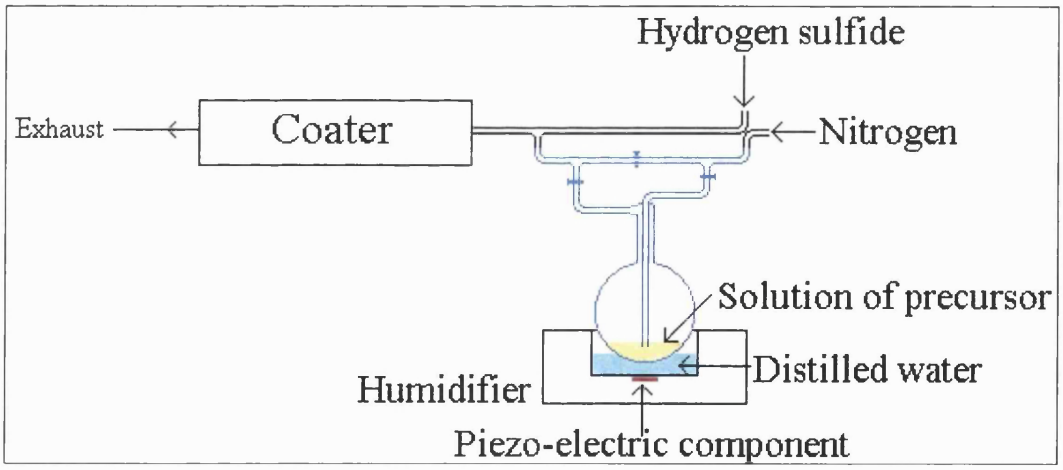


**Figure 2.3** **Modification of rig for aerosol delivery of air sensitive precursors.**

A minimal flow of nitrogen was admitted to the hydrogen sulfide/nitrogen line. The reactor was heated as normal, but the nitrogen line was not. A small amount of the precursor (*ca.* 0.1 g) was dissolved in a suitable solvent (*ca.* 50 $cm^3$). When the reactor had reached the required temperature, the solution was poured into the round-bottomed flask and the top replaced. This was not done sooner, as passing nitrogen through the solvent caused it to evaporate. Hydrogen sulfide was introduced to the system at this

time and the humidifier turned on. The total gas flow through the round-bottomed flask was *ca.* 1-2 $dm^3min^{-1}$. Adjustments were made to the position of the humidifier and flask to achieve the maximum aerosol activity. The reaction was run until there was no more misting as the solution ran out. Hydrogen sulfide was stopped and the reactor cooled with a minimal flow of nitrogen.

Air-sensitive materials could not be used in this way. A specially designed piece of glassware was made for admitting any compound which could not be exposed to air for short periods of time. This comprised a round bottomed flask with a side-arm allowing it to be attached to a Schlenk line, and a system of three taps which allowed nitrogen to pass through the solution, or to bypass the flask. The tap setup was modelled on the system used with bubblers. The precursor was put into the flask in a glove box. The solvent was added using Schlenk techniques, and the taps were then closed, isolating the solution. This was attached to the rig with PTFE tubing as described above. Reactions were carried out without heating nitrogen in the lines, and timing of the reactions was from the start of mist formation to the expenditure of all the solution.

## 2.2 X-ray diffraction

Glancing angle X-ray diffraction was carried out on a Philips XPert θ-2θ diffractometer. Cu Kα radiation was used in the reflection mode with PC-APD version 4.0b software. The angle of incidence in the diffractometer was 1.5 °. Most spectra were recorded from 14 to 70 ° as this covered all the major peaks for tin sulfides and tin oxides. Some spectra were recorded by transmission on a Siemens D5000 diffractometer using monochromatic Cu $K_{\alpha 1}$ radiation. Samples on glass could not be recorded in this way and this was only used for pyrolysis products and residues from Thermal Gravimetric Analysis and Differential Scanning Calorimetry. Reference spectra of tin sulfides and oxides are given in Figures 2.4 and 2.5.

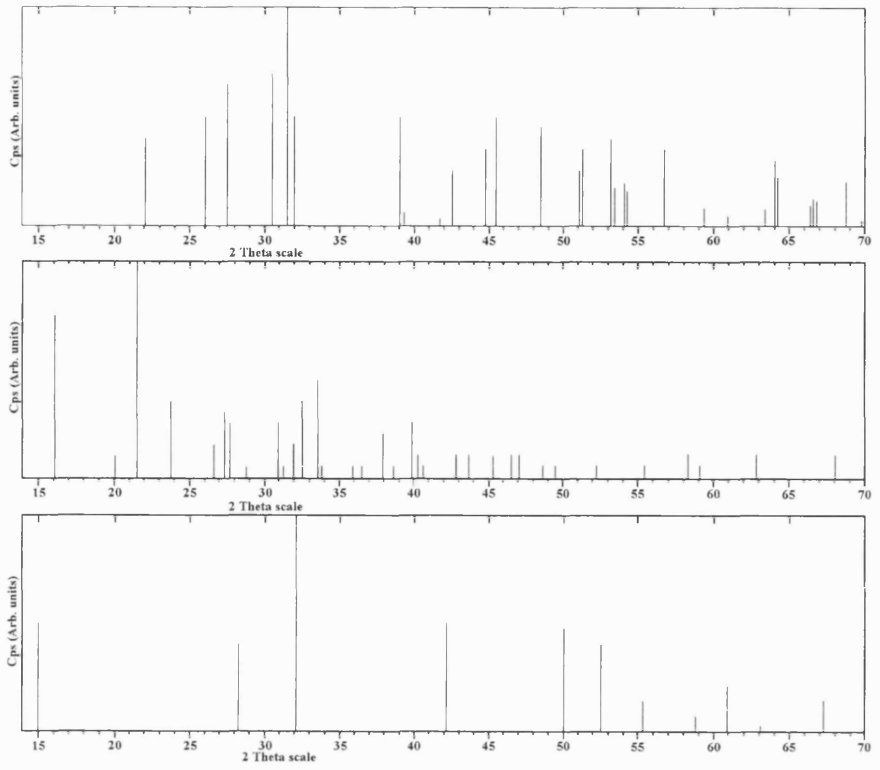


**Figure 2.4** X-ray diffraction stick patterns of tin sulfides. ($SnS$[79] – top; $Sn_2S_3$[80] – middle; $SnS_2$[81] – bottom)

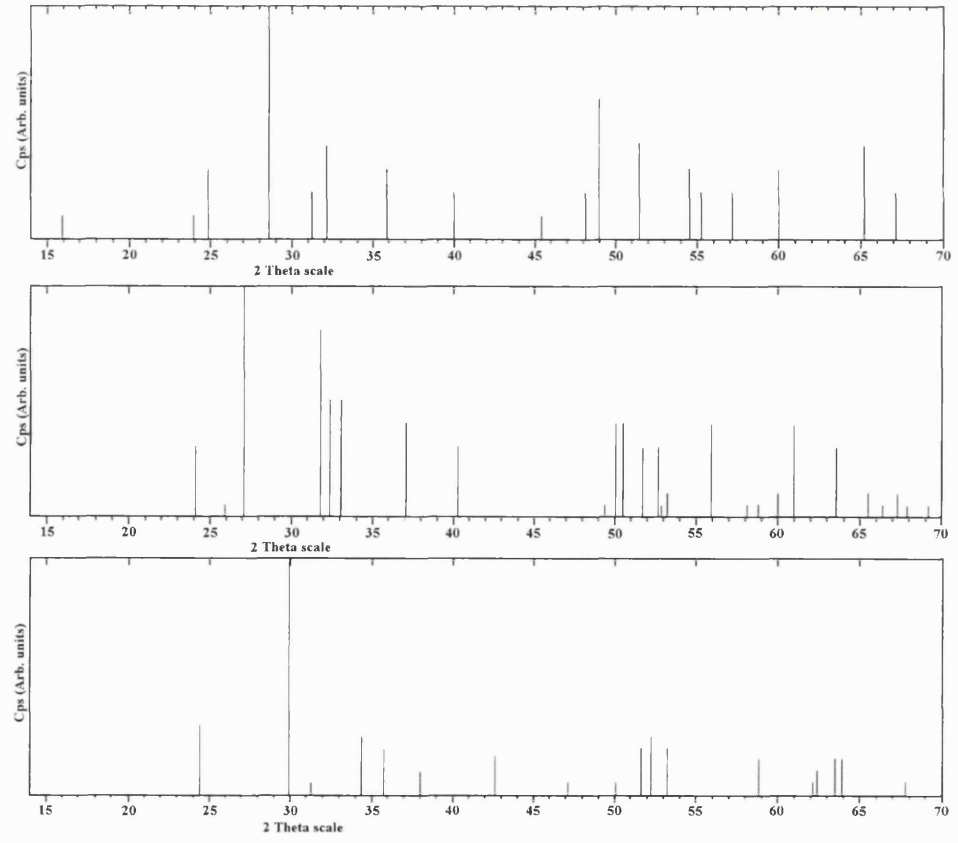


**Figure 2.5** X-ray diffraction stick patterns of tin oxides. ($SnO$[82] – top; $Sn_3O_4$[83] – middle; $SnO_2$[84] – bottom)

# 2.3 Raman microscopy

Four spectrometers were used during the course of this project. The details of these are given in Table 2.1. All spectra were calibrated against neon emission lines.

**Table 2.1 Raman microscopes used in this thesis.**

| Spectrometer | Microscope | Excitation line | Wavelength |
|---|---|---|---|
| Dilor Infinity with a notch filter and a CCD detector | Olympus | HeNe | 632.8 nm |
| Dilor XY triple grating | Olympus BH-2 | Coherent Innova 300 $Kr^+$ laser | 647.1 nm |
| Renishaw Raman System 1000 | Olympus BH-2 | HeNe | 632.8 nm |
| Renishaw Raman System 1000 | Lecia | HeNe | 632.8 nm |

Reference spectra of tin sulfides and oxides are given in Figures 2.6 and 2.7.

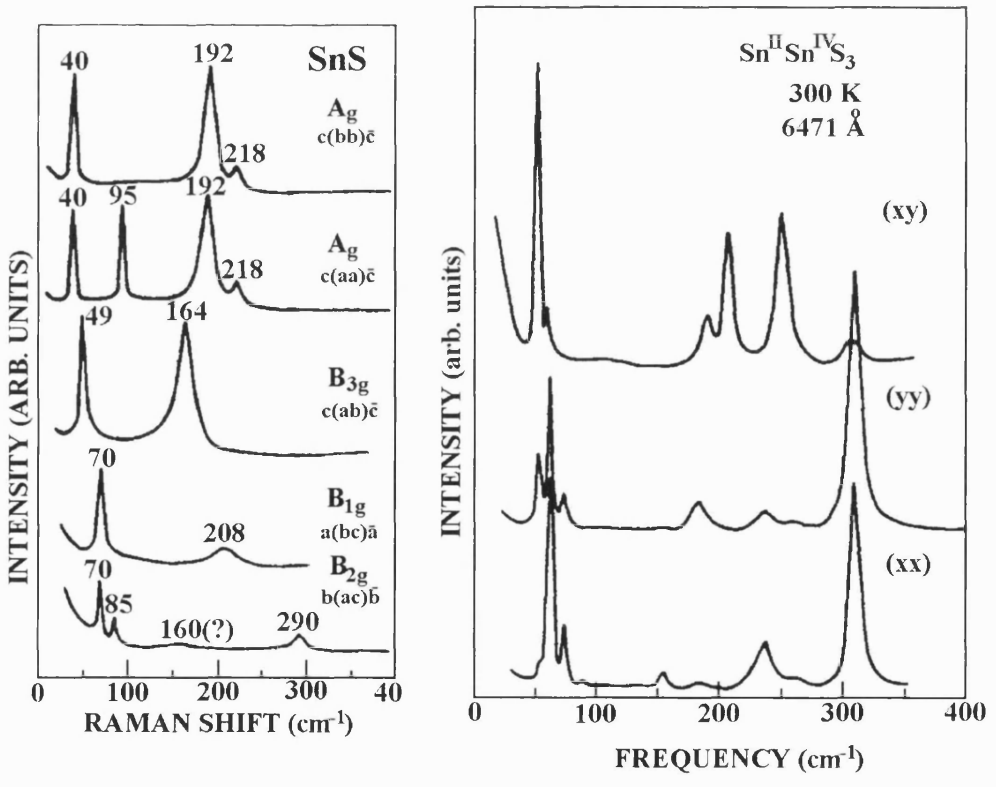


**Figure 2.6 Raman spectra of tin sulfides. ($SnS$[85] – left; $Sn_2S_3$[86] – right)**

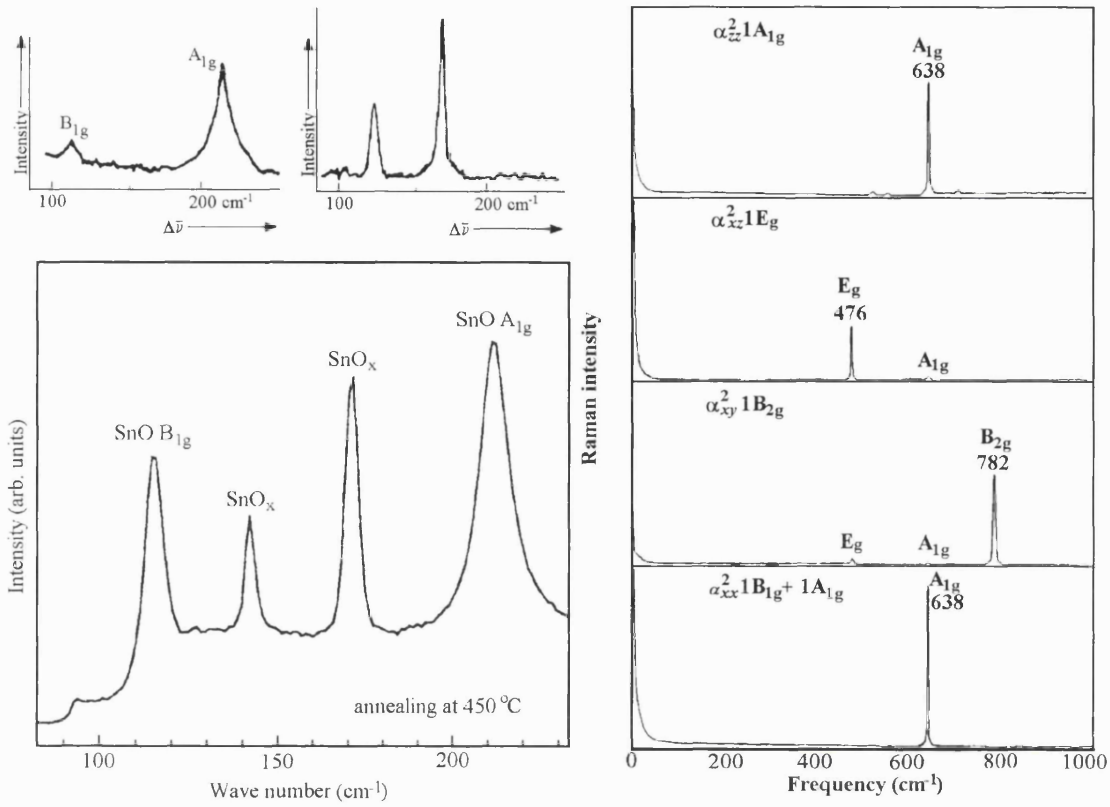


**Figure 2.7 Raman spectra of tin oxides. ($SnO^{87}$ – top left; $Sn_3O_4$[87] – top middle; mixture of SnO and $Sn_3O_4$ achieved by oxidising $SnO^{88}$ – bottom left; $SnO_2$[89] – right)**

# 2.4 Energy dispersive analysis by X-rays

EDAX was used to determine the tin:sulfur ratio in the films. Analysis was carried out on a Hitachi S570 Filament Scanning Electron Microscope with a beryllium window. The beryllium window is to protect the detector from certain X-rays, and prohibits detection of elements lighter than sodium. Oxygen and carbon, therefore, are not observed. All elements are standardised relative to cobalt. Data are quantified using an Oxford Instruments AM10, 000 software package. The excitation voltage used was 20 kV. Escape depth is determined by density of material and excitation voltage. In the case of tin sulfide films, tin(II) sulfide and tin(IV) sulfide have respective densities of 5.2 and 4.5 g.cm$^{-3}$ and glass has a density within the range 2.1-2.3. Tin sulfides would have an escape depth of *ca.* 2 μm while glass would have an escape depth of *ca.* 5 μm. Film thicknesses within this thesis are calculated by comparing tin and sulfur counts with those observed in a film where tin and sulfur were the only components. This film was taken as being 2 μm thick.

For the thinner films, much of the excitation volume was made up of the underlying glass substrate. This leads to larger errors in the quantification of atomic ratios (normally ~1 %). In addition, in the case of the tin oxide/silica undercoated glass, the glass interfered with the signal, leading to erroneous results. A further problem is the presence of calcium in the glass. The calcium Kα line coincides with the tin $L\alpha_1$ line used for quantification. This leads to an enhanced tin concentration. Very few of the films were sufficiently thick for the underlying glass not to be observed.

## 2.5 Scanning electron microscopy

SEM was carried out on the same instrument as the EDAX analysis - a Hitachi S570 Filament Scanning Electron Microscope. Magnification ranged from x 1, 000 to x 30, 000.

## 2.6 X-ray photoelectron spectroscopy

XPS is used as an analytical technique for two purposes. Primarily it is used to determine the elemental composition of a sample, but it may also be used to indicate the oxidation state and local environment of atoms. Spectra were recorded using a VG ESCALAB 220I XL instrument with monochromatic Al $K_\alpha$ radiation. Depth profiling was carried out using an $Ar^+$ ion gun. All spectra were calibrated relative to a graphitic carbon peak at 284.5 eV. Table 2.1 lists binding energies for various oxidation states and local environments. The X-ray lines investigated are C 1s, O 1s, S 2p and Sn $3d_{5/2}$.

Tin binding energies are observed at 884 ($3s_{1/2}$), 757 ($3p_{1/2}$), 715 ($3p_{3/2}$), 494 ($3d_{3/2}$), 486 ($3d_{5/2}$), 137 ($42_{1/2}$), 91 (4p) and 24 eV (4d). Sulfur lines are seen at 226 ($2s_{1/2}$), 163 ($2p_{1/2}$), 162 ($2p_{3/2}$), and 14 eV ($3s_{1/2}$). Oxygen lines are seen at 531 ($1s_{1/2}$) and 24 eV ($2s_{1/2}$).

A major problem with using XPS as a tool for determining the elemental composition of a sample is that atoms are not sputtered away at the same rate. The surface is

heavily contaminated with oxygen and carbon adsorbed from the atmosphere, so etching with $Ar^+$ ions is essential. However, lighter elements are more easily removed, leading to a surface richer in heavy metal ions.[99]

**Table 2.2 Common carbon, oxygen, sulfur and tin lines observed in XPS.**

| Element | Oxidation state | Compound | Binding energy (eV) | reference |
|---|---|---|---|---|
| C | | Graphite | 284.3 | 90 |
| O | -2 | $SnO_2$ | 530.6 | 91 |
| O | -2 | $H_2O$ | 533.1 | 92 |
| S | | Sulfur | 164.25 | 93 |
| S | -2 | ZnS | 161.7 | 94 |
| S | -2 | $H_2S$ | 170.44 | 95 |
| Sn | | Tin | 484.92 | 96 |
| Sn | +2 | SnS | 485.4 | 97 |
| Sn | +2 | SnO | 487.1 | 98 |
| Sn | +4 | $SnO_2$ | 486.9 | 98 |

# 2.7 Transmittance/reflectance spectroscopy

This was carried out to determine the optical properties of the coatings, in particular to investigate their suitability as heat mirrors. Measurements were carried out on a computer controlled, purpose built spectrometer. The light source was a Xenon bulb. Light transmitted through the sample, or reflected off the surface of the sample at 5°, is transmitted along a fibre optic cable. The fibre optic cable receives light across a circular cross-section, and converts this to a linear beam at the detector. Two detectors were used sequentially. These were Monolithic Miniature Spectrometers, MMS1 and MMS NIR supplied by Zeiss. MMS 1 contained 256 diodes that detected in the range 360-900 nm, with a spectral resolution of *ca.* 3.3 nm at each diode. The MMS NIR detector contained 128 InGaAs diodes capable of detecting in the range 900-1700 nm, each diode having a spectral resolution of *ca.* 6 nm. Measurements were averaged over 100 readings in order to minimise noise.

## 2.8 Scotch tape test

This is the standard test carried out to determine the adhesion of thin films to substrates. A cross of Scotch tape is place on the films, sticky side down. This is then peeled off and inspected. If any of the film is removed onto the Scotch tape, then the sample has failed. In the case of tin sulfide films, no material appears on the tape, although the film is easily removed by wiping. This is due to the structure of the material. The weak van der Waals bonds between the layers break easily, removing some of the film to the tape, but this is such a small amount – possible only a few atomic layers thick – that there appears to be nothing on the tape and the entire film remains on the glass. This is the case for all phases of tin sulfide, so the test was only carried out on the first few films produced. Later films were tested for adhesion by wiping with a paper towel.

## 2.9 Band gaps

UV-visible absorption spectra were recorded on a Shimadzu double beam instrument in the range 200-1100 nm. Uncoated glass was used as the reference. Band gaps were calculated using the direct method.

# Chapter 3
# Tin sulfide films from the reaction of tin tetrahalides with hydrogen sulfide

Transition and p-block metal halides are often used as CVD precursors because of their high volatility and reactivity.[100] Tetrahalides of tin are no exception. Tin tetrachloride is used to deposit tin oxide films in the commercial coating of glass.[101]

In this chapter, tin tetrahalides are used with hydrogen sulfide gas in order to deposit tin sulfide films. The aim is to determine how different parameters affect the nature of the film deposited. Reactions were carried out varying a number of parameters, and results are reported discussing each parameter in turn.

Firstly, deposition temperatures will be discussed, and how variation of these leads to different compositions of the final film. Secondly, variation of hydrogen sulfide flow rate during reaction will be discussed. The third parameter to be varied in this chapter was the volatile tin precursor used. Finally, any alterations in properties of the film due to the substrate onto which the film was deposited will be discussed. Conditions will be compared in order to determine which variables have the greatest effect on the resultant film.

# 3.1 Precursors used

The precursors used in this section were tin tetrachloride and tin tetrabromide. Tin tetrachloride is a liquid at room temperature and boils at 114 °C. It is highly air and moisture sensitive, and is packaged in Aldrich SureSeal bottles. It must be loaded into the bubbler *via* the use of a syringe. The vapour pressure curve is given in Figure 3.1.[78] This shows that vapour pressures of almost 200 torr (25 kPa) may be achieved at temperatures as low as 70 °C.

Tin tetrabromide is a solid at room temperature with a melting point of 34 °C and a boiling point of 202 °C. This is packaged under nitrogen and loaded into the bubbler in a glove box. The vapour pressure *vs.* temperature curve for tin tetrabromide is also shown in Figure 3.1 and it is seen that 150 °C gives approximately the same vapour pressure above $SnBr_4$ as 70 °C does above $SnCl_4$.

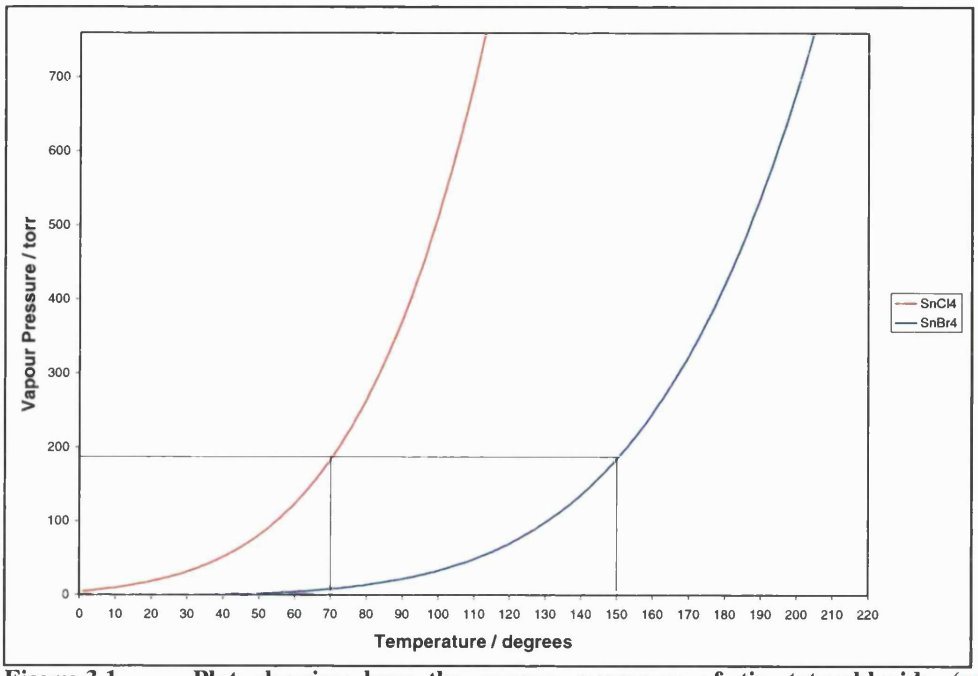


**Figure 3.1 Plot showing how the vapour pressures of tin tetrachloride (red) and tin tetrabromide (blue) vary with temperature.**

## 3.2 Reactions carried out

For each precursor, an extensive series of reactions was carried out. Tin tetrachloride reactions were carried out with a coater temperature between 300 and 550 °C at intervals of 25 degrees. The bubbler temperature was approximately 70 °C for all reactions. Reactions were carried out over a 30 s period. The hydrogen sulfide flow for each reaction was 0.3 or 0.6 $dm^3min^{-1}$ and nitrogen diluting this was adjusted to maintain a total flow in this line of 1.8 $dm^3min^{-1}$. The nitrogen flow through the bubbler was set to 0.4 $dm^3min^{-1}$ and was further diluted by a main flow of 10 $dm^3min^{-1}$. The plain nitrogen line, which passed straight to the exhaust during reaction, carried a flow of 10 $dm^3min^{-1}$. Films were deposited on carbon-doped silica coated glass. Full details of reaction conditions are summarised in Table 3.1.

For tin tetrabromide, reactions were carried out with a substrate temperature between 200 and 600 °C at intervals of 50 degrees. Reactions were also carried out at 525 °C, as this temperature had proved to be interesting in the case of the tin tetrachloride / hydrogen sulfide system. The bubbler temperature was set to approximately 150 °C for all reactions. Depositions were carried out over 30 s. The hydrogen sulfide flow was

set to 0.6, 1.2 or 1.8 $dm^3min^{-1}$ and the nitrogen diluting this was adjusted to maintain a total flow of 1.8 $dm^3min^{-1}$ in this line. The nitrogen flow through the bubbler was 0.4 $dm^3min^{-1}$ and was further diluted by a flow of 10 $dm^3min^{-1}$. The plain line, which passed straight to the exhaust, contained a 10 $dm^3min^{-1}$ flow of nitrogen. Films were deposited on tin oxide / silica coated glass. Full details of reaction conditions are summarised in Table 3.1.

**Table 3.1 Summary of reaction conditions for depositions from tin tetrahalides with hydrogen sulfide.**

| | Reactions of tin tetrachloride | Reactions of tin tetrabromide |
|---|---|---|
| Precursor temperature | 70 °C | 150 °C |
| Nitrogen flow rate through bubbler line | 0.4 $dm^3min^{-1}$ | 0.4 $dm^3min^{-1}$ |
| Nitrogen flow rate diluting line from bubbler | 10 $dm^3min^{-1}$ | 10 $dm^3min^{-1}$ |
| $H_2S$ flow rate | 0.3 or 0.6 $dm^3min^{-1}$ | 0.6, 1.2 or 1.8 $dm^3min^{-1}$ |
| Nitrogen flow rate diluting $H_2S$ | 1.5 or 1.2 $dm^3min^{-1}$ | 1.2, 0.6 or 0 $dm^3min^{-1}$ |
| Substrate | Carbon-doped silica coated glass | Tin oxide / silica coated glass |
| Deposition time | 30 s | 30 s |

The setting up and execution of each reaction is detailed in Section 2.1.2.

# 3.3 Effect of substrate temperature on film produced

## 3.3.1 Visual appearance of films

Films deposited exhibited different colours depending on deposition temperature regardless of which precursor was used. Films deposited at all temperatures up to and including 450 °C were yellow in colour. At very low temperatures (*ca.* 200 °C), the films had a brown tinge to them. The films deposited at 550 and 600 °C were silver. Films deposited between 475 and 525 °C contained a mix of yellow and silver regions, some also including large areas of brown film. All films contained areas of yellow at

the extremities. This was attributed to non-uniform temperatures across the substrate, probably due to heat losses from the edges of the reactor coater.

## 3.3.2 X-ray diffraction

Reference spectra of tin sulfides are available in Figure 2.4. Details of the diffractometer used are given in Section 2.2.

X-ray diffraction patterns of various films were recorded. The analysed area did not include the edges of the film which were characteristic of films deposited at a lower substrate temperature. Each film was found to contain a single phase. As the results were consistent regardless of precursor, and films deposited from tin tetrachloride were thicker than those deposited from tin tetrabromide, only the diffraction patterns of films deposited from tin tetrachloride are shown as figures in this section. Diffraction patterns of the films deposited from tin tetrachloride with a hydrogen sulfide flow of 0.3 $dm^3min^{-1}$ at substrate temperatures of 300, 525 and 545 °C are shown in Figures 3.2, 3.3 and 3.4 respectively.

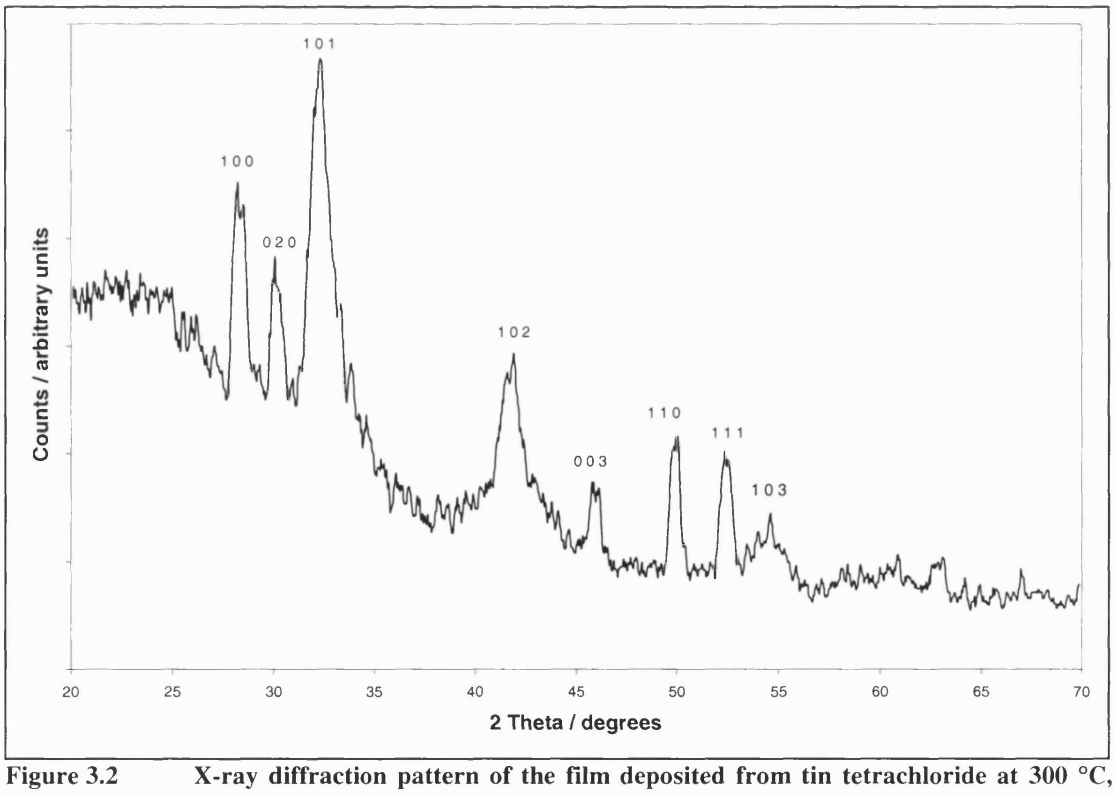


**Figure 3.2 X-ray diffraction pattern of the film deposited from tin tetrachloride at 300 °C, with a hydrogen sulfide flow rate of 0.3 $dm^3min^{-1}$.**

It may be seen, by comparing these spectra with the reference spectra shown in Figure 2.4, that the film deposited at 300 °C was tin(IV) sulfide, the film deposited at 525 °C was tin(II) tin(IV) trisulfide and the film deposited at 545 °C was tin(II) sulfide. Films deposited from the tetrabromide, or films deposited with different hydrogen sulfide flows gave diffraction patterns consistent with these observations, although different polytypes may be observed in some cases. This is discussed in later sections.

Lattice parameters were calculated using UnitCell. Table 3.2 gives the lattice parameters determined from the diffraction patterns shown in Figures 3.2, 3.3 and 3.4, along with the literature values. It can be seen from this that the lattice parameters match well enough to conclude that the films deposited at 300, 525 and 545 °C are $SnS_2$, $Sn_2S_3$ and SnS respectively.

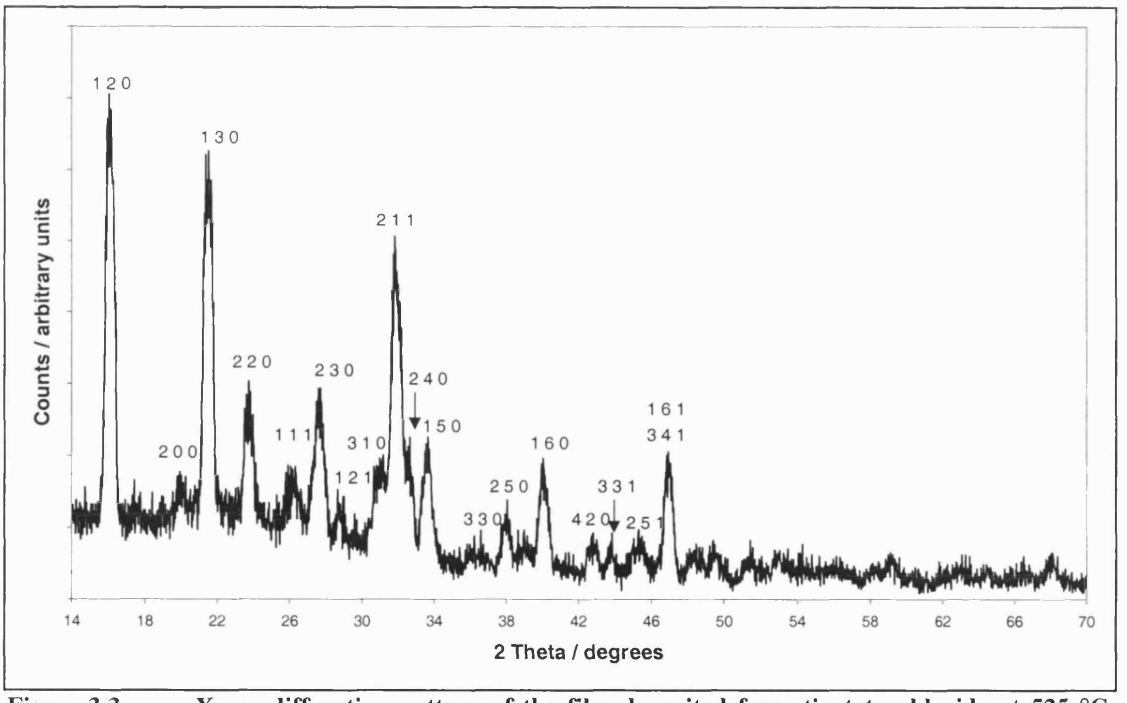


**Figure 3.3 X-ray diffraction pattern of the film deposited from tin tetrachloride at 525 °C, with a hydrogen sulfide flow rate of 0.3 $dm^3min^{-1}$.**

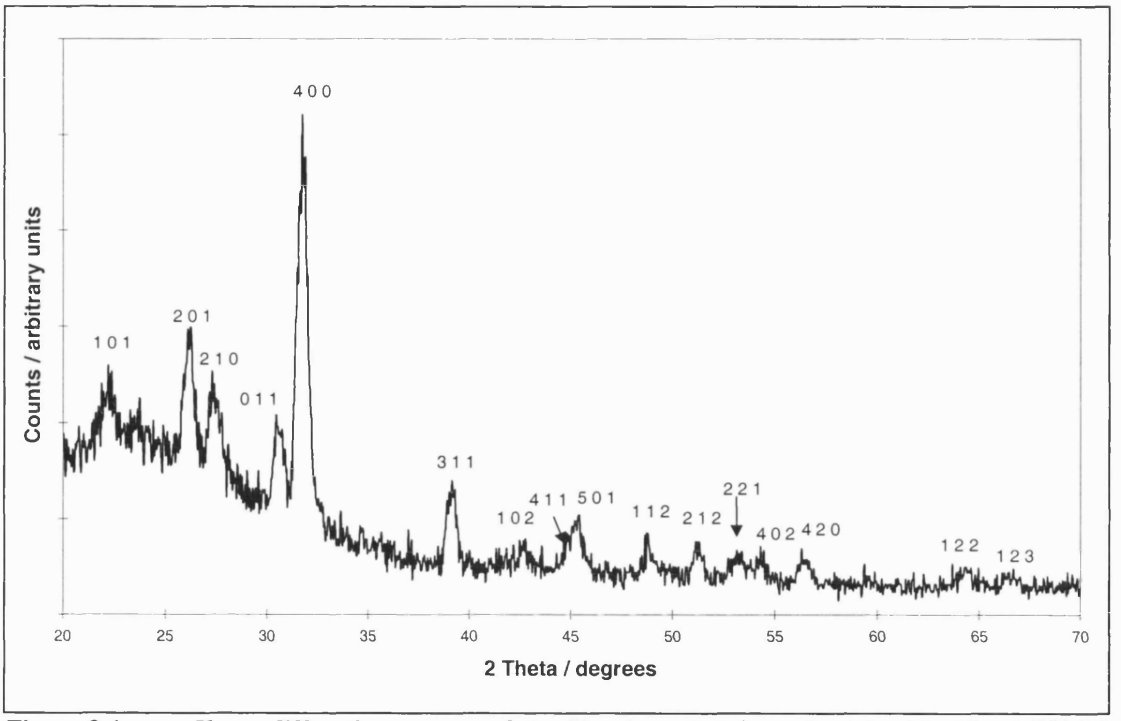


**Figure 3.4** **X-ray diffraction pattern of the film deposited from tin tetrachloride at 545 °C, with a hydrogen sulfide flow rate of 0.3 $dm^3min^{-1}$.**

**Table 3.2** **Comparison of lattice parameters of films deposited at 300, 525 and 545 °C from tin tetrachloride with hydrogen sulfide with literature values.**

| Compound | a | b | c | Crystal system |
|---|---|---|---|---|
| Film deposited at 300 °C | 3.642(7) | | 5.92(1) | Hexagonal |
| Film deposited at 525 °C | 8.83(1) | 3.76(1) | 14.03(1) | Orthorhombic |
| Film deposited at 545 °C | 11.20(1) | 3.99(1) | 4.32(1) | Orthorhombic |
| Literature $SnS_2$[18] | 3.6472(8) | | 5.8990(5) | Hexagonal |
| Literature $Sn_2S_3$[19] | 8.878(2) | 3.751(1) | 14.020(3) | Orthorhombic |
| Literature SnS[14] | 11.180(6) | 3.982(2) | 4.329(3) | Orthorhombic |

## 3.3.3 Raman microscopy

The Raman microscopes used and the experimental setup are described in Section 2.3. Reference Raman spectra are given in Figure 2.6.

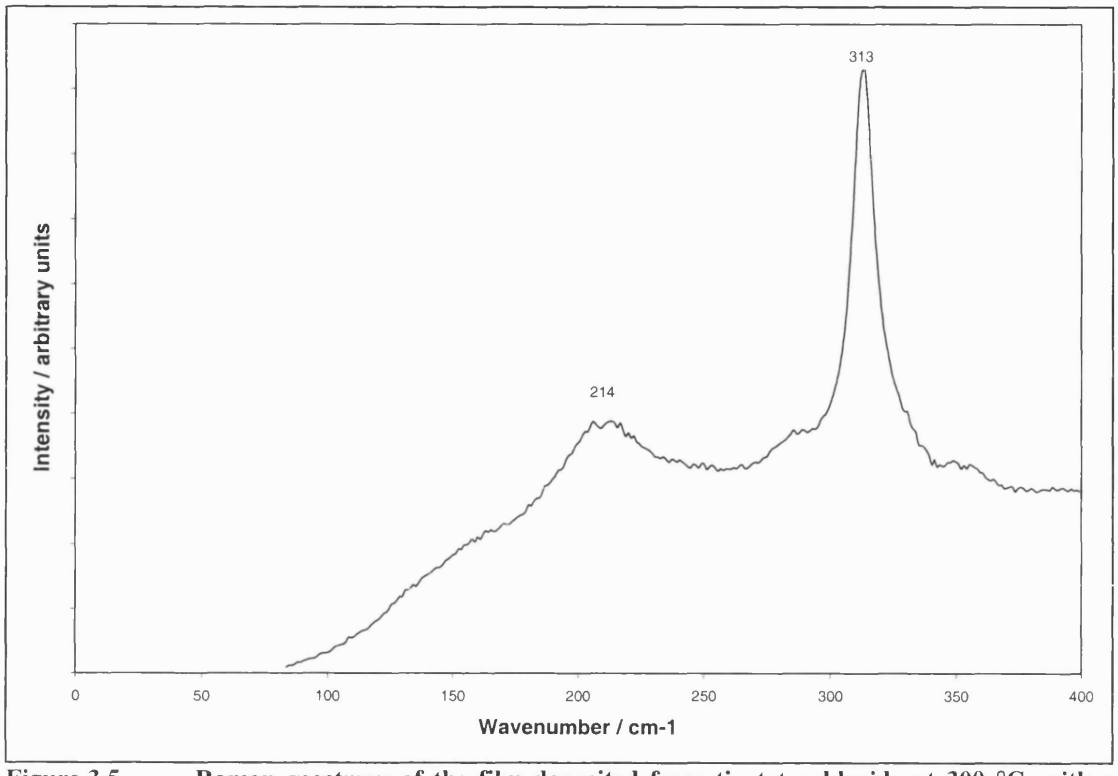


**Figure 3.5 Raman spectrum of the film deposited from tin tetrachloride at 300 °C, with a hydrogen sulfide flow rate of 0.3 $dm^3min^{-1}$.**

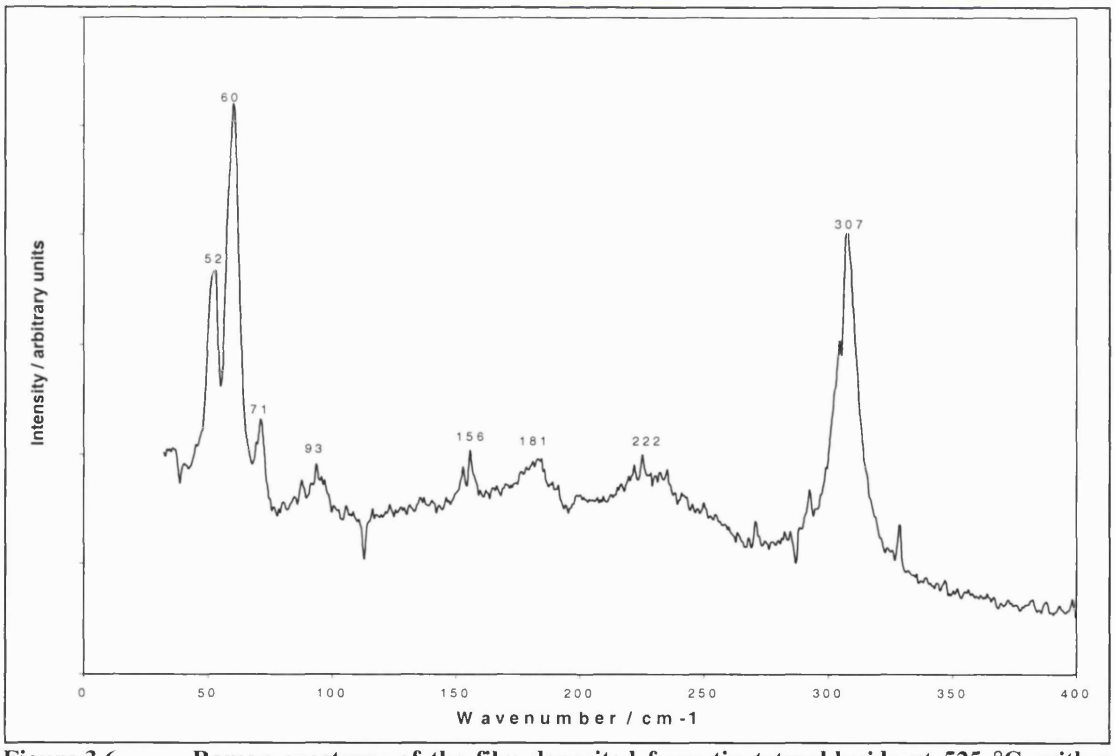


**Figure 3.6 Raman spectrum of the film deposited from tin tetrachloride at 525 °C, with a hydrogen sulfide flow rate of 0.3 $dm^3min^{-1}$.**

As Raman is particularly sensitive to tin sulfides, it is possible to record a spectrum in a relatively short length of time. This allowed Raman microscopy to be carried out

routinely on many samples. The spectra of films deposited at 300, 525 and 545 °C from tin tetrachloride with a 0.3 $dm^3min^{-1}$ flow of hydrogen sulfide are given in Figures 3.5, 3.6 and 3.7 respectively.

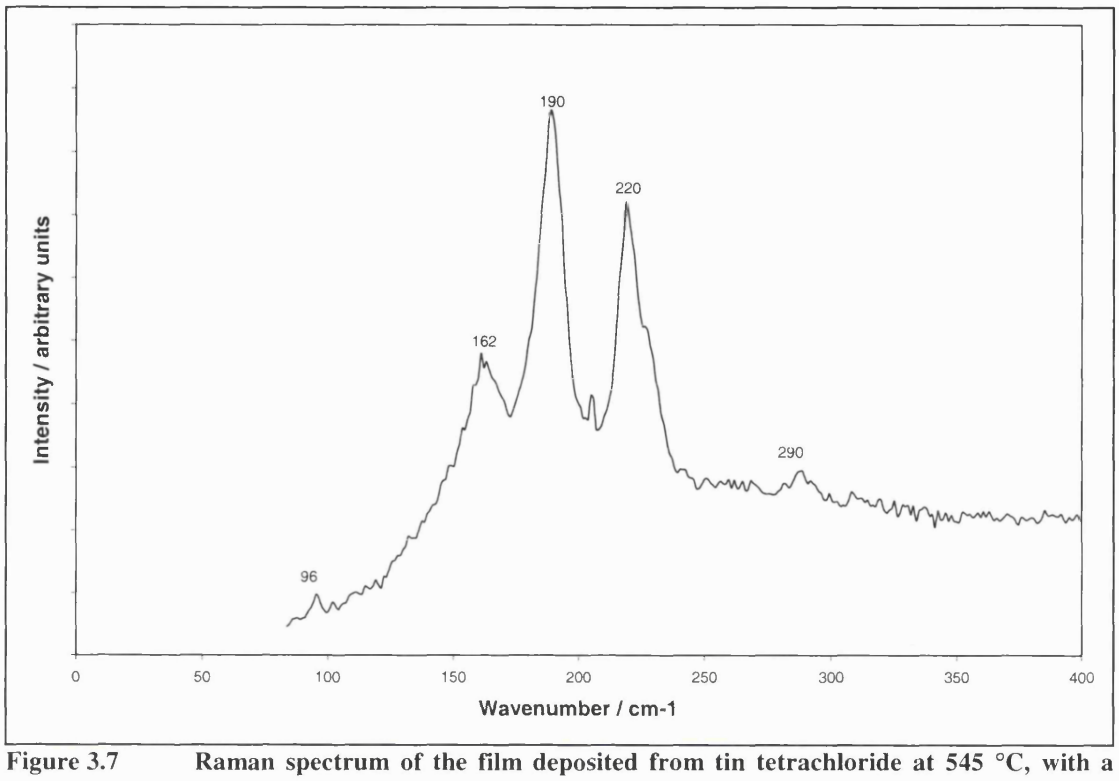


**Figure 3.7 Raman spectrum of the film deposited from tin tetrachloride at 545 °C, with a hydrogen sulfide flow rate of 0.3 $dm^3min^{-1}$.**

The positions of the bands are labeled. In this thesis, we have used Raman as a fingerprint technique alone, and this enables comparisons to be made with spectra in the literature recorded by other groups (shown in Figure 2.6). In doing this it is possible to say that the film deposited at 300 °C is tin(IV) sulfide, the film deposited at 525 °C is tin(II) tin(IV) trisulfide and that deposited at 545 °C is tin(II) sulfide.

## 3.3.4 Energy dispersive analysis by X-rays

EDAX was carried out on all films. As the films are very thin, some breakthrough to the underlying glass was observed. In the case of the films laid down on tin oxide / silica precoated glass, tin from the undercoating interfered with the results and an accurate tin:sulfur ratio could not be determined. This was the case for all coatings deposited from tin tetrabromide with hydrogen sulfide.

The elements observed in the glass were silicon, sodium, potassium, magnesium and aluminium. Oxygen is not observed by EDAX on the machine used.

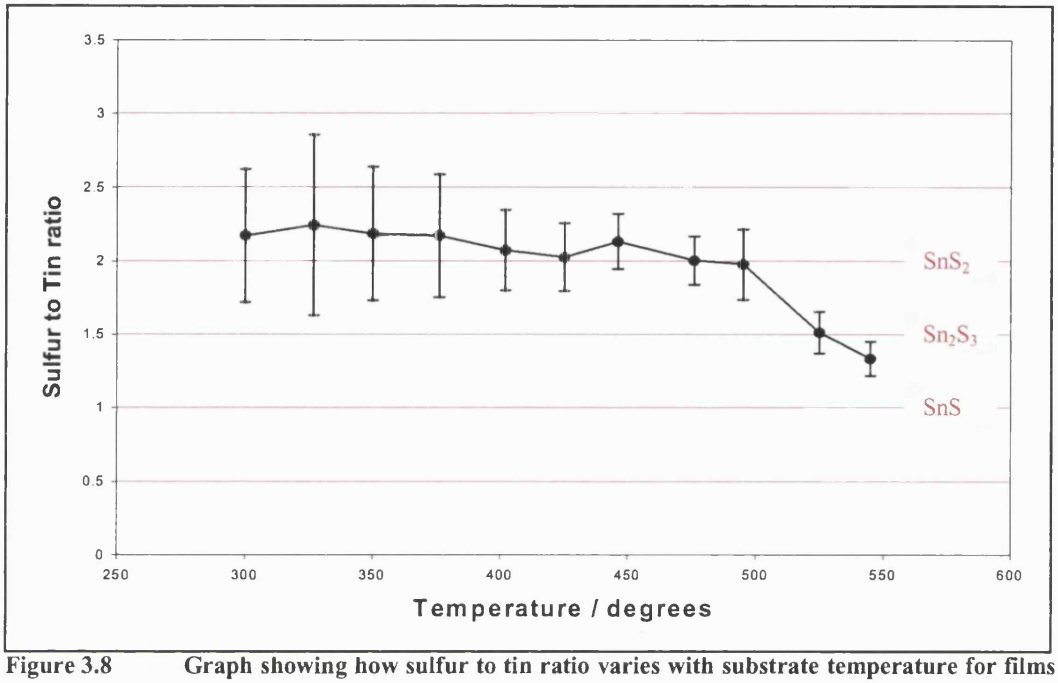


**Figure 3.8 Graph showing how sulfur to tin ratio varies with substrate temperature for films deposited from tin tetrachloride with hydrogen sulfide at a 0.3 $dm^3min^{-1}$ hydrogen sulfide flow.**

Figure 3.8 shows a plot of substrate temperature *vs.* sulfur to tin ratio for films deposited from the reaction of tin tetrachloride with hydrogen sulfide deposited with a 0.3 $dm^3min^{-1}$ hydrogen sulfide flow.

The error in EDAX measurements carried out with an accelerating voltage of 20 kV is approximately 1 % of the total volume observed. The error bars on Figure 3.8 are calculated in accordance with this. It can be seen that the error is larger for films deposited at lower substrate temperatures, and this is due simply to the films being thinner. The tin:sulfur ratio depends on substrate temperature, lower substrate temperatures giving rise to a 1:2 ratio of these elements and higher substrate temperatures giving ratios approaching 1:1.

Film thicknesses were also determined by EDAX. The film deposited at 300 °C from tin tetrachloride and hydrogen sulfide was found to be 0.9 μm thick. The film deposited at 525 °C was 1.3 μm thick and that deposited at 545 °C was 0.8 μm thick.

## 3.3.5 Scanning electron microscopy

SEM images of various films are given in Figure 3.9.

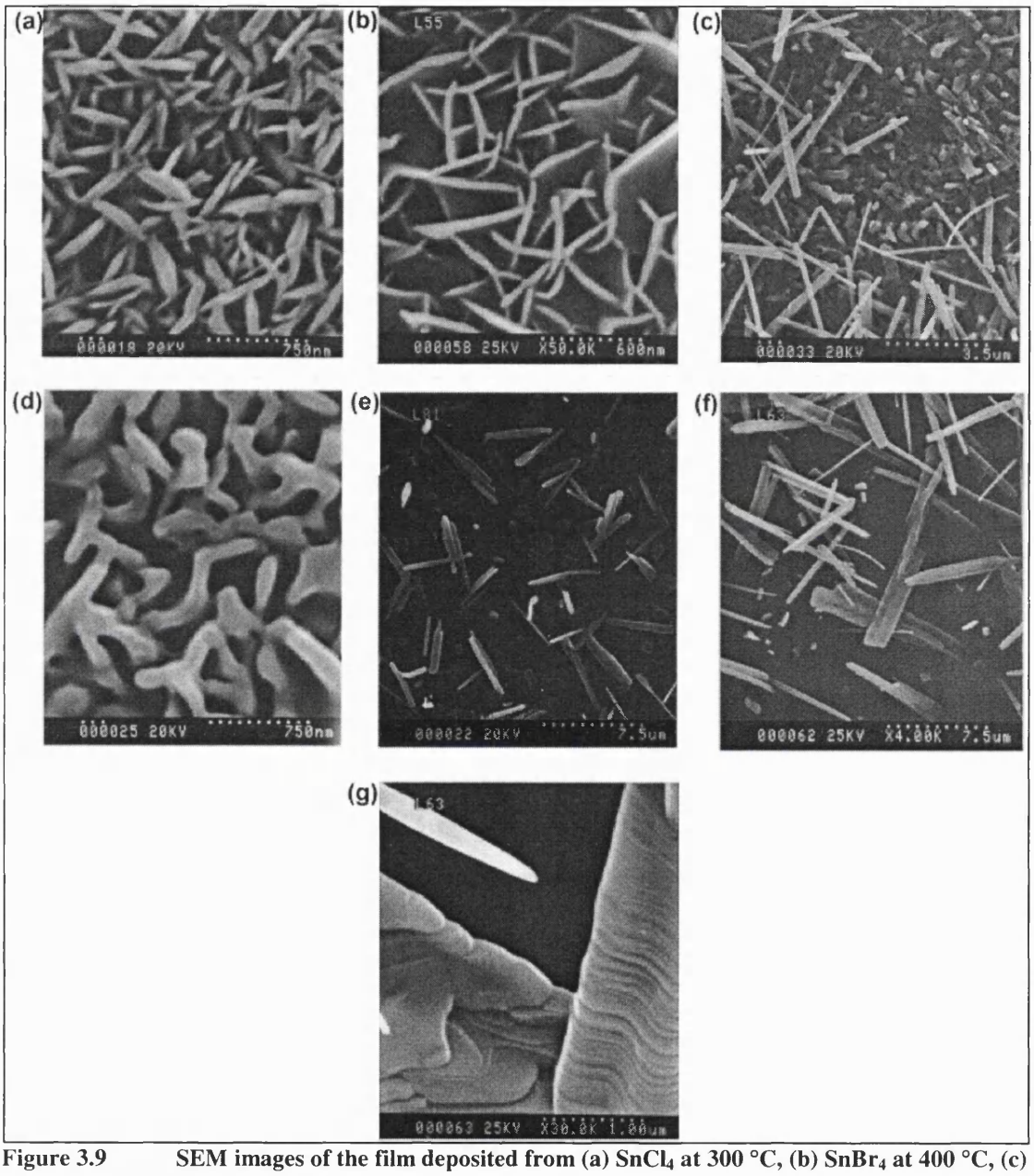


**Figure 3.9 SEM images of the film deposited from (a) $SnCl_4$ at 300 °C, (b) $SnBr_4$ at 400 °C, (c) $SnCl_4$ at 525 °C, (d) $SnCl_4$ at 545 °C, (e) $SnBr_4$ at 525 °C and (f and g) $SnBr_4$ at 550 °C.**

Figure 3.9a is the film deposited from tin tetrachloride at 300 °C, with a hydrogen sulfide flow rate of 0.3 $dm^3min^{-1}$. The irregular needle-like shapes are exhibited by all films deposited at temperatures up to and including 350 °C from either precursor. Figure 3.9b is an image of the film deposited from tin tetrabromide at 400 °C, with a 0.6 $dm^3min^{-1}$ hydrogen sulfide flow. This shows interlocking plates, which is the

morphology of all films deposited at temperatures between 375 and 475 °C. Another observation made in this study was that particle size increases with deposition temperature.

The film deposited at 525 °C from tin tetrachloride with a hydrogen sulfide flow of 0.3 $dm^3min^{-1}$ is shown in Figure 3.9c. This includes two different morphologies – rounded ill-defined masses similar to those exhibited by the film deposited at 545 °C depicted in Figure 3.9d and long needles. Although these areas were analysed separately by Raman and EDAX, no compositional differences were observed. Figures 3.9e and 3.9f show the images taken from films deposited at 525 and 550 °C respectively from tin tetrabromide with 1.2 $dm^3min^{-1}$ hydrogen sulfide flow rate. These are different from the films deposited from the tetrachloride in that the needles on top are less regular and the underlying forms are more regular. The overlying needles are seen in all films deposited at temperatures above 525 °C from the tetrabromide, whereas in the case of films deposited from the tetrachloride they are only seen at 525 °C.

Figure 3.9g shows a high magnification image of the film deposited from tin tetrabromide at 550 °C, with 1.2 $dm^3min^{-1}$ $H_2S$ flow. This shows that the particles are made up of thin layers. Tin-sulfur double layers in SnS are *ca.* 1.1 nm thick and they could not be observed with the microscope used in this work.

## 3.3.6 X-ray photoelectron spectroscopy

XPS was only carried out on a few films. The full XPS of the film deposited at 545 °C from tin tetrachloride with hydrogen sulfide is shown in Figure 3.10. The surface of each film was highly contaminated with carbon and oxygen, so etching was essential. This led to alterations in the compositions of films as discussed in Section 2.6. As such, the elemental composition of the films determined by this technique cannot be relied on. The most important result obtained from XPS is the binding energy of the elements, which indicates the oxidation state and local environment.

The films deposited from the reactions of tin tetrachloride with hydrogen sulfide at 300, and 545 °C were analysed. Table 3.3 gives the binding energies of tin and sulfur in the

films. Table 3.4 gives the elemental ratios of the bulk of the film. Etching times varied, and the ratios given here are those determined after the oxygen concentration ceased to drop.

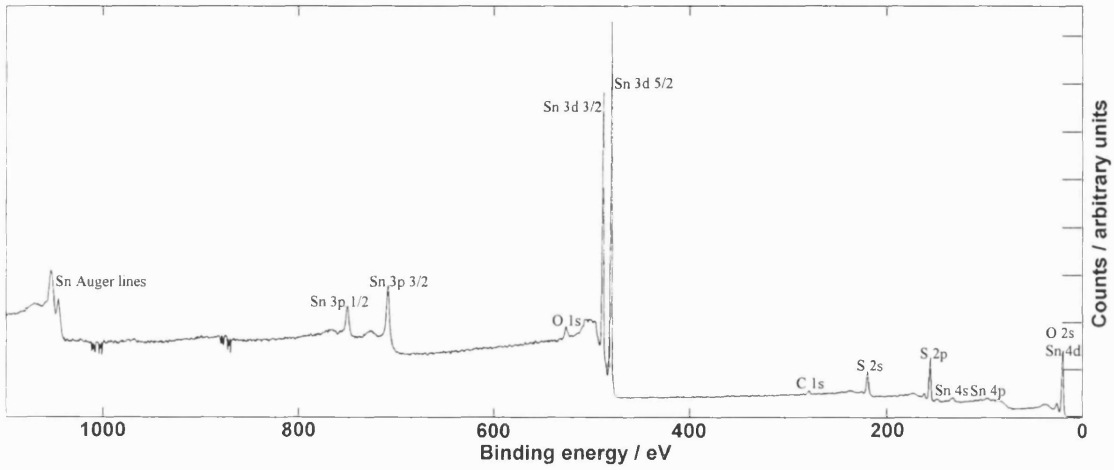


**Figure 3.10 XPS of film deposited at 545 °C from tin tetrachloride with hydrogen sulfide.**

**Table 3.3 XPS binding energies of tin and sulfur observed in films deposited from tin tetrachloride with hydrogen sulfide.**

| Substrate Temperature | Element | Binding Energy / eV |
|---|---|---|
| 300 | Tin $3d_{5/2}$ | 486.4 |
| | Sulfur 2p | 162.2 |
| 545 | Tin $3d_{5/2}$ | 485.9 |
| | Sulfur 2p | 161.2 |

Tin binding energies have a relatively narrow range, going from 484.9 eV for elemental tin, to 488.2 for $SnF_4$ where tin is in the +4 oxidation state and bound to a highly electronegative atom. The binding energy of tin is reported as 485.4 eV in bulk tin(II) sulfide, and 486.4 – 486.6 eV in tin(IV) sulfide. The tin binding energies reported in Table 3.3 are consistent with the film deposited at 300 °C containing tin(IV) sulfide and the film deposited at 545 °C containing tin(II) sulfide. Sulfur has a range of binding energies from 161.7 for ZnS to 180.3 for $SF_6$. The sulfur binding energies displayed in Table 3.3 are all consistent with a metallic $S^{2-}$ environment, when compared with ZnS(161.7 eV), NiS (162.8eV) and $WS_2$ (162.8 eV).

**Table 3.4 Atomic percentages of elements in films deposited from the reaction of tin tetrachloride with hydrogen sulfide after etching.**

| Substrate Temperature | At. % tin | At. % sulfur | At. % oxygen | At. % carbon |
|---|---|---|---|---|
| 300 | 49 | 50 | 1 | 0 |
| 545 | 61 | 7 | 22 | 10 |

From Table 3.4, it can be seen that there is a sulfur deficiency in all films. This is not due to a proportion of the tin being bound to oxygen in place of sulfur, as is the case on the surface, as the oxygen content is also very low. This sulfur deficiency is attributed to preferential sputtering of lighter elements by the ion gun.

## 3.3.7 Transmittance/reflectance spectroscopy

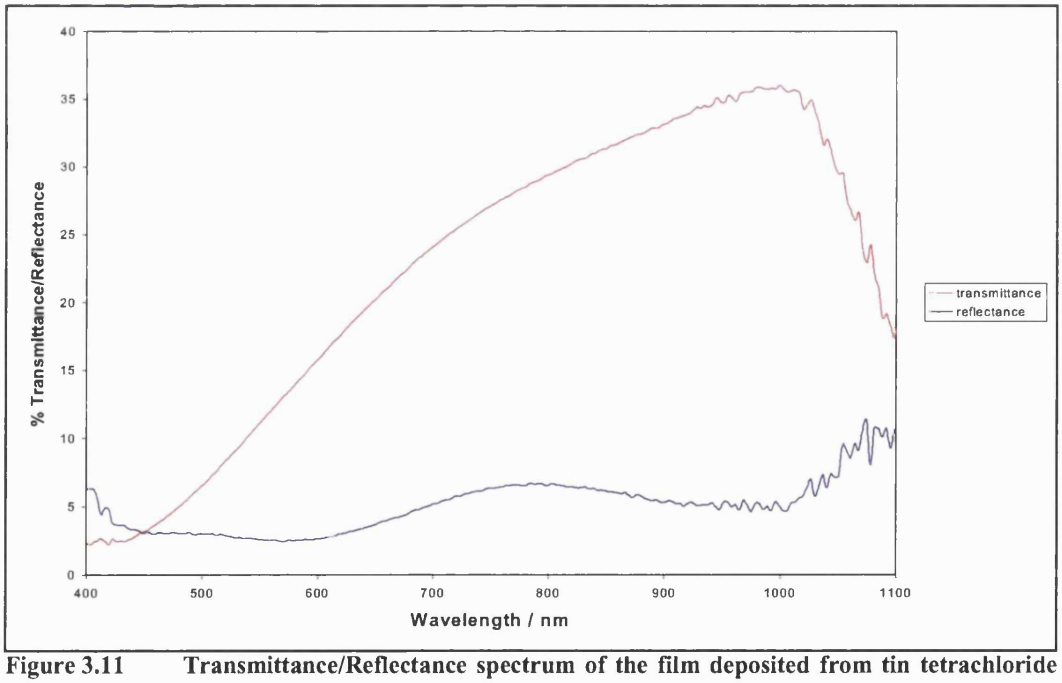


**Figure 3.11 Transmittance/Reflectance spectrum of the film deposited from tin tetrachloride with hydrogen sulfide at 300 °C.**

Transmittance/reflectance spectroscopy was carried out routinely on all samples. Figures 3.11, 3.12 and 3.13 give the transmittance/reflectance spectra of films deposited at 300, 525 and 545 °C respectively from the reaction of tin tetrachloride with hydrogen sulfide. For a perfect heat mirror, transmission should be high in the visible region and reflection high in the infrared. None of the spectra recorded for films deposited from

these precursors exhibit ideal heat mirror properties. In addition, for a material to be commercially viable as a heat mirror, the colour should not be yellow, brown or grey for aesthetic reasons.

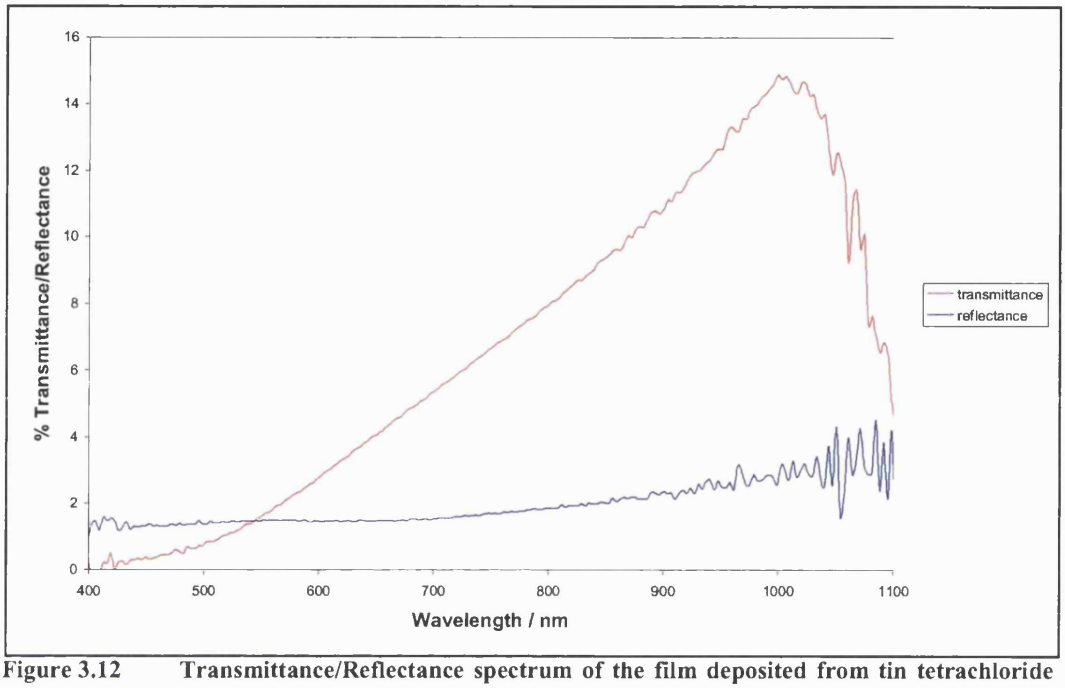


**Figure 3.12 Transmittance/Reflectance spectrum of the film deposited from tin tetrachloride with hydrogen sulfide at 525 °C.**

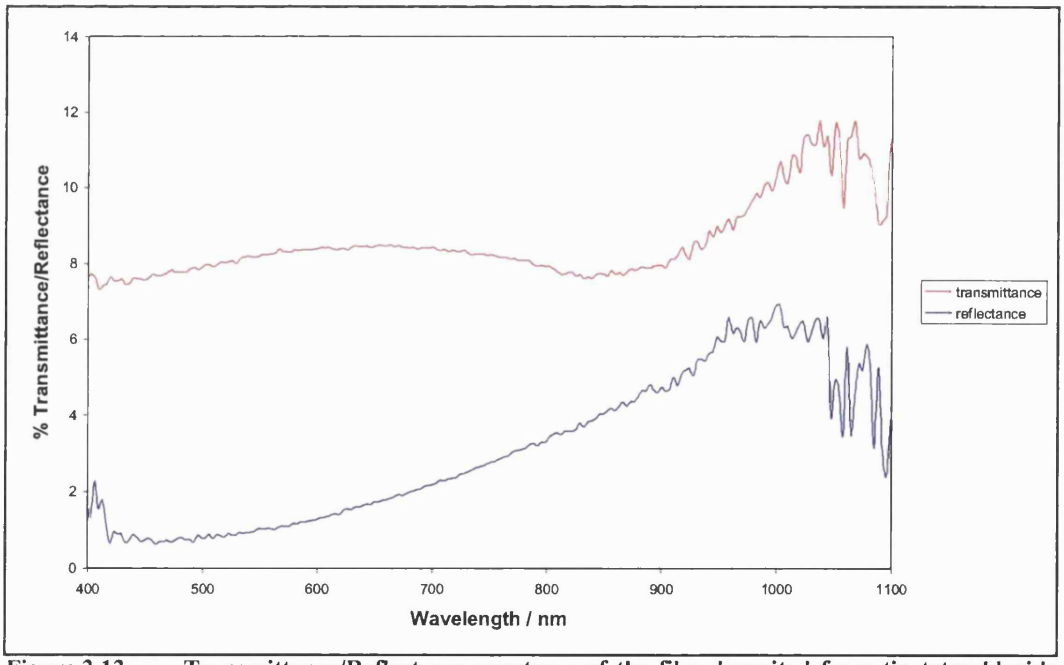


**Figure 3.13 Transmittance/Reflectance spectrum of the film deposited from tin tetrachloride with hydrogen sulfide at 545 °C.**

## 3.3.8 Band gaps

Band gaps were recorded for a small number of films. It was found that the band gap of the film deposited from tin tetrachloride with hydrogen sulfide at 300 °C was 2.14 eV. This is comparable with the literature band gap of $SnS_2$, namely 2.2-2.3 eV.[43,48] The band gap of the film deposited from tin tetrachloride and hydrogen sulfide at 545 °C was determined as 1.3 eV, which is exactly the same as that reported in the literature.[30]

## 3.3.9 Discussion

Deposition temperature plays an important role in determining which phase of tin sulfide is deposited in the CVD reaction. The phase diagram of tin sulfide is given in Figure 1.1. This shows that all three phases of tin sulfide are accessible at temperatures up to and including 760 °C. It is also seen that no change occurs to any phase below 602 °C where αSnS changes to βSnS. $Sn_2S_3$ and $SnS_2$ undergo no changes until 661 and 680 °C respectively.

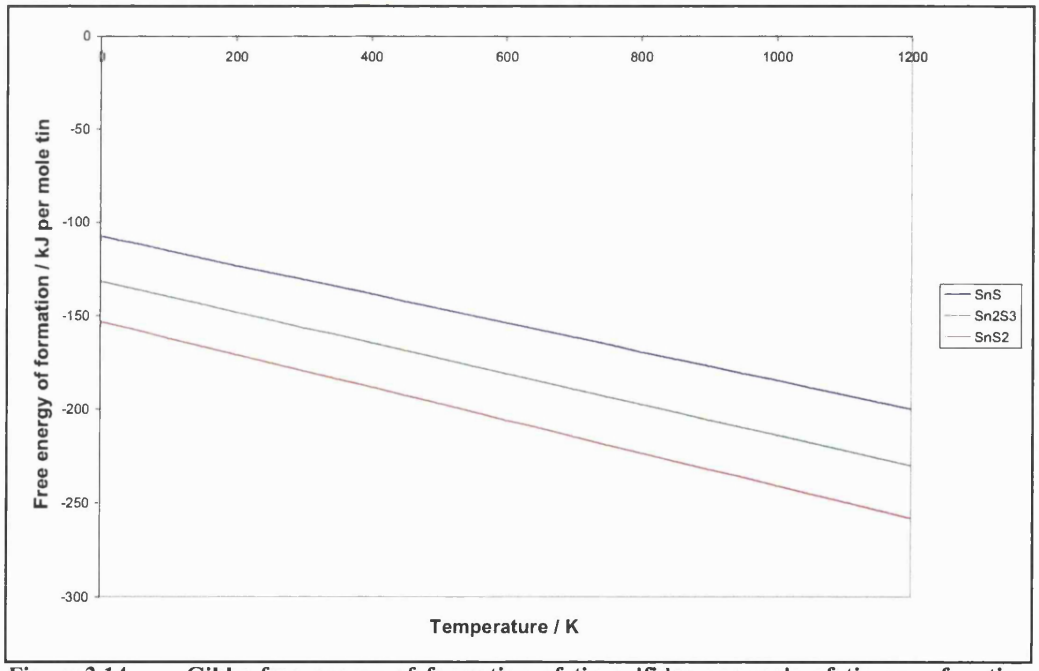


**Figure 3.14 Gibbs free energy of formation of tin sulfides per mole of tin as a function of temperature.**

The Gibbs free energy of formation per mole of tin is plotted against temperature in Figure 3.14.

From Figure 3.14 it is clear that $SnS_2$ is the most thermodynamically stable at all temperatures. As tin(II) sulfide and mixed valent species are deposited, it is clear that the other species in the reaction must be taken in to account. The reaction of tin tetrachloride with hydrogen sulfide to give tin(IV) sulfide is given in Equation 3.1. Reactions forming tin(II) involve reduction of tin from the +4 oxidation state, and so must also entail oxidation of either chlorine or sulfur. The possible reaction schemes are given in Equations 3.2 – 3.5. The Gibbs free energy of each of these reactions is plotted against temperature in Figure 3.15.

$SnCl_{4\,(g)} + 2\ H_2S_{(g)} \rightarrow SnS_{2\,(s)} + 4\ HCl_{(g)}$ **Equation 3.1**

$SnCl_{4\,(g)} + 1½\ H_2S_{(g)} \rightarrow ½\ Sn_2S_{3\,(s)} + 3\ HCl_{(g)} + ½\ Cl_{2\,(g)}$ **Equation 3.2**

$SnCl_{4\,(g)} + H_2S_{(g)} \rightarrow SnS_{(s)} + 2\ HCl_{(g)} + Cl_{2\,(g)}$ **Equation 3.3**

$SnCl_{4\,(g)} + 2\ H_2S_{(g)} \rightarrow ½\ Sn_2S_{3\,(s)} + 4\ HCl_{(g)} + ½\ S_{(g)}$ **Equation 3.4**

$SnCl_{4\,(g)} + 2\ H_2S_{(g)} \rightarrow SnS_{(s)} + 4\ HCl_{(g)} + S_{(g)}$ **Equation 3.5**

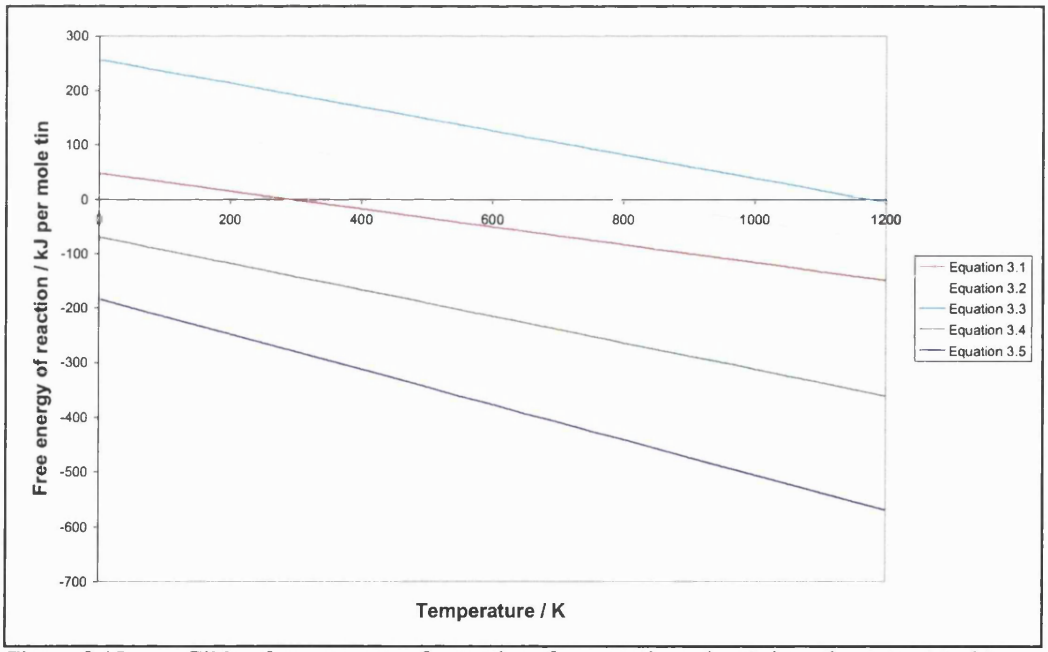


**Figure 3.15 Gibbs free energy of reaction for reactions involving tin tetrachloride and hydrogen sulfide as detailed in Equations 3.1 to 3.5.**

Figure 3.15 shows that it is more likely for sulfur to be reduced than chlorine as the reactions involving evolution of sulfur are exoergic and those involving evolution of

chlorine tend to be endoergic. This is in accordance with the electron affinities of the two elements: E.A. of Cl = 348 kJ $mol^{-1}$; E.A. of S = 200 kJ $mol^{-1}$. However, this is not the general trend seen in the reactions of tin tetrahalides with hydrogen sulfide. In this section, we have seen that tin disulfide is formed at lower temperatures and sulfides containing tin(II) atoms are only deposited at temperatures above 500 °C. This indicates that tin(IV) sulfide is the kinetic product of the reaction and tin(II) sulfide and tin(II) tin(IV) trisulfide are only accessible at higher temperatures.

It is possible that the primary product of the reaction is $SnS_2$ and loss of sulfur is a second step to the process. To confirm this, samples of films deposited from the reaction of tin tetrabromide with hydrogen sulfide were heated under a nitrogen flow for 20 minutes to see if there was any change in composition. The samples used were those deposited at 400 and 550 °C with a 0.6 $dm^3min^{-1}$ flow of hydrogen sulfide. The resulting films were only analysed by visual inspection of colour and Raman microscopy, and the results are given in Table 3.5.

**Table 3.5** **Results of heating previously deposited tin sulfide films under a flow of nitrogen.**

| Original film | 400 °C | 500 °C | 550 °C | 600 °C |
|---|---|---|---|---|
| $SnS_2$ | No change | No change | SnS | SnS |
| SnS | No change | No change | | No change |

This shows that tin(II) sulfide is unchanged on heating and that tin(IV) sulfide is reduced to tin(II) sulfide at temperatures above 550 °C, presumably with the evolution of sulfur gas. An interesting observation is that the films deposited as tin disulfide and subsequently heated are not homogeneous as is the case with those initially deposited at higher temperatures. Also, heating previously deposited films in a flow of hydrogen sulfide tends to reduce them more easily – the tin(IV) sulfide film, when heated to 500 °C under a 0.4 $dm^3min^{-1}$ flow of hydrogen sulfide for 15 minutes, turned brown and exhibited a Raman spectrum consistent with it being the mixed valent sesquisulfide.

These results imply that the primary product of the reaction is a form of tin sulfide, which, at sufficiently higher temperatures, can undergo sulfur loss to leave tin monosulfide or ditin trisulfide. On cooling to room temperature, this form of tin sulfide

results in crystalline tin disulfide, which is not as reactive as the initially formed high temperature intermediate, and as such is not as readily reduced with the loss of sulfur.

# 3.4 Effect of hydrogen sulfide flow rate

## 3.4.1 Visual appearance of films

For the reactions of tin tetrachloride with hydrogen sulfide, two different flow rates of hydrogen sulfide were used – 0.3 and 0.6 $dm^3min^{-1}$. The films deposited with the lower flow were visibly thinner than those deposited with higher flow.

In the case of the reactions of tin tetrabromide with hydrogen sulfide, flow rates of 0.6, 1.2 and 1.8 $dm^3min^{-1}$ were investigated. A small number of films were deposited with lower flow rates, but the coating was extremely thin over the 30 s reaction time and this made films harder to analyse. It was observed that, in most cases, hydrogen sulfide flow rate led to no difference other than the visual appearance of the films. However, at temperatures around 500 °C, where a change of phase of deposited film is observed, the colours of the films were not always the same if different hydrogen sulfide flow rates were used. Table 3.6 describes the colours of films deposited from tin tetrabromide with varying flow of hydrogen sulfide at these critical temperatures.

**Table 3.6 Colour of films deposited from tin tetrabromide with hydrogen sulfide with varying hydrogen sulfide flow rates.**

| Temp \ $H_2S$ flow rate | 0.6 $dm^3$ $min^{-1}$ | 1.2 $dm^3$ $min^{-1}$ | 1.8 $dm^3$ $min^{-1}$ |
|---|---|---|---|
| 450 | Yellow | Yellow | Yellow |
| 500 | Brown | Grey and Brown | Silver and Brown (2:3) |
| 525 | Silver | Silver | Silver |
| 550 | Silver | Grey | Grey |

### 3.4.2 Raman microscopy

Raman spectra were recorded from films deposited from tin tetrabromide and hydrogen sulfide at 500 °C with different hydrogen sulfide flow rates. It was seen that when the hydrogen sulfide flow rate was 0.6 $dm^3min^{-1}$ the film comprised mainly tin sesquisulfide. At higher hydrogen sulfide flow rates of 1.2 and 1.8 $dm^3min^{-1}$ tin monosulfide was the main phase formed.

### 3.4.3 Discussion

The results reported in this section are in agreement with those reported in Section 3.3.9 regarding the heating of films deposited previously. It appears that, whether during deposition or during subsequent heating of films, higher hydrogen sulfide flow rates afford a more facile route to the reduction of tin atoms. This implies that hydrogen sulfide is involved in the mechanism of sulfur loss. Therefore, it is possible that the sulfur species that results from this decomposition is not sulfur gas, but a polyanionic species such as $H_2S_2$. Equation 3.6 gives a possible example of this reaction.

$$SnS_2 + H_2S \rightarrow SnS + H_2S_2 \qquad \textbf{Equation 3.6}$$

This is unlikely, as the overall process

$$SnCl_4 + 3H_2S \rightarrow SnS_2 + 4HCl + H_2S \rightarrow SnS + 4HCl + H_2S_2$$

is less favourable than

$$SnCl_4 + 2H_2S \rightarrow SnS_2 + 4HCl \rightarrow SnS + 4HCl + S$$

from both enthalpy and entropy considerations.

## 3.5 Effect of precursor on films produced

In general, little difference was observed in the films deposited from the two different precursors, tin tetrachloride and tin tetrabromide. It should be made clear again here that the substrates films were deposited onto were different for the reactions of tin

tetrachloride and tin tetrabromide. Films deposited from tin tetrachloride were deposited onto glass with a pre-coating of carbon-doped silica, whereas the substrate used in reactions involving tin tetrabromide was glass with two coatings – tin oxide first and silica on top. A difference in morphology was observed between films deposited from the different precursors, but this was attributed to the substrate and will be discussed in Section 3.6.

### 3.5.1 Visual appearance of the films

Films deposited under the same conditions from the two different precursors showed the same colours. The most significant difference in the appearance was that films deposited from tin tetrabromide with hydrogen sulfide were visibly thinner than those deposited from tin tetrachloride. Yellow films could appear orange when deposited from the tetrachloride due to thickness. Silver films deposited from the tetrabromide were almost invisible in some cases.

### 3.5.2 X-ray diffraction

X-ray diffraction patterns of films deposited at the same temperature appeared to be different. Some peaks that are evident in films produced from the tetrachloride do not appear in the X-ray diffraction patterns of films deposited from the tetrabromide. Relative intensities also vary depending on the film. Figure 3.16 shows the diffraction patterns of films deposited from tin tetrabromide with hydrogen sulfide at 450, 500 and 600 °C. If these are compared with Figures 3.2, 3.3 and 3.4, which show the diffraction patterns of films deposited from tin tetrachloride at 300, 525 and 545 °C, it is seen that the films are similar. Indexing the films gives the same lattice parameters, as seen in Table 3.7. It is impossible to calculate lattice parameters for the film deposited at 600 °C from tin tetrabromide with hydrogen sulfide, as only three peaks are evident. Changes in relative intensities could be due to deposition of different polytypes, or preferred orientation on the different types of glass.

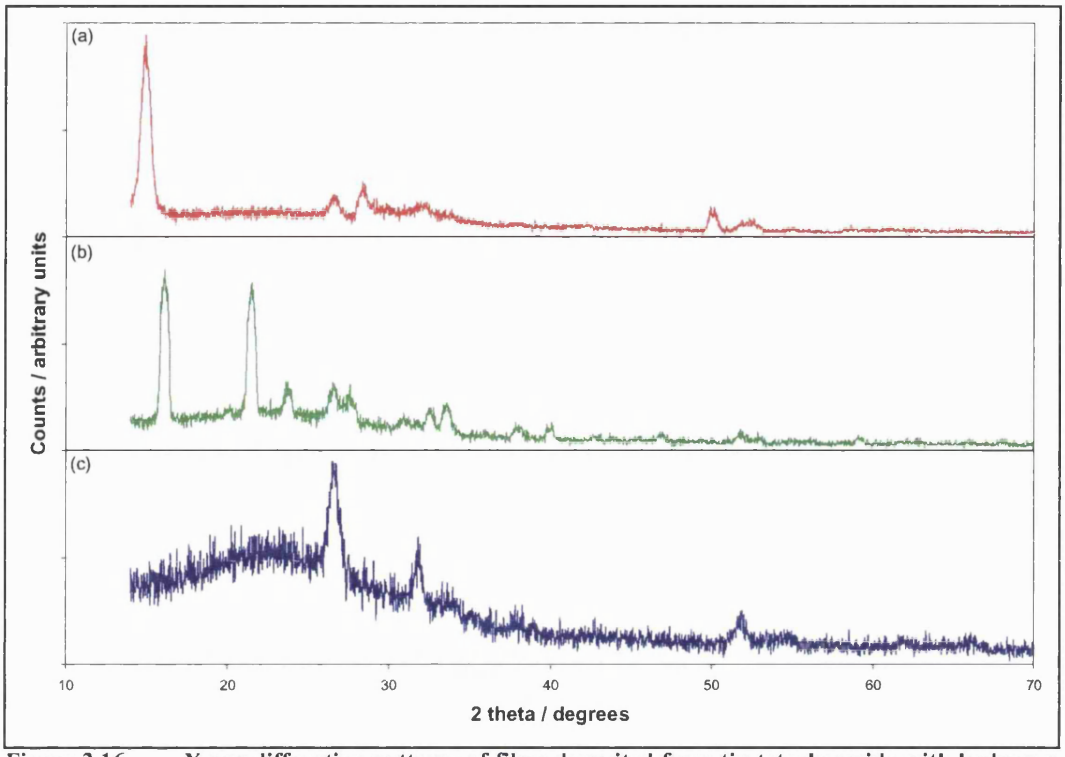


**Figure 3.16** **X-ray diffraction patterns of films deposited from tin tetrabromide with hydrogen sulfide at (a) 450 °C, (b) 500 °C and (c) 600 °C.**

**Table 3.8** **Comparison of the calculated lattice parameters of films deposited from tin tetrachloride and films deposited from tin tetrabromide with existing literature values.**

| Film/reference | a-parameter | b-parameter | c-parameter |
|---|---|---|---|
| Film from $SnCl_4$ at 300 °C | 3.642(7) | | 5.92(1) |
| Film from $SnBr_4$ at 400 °C | 3.638(5) | | 5.93(3) |
| Literature $SnS_2$ [18] | 3.6472(8) | | 5.8990(5) |
| Film from $SnCl_4$ at 525 °C | 8.83(1) | 3.76(1) | 14.03(1) |
| Film from $SnBr_4$ at 500 °C | 8.85(1) | 3.767(6) | 13.99(1) |
| Literature $Sn_2S_3$ [19] | 8.878(2) | 3.751(1) | 14.020(3) |
| Film from $SnCl_4$ at 545 °C | 11.20(1) | 3.99(1) | 4.32(1) |
| Literature SnS [14] | 11.180(6) | 3.982(2) | 4.329(3) |

### 3.5.3 Raman microscopy

The Raman spectra of films deposited from tin tetrachloride with hydrogen sulfide are shown in Figures 3.5, 3.6 and 3.7. Spectra collected from films deposited from the reactions of tin tetrabromide with hydrogen sulfide are given in Figure 3.17. It is clear from these that reactions at the same temperature from the two different precursors yield the same product.

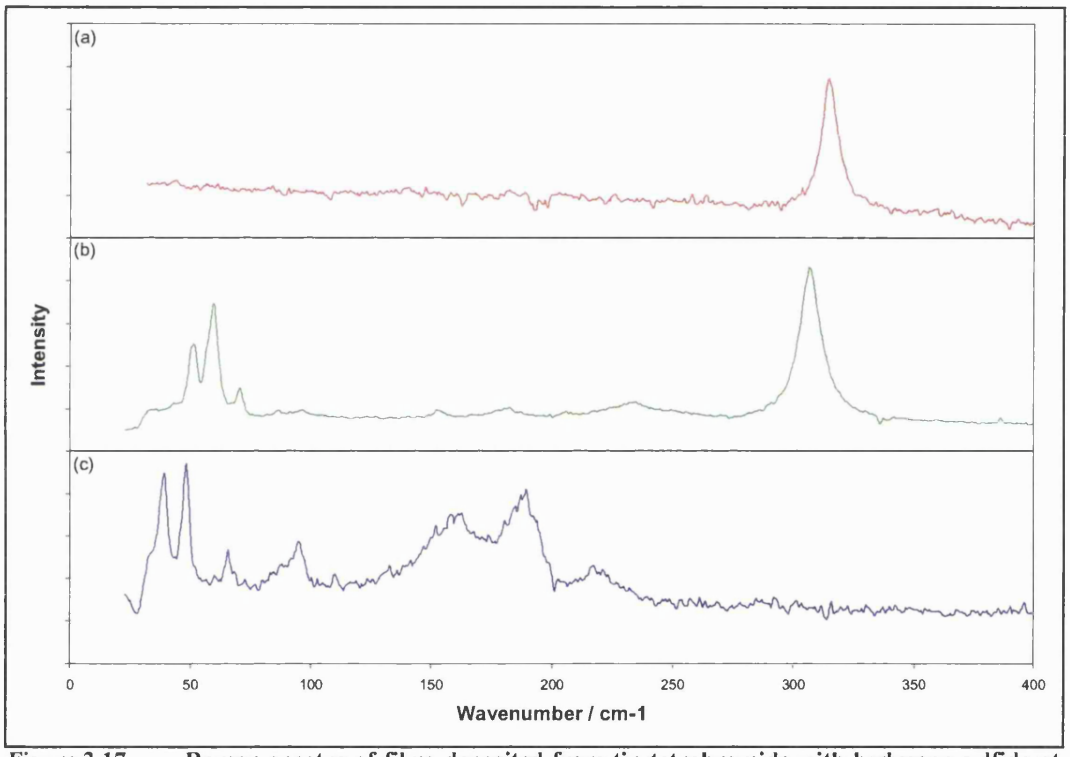


**Figure 3.17 Raman spectra of films deposited from tin tetrabromide with hydrogen sulfide at (a) 300 °C, (b) 525 °C and (c) 545 °C.**

### 3.5.4 Energy dispersive analysis by X-rays

This technique would be useful to quantify the difference in thickness observed visually between films deposited from the two different precursors. However, since films deposited from reactions of tin tetrabromide with hydrogen sulfide were deposited onto substrates containing tin, results from this analysis method can tell us only that the films contain sulfur. It would be possible to compare sulfur content of the films, but the error in EDAX is *ca.* 1 % at accelerating voltages of 20 kV and sulfur comprises 2 % of the excitation volume of some films deposited from the tetrabromide.

Film thicknesses were also determined from EDAX measurements. As reported in Section 3.3.4, the film deposited from tin tetrachloride and hydrogen sulfide were found to be 0.9 μm thick at a deposition temperature of 300 °C, 1.3 μm at a deposition temperature of 525 °C and 0.8 μm thick at a deposition temperature of 545 °C. For film deposited from tin tetrabromide with hydrogen sulfide, thicknesses of *ca.* 0.1 μm were recorded for films deposited at 400 and 525 °C, while a film 0.5 μm thick was formed at 550 °C. This quantitatively shows that which was observed in the visual appearance - that films deposited from the tetrabromide are thinner than those deposited from the tetrachloride under equivalent conditions.

## 3.5.5 Transmittance/reflectance spectroscopy

It was clear from transmittance/reflectance spectroscopy that the tetrabromide led to deposition of thinner films, even though the deposition temperature, $H_2S$ flow rate and vapour pressure in the bubbler were all identical. This is shown in Figure 3.18, which gives the transmittance and reflectance spectra for two films deposited at 400 °C from the reactions of the two precursors.

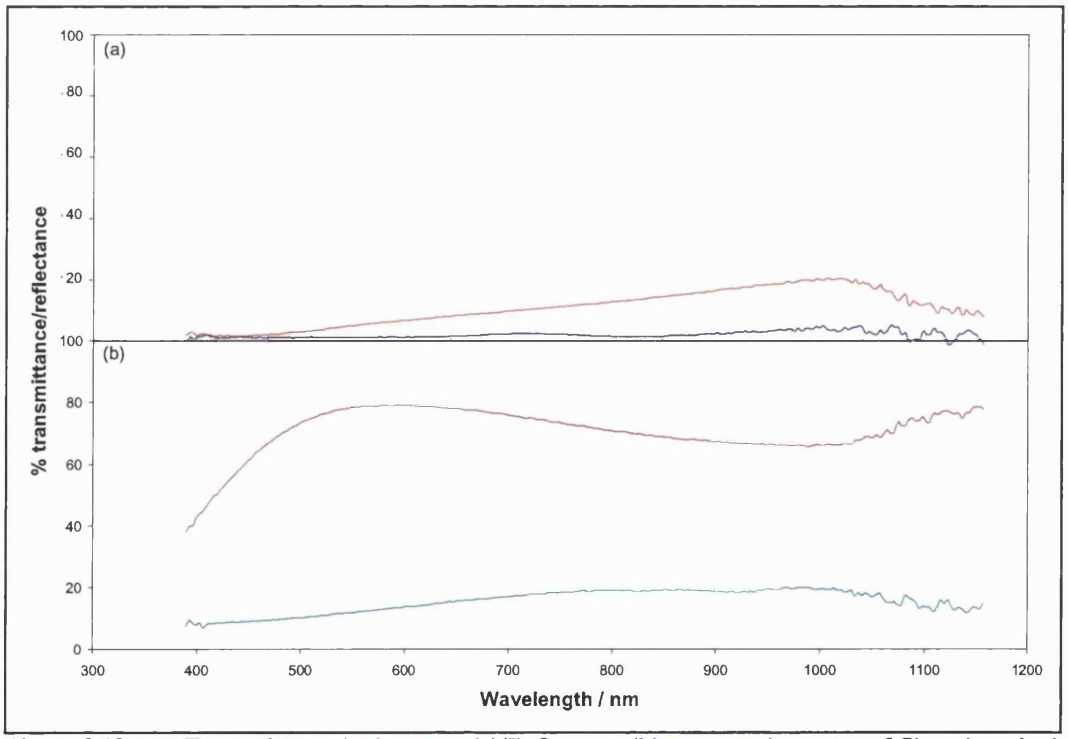


**Figure 3.18 Transmittance(red or purple)/Reflectance(blue or grey) spectra of films deposited from (a) tin tetrachloride and (b) tin tetrabromide at 400 °C.**

Transmittance is much higher for films deposited from the tetrabromide. This is because the films are much thinner. Reflectance is also higher in the film deposited from the tetrabromide. This suggests that the reflectance measured is that from the glass substrate. It is higher in the case of the film deposited from tin tetrabromide, because the thinner film permits more transmittance.

### 3.5.6 Discussion

The difference in volatility of the precursors should not have had any effect on films deposited, as bubbler temperatures were adjusted to suit. Figure 3.1 shows the vapour pressure curve for the tin tetrahalides. This shows that a bubbler temperature of 70 °C for tin tetrachloride, which gives rise to a vapour pressure of 200 torr (25 kPa), is equivalent to a bubbler temperature of 150 °C for tin tetrabromide. Given that the vapour pressure above the precursors, the flow of nitrogen through the bubblers and the time allowed for reaction were all the same, the amount of precursor reaching the substrate in all reactions would be the same.

The strengths of tin-chlorine and tin-bromine bonds in diatomic molecules have previously been measured. These were determined spectroscopically from the hot gases effusing from a Knudsen cell.[102] A tin-bromine bond has a strength of 47 +/- 23 kcal $mol^{-1}$ and a tin-chloride bond has a strength of 75 kcal $mol^{-1}$.[103] This would tend to indicate that tin tetrabromide would be the more reactive species as its bonds are weaker. Also supporting this are the relative heats of formation of tin tetrabromide and tin tetrachloride - $\Delta H_f^\circ$ ($SnCl_4$) = 545.2 kJ $mol^{-1}$, $\Delta H_f^\circ$ ($SnBr_4$) = 406.3 kJ $mol^{-1}$.

The driving force making the reaction of tin tetrachloride more vigorous than that of tin tetrabromide is the energy released in the formation of the hydrogen halide. The heats of formation of the two species are $\Delta H_f^\circ$ (HCl) = -92.3 kJ $mol^{-1}$ and $\Delta H_f^\circ$ (HBr) = -36.3 kJ $mol^{-1}$. The entropy of hydrogen bromide is slightly higher than that of hydrogen chloride, but, with such a vast difference in enthalpy of formation, this is negligible. At all temperatures the release of energy forming HCl is much higher, and this reaction proceeds faster. Figure 3.19 shows the overall energy of reaction for Reactions 3.1 and 3.7 as a function of temperature.

$SnCl_4 + 2\ H_2S \rightarrow SnS_2 + 4\ HCl$ **Equation 3.1**

$SnBr_4 + 2\ H_2S \rightarrow SnS_2 + 4\ HBr$ **Equation 3.7**

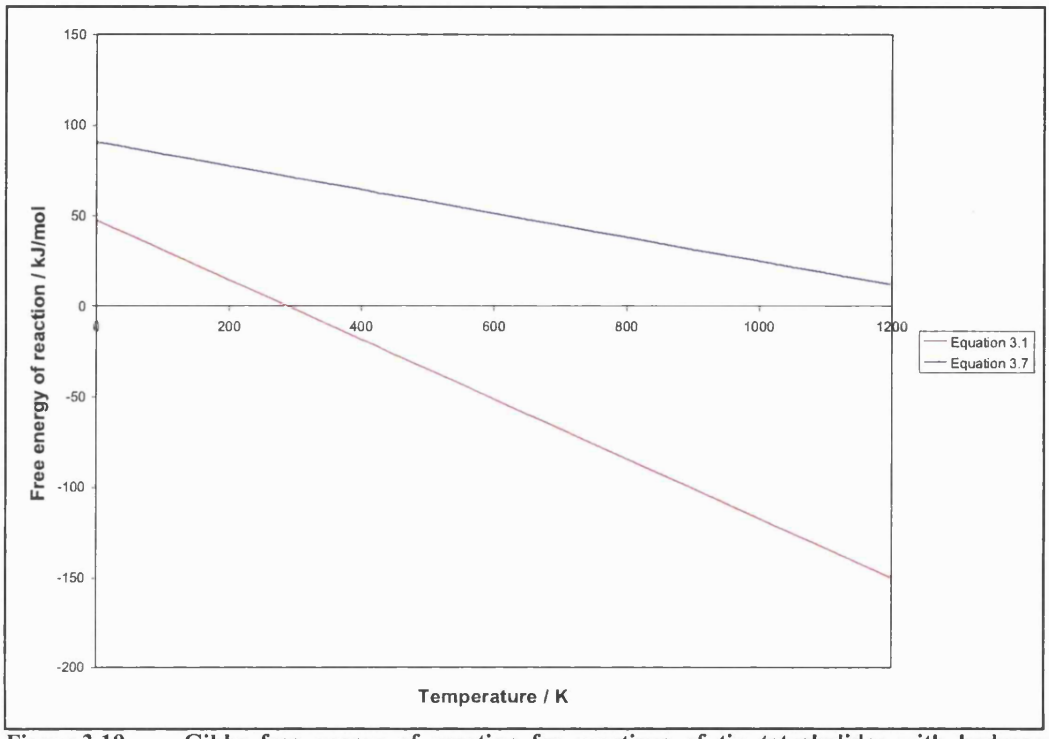


**Figure 3.19 Gibbs free energy of reaction for reactions of tin tetrahalides with hydrogen sulfide to form tin disulfide.**

Figure 3.19 shows that the reaction of tin tetrabromide with hydrogen sulfide is endoergic at all temperatures. Reactions involving the reduction of tin(IV) to tin(II) accompanied by the evolution of sulfur gas are exoergic overall, but if the first step involves the formation of a tin(IV) sulfide species, as discussed in Section 3.3.9, the overall process would not occur. Nor would tin(IV) sulfide be deposited as the final film in any reaction.

In the case of films deposited from tin tetrabromide, the thermodynamics of the reaction suggest that it would not occur. The equilibrium position of Reaction 3.7 and other related reactions of tin tetrabromide would be close to the reactants. However, the high rate of flux of reactants to the surface, the ease of transport of by-products away from the surface and the fact that one product is a solid all contribute to the reaction occurring.

# 3.6 Effect of substrate on films deposited

## 3.6.1 Scanning electron microscopy

Scanning electron microscopy was carried out on all the films deposited. It was observed that films deposited at temperatures up to and including 475 °C gave similar morphologies irrespective of the substrate or precursor. The main difference was observed when tin(II) sulfide films were deposited at temperatures of 500 °C and above. This was seen in Figure 3.9 by comparing 3.9c and 3.9d deposited from the tetrachloride with 3.9e and 3.9f deposited from the tetrabromide. Figures 3.9c and 3.9d showed wavy ill-defined shapes on the surface of the glass, with long, straight, discreet needles covering them in 3.9c (deposited at 525 °C). These needles were not observed on any other film deposited from the chloride. In the case of the films deposited from the bromide, the shape of the particles on the surface of the glass was more regular. They had straight edges and were uniform in size. The long needles on the surface of the film were formed into clusters and were seen on all films deposited at 500 °C and above.

## 3.6.2 Discussion

The shape and size of the particles formed on the surface of the glass is likely to differ according to the nucleation and growth mechanisms dictated by the surface. The needles are probably formed from gas phase reactions, so are not related to the substrate. The coverage of particles on the surface of the carbon-doped silica coated glass is greater than that on the tin oxide / silica coated glass. As temperature increases on the carbon-doped silica coated glass the coverage is greater, so less reaction occurs in the gas phase and fewer needle-like particles are formed. On the tin oxide / silica coated glass the coverage is low, so the proportion of material formed into needles is greater. The higher number means that, statistically speaking, they are more likely to form into clusters.

## 3.7 Discussion and conclusions

In summary, films may be deposited from the reaction of tin tetrahalides with hydrogen sulfide by atmospheric pressure chemical vapour deposition. Films deposited contain very little impurity, most of which is in the form of surface adsorbed oxygen and carbon species. All three phases of tin sulfide may be deposited.

The factors that control the properties of film are the deposition temperature, precursor, hydrogen sulfide flow rate and the substrate.

Deposition temperature is the variable that has the greatest influence over the phase of tin sulfide deposited. It was observed that, in all cases, films deposited at temperatures up to and including 450 °C were tin(IV) sulfide. Raman spectra, X-ray diffraction patterns, unit cell parameters, band gaps and colours of the films all agreed that this was the case. Binding energies in XPS and elemental compositions recorded *via* EDAX were also used to confirm this.

Films deposited at temperatures of 550 °C and above, were found to be predominantly tin(II) sulfide. Again, all the analytical techniques carried out confirmed this. Edges of the films deposited were yellow in colour, and exhibited properties of tin(IV) sulfide. This was attributed to heat losses at the edge of the graphite block in the reactor.

Intermediate temperatures led to the deposition of films of tin(II) tin(IV) trisulfide. In some cases, there was a mixture of phases in the film deposited.

The reason why different phases are deposited at different temperatures stems from the thermodynamics of the system. Although tin disulfide is the most thermodynamically stable phase at all temperatures, the evolution of a gas increases the entropy of the system and permits the reduction to tin(II). Figure 3.15 shows that sulfur gas is more likely to be lost than chlorine or bromine gas. This is due to the higher enthalpy of formation of sulfur gas, and the higher electron affinity of the halogens, which make them more stable in the -1 oxidation state.

Heating films of tin(IV) sulfide in streams of nitrogen cause them to be reduced to tin(II) sulfide at temperatures of 500 °C and above. This concurs with the thermodynamic observations already made. Visual observations made of the films indicate that films deposited at higher initial temperatures are of a single phase, whereas those deposited at the lower temperature and heated are more likely to be inhomogeneous. This may be due to a high temperature intermediate that is more active than $SnS_2$. This would have a different mechanism of reduction and possibly a lower energy pathway to tin(II) sulfide and sulfur gas. A more likely explanation is that the structure of tin(IV) sulfide inhibits the loss of sulfur to tin(II) sulfide. This is shown schematically in Figure 3.20.

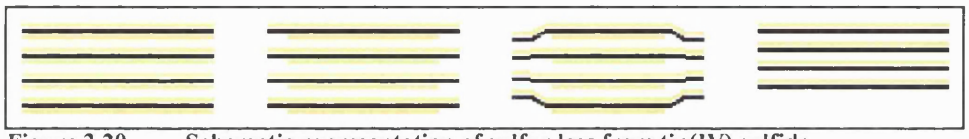

**Figure 3.20 Schematic representation of sulfur loss from tin(IV) sulfide.**

Figure 3.20 shows that as sulfur is lost from between the layers, the layers close up which would impede further sulfur loss. If tin(IV) is reduced to tin(II) during the CVD process, this circumstance does not arise as the film is deposited as tin(II) sulfide.

The second factor that alters the properties of the film is the precursor. Films deposited from tin tetrabromide were thinner than those deposited from tin tetrachloride under comparable conditions. This was demonstrated using transmittance/reflectance spectra.

Tin tetrachloride and tin tetrabromide are similar in many ways. The vapour pressure of each was constant throughout the entire study and the flow rates through the bubbler were constant. The strength of tin-bromine bonds is less than that of tin-chlorine bonds, so tin tetrabromide would be more reactive. The reason why the tetrachloride reacts more actively is that the energy released on formation of hydrogen chloride is greater than that released on formation of the corresponding bromide.

Hydrogen sulfide flow rate into the reaction chamber plays an important part in the formation of the films. Higher hydrogen sulfide flows lead to thicker films. The tin tetrahalide is the limiting reactant in the system, so the hydrogen sulfide is playing a role in lowering the barrier to reaction. When tin(IV) sulfide films are deposited and

subsequently heated to produce mixed valent or tin(II) sulfide, they are reduced more easily in the presence of hydrogen sulfide.

The substrate onto which the film is deposited has no effect on tin disulfide films, however, films of tin monosulfide exhibit different structures on the two substrates used in this study. Tin monosulfide forms particles of two different types – long needles and flat particles on the surface of the glass. On tin oxide / silica coated glass the flat particles are less numerous indicating that nucleation on this substrate is harder than on carbon-doped silica coated glass. Particles deposited on each substrate are of similar size, but on carbon-doped silica coated glass, the irregular shape suggests that particles stop growing due to contact with adjacent particles. This implies that growth on this substrate is faster than on tin oxide / silica coated glass.

The needles also differ on the two substrates. As much of the film is able to deposit as the ill-defined shapes on the carbon-doped silica coated glass there are very few needles covering them. At higher substrate temperatures the formation of the particles on the surface is facilitated so no needles are formed. On tin oxide / silica coated glass there are many more needle-like particles. As the number of needles increases the likelihood that they will form into clusters is increased.

# Chapter 4
# Tin sulfide films from the reaction of tributyl tin trifluoroacetate with hydrogen sulfide

Tri(n-butyl) tin trifluoroacetate is a known precursor for CVD reactions. It is used to deposit tin oxide films,[104] which are used as heat mirrors. The presence of fluorine in the precursor leads to incorporation of a low level of fluorine in the film deposited. This level is sufficient to alter the heat mirror properties of the films, but cannot be detected by methods such as XPS.

In this chapter the use of tributyl tin trifluoroacetate to deposit tin sulfide films will be reported. Hydrogen sulfide gas is necessary, as the precursor does not contain sulfur. The aim is to deposit films of tin sulfide with fluorine doping, to investigate their heat mirror properties and compare them with those of pure tin sulfide films deposited by other means. Within detection limits, XPS will be used to examine fluorine content of the films.

# 4.1 The precursor

## 4.1.1 Previous work with this precursor

Tributyl tin trifluoroacetate has previously been prepared and used for chemical vapour deposition. It is used in the atmospheric pressure deposition of tin oxide and incorporates *ca.* 0.5 % fluorine in the resultant film. This enhances heat mirror properties of the film.

## 4.1.2 Preparation of the precursor

The precursor was prepared at The University of Bath by Dr. T. Hibbert using the previously published method of Tiekink.[104] Sodium trifluoroacetate, 3.83 g (28 mmol), was refluxed with tri-*n*-butyltin chloride, 9.14 g (28 mmol), in ethanol, 0.12 $dm^3$ for 2 h. The solvent was removed *in vacuo* and the resulting solid recrystallised from diethyl ether. This yielded colourless crystals in 68 % yield. The melting point was determined as 49 - 50 °C.

## 4.1.3 Analysis and physical properties of the precursor

The melting point of the precursor was determined as 49 - 50 °C, although Tiekink determined it previously as 55 °C.[104]

Differential scanning calorimetry was carried out on the precursor before using it in CVD reactions. A sharp endotherm was observed at 57 °C, which is consistent with being the melting point of the compound. A broad endotherm was observed with maximum at 174 °C, although the onset of change was as low as 120 °C. A second sharp endotherm at 208 °C is likely to be the vaporisation point of the compound. The DSC of tributyl tin trifluoroacetate is shown in Figure 4.1.

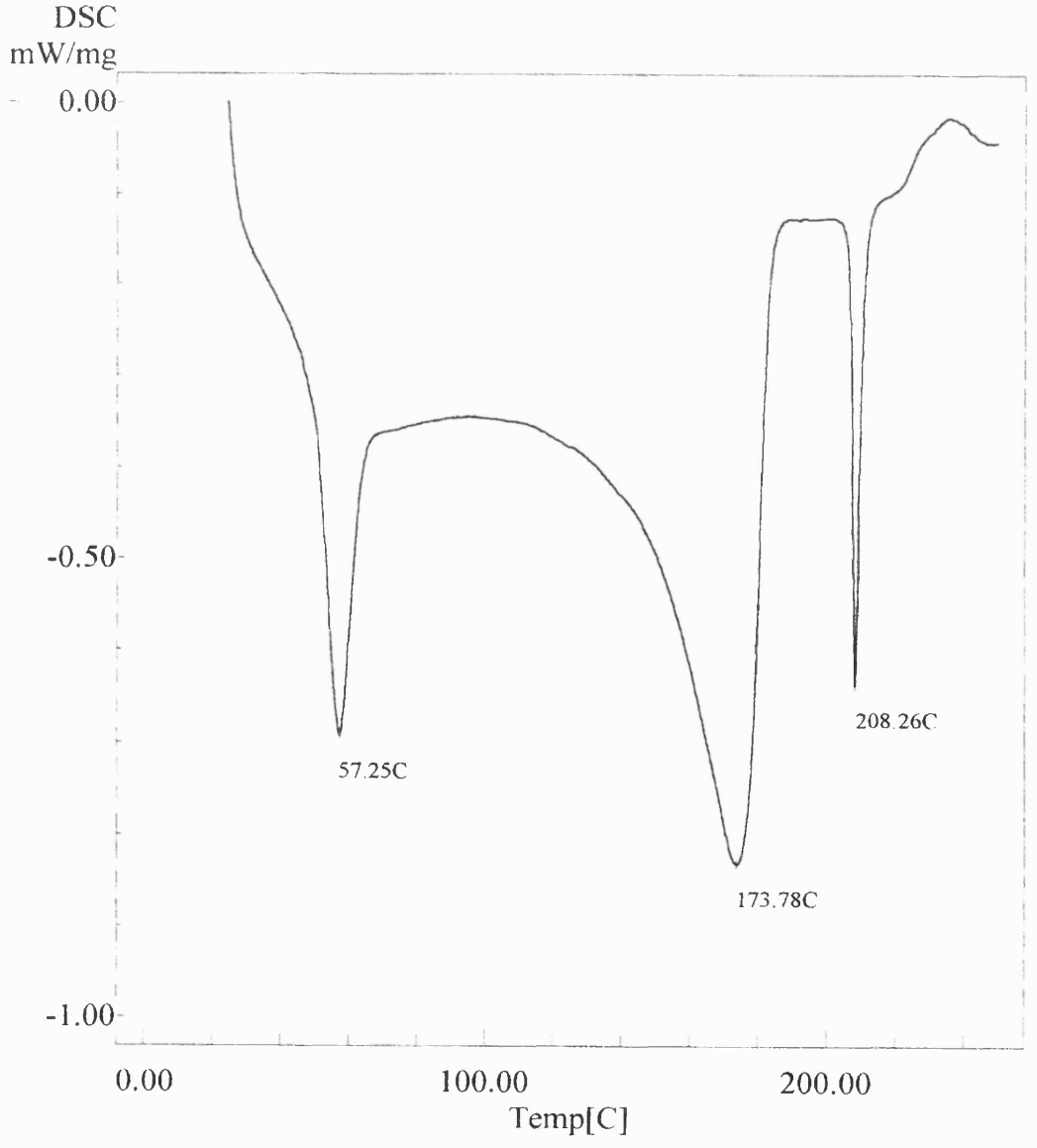


**Figure 4.1** **DSC of tributyl tin trifluoroacetate**

It was found, through carrying out the CVD reaction, that the precursor sublimes at a temperature of approximately 150 °C. The precursor is a waxy solid initially, and sublimation yields 2 products – around the top of the bubbler needle-like crystals were formed and in the bottom of the bubbler a dry, beige solid was found. The needles were wet looking and *ca.* 8 mm long. They formed into clusters. The beige powder was not at all similar in appearance to the starting material.

The colourless crystals, beige powder and starting material were all analysed by IR spectroscopy and powder X-ray diffraction to determine any similarities and differences between the three. Powder X-ray diffraction of the starting material showed that it was amorphous. The needle-like crystals deposited at the top of the bubbler were also amorphous, but the beige powder showed some crystallinity.

Infrared absorption spectra of the three phases showed very similar spectra. These are shown in Figure 4.2.

In all cases, four bands were observed at 2800 – 3000 $cm^{-1}$ associated with C-H stretches. A broad band was observed at *ca.* 1700 $cm^{-1}$ that was sharper in the beige powder. This is probably due to the acetate functionality, although one would expect two bands associated with the symmetric and asymmetric stretching modes. A sharp band was seen at 1430 $cm^{-1}$ in the starting material, and this moved to 1460 $cm^{-1}$ in both the needle-like crystals and the beige powder. This would be due to C-H bending modes. Two weak absorptions were noticed at 1310 and 1350 $cm^{-1}$, which were significantly stronger in the spectrum of the needle-like crystals. A broad band appeared at *ca.* 1200 $cm^{-1}$ in all spectra. In the starting material and the beige powder other bands were observed at 830 (C-F stretching), 800 (C-F stretching), 720 (C-H bending), 600 and 500 $cm^{-1}$, however many more bands were observed in the spectrum of the needle-like crystals (at least eleven were noted).

Heating probably induced the increase in crystallinity between the precursor and the beige powder found in the bottom of the bubbler. The only difference observed in the infrared absorption spectrum was a slight shift in the position of the carbonyl stretching mode. The needle-like crystals appeared wet, as though they were on the point of melting, or had absorbed moisture from the air. With this in mind, it appears that they may have melted on grinding, so giving no diffraction pattern.

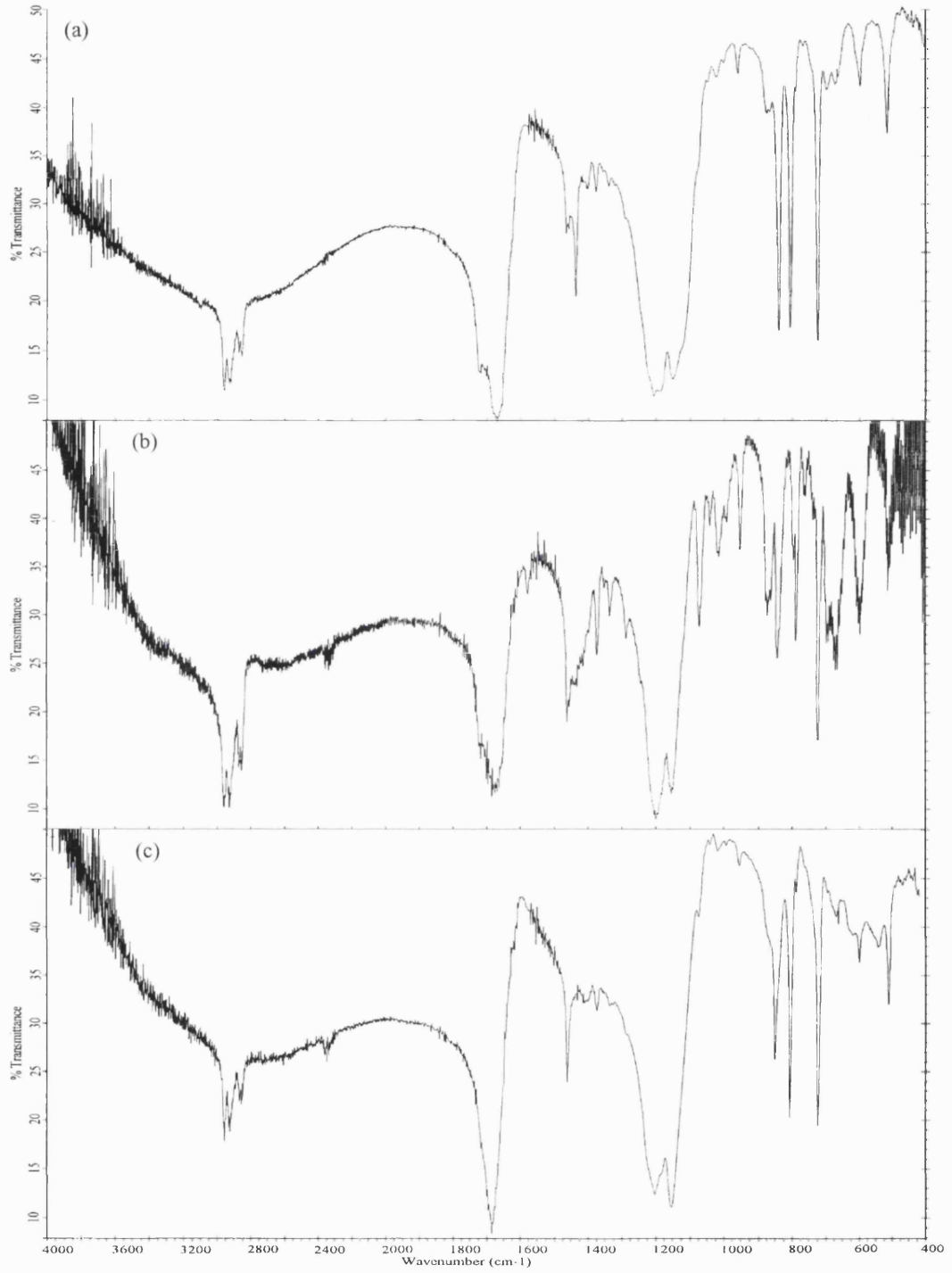


**Figure 4.2 Infra-red absorption spectra of the precursor and products to which it decomposed in the bubbler. (a - before heating; b – crystals around top of bubbler; c – beige powder in bottom of bubbler)**

Although the major bands observed in the infrared were essentially identical to those observed in the spectra of the precursor and beige powder, the existence of a large number of bands in the fingerprint region indicates a significant change in the material. In the needle-like crystals, the molecules are structurally identical, but may be locked

into a configuration with a different symmetry from those in the precursor or beige powder, which are the same.

In the light of observations made after reactions had been carried out with a bubbler temperature of 150 °C, it is likely that the endotherm observed in the differential scanning calorimetry at 174 °C is due to an alteration in the structure of the compound. Two different products are formed, both with the same structural formula as the precursor. One sublimes to form needle-like crystals with a different symmetry within each molecule. The other compound, which is slightly discoloured, is more crystalline, and has a low vapour pressure (indicated by the fact that no further reactions could be carried out).

## 4.2 Reactions carried out

A large number of reactions were carried out using this precursor. Reactions were carried out with a coater temperature between 300 and 600 °C at intervals of 50 degrees. The bubbler temperature was *ca.* 120 - 130 °C for all reactions. A few reactions were carried out with a bubbler temperature of *ca.* 150 °C, but this caused the precursor to sublime, as discussed in Section 4.1.3. Reactions were carried out over a 15 min period, due to the limited volatility of the precursor at 120 – 130 °C. The hydrogen sulfide flow for each reaction was 0.6 $dm^3min^{-1}$ and the nitrogen diluting this flowed at 1.2 $dm^3min^{-1}$. The nitrogen flow through the bubbler was 0.4 $dm^3min^{-1}$ and a 10 $dm^3min^{-1}$ flow of nitrogen was used to dilute this. The plain nitrogen line, which passed straight to the exhaust during reaction, carried a flow of 10 $dm^3min^{-1}$. Most films were deposited on tin oxide / silica precoated glass although those deposited initially with the higher bubbler temperature were laid down on carbon-doped silica coated glass. Full details of reaction conditions are summarised in Table 4.1.

**Table 4.1 Summary of reaction conditions for films deposited from tin trifluoroacetate with hydrogen sulfide.**

| | |
|---|---|
| Precursor temperature | 130 or 150°C |
| Nitrogen flow rate through bubbler line | 0.4 $dm^3min^{-1}$ |
| Nitrogen flow rate diluting line from bubbler | 10 $dm^3min^{-1}$ |
| $H_2S$ flow rate | 0.6 $dm^3min^{-1}$ |
| Nitrogen flow rate diluting $H_2S$ | 1.2 $dm^3min^{-1}$ |
| Substrate | Tin oxide / silica or carbon-doped silica coated glass |
| Deposition time | 15 min |

# 4.3 Results

## 4.3.1 Visual appearance of films

The reaction of tributyl tin trifluoroacetate with hydrogen sulfide carried out at 300 °C deposited no film. At all temperatures from 350 to 600 °C, a silver-grey film was deposited. The films were not as uniform as those deposited from the reactions of tin tetrahalides with hydrogen sulfide, although they were of similar thickness. There was no obvious cause for the non-uniformity of coverage. It was noticed that the films deposited with a higher bubbler temperature were thicker. This was due to the vapour pressure over the precursor being higher and more of the precursor being carried over to the substrate. These thicker films were deposited on carbon-doped silica coated glass, whereas all others were laid down on tin oxide / silica coated glass.

## 4.3.2 X-ray diffraction

As typical growth conditions produced thin films, only those deposited with the higher bubbler temperature gave an X-ray diffraction pattern. Figure 4.3 shows the X-ray

diffraction pattern recorded of the film deposited from tributyl tin trifluoroacetate with a bubbler temperature of 150 °C and a coater temperature of 450 °C.

If the diffraction pattern shown in Figure 4.3 is compared with the reference spectrum of tin(II) sulfide shown in Figure 2.4 it is seen that they are identical. Table 4.2 gives the calculated cell parameters for the film deposited from [$^{n}Bu_3SnOC(O)CF_3$] along with literature parameters for tin monosulfide. The *a*-parameter is slightly longer and the *c*-parameter shorter than those reported previously. Overall, the unit cell is *ca.* 2 % smaller than that found in other works.

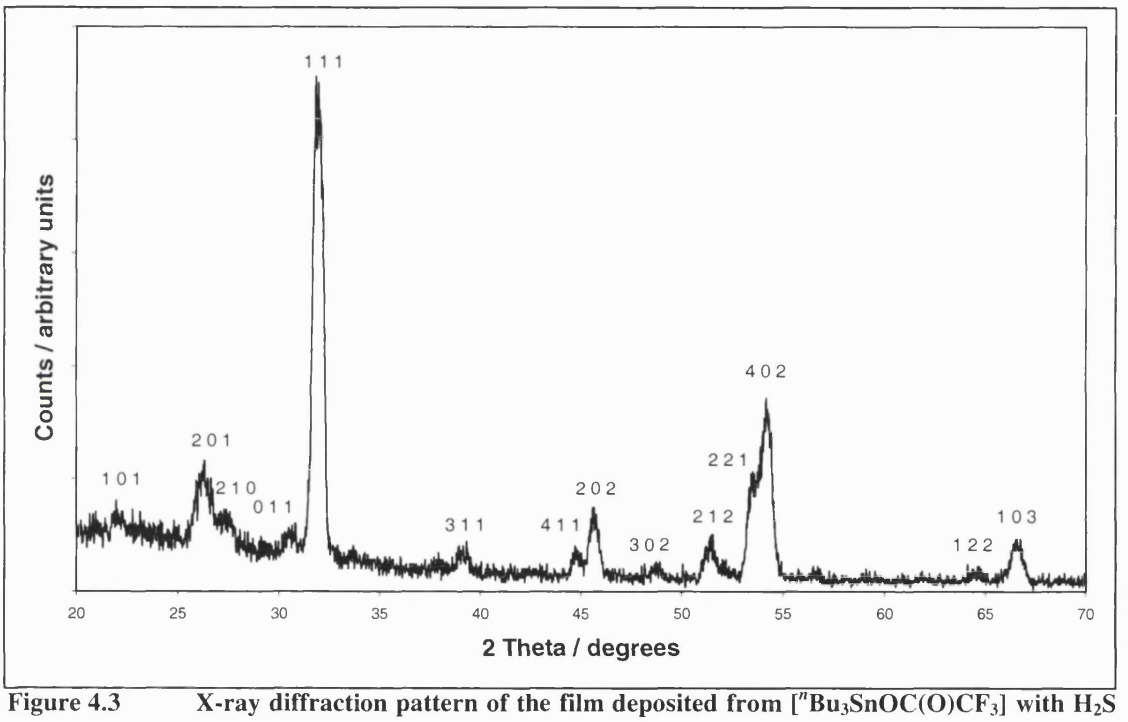


**Figure 4.3 X-ray diffraction pattern of the film deposited from [$^{n}Bu_3SnOC(O)CF_3$] with $H_2S$ at 450 °C on carbon-doped silica coated glass with a bubbler temperature of 150 °C.**

**Table 4.2 Comparison of cell parameters determined in this work with those reported previously.**

| Parameter | Calculated from Figure 4.3 | Literature values[15] |
|---|---|---|
| a | 11.27(4) Å | 11.180(6) Å |
| b | 3.972(6) Å | 3.982(2) Å |
| c | 4.24(1) Å | 4.329(3) Å |

No peaks corresponding to any other phase of tin sulfide or tin oxide were observed in the X-ray diffraction pattern.

## 4.3.3 Raman microscopy

Raman spectra were recorded for all the films deposited and it was found that they exhibited the spectra of tin(II) sulfide for all deposition temperatures. The Raman spectra of the films deposited at 400 °C for each of the bubbler temperatures and substrates is shown in Figure 4.4. These are identical and show that there is no difference in altering the bubbler temperature or substrate other than an alteration in thickness.

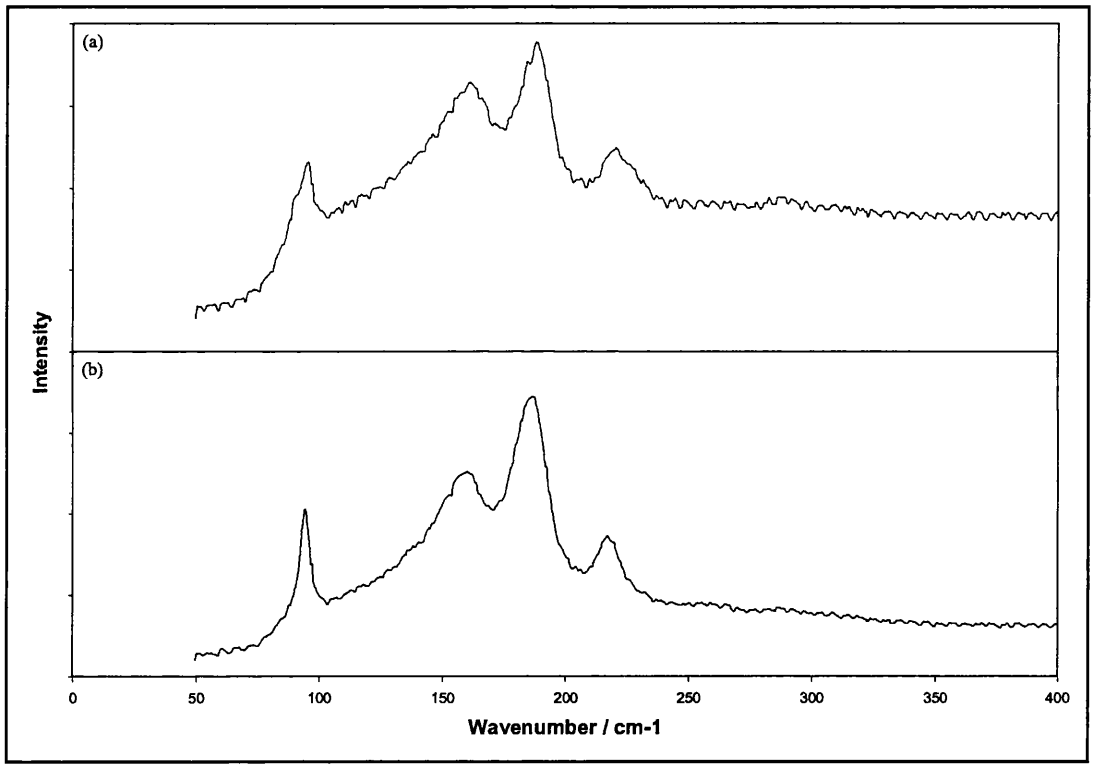


**Figure 4.4 Raman spectra of the two films deposited at 400 °C (a) with a bubbler temperature of 150 °C on carbon-doped silica coated glass and (b) with a bubbler temperature of 130 °C on tin oxide / silica coated glass.**

No evidence for other phases of tin sulfide or oxide was observed by Raman microscopy.

## 4.3.4 X-ray photoelectron spectroscopy

XPS was carried out on the film deposited at 450 °C with a bubbler temperature of 150 °C. It was observed that there was a high level of oxygen contamination in the

film. Sputtering was not carried out and only information on the surface of the film is reported here. Table 4.3 gives the binding energy of each element and composition of the film.

**Table 4.3 Binding energies and composition of the film deposited from tributyl tin trifluoroacetate at 450 °C, with a bubbler temperature of 150 °C on carbon-doped silica coated glass.**

| Element | Binding Energy | Composition after etching |
|---|---|---|
| Sn $3d_{5/2}$ | 485.8 and 484.8 eV | 38 % |
| S 2p | 161.1 eV | 18 % |
| O 1s | 533.3 eV | 40 % |
| C 1s | 284.5 eV | 4 % |

Two tin environments were observed. Tin(II) sulfide has a Sn $3d_{5/2}$ binding energy of 485.4 and tin(IV) sulfide is observed at *ca.* 486.4 – 486.6 eV, so the first of these peaks is indicative of tin(II) sulfide. Tin oxides have Sn $3d_{5/2}$ binding energies of 487.1 and 486.9 eV for tin in the +2 and +4 oxidation states respectively, so it is unlikely that the second environment observed is due to either of these. Tin metal has a binding energy of 484.9, so it is possible that this is observed.

Sulfur in the –2 oxidation state, when bound to a metal has a binding energy of 161.7 – 162.8 eV. It is, therefore, likely that the binding energy observed in this case is due to sulfur in a metallic environment. The low sulfur to tin ratio is consistent with some of the tin being bound to oxygen.

The level of oxygen observed in this film is relatively high. This is possibly due to oxidation of the surface of the coating to form tin oxide. The binding energy of oxygen normally falls within the range 529 to 534 eV. Metal oxides have binding energies at the lower end of this range, typically O 1s (CdO) = 529.2 eV; O 1s (NiO) = 529.5 eV. The highest binding energy of a metal oxide is found at 531.0 and is observed in $Al_2O_3$. Binding energies for oxygen higher than these are indicative of non-metallic environments. Water has an O 1s binding energy of 533.1 eV and $Co(CO)_6$ has an O 1s binding energy of 533.9 eV. Other tabulated data in this region include chlorate anions and alcohols. Considering this, it appears that the oxygen detected in this coating is due to water or reaction byproducts adsorbed onto the surface of the film.

Fluorine was not observed in the XPS. In the region where fluorine would be expected there was no indication of a peak. This implies that less than 1 % is present in the film.

The carbon found in the films is usually a result of the vacuum pumps in the XPS chamber. It is graphitic in nature and used to calibrate the binding energies of other elements.

## 4.3.5 Energy dispersive analysis by X-rays

EDAX was carried out on all samples, although those deposited on tin oxide / silica coated glass have their elemental ratios distorted by the undercoatings on the glass. The films deposited on carbon-doped silica coated glass exhibit near 1:1 ratios of tin and sulfur. Table 4.4 shows the percentages of tin, sulfur and silicon in the films deposited.

**Table 4.4 Composition of films deposited from [$Bu_3SnOC(O)CF_3$] with a bubbler temperature of 150 °C on carbon-doped silica coated glass.**

| Coater temperature | At. % tin | At. % sulfur | At. % silicon |
|---|---|---|---|
| 450 | 14.8 | 14 | 47.3 |
| 420 | 6.1 | 5.4 | 56 |
| 400 | 2.9 | 1.4 | 57.7 |

As seen in Table 4.4, decreasing bubbler temperature leads to lower tin and sulfur contents in the deposited films. This is not due to lower reactivity, but the sequence in which the films were deposited. The film deposited at 450 °C was produced first, followed by that at 420 °C, with that deposited at 400 °C coming last. As reported in section 4.1.3, the precursor was altered in the bubbler to give involatile products. As more reactions were carried out, the amount of precursor in the bubbler was being reduced dramatically because of this. In the case of films deposited with a precursor temperature of 130 °C, only a small change is observed in the sulfur content with increasing substrate temperature.

The ratio of tin to sulfur in films deposited from [$Bu_3SnOC(O)CF_3$] with a bubbler temperature of 150 °C, is near 1:1, although there is a slight excess of tin in all films. This is due to there being calcium in the glass. An X-ray line for calcium exists very

close to the tin line measured in EDAX, and elemental compositions of the two are distorted.

## 4.3.6 Scanning electron microscopy

SEM images were obtained from all samples. Figure 4.5 shows a representative sample of these.

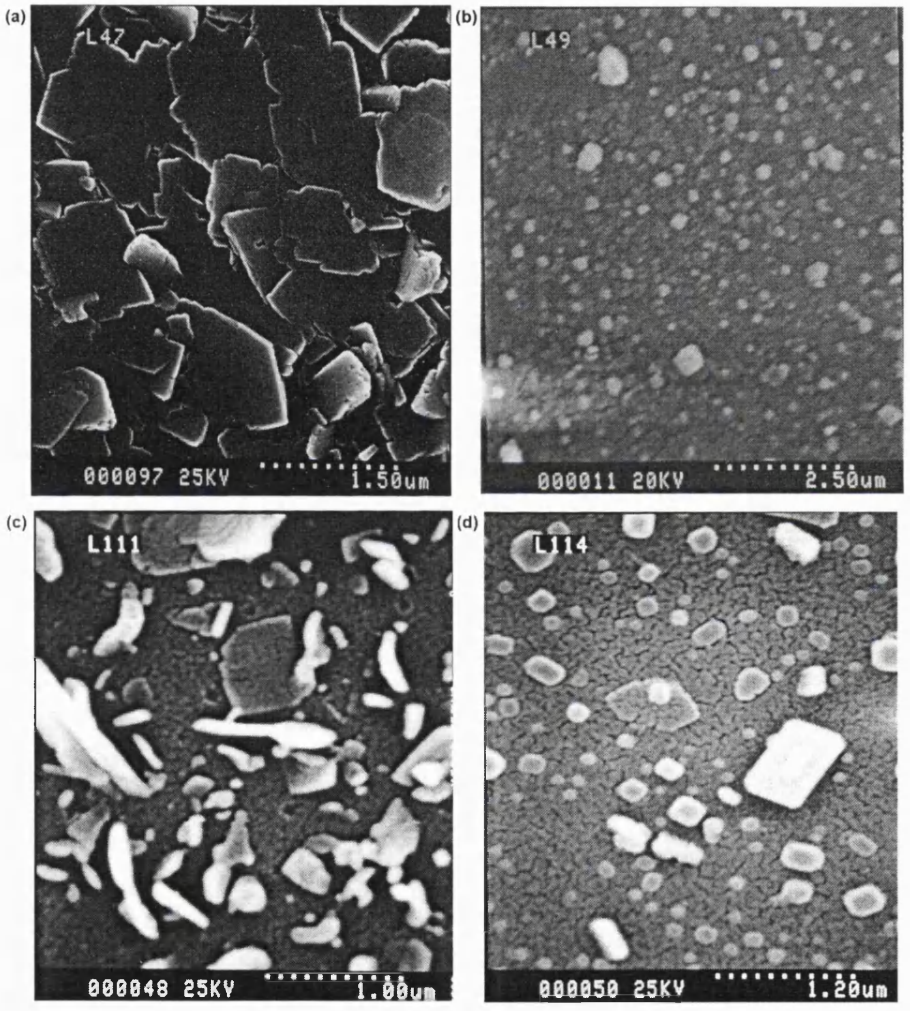


**Figure 4.5 SEM images of films deposited from the reaction of tributyl tin trifluoroacetate with hydrogen sulfide. (See next paragraph for more details)**

Figure 4.5a shows the scanning electron micrograph of the film deposited at 450 °C on carbon-doped silica coated glass with a precursor temperature of *ca.* 150 °C. This shows large regular shaped particles. A film deposited later, at 400 °C, with the same bubbler temperature is depicted in Figure 4.5b. The film deposited at 400 °C shows

much lower surface coverage, due to the precursor becoming involatile as it decomposed in the bubbler.

Figures 4.5c and 4.5d show films deposited on tin oxide / silica coated glass with a precursor temperature of 130 °C with coater temperatures of 400 and 500 °C respectively. Here, there is less variation in surface coverage, but films show less coverage than that imaged in Figure 4.5a. The particles are less regular in shape in the film deposited at the lower coater temperature. This is because the surface diffusion rate is lower.

Figure 4.5d clearly shows a wavy structure to the film. This is characteristic of island growth. The film was not deposited for long enough for all particles to coalesce forming a continuous film.

### 4.3.7 Transmittance/reflectance spectroscopy

Transmittance/reflectance spectra were recorded for all films. Figure 4.6 shows various spectra recorded from films deposited from tributyl tin trifluoroacetate. Figure 3.13 was recorded for a film which was analysed by other means to be tin(II) sulfide.

In all the films deposited from tributyl tin trifluoroacetate, reflectance is low. Transmittance is low in the case of the film deposited at 450 °C with a bubbler temperature of *ca.* 150 °C. This is due to the thickness of the film. The two films deposited at 400 °C show similar profiles of transmittance across the spectral range. The film deposited with a bubbler temperature of *ca.* 150 °C has higher transmittance, indicating a thinner film. In general, a higher bubbler temperature leads to higher vapour pressure and so thicker films as more of the precursor is reaching the substrate. In this case, the film deposited at the higher bubbler temperature is thinner because it was the third film deposited at this bubbler temperature and the precursor was being rendered involatile by the high temperature.

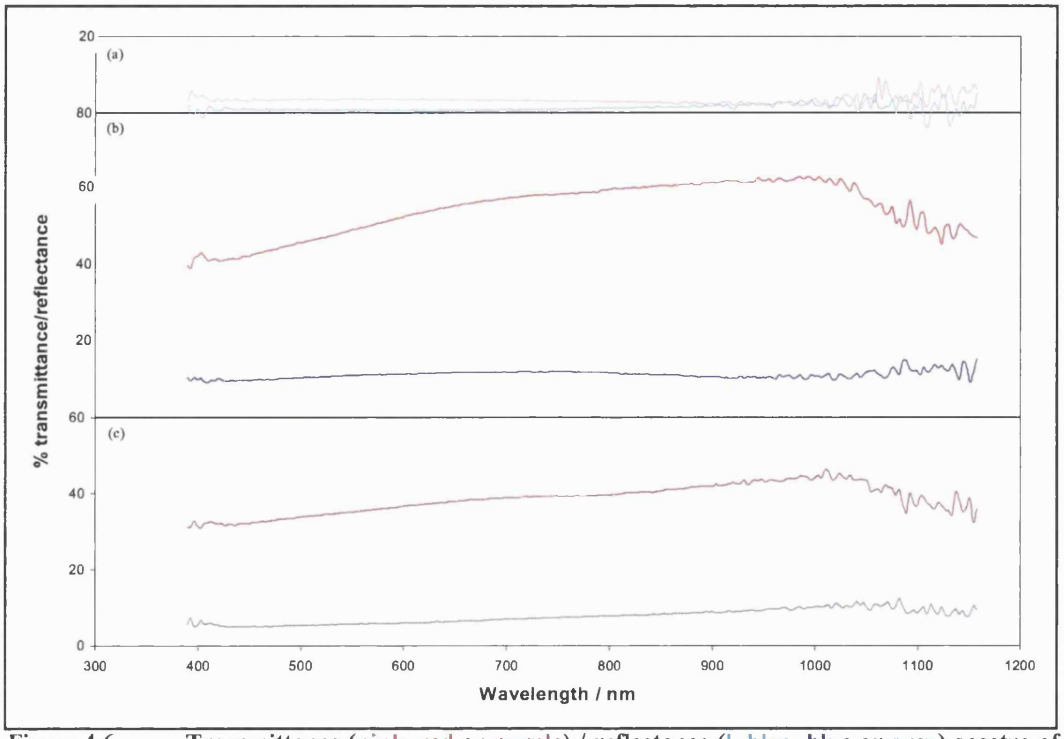


**Figure 4.6 Transmittance (pink, red or purple) / reflectance (l. blue, blue or grey) spectra of films deposited from tributyl tin trifluoroacetate at (a) 450 °C with a bubbler temperature of *ca.* 150 °C, (b) 400 °C with a bubbler temperature of *ca.* 150 °C and (c) 400 °C with a bubbler temperature of *ca.* 130 °C.**

Figure 3.13 was recorded for a film which was analysed by other means to be tin(II) sulfide. When this is compared with the spectra recorded from films deposited by the reaction of tributyl tin trifluoroacetate with hydrogen sulfide, some similarities are observed. In the cases of the films deposited at 420 and 400 °C from tributyl tin trifluoroacetate with either bubbler temperature, thinner films are deposited than those formed by the reaction of tin tetrachloride with hydrogen sulfide. The shapes of the transmittance/reflectance spectra are very different, and many of the features observed in Figures 4.6b and 4.6c are due to the glass rather than the coating. The film deposited from tributyl tin trifluoroacetate and hydrogen sulfide at 450 °C with a bubbler temperature of *ca.* 150 °C is much thicker. This is demonstrated by the transmittance/reflectance percentages having much lower values. Here, the film is of comparable thickness to that deposited from tin tetrachloride and hydrogen sulfide at 545 °C.

### 4.3.8 Band gaps

The UV-visible absorption spectrum was recorded for the film deposited from tributyl tin trifluoroacetate with hydrogen sulfide at 400 °C and a bubbler temperature of *ca.* 150 °C. From this, the band gap was calculated as 1.5 eV. Tin(II) sulfide has previously been recorded as having a band gap of 1.3 eV.[30] This is lower than the value recorded for the film deposited from [$^{n}Bu_3SnO_2CCF_3$] with hydrogen sulfide.

## 4.4 Summary and Discussion

### 4.4.1 Summary of results

The aim of the work in this chapter was to attempt to deposit tin sulfide films with fluorine doping. This was in an attempt to mirror previous work on tin oxide films using this precursor. It was accepted from the outset, that any fluorine incorporation would probably not be observed directly by the techniques employed in this thesis, but may possibly be observed indirectly from the transmittance/reflectance measurements.

X-ray diffraction and Raman microscopy were used to determine the phases present in the films. Only tin(II) sulfide was observed by these techniques, with no evidence for contamination by other phases of tin sulfide or oxide. Calculation of the unit cell parameters showed it was slightly smaller than unit cells reported in the literature.

XPS demonstrated that there was a high level of oxygen contamination in the films. This was not in the form of a metal oxide, but had a 1s binding energy indicative of a covalently bound species such as water or oxygen bound to carbon or chlorine. Such species would have been observed in Raman spectroscopy, if they formed part of the bulk film. It is thought that one of the reaction byproducts may have been adsorbed onto the surface of the film and detected only in the XPS due to its high surface sensitivity. Tin was shown to have two environments – tin(II) sulfide and metallic tin. This was not observed in the films studied in Chapter 3. The observed tin-sulfur ratio was sulfur deficient, which is in agreement with this.

EDAX carried out on the films showed a near 1:1 ratio of tin to sulfur in the films deposited with a bubbler temperature of 150 °C on carbon-doped silica coated glass. Deviations from the perfect 1:1 ratio were caused by calcium in the substrate interfering with the tin signal in analysis. Films deposited later had less coating, due to the reaction in the bubbler yielding involatile products. Films deposited on tin oxide / silica coated glass with lower precursor temperatures were also analysed, but it was impossible to calculate an accurate tin to sulfur ratio. This was due to the tin oxide precoating on the substrate.

SEM images showed that films deposited with the higher precursor temperature had larger particles and greater surface coverage, but confirmed that both decreased with later deposition reactions. With the lower precursor temperature, smaller particles were observed. In this case, it was observed that higher deposition temperatures led to more regularly shaped particles in the film. This was due to faster surface diffusion. Underneath, the film was seen to exhibit island growth.

## 4.4.2 Discussion

Films of tin(II) sulfide may be deposited by the reaction of tri-*n*-butyl tin trifluoroacetate with hydrogen sulfide. No tin(IV) sulfides may be deposited despite the fact that the precursor was a tin(IV) species. This is in contrast with work carried out in Chapter 3, where tin(IV) halides deposited tin(II), tin(IV) and mixed valent sulfides. Although tin(II) sulfides were formed, they were only accessible at high temperatures. This was because the kinetic product of the reaction was tin(IV) sulfide. The reaction pathway of tributyl tin trifluoroacetate with hydrogen sulfide must experience lower energy barriers to the thermodynamically more stable tin(II) sulfide.

The overall reaction of tributyl tin trifluoroacetate could result in a number of products. Some of the possible reactions are given below.

$[Bu_3SnO_2CCF_3] + 2H_2S \rightarrow SnS + 3BuH + HOC(O)CF_3 + S$ **Equation 4.1**

$[Bu_3SnO_2CCF_3] \rightarrow [Bu_2Sn] + BuOC(O)CF_3$

$\downarrow H_2S$ **Equation 4.2**

$SnS + 2BuH$

In Equation 4.1, reduction of tin is accompanied by oxidation of sulfur as was assumed to be the case in Chapter 3 for the reaction of tin(IV) chloride to yield tin(II) sulfide. Equation 4.2 assumes reductive elimination to give butyl trifluoroacetate, followed by reaction of the 16 electron species, dibutyl tin, with hydrogen sulfide to give tin(II) sulfide. Without analysis of effluent gases, it is impossible to determine which of these is occurring in the reaction.

The oxygen incorporation observed in the XPS, while possibly coming from the glass, may have been due to one or other of these by-products. Reaction by-products could easily remain adsorbed on the surface of the coating.

A further possibility is that the film is formed by two-step surface reaction. In the first step, tributyl tin trifluoroacetate may react with the surface to form a surface bound tin species with the loss of one or all of the butyl groups. The second step would then involve reaction of hydrogen sulfide or an HS species with the tin-oxygen bond. This would be slower as the bulky groups surrounding the tin atom would impede the hydrogen sulfide.

If this were the case, a large amount of tin, which is not yet part of the forming tin sulfide film, would be found near the surface. In addition, the large proportion of oxygen observed in the XPS can be accounted for. The binding energy of tin in this case would not be the same as that observed for tin sulfides. Nor would it be similar to binding energies observed for tin oxides, as the oxygen atom is a covalent species rather than an $O^{2-}$ ion.

As both the Raman and X-ray diffraction showed the films were consistent with being tin(II) sulfide alone, it is likely that the oxygen is only a surface bound entity. A high level of incorporation of another phase would be observed in the Raman microscopy, although an amorphous species could escape X-ray detection.

None of these proposed reaction mechanisms can be confirmed without analysis of the reaction byproducts. *In situ* spectroscopy would also be required to determine the actual mechanism of film growth. The setup of the reactor used in this work makes both these unfeasible.

### 4.4.3 Comparison with results from reactions of tin tetrahalides

Films deposited from the reaction of tributyl tin trifluoroacetate with hydrogen sulfide show some differences from those deposited from the reaction of tin tetrahalides with hydrogen sulfide. These differences include unit cell dimensions and morphology. The difference in unit cell parameters was slight.

Transmittance / reflectance spectroscopy showed similarities with films deposited from the reaction of tin tetrahalides with hydrogen sulfide. It appears that in contrast with the case of tin oxide, use of a fluorine-containing precursor has little effect on the optical properties of the film deposited by CVD.

The films deposited from tributyl tin trifluoroacetate exhibited a different morphology from those deposited from tin tetrachloride or tin tetrabromide. In the case of the tin tetrahalides, different morphologies were observed dependant on the substrate, whereas, in the case of tributyl tin trifluoroacetate, morphology was similar in all cases. This may be because the film deposited was not entirely composed of tin monosulfide, but another phase was present. The presence of another phase may alter the nucleation properties of the films, making the substrates alike enough for the same film to be deposited.

# Chapter 5
# Tin sulfide films deposited from single source precursors

Chemical vapour deposition is often carried out using dual sources, as was the case in Chapters 3 and 4. One of the problems with this method is that it is hard to control stoichiometries in the final film. If one of the precursors is in vast excess, there is the likelihood that more of this may be incorporated into the film. Another problem sometimes encountered is that one component of the film is easily lost during deposition.

The solution to these problems is to construct a single-source precursor. This should have direct bonds between atoms that are to form the final film, along with weaker bonds that are easily broken, to remove other parts of the molecule. The simplest molecules containing tin and sulfur are thiolates. The general formula of these is $[Sn(SR)_n]$ where R is an alkyl or aryl group and n is 2 or 4 depending on the oxidation state of tin. Other simple molecules are dithiocarbamates, whose general formula is $[Sn(SC(S)NR_2)_n]$ again where R is an alkyl group and n is 2 or 4.

In this chapter, the synthesis of various single source precursors is outlined. Thermal Gravimetric Analysis (TGA) and Differential Scanning Calorimetry (DSC) were used to investigate precursors for suitability as CVD precursors. CVD reactions were carried out and the resulting films analysed by XRD, Raman, XPS, EDAX and SEM.

# 5.1 Preparation of the precursors

All precursors used in this chapter were synthesised at The University of Bath by Dr. T. Hibbert. Differential Scannign Calorimetry and all CVD reactions (except where otherwise noted) were carried out at University College London. The precursors investigated in this chapter fall into one of the following categories.

- Homoleptic tin(IV) thiolates
- Homoleptic tin(II) thiolates
- Homoleptic tin(IV) dithiocarbamates
- Alkyl tin(IV) dithiocarbamates

## 5.1.1 Preparation of homoleptic tin(IV) thiolates

Tin(IV) phenyl thiolate was prepared by the method of Backer and Kramer.[106] A solution of tin tetrachloride, 2 $cm^3$ (17.4 mmol), in dry, degassed toluene, 100 $cm^3$, was prepared. Sodium phenylthiolate, 9.42 g (71.3 mmol), was added and refluxed for 2 h. The solution was cooled to room temperature. NaCl and excess sodium thiolate were removed by filtration. The remaining solution was evaporated to dryness *in vacuo*. The product was recrystallised from diethyl ether to yield colourless crystals in 80 % yield. The melting point was determined as 52 °C, which is lower than the literature value of 67 °C.[106]

Tin(IV) $\eta^2$-ethane 1,2-diothiolate was prepared in a similar manner. Ethane-1,2-dithiol, 1.45 $cm^3$ (17.2 mmol), was dissolved in THF, 50 $cm^3$. $^n$BuLi (2.5 M), 13.7 $cm^3$ (34.2 mmol), in hexane was added under constant stirring. This led to the formation of a white precipitate. After stirring at room temperature for 30 min, $SnCl_4$, 1.0 $cm^3$ (8.55 mmol), was added dropwise, causing an exothermic reaction. The solution was stirred for 16 h and the THF removed *in vacuo*. The resulting solid was dissolved in $CH_2Cl_2$ and insoluble LiCl removed by filtration. The solvent was again removed *in vacuo* to leave a white powder in 91 % yield. The melting point was determined as 180-181 °C, comparable with 178 °C[107] and 182 °C[108] previously reported.

Tin(IV) 2,2,2-trifluoroethane thiolate was prepared by an alternative route. $CF_3CH_2SH$, 3.05 $cm^3$ (34.3 mmol), was syringed into a pre-cooled flask at –78 °C. Once fully frozen, $SnCl_4$, 1.0 $cm^3$ (8.55 mmol), was added and allowed to freeze. The cooling bath was then removed and the reagents allowed to warm slowly to room temperature under vigorous stirring. Stirring was continued at room temperature for 1 hr, and the flask periodically vented of emerging hydrogen chloride. Once evolution of HCl was complete, as determined using universal indicator paper, $[Sn(SCH_2CF_3)_4]$ remained as a clear colourless liquid. The boiling point was determined as 35 °C.

## 5.1.2 Preparation of homoleptic tin(II) thiolates

Homoleptic tin(II) thiolates were prepared by reacting stannocene with the appropriate thiolate in toluene. Products were polymeric and so both insoluble and involatile making them unsuitable for CVD. The only exception was $[Sn(SCPh_3)_2]$. This compound contains exceptionally bulky groups, rendering polymerisation difficult from steric considerations. As such, although involatile, it could be dissolved in toluene and aerosol assisted CVD reactions carried out.

## 5.1.3 Preparation of homoleptic tin(IV) dithiocarbamates

Dithiocarbamates were prepared by the route of Lalancette *et al.*[109] An appropriate dialkyl amine was reacted with butyl lithium in toluene to form the dialkylamino lithium salt. This was then reacted with $CS_2$ in toluene to give a dithiocarbamate lithium salt. A number of precursors were also used where the dithiocarbamate precursor had two different alkyl groups. In this case $Li[S_2CNMeBu]$ was prepared by using MeBuNH as the starting amine.

$SnCl_4$ and a stoichiometric amount of $Li[S_2CNMeBu]$ were placed in a Schlenk tube under a nitrogen counter-flow. Dichloromethane was added and the reagents stirred at room temperature for 16 h. LiCl was removed by filtration and the solvent removed *in vacuo*. Products were recrystallised from diethyl ether.

## 5.1.4 Preparation of alkyl tin(IV) dithiocarbamates

Reagents were prepared as above using $[R_nSnCl_{4-n}]$ as the tin source to give $[R_nSn(dtc)_{4-n}]$ precursors, where dtc is any dithiocarbamate ligand.

## 5.2 Reactions and results of homoleptic tin(IV) thiolates

Many of the precursors synthesised were investigated for their suitability as CVD precursors by Differential Scanning Calorimetry. This indicated which could be used with thermal evaporation and which required aerosol delivery methods.

Five precursors were investigated for use as CVD precursors. Tin(IV) benzyl thiolate was thought to be suitable for bubbler delivery, and a small number of reactions were carried out. All were unsuccessful.

Tin(IV) cyclohexyl thiolate and tin(IV) phenyl thiolate were investigated by DSC and thermal decomposition. It was found that they both had very high boiling points (*ca.* 350 °C), and so were unsuitable for thermal delivery methods. They were each investigated as CVD precursors using the aerosol delivery method. Tin(IV) cyclohexyl thiolate was dissolved in trichloromethane and a small number of reactions were carried out. All were unsuccessful. On the other hand, tin(IV) phenyl thiolate could be dissolved in trichloromethane, hexane or acetone and films deposited.

In order to produce more volatile tin(IV) thiolates, alkyl compounds were investigated, with fluorine substituted for hydrogen. This is likely to increase the volatility. One such compound investigated was tin(IV) 2,2,2-trifluoroethane thiolate. This has a boiling point of 35 °C, so may be admitted to the CVD reactor using the bubbler delivery method.

Another precursor investigated for CVD was a chelating thiolate. Ethane 1,2-dithiol was reacted with tin(IV) chloride in the same manner as other thiolates, to produce tin(IV) $\eta^2$-ethane 1,2-dithiolate.

## 5.2.1 Reactions of tin(IV) phenyl thiolate

The first reactions involving tin(IV) phenyl thiolate were carried out at the University of Bath by Dr. T. G. Hibbert. A solution of 0.5 g tin(IV) phenyl thiolate in 20 ml toluene was used to create a mist, which was transported to the CVD reactor in a 1 $dm^3min^{-1}$ stream of nitrogen. The reaction was carried out until the entire precursor was expended. The coater temperature during reaction was 300 °C. The substrate used was carbon-doped silica coated glass, and no hydrogen sulfide was admitted to the system. The resulting films were yellow in colour. These were investigated by X-ray diffraction and Raman microscopy. The X-ray diffraction pattern of the film deposited at 400 °C is shown in Figure 5.1 and the Raman spectrum of the same film is given in Figure 5.2.

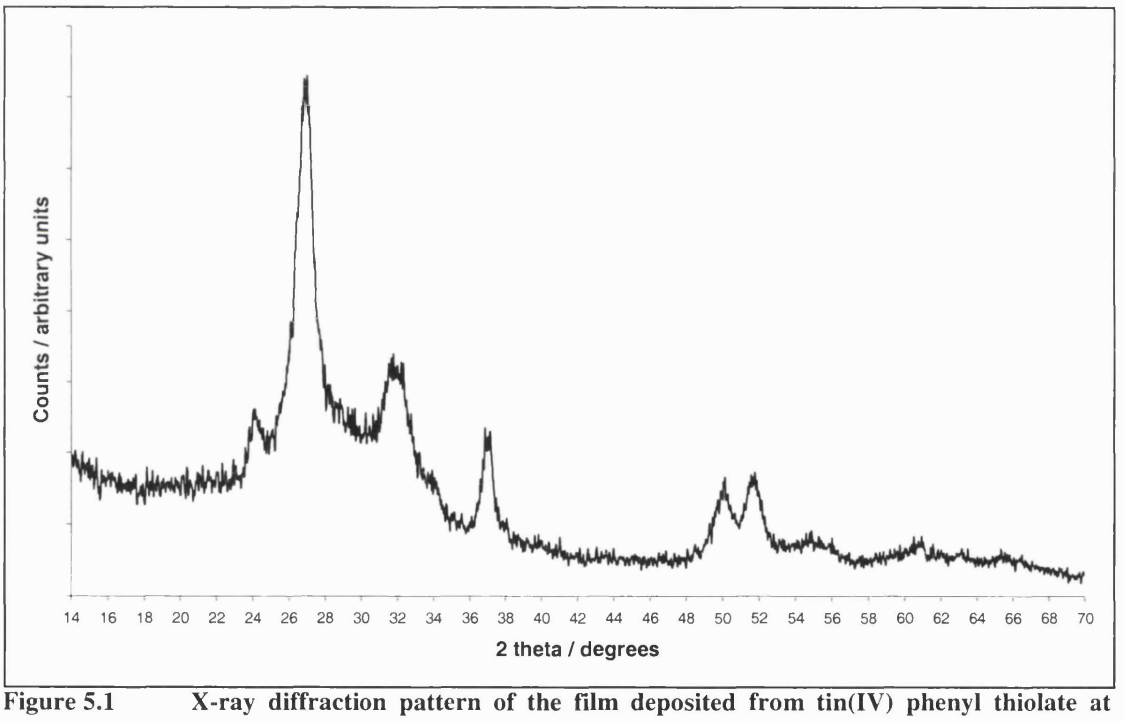


**Figure 5.1 X-ray diffraction pattern of the film deposited from tin(IV) phenyl thiolate at 400 °C.**

Both Figure 5.1 and Figure 5.2 bear no resemblance to any of the tin sulfide reference X-ray diffraction patterns and Raman patterns in Figures 2.4 and 2.6 respectively. Comparison with Figures 2.5 and 2.7 showed that both the X-ray diffraction and Raman data were consistent with the film being tin(II) tin(IV) oxide ($Sn_3O_4$).

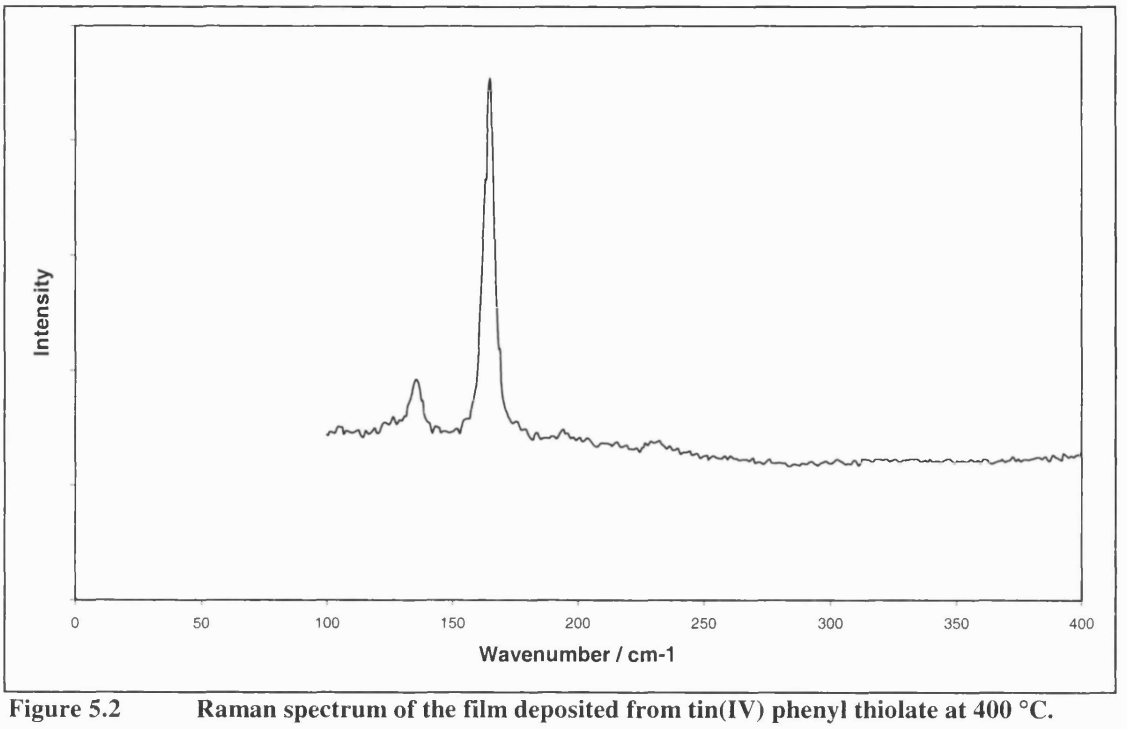


**Figure 5.2** **Raman spectrum of the film deposited from tin(IV) phenyl thiolate at 400 °C.**

Further reactions were carried out at University College, using tin(IV) phenyl thiolate and hydrogen sulfide. Many of these were successful. The full details of all reactions carried out and the visual appearances of the resulting films are listed in Table 5.1.

**Table 5.1** **Reaction conditions for the CVD reaction of tin(IV) phenyl thiolate.**

| Coater temperature (°C) | Solvent | Hydrogen sulfide ($dm^3min^{-1}$) | Visual appearance |
|---|---|---|---|
| 400 | Acetone | 0.2 | Thin, yellow |
| 405 | Hexane | 0.4 † | Thin, yellow |
| 448 | Hexane | 0.4 † | Yellow |
| 454 | $CHCl_3$ | 0.2 | Grey & brown |
| 502 | Hexane | 0.4 † | Thin, grey |
| 550 | Hexane | 0 | Grey |
| 550 | Acetone | 0.4 † | Grey |
| 550 | $CHCl_3$ | 0 | Thin, brown |
| 550 | $CHCl_3$ | 0.2 | Grey |

For the reactions marked †, hydrogen sulfide flowed through the reaction solution while the mist was being created. In the case of all other reactions, hydrogen sulfide did not meet the precursor until immediately prior to the reaction chamber. In the case of the reactions marked †, it is possible that a small amount of reaction occurred in the flask

where the aerosol was created. This may account for some of the differences in reaction product.

The films were too thin for investigation by X-ray diffraction.

### 5.2.1.1 Raman microscopy

Raman microscopy was carried out on all films. It was noted that in many cases the films were not of a single phase. Figure 5.3 shows the Raman spectra of films deposited at 450 and 500 °C with a hydrogen sulfide flow of 0.4 $dm^3min^{-1}$.

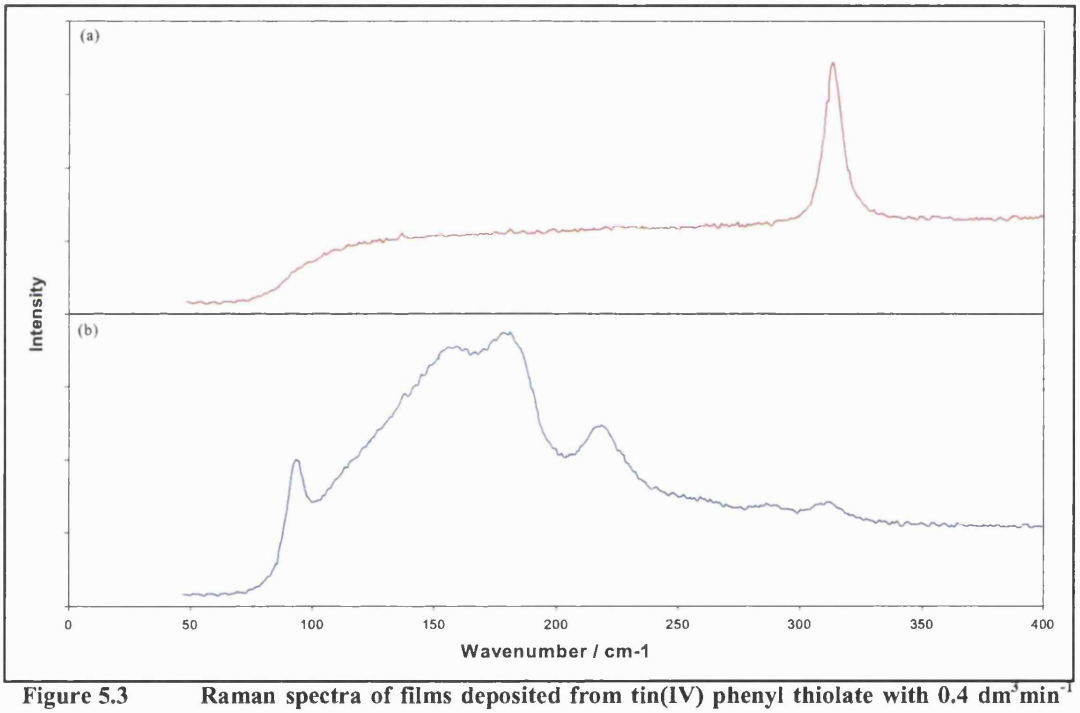


**Figure 5.3 Raman spectra of films deposited from tin(IV) phenyl thiolate with 0.4 $dm^3min^{-1}$ hydrogen sulfide at (a) 450 and (b) 500 °C.**

This shows that at 450 °C tin(IV) sulfide is the predominant phase formed, while at 500 °C a mixture is seen. At this higher temperature, the major phase is tin(II) sulfide, however a small band is observed at 310 $cm^{-1}$. This could be due to the major peaks of both tin(IV) sulfide and mixed valent $Sn_2S_3$.

Figure 5.4 shows the Raman spectra of films deposited at 400 and 450 °C with a 0.2 $dm^3min^{-1}$ flow of hydrogen sulfide. In these reactions hydrogen sulfide did not meet the tin(IV) phenyl thiolate until the reaction chamber, so there was no chance of the solution reacting prior to aerosol creation.

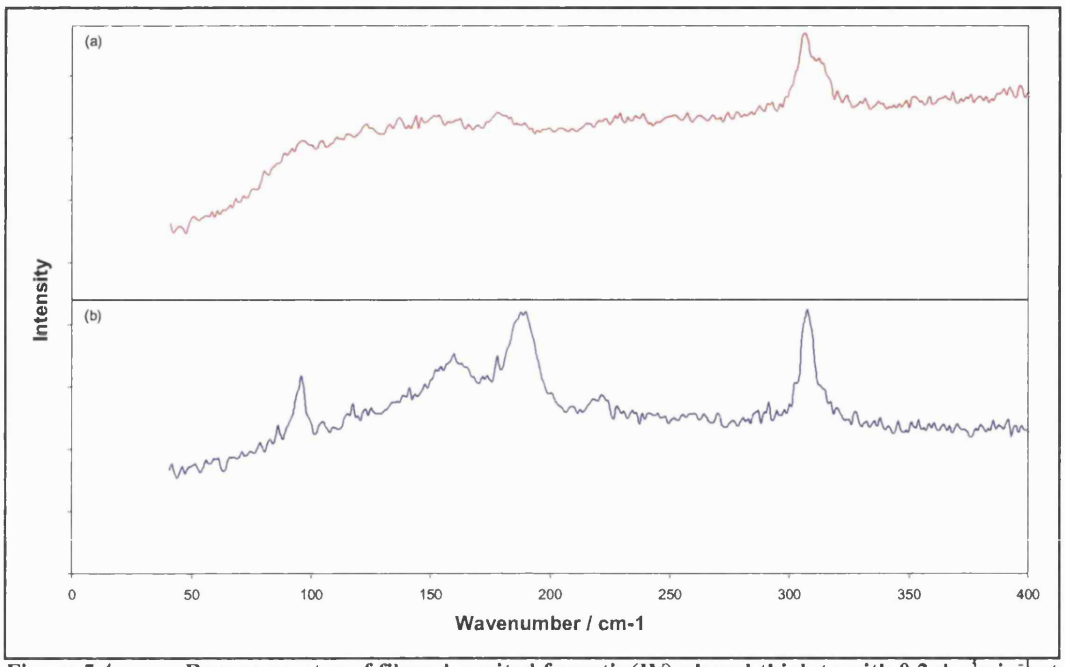


**Figure 5.4 Raman spectra of films deposited from tin(IV) phenyl thiolate with 0.2 $dm^3 min^{-1}$ at (a) 400 and (b) 450 °C.**

Figure 5.4 shows the same trend, of tin sulfides of lower oxidation states being available at higher temperatures. At 400 °C a mixture of tin(IV) sulfide and mixed valent tin(II) tin(IV) trisulfide is observed, while at 450 °C a mixture of tin(II) tin(IV) trisulfide and tin(II) sulfide is seen. A significant difference between Figures 5.3 and 5.4 is that mixed valent tin sulfide is more prominent when there was no pre-reaction of the precursor with $H_2S$ in the round-bottomed flask.

### 5.2.1.2 Energy dispersive analysis by X-rays

All films analysed were found to contain tin and sulfur. As the films were very thin much of the excitation volume contained glass. Some of the films were deposited on tin oxide / silica coated glass, so the tin in the undercoating interfered with the result. Other films, which were deposited on silica coated glass, were so thin that the calcium content in the underlying glass also interfered with the tin signal, but the tin to sulfur ratio was approximately 1:1.

#### 5.2.1.3 Scanning electron microscopy

The SEM image of the film deposited from tin(IV) phenyl thiolate with hydrogen sulfide at 500 °C from a hexane solution is shown in Figure 5.5. The substrate was tin oxide / silica coated glass. Small particles are observed, in discreet clusters.

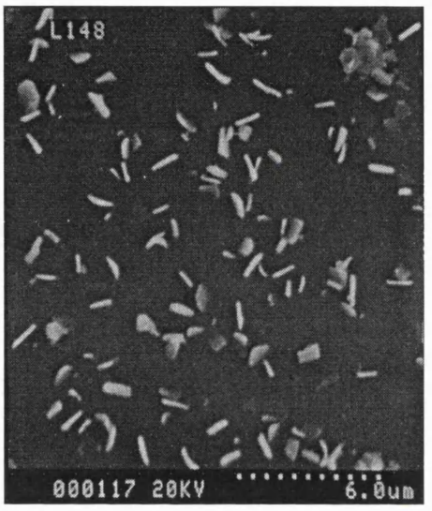


**Figure 5.5 SEM image of a film deposited from tin(IV) phenyl thiolate with hydrogen sulfide at 500 °C.**

## 5.2.2 Reactions of tin(IV) 2,2,2-trifluoroethane thiolate

Tin(IV) 2,2,2-trifluoroethane thiolate was found to have a boiling point of 35 °C. At room temperature it is a liquid. It was admitted to the reaction *via* a bubbler. Reactions were carried out without heating the bubbler. This meant that, as ambient temperatures in the room changed from day to day and throughout the day, the bubbler temperature ranged from 9 to 18 °C. Depositions were carried out over one or three minutes. Those carried out over three minutes were thick enough to analyse by X-ray diffraction.

A small number of reactions were carried out in the absence of hydrogen sulfide, but no film was deposited.

Reaction conditions are detailed in Table 5.2.

**Table 5.2 Reaction conditions for the reaction of tin(IV) 2,2,2-trifluoroethane thiolate.**

| | |
|---|---|
| Precursor temperature | 9 – 18 °C |
| Nitrogen flow rate through bubbler line | 0.5 $dm^3min^{-1}$ |
| Nitrogen flow rate diluting line from bubbler | 10 $dm^3min^{-1}$ |
| $H_2S$ flow rate | 0.3 $dm^3min^{-1}$ |
| Nitrogen flow rate diluting $H_2S$ | 1.5 $dm^3min^{-1}$ |
| Substrate | Silica coated glass |
| Deposition time | 1 – 3 min |

### 5.2.2.1 Visual appearance of films

Films deposited at 300 and 400 °C were yellow in colour. The film deposited at 450 °C was mostly brown, but large areas of yellow film were apparent at the edges. The film deposited at 500 °C was predominantly brown. At 550 °C, a film was produced which had large regions of both grey and brown, the brown region being nearer the gas inlet of the reactor. The film deposited at 600 °C was grey in colour. No film was deposited at 200 °C.

### 5.2.2.2 X-ray diffraction

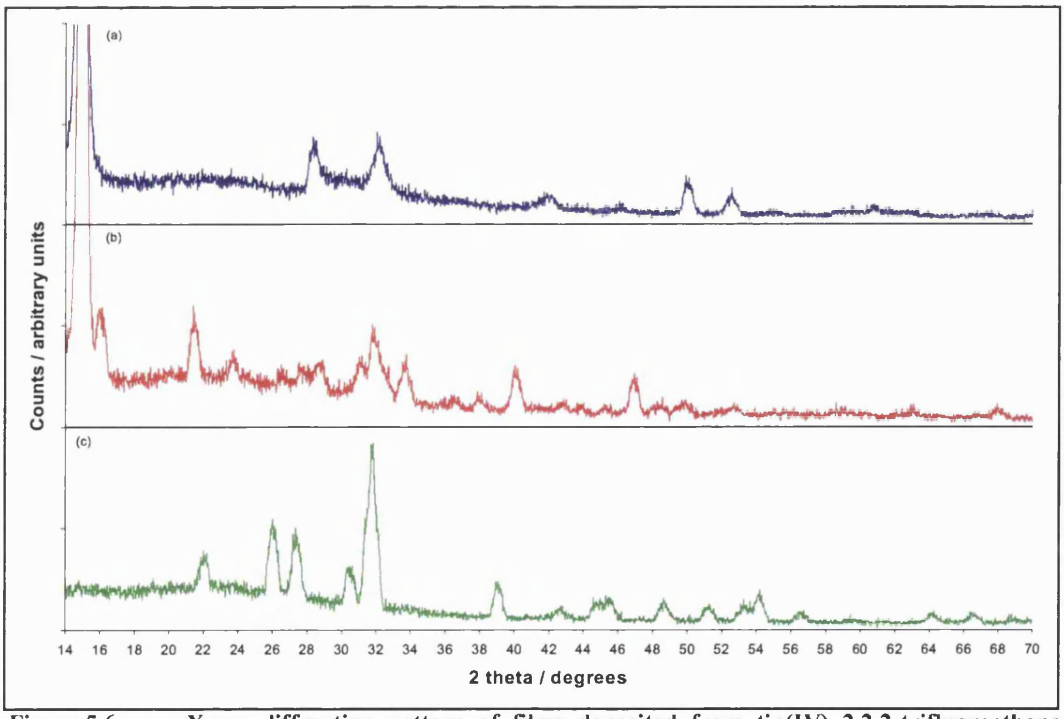


**Figure 5.6 X-ray diffraction pattern of films deposited from tin(IV) 2,2,2-trifluoroethane thiolate at (a) 400, (b) 450 and (c) 600 °C over 3 minutes.**

X-ray diffraction patterns were recorded for the films deposited at 400, 450 and 600 °C over 3 minutes. These are all shown in Figure 5.6.

Figure 5.6a shows the X-ray diffraction pattern of tin(IV) sulfide. The spectrum in Figure 5.6b is that of tin(II) tin(IV) trisulfide, although some tin(IV) sulfide is shown by the peak at 14 °. Figure 5.6c is the characteristic spectrum of tin(II) sulfide.

### 5.2.2.3 Raman microscopy

The Raman spectrum was recorded for all films. The films deposited at 300 and 400 °C both exhibited the pattern of tin(IV) sulfide. Figure 5.7 shows the Raman pattern of the film deposited with a substrate temperature of 400 °C.

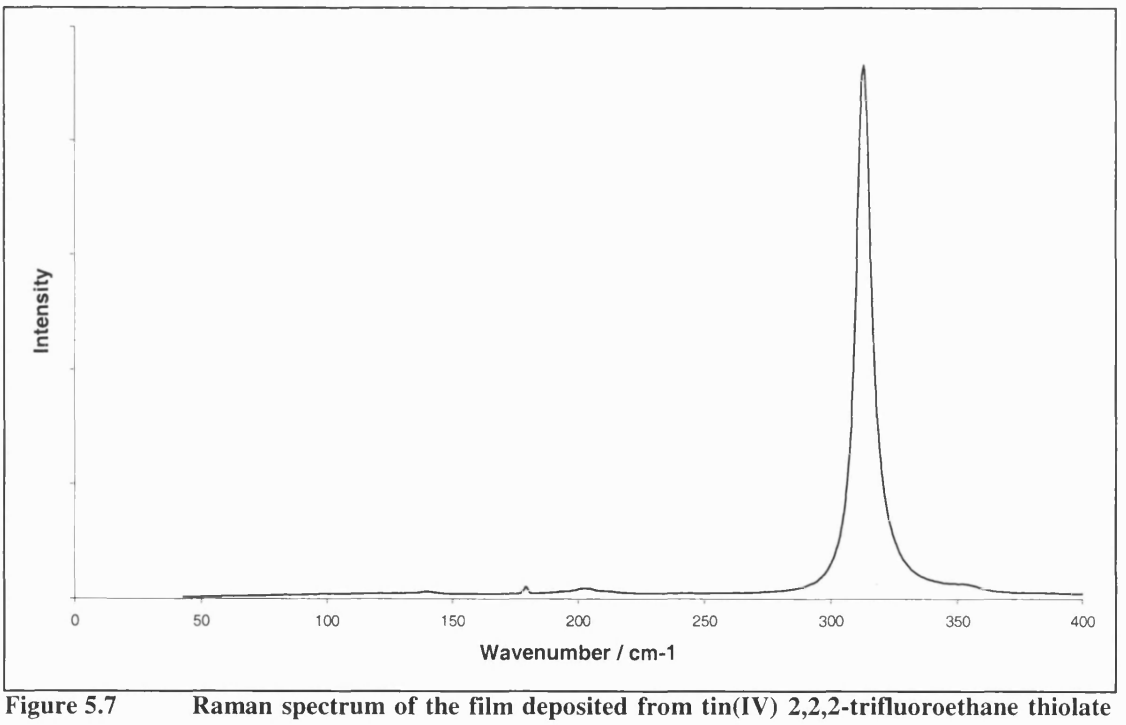


**Figure 5.7 Raman spectrum of the film deposited from tin(IV) 2,2,2-trifluoroethane thiolate with hydrogen sulfide at 400 °C.**

The film deposited at 450 °C was brown in colour, with a large amount of yellow film around the edges. The brown portion of the film was analysed by Raman to be tin(II) tin(IV) trisulfide and the yellow region tin(IV) sulfide. The film deposited at 500 °C showed that only $Sn_2S_3$ was present. This Raman spectrum is shown in Figure 5.8.

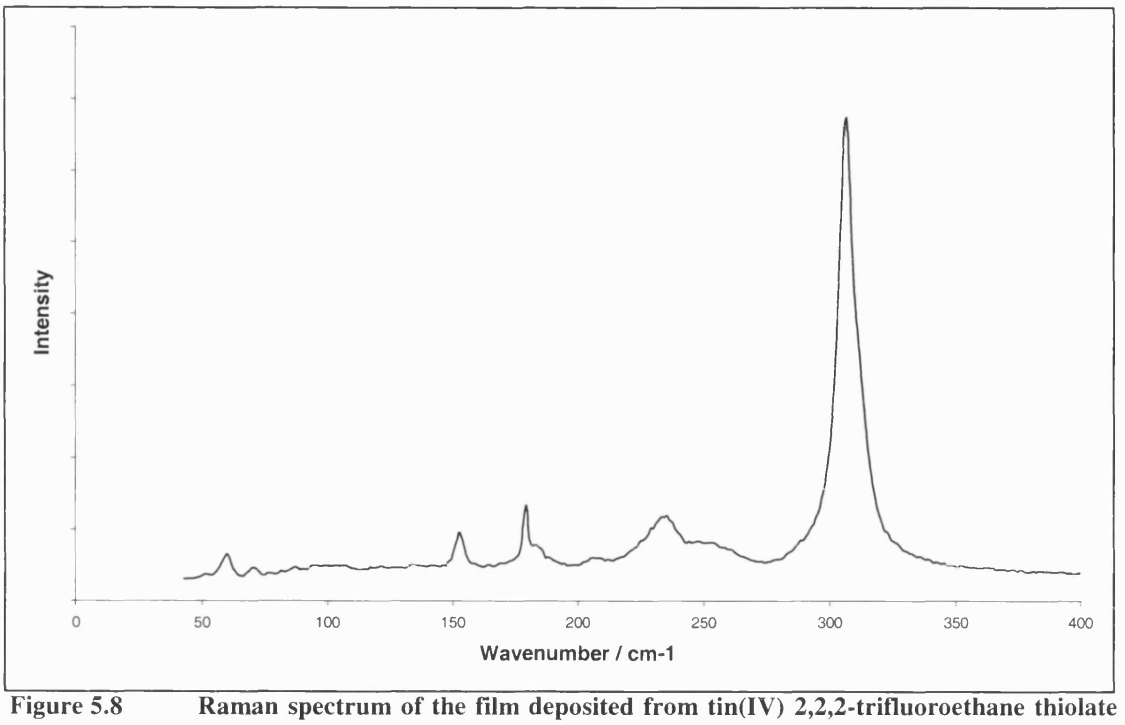


**Figure 5.8 Raman spectrum of the film deposited from tin(IV) 2,2,2-trifluoroethane thiolate with hydrogen sulfide at 500 °C.**

At 525 and 550 °C a mixture of tin(II) sulfide and mixed valent $Sn_2S_3$ is observed by Raman. In the film deposited at 550 °C two different regions were analysed separately, which showed the different Raman spectra. The Raman spectrum of the film deposited at 600 °C is shown in Figure 5.9. This shows that only the tin(II) sulfide phase is formed at this temperature.

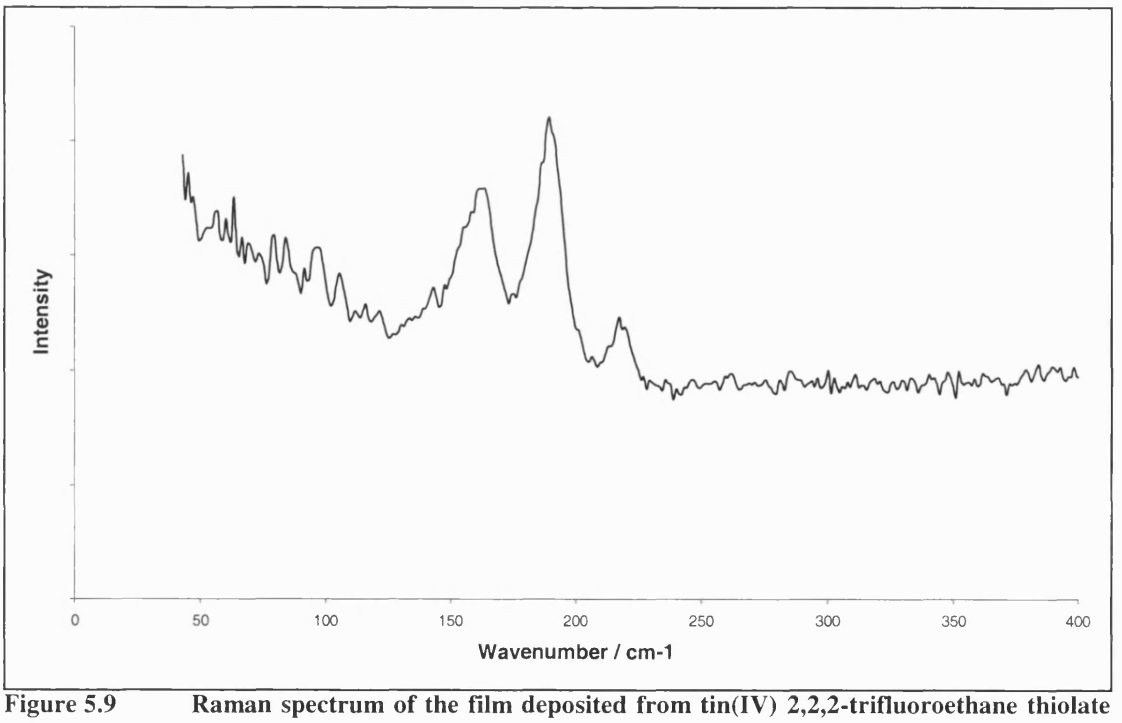


**Figure 5.9 Raman spectrum of the film deposited from tin(IV) 2,2,2-trifluoroethane thiolate with hydrogen sulfide at 600 °C.**

### 5.2.2.4 Energy dispersive analysis by X-rays

EDAX was carried out on all films. Although some breakthrough to the underlying glass occurred, the films were found to be much thicker than those deposited from tin(IV) phenyl thiolate. EDAX analysis of films deposited from tin(IV) 2,2,2-trifluoroethane thiolate showed approximately 20 – 30 % of the excitation volume to be tin and sulfur. In contrast, films deposited from tin(IV) phenyl thiolate showed a maximum of 10 % of the excitation volume to be tin and sulfur. A plot of tin to sulfur ratio as a function of temperature is given in Figure 5.10.

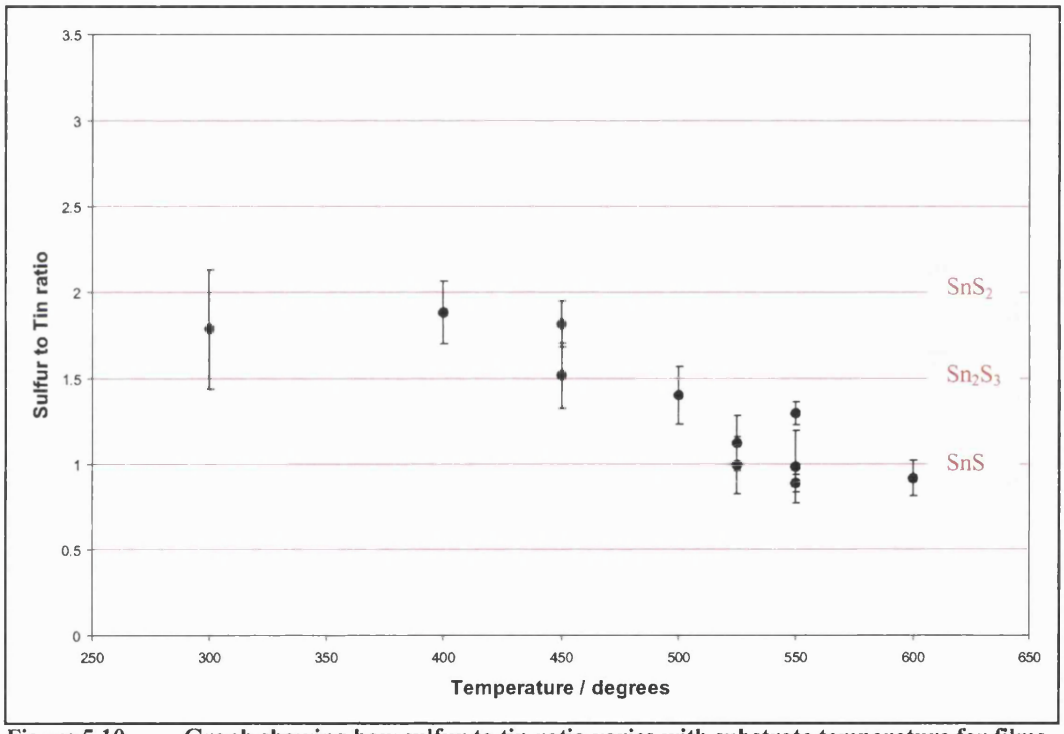


**Figure 5.10 Graph showing how sulfur to tin ratio varies with substrate temperature for films deposited from tin(IV) 2,2,2-trifluoroethane thiolate with hydrogen sulfide.**

Figure 5.10 is similar to Figure 3.8 which showed the variation of sulfur to tin ratio with substrate temperature for films deposited from tin tetrachloride with hydrogen sulfide. In both cases, there is a lower sulfur content in the films with increasing temperature.

In agreement with Figure 3.8, the sulfur to tin ratios shown in this section are not the ideal values of 1, 1.5 or 2 for tin(II) sulfide, tin(II) tin(IV) trisulfide and tin(IV) sulfide. However, in the case of films deposited from tin tetrachloride and hydrogen sulfide, sulfur content was high, whereas here sulfur content is low. This is because the

substrate used for the depositions from tin(IV) 2,2,2-trifluoroethane thiolate is silica coated glass and carbon-doped silica coated glass was used for the reactions of tin tetrachloride.

A further difference is in the presence of multiple phases after reaction of tin(IV) 2,2,2-trifluoroethane thiolate with hydrogen sulfide. This could be a function of the precursor, or the substrate.

#### 5.2.2.5 Scanning electron microscopy

SEM images were obtained for all films. Figure 5.11 shows a representative sample of these.

Figure 5.11a shows the film deposited at 400 °C. Figures 5.11b and 5.11c are two different regions of the film deposited at 450 °C – 5.11b being the yellow area at the edge and 5.11c the brown area in the middle. Figure 5.11d is the SEM image of the film deposited at 500 °C. Figures 5.11e and 5.11f show the images of the film deposited at 550 °C, 5.11e being the brown area nearer the inlet to the reactor and 5.11f the grey area further along the reactor bed. Figure 5.11g shows the film deposited at 600 °C.

The films depicted in Figures 5.11a and 5.11b were analysed by Raman to be tin(IV) sulfide. Here, they exhibit ill-defined, needle-like particles. Films that were analysed by Raman to be mixed valent tin sulfide are shown in Figures 5.11c, 5.11d and 5.11e. All have long needle crystals, which are longer and thicker with increasing deposition temperature (5.11c → 5.11d → 5.11e). The films shown in Figures 5.11f and 5.11g were both shown to be tin(II) sulfide by Raman. The morphology of the two is the same, however it is clear from the SEM images that the film deposited at 600 °C has a poorer surface coverage than that deposited at 550 °C.

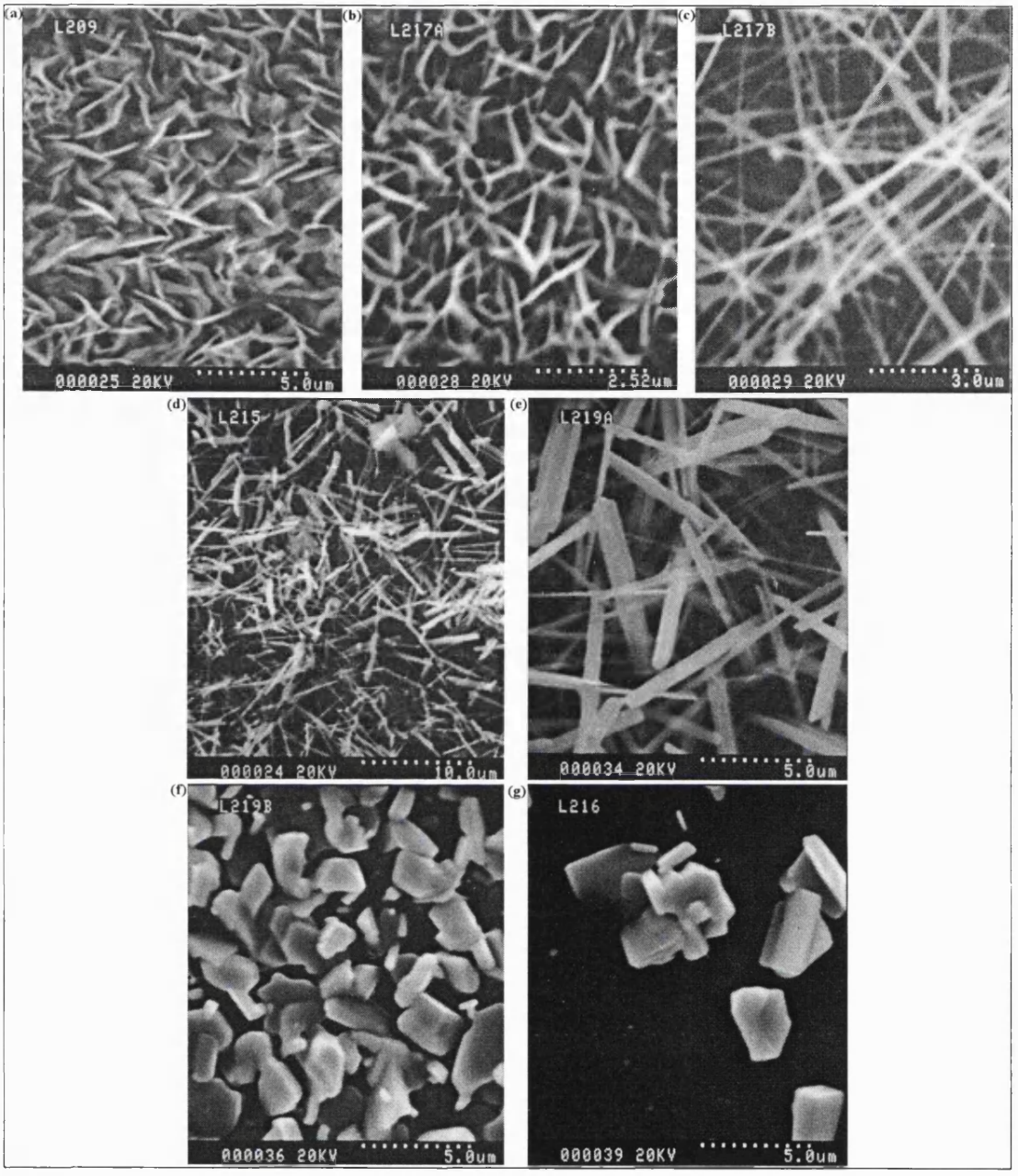


**Figure 5.11 SEM images of films deposited from tin(IV) 2,2,2-trifluoroethane thiolate. (See previous paragraph for details.)**

## 5.2.3 Reactions of tin(IV) $\eta^2$-ethane 1,2 dithiolate

Tin(IV) $\eta^2$-ethane 1,2 dithiolate was investigated by Differential Scanning Calorimetry and Thermal Gravimetric Analysis. These methods showed that it melted at 101 °C and decomposed at *ca.* 180 °C. TGA also showed decomposition consistent with a mass similar to that of two sulfur atoms, or a $CH_2CH_2S$ moiety being lost at 180 °C and a

further decomposition to $SnS_2$ at 250 °C. Considering these observations, this precursor would be unsuitable for bubbler delivery, but aerosol delivery might be appropriate.

In each reaction 0.1 g of the precursor was dissolved in acetone, 50 $cm^3$. The reactions were allowed to run until the entire precursor in the round-bottomed flask had been used up. Hydrogen sulfide, if used in the reaction, did not meet the precursor until immediately prior to the reaction chamber. Films were deposited onto silica coated glass.

Reactions were carried out at temperatures from 350 – 600 °C with a 0.2 $dm^3min^{-1}$ flow of hydrogen sulfide. Reactions were also carried out without hydrogen sulfide at temperatures from 350 – 600 °C.

The films were all too thin for analysis by X-ray diffraction.

#### 5.2.3.1 Visual appearance of films

The films deposited with a hydrogen sulfide flow of 0.2 $dm^3min^{-1}$ exhibited varying colours with substrate temperature. The film deposited at 350 °C was yellow in colour, that deposited at 400 ° C was brown and those deposited at 500 and 550 ° C were grey. No film was laid down when the substrate temperature was 600 °C. In the absence of hydrogen sulfide films could not be deposited at 350 °C or at 600 °C. All films produced at 400 – 550 °C were grey.

#### 5.2.3.2 Raman microscopy

Raman spectra were recorded for all films. The spectra of the films deposited with a 0.2 $dm^3min^{-1}$ flow of hydrogen sulfide are shown in Figure 5.12.

Figure 5.12 shows that the film deposited at 350 °C is tin(IV) sulfide, that deposited at 400 °C is tin(II) tin(IV) trisulfide and that deposited at 500 °C is tin(II) sulfide. This is in agreement with all other results that higher temperatures lead to accessibility of the +2 oxidation state.

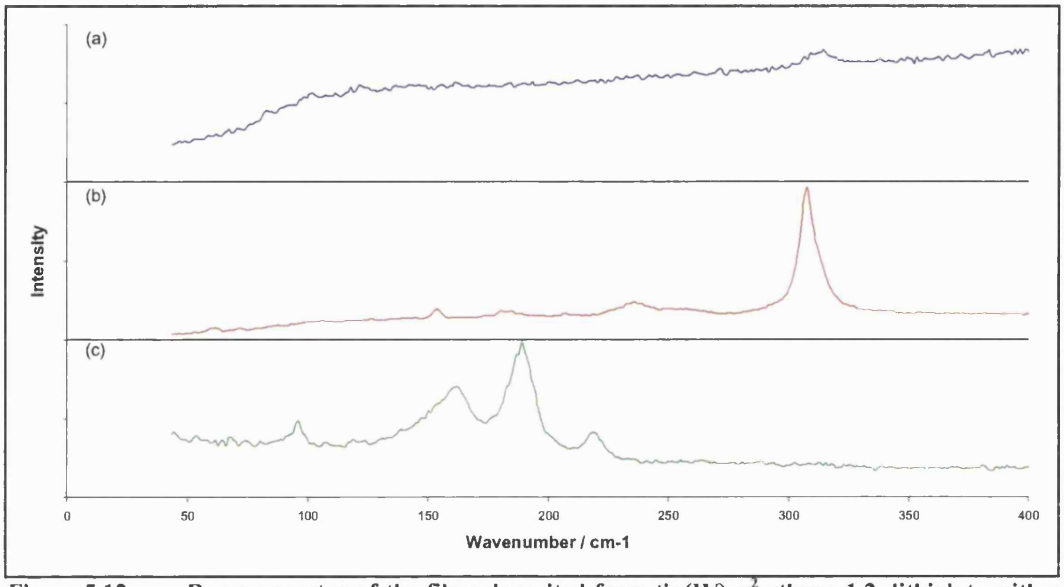


**Figure 5.12 Raman spectra of the films deposited from tin(IV) $\eta^2$-ethane 1,2-dithiolate with a 0.2 $dm^3min^{-1}$ flow of hydrogen sulfide at (a) 350, (b) 400 and (c) 500 °C.**

Figure 5.13 shows Raman spectra of films deposited from tin(IV) $\eta^2$-ethane 1,2-dithiolate without hydrogen sulfide. In contrast with other results in this series, temperature has no effect on the phase deposited.

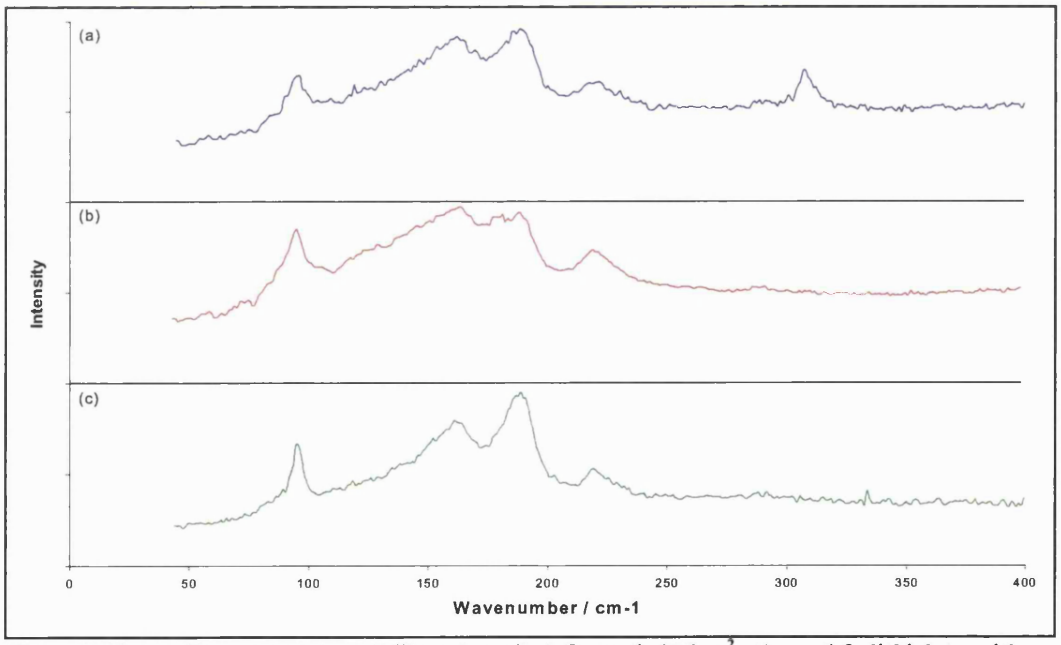


**Figure 5.13 Raman spectra of films deposited from tin(IV) $\eta^2$-ethane 1,2-dithiolate with no hydrogen sulfide at (a) 400, (b) 450 and (c) 500 °C.**

Figures 5.12 and 5.13 demonstrate that the hydrogen sulfide plays an important role in which phase is deposited. When hydrogen sulfide is present, all phases of tin sulfide are accessible, whereas in its absence only tin(II) sulfide may be deposited.

### 5.2.3.3 Energy dispersive analysis by X-rays

The films were all very thin, and EDAX showed a large amount of the underlying glass. Tin and sulfur were observed in all films, although a maximum of just 5 % of the excitation volume was made up of these two elements. As calcium in the underlying glass interfered with the tin signal all films appear to contain more tin that sulfur. This meant that accurate elemental ratios could not be obtained, however EDAX indicated that ratios were near 1:1

### 5.2.3.4 Scanning electron microscopy

Images were obtained from all films deposited. A representative selection of these is shown in Figure 5.14.

Figure 5.14a shows the image of the film deposited at 350 °C with 0.2 $dm^3min^{-1}$ flow of hydrogen sulfide. Small particles are seen. The familiar image of interlocking plates is observed in the film deposited at 400 °C with 0.2 $dm^3min^{-1}$ hydrogen sulfide, depicted in Figure 5.14b. Figure 5.14c shows the film deposited at 500 °C with 0.2 $dm^3min^{-1}$ hydrogen sulfide. Small square plates are observed in this image, some of which are interlocking.

Figures 5.14d, 5.14e, 5.14f and 5.14g show images of the films deposited without hydrogen sulfide in the reaction chamber. The deposition temperatures of these films were 400, 450, 500 and 550 °C respectively. Two observations may be made. The first is that with increasing deposition temperature the morphology of the particles becomes more regular. The second observation is that low temperature and high temperature conditions lead to lower surface coverage. This is due to lower reaction rate at lower temperatures. Looking at the particle sizes in the films, higher temperature conditions lead to large particle sizes. It is possible that at 550 °C nucleation is low and surface migration high. This would lead to a smaller number of larger particles, with larger spaces between them.

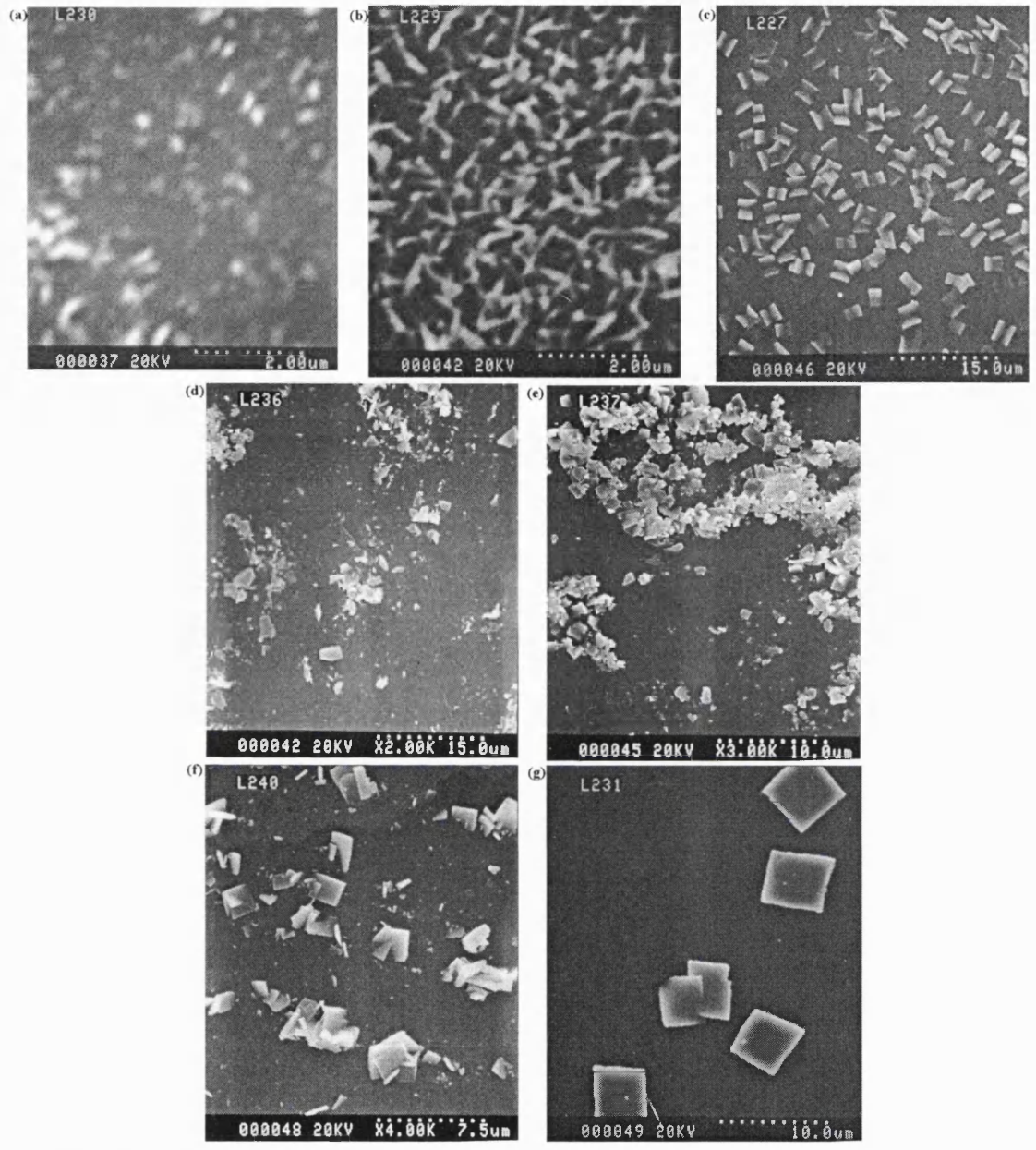


**Figure 5.14** **SEM images of the films deposited from tin(IV) $\eta^2$-ethane 1,2-dithiolate. (See previous paragraph for details.)**

## 5.2.4 Conclusions

Certain tin(IV) thiolates may provide useful precursors to the CVD formation of tin sulfides. Of those studied, each had advantages and disadvantages. Homoleptic alkyl and aryl thiolates investigated turned out to yield tin oxides in the absence of hydrogen sulfide and the entire range of tin sulfides when hydrogen sulfide was admitted. This has been reported previously for the case of indium sulfide being deposited from $Bu_2InS^iPr$.[110] If 99.999 % argon was used as the carrier gas, $In_2S_3$ could be produced,

but lower purity gases led to the formation of $In_2O_3$. Formation of the oxide was due to there being water in the carrier gas.

Use of a fluorinated thiolate allowed the bubbler delivery method to be used. The precursor, tin(IV) 2,2,2-trifluoroethane thiolate, was as volatile at room temperature as tin tetrachloride at 70 °C. This allowed thick films to be deposited over much shorter timescales than other thiolate precursors. All phases of tin sulfide were accessible, and films thick enough to investigate by X-ray diffraction could be produced.

Although neither of the other two precursors investigated could produce a film without hydrogen sulfide being present, the chelating tin(IV) $\eta^2$-ethane 1,2-dithiolate deposited tin(II) sulfide when no $H_2S$ was used. The precursor could only be used with the aerosol method of delivery, as it was involatile. No forms of tin oxide were observed in the Raman, and the EDAX ratio was consistent with tin sulfide being the major component. This was despite undried acetone being used as the solvent.

A reason why neither tin(IV) phenyl thiolate nor tin(IV) 2,2,2-trifluoroethane thiolate could produce tin sulfide in the absence of hydrogen sulfide came to light when tin(IV) phenyl thiolate was analysed by mass spectroscopy. No tin containing species were observed in the EI mass spectrum. The major species observed were PhS and PhSSPh fragments. This result agrees with observations made from the thermal decomposition study. Tin(IV) phenyl thiolate was heated to 200 °C for 2 hr, and the resulting powder analysed by Mössbauer. A tin(II) species, with parameters similar to those of tin(II) phenyl thiolate, and a small amount of tin(IV) oxide were observed. Further heating led to decrease of the tin(II) signal and increase of the tin oxide signal.

From these results, it is likely that the first step of the CVD reaction involves decomposition of the precursor accompanied by loss of RSSR. A further RSSR entity may be lost, leaving an active tin species, which, in the presence of water in the carrier gas, yields tin oxide. If hydrogen sulfide was also present in the system, tin oxide will react to form tin sulfide as was reported in Section 3.3.9.

In the case of tin(IV) $\eta^2$-ethane 1,2-dithiolate, loss of a RSSR entity is unlikely. To lose one of the ligands in this fashion would result in an unstable 4-membered SCCS ring

being formed. If a bond was formed between sulfur atoms from the two different ligands, they would still be locked to the tin atom and may revert anyway.

It is interesting that only tin(II) sulfide is formed from the AACVD reaction of $[\overline{Sn(-SCH_2CH_2S)}_2]$ when no hydrogen sulfide is present. If the TGA of tin(IV) $\eta^2$-ethane 1,2-dithiolate is studied, it appears that a group corresponding to the mass of $CH_3CHS$ is lost. This would leave $[(\overline{SCH_2CH_2S-)Sn}=S]$. At higher temperatures in the CVD reactor, the second ligand may be lost in its entirety. It may react with water in the nitrogen carrier, or may undergo internal rearrangement, but the stronger tin-sulfur double bond would remain intact. This resulting species $SnS_{(g)}$, on reaching the surface, may be adsorbed and form a tin sulfide film. As tin(II) sulfide is the most useful of all the phases in terms of electronic applications, a route to the single phase compound is very useful.

## 5.3 Reactions and results of homoleptic tin(II) thiolates

Many homoleptic tin(II) thiolates were prepared by the method outlined in section 5.1.2. It was found that almost all of them were polymeric. As polymeric compounds their melting and boiling points were very high, so bubbler delivery was impossible. Also, they were insoluble in all of the solvents tried.

Polymerisation came about because the coordination sphere around the tin atom was not full. Each tin atom became 4-coordinate, with bridging thiolate groups between. It was speculated that, if the thiolate group around the tin atom was very large, polymerisation would not be possible and the monomeric form of the molecule would prevail. With this in mind, a triphenyl methane thiolate was produced. Four of these very bulky groups are unlikely to fit around a tin atom, so polymerisation would be prohibited and the molecule may be volatile or soluble.

It transpired that the molecule was indeed monomeric, but the bulky groups also led to high melting and boiling points along with low volatility. It was, however, soluble in

tetrahydrofuran and toluene. The compound was air- and moisture-sensitive, so had to be handled in a glove box. Dried, degassed solvents were used for all reactions.

#### 5.3.3.1 Reactions carried out

Reactions were carried out using the aerosol delivery method. Some reactions were carried out in tetrahydrofuran, but polymerisation of this in the heated section of pipe immediately prior to the reaction chamber led to blockages. Therefore, toluene was selected as a more appropriate solvent. In all reactions, 0.1 g of the precursor was dissolved in 50 $cm^3$ of the solvent.

Reactions were carried out with 0.2 $dm^3min^{-1}$ hydrogen sulfide at temperatures of 400, 500 and 575 °C. The substrate used was silica coated glass, and depositions lasted until all the precursor had been used up.

Unfortunately, none of the reactions produced a film.

## 5.4 Reactions and results of homoleptic tin(IV) dithiocarbamates

Two homoleptic dithiocarbamate precursors were investigated. These were $[Sn(S_2CNR_2)_4]$ where R=Me, Et. Both were solids at room temperature. Differential scanning calorimetry was carried out to determine suitability of these as CVD precursors, and it was found that the boiling points were prohibitively high. With this in mind, the precursor was admitted using the aerosol delivery method. A small number of reactions were carried out using $[Sn(S_2CNMe_2)_4]$ and the bubbler delivery method, but volatility problems made these unsuccessful.

## 5.4.1 Reactions carried out

Reactions involving $[Sn(S_2CNEt_2)_4]$ were carried out at three temperatures – 350, 450 and 520 °C. $[Sn(S_2CNEt_2)_4]$, 0.3 g, was dissolved in chloroform, 50 $cm^3$, and admitted using the humidifier. No hydrogen sulfide was used in any reaction, and reactions were carried out until the entire precursor had run out (typically 30 min). Tin oxide / silica coated glass was used as the substrate.

For methodology of reaction, refer to Section 2.1, particularly 2.1.3 for aerosol modifications.

## 5.4.2 Visual appearance of films

The films deposited from $[Sn(S_2CNEt_2)_4]$ using the aerosol delivery method at 450 and 520 °C coated only the first *ca.* 10 cm of the substrate. Films were thin and grey in colour. No film was deposited at 350 °C.

## 5.4.3 Raman microscopy

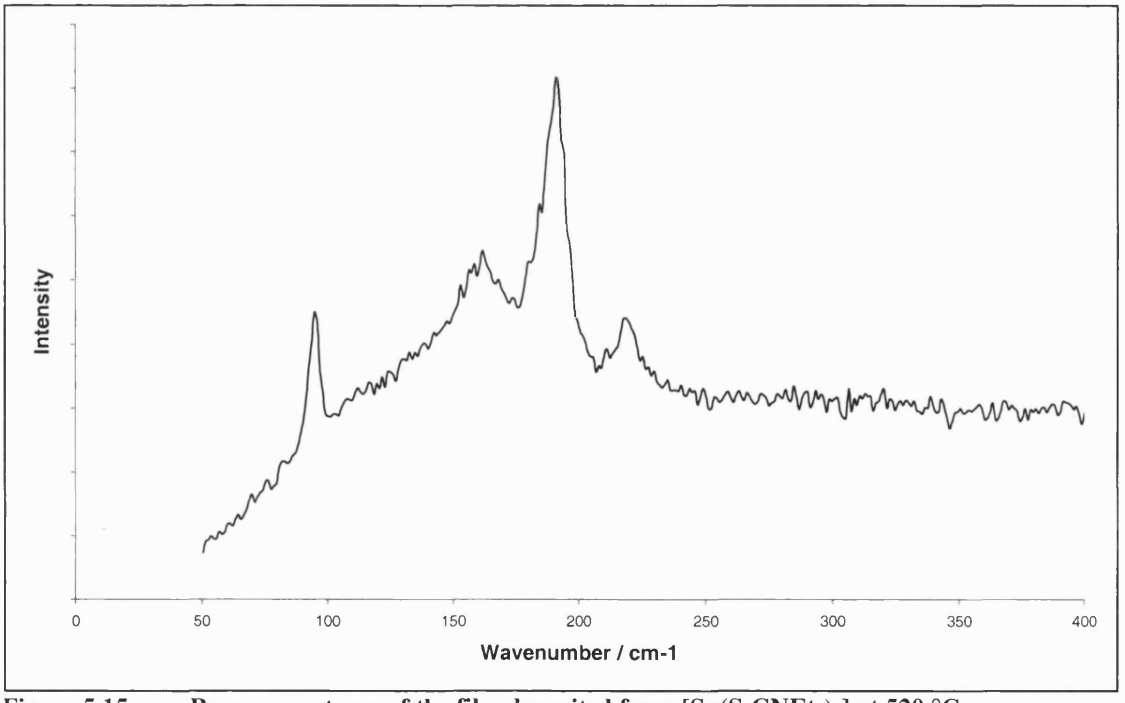


**Figure 5.15 Raman spectrum of the film deposited from $[Sn(S_2CNEt_2)_4]$ at 520 °C.**

The Raman spectra of films deposited from $[Sn(S_2CNEt_2)_4]$ were recorded. The spectrum of the film deposited at 520 °C is shown in Figure 5.15.

Figure 5.15 shows the characteristic Raman spectrum of tin(II) sulfide. The spectrum recorded from the film deposited at 450 °C shows the same pattern.

## 5.4.4 Energy dispersive analysis by X-rays

EDAX measured the elemental ratio for both the films deposited. As the films were deposited on tin oxide / silica coated glass, elemental ratios were found to be tin rich. Sulfur was observed in the films, although at low levels. Accurate tin to sulfur ratios could not be determined.

## 5.4.5 Scanning electron microscopy

SEM showed that the films were not uniform. Images of each of the films deposited from $[Sn(S_2CNEt_2)_4]$ are given in Figure 5.16. These show that the film is deposited in large clusters of particles. Underneath the particles no morphology is observed, so it was thought that this is uncoated glass.

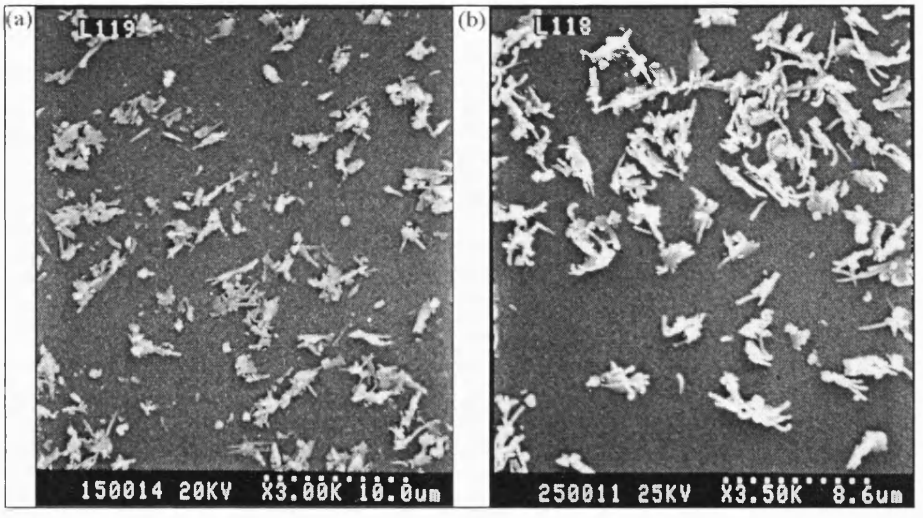


**Figure 5.16 SEM images of films deposited from $[Sn(S_2CNEt_2)_4]$ at (a) 450 and (b) 520 °C.**

### 5.4.6 Conclusions

In this section, only a small number of films were attempted. Only those reactions using the aerosol delivery method could deposit a film. This was due to involatility of the precursor.

Films were only attempted without hydrogen sulfide. This led to only tin(II) sulfide being deposited, although the precursor contained tin(IV). This is in accordance with observations made in Section 5.2.3.

Films were deposited on tin oxide / silica coated glass. This meant that accurate data from EDAX could not be obtained, although sulfur was observed in the films. The morphology of the films was dissimilar to that observed using other precursors. Using a different substrate is an important factor in this observation.

## 5.5 Reactions and results of alkyl tin dithiocarbamates

A number of precursors were used in this section with varying degrees of success. $[R_3Sn(S_2CNR'_2)]$ R=Me, $^n$Bu; R'=Me, Et were all used with both the bubbler and aerosol delivery methods. Although aerosol delivery was successful, no film was formed with any precursor using the bubbler delivery method. The more volatile asymmetric dithiocarbamate precursors $[Me_3SnS_2CNMeBu]$ and $[BuSn(S_2CNMeBu)_3]$ were also used with the bubbler delivery method.

## 5.5.1 Reactions of the asymmetric dithiocarbamate [$Me_3SnS_2CNMeBu$] with hydrogen sulfide *via* bubbler delivery method

### 5.5.1.1 Reactions carried out

Using asymmetric dithiocarbamate groups in the precursor leads to lower boiling points. Consequently, reactions of [$Me_3SnS_2CNMeBu$] were carried out using the bubbler delivery method. Reactions were carried out with a bubbler temperature of *ca.* 90 °C. 0.5 $dm^3min^{-1}$nitrogen flowed through the bubbler and this was diluted by 10 $dm^3min^{-1}$ of nitrogen. 0.3 $dm^3min^{-1}$ hydrogen sulfide was used in all reactions and this was diluted by a nitrogen flow of 1.5 $dm^3min^{-1}$. Reactions were carried out over 15 minutes and silica coated glass was used as the substrate. Substrate temperatures in the range 450 – 600 °C were used at intervals of 50 degrees.

### 5.5.1.2 Visual appearance of films

The bubbler delivery reactions of the asymmetric dithiocarbamate [$Me_3SnS_2CNMeBu$] led to brown films at 450 °C. At 500 and 550 °C grey films were deposited, although the higher temperature led to a thinner film. No film was deposited at 600 °C.

### 5.5.1.3 Raman microscopy

Of the reactions carried out using the asymmetric dithiocarbamate precursor, [$Me_3SnS_2CNMeBu$], with hydrogen sulfide, most spectra recorded showed the familiar pattern of tin(II) sulfide. No film was deposited at the highest temperature of 600 °C, while at 450 °C $Sn_2S_3$ was the predominant component of the film. At 500 and 550 °C SnS was the major component.

### 5.5.1.4 Energy dispersive analysis by X-rays

Films deposited from [$Me_3SnS_2CNMeBu$] were on silica coated glass. Here, near 1:1 ratios of tin to sulfur were detected, with the film deposited at 450 °C showing a slightly

higher sulfur content. This agrees with the Raman result, where tin(II) tin(IV) trisulfide was observed as the major phase along with a small amount of tin(II) sulfide.

### 5.5.1.5 Scanning electron microscopy

Figure 5.17 shows a selection of SEM images recorded from films deposited from the AACVD reaction of [$Me_3SnS_2CNMeBu$] with hydrogen sulfide.

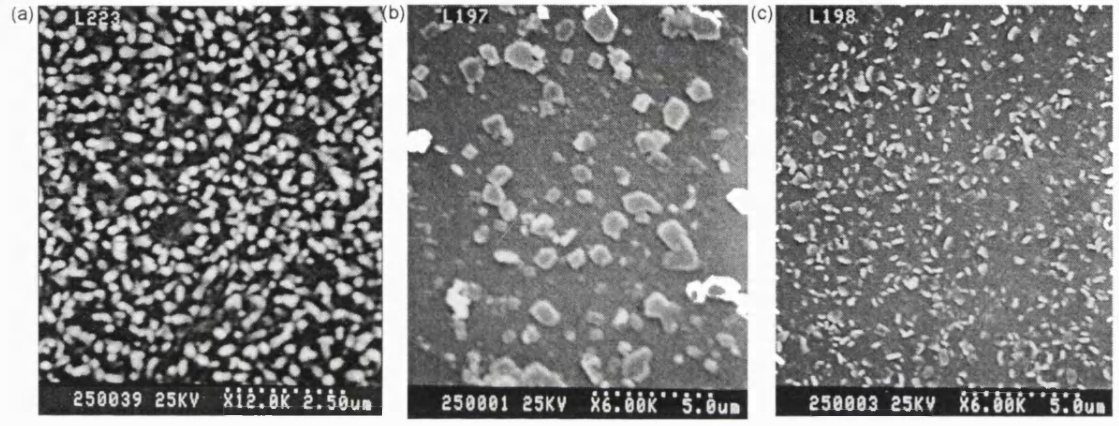


**Figure 5.17 SEM images of films deposited from the reaction of [$Me_3SnS_2CNMeBu$] with 0.2 $dm^3min^{-1}$ at (a) 450 °C, (b) 500 °C and (c) 550 °C.**

Figure 5.17a shows that at 450 °C small particles are deposited (typically 0.1 - 0.2 μm). The Raman data indicated that the films deposited at 500 and 550 °C were a different material from that deposited in the reaction at 450 °C. With this in mind, comparison of Figures 5.17b and 5.17c show that increasing deposition temperature leads to more particles, of a smaller size. This implies that nucleation is increased, and that either growth rate decreases or amount of material in the reaction chamber limits the size of the particles.

### 5.5.1.6 Conclusions

[$Me_3SnS_2CNMeBu$] was found more volatile than a number of other alkyl dithiocarbamates studied in this section. It could be admitted to the CVD system using the bubbler delivery method. A number of reactions were carried out with the substrate temperature in the range 450 to 600 °C. At 450 °C the predominant phase was found to be mixed valent tin(II) tin(IV) trisulfide. A small amount of tin(II) sulfide was also observed. At 500 and 550 °C tin(II) sulfide was the phase deposited, while no film was laid down at 600 °C. This is in accordance with work carried out in Chapter 3, where

films deposited at higher substrate temperatures consisted of tin in a lower oxidation state.

## 5.5.2 Reactions of $[Me_3SnS_2CNMe_2]$ *via* aerosol delivery method

### 5.5.2.1 Reactions carried out

Reactions of $[Me_3SnS_2CNMe_2]$ were carried out dissolving 0.25 g of the precursor in 50 ml acetone. A flow of 1 $dm^3min^{-1}$ nitrogen passed through the round bottomed flask above the humidifier during reaction. The reaction was run until the entire precursor was used up (typically 20 min). No hydrogen sulfide was used in reactions. Substrate temperatures were between 400 and 600 °C and tin oxide / silica coated glass was used as the substrate.

### 5.5.2.2 Visual appearance of films

The reactions of $[Me_3SnS_2CNMe_2]$ as a solution in acetone using the aerosol delivery method deposited films at 500 and 550 °C. No film was observed at 400 °C. Brown and grey films were deposited at both 500 and 550 °C.

### 5.5.2.3 Raman microscopy

Films deposited from $[Me_3SnS_2CNMe_2]$ using the aerosol delivery method and no hydrogen sulfide showed two different spectra. Figure 5.18 shows spectra recorded from films deposited at 500 and 550 °C under these conditions.

Figure 5.18 shows that the film deposited at 500 °C from $[Me_3SnS_2CNMe_2]$ using the aerosol delivery method and no hydrogen sulfide does not depict a tin sulfide. The film deposited at 550 °C from the same precursor gives tin(II) sulfide.

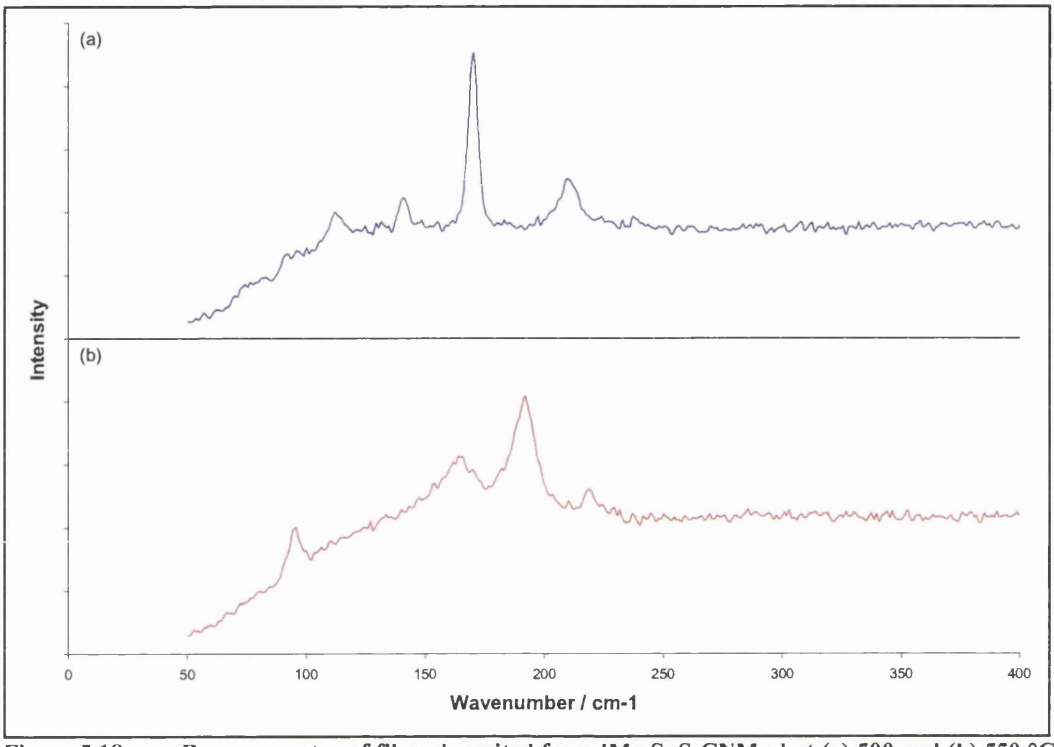


**Figure 5.18 Raman spectra of films deposited from [$Me_3SnS_2CNMe_2$] at (a) 500 and (b) 550 °C with no hydrogen sulfide on tin oxide / silica coated glass using the aerosol delivery method.**

### 5.5.2.4 Energy dispersive analysis by X-rays

In the case of films deposited from [$Me_3SnS_2CNMe_2$] without hydrogen sulfide using the aerosol delivery method, sulfur contents were all too low to be detected. Tin was observed, but this was due to tin oxide precoating on the substrate.

### 5.5.2.5 Scanning electron microscopy

Figure 5.19 shows a selection of SEM images recorded from films deposited from the reaction of [$Me_3SnS_2CNMe_2$].

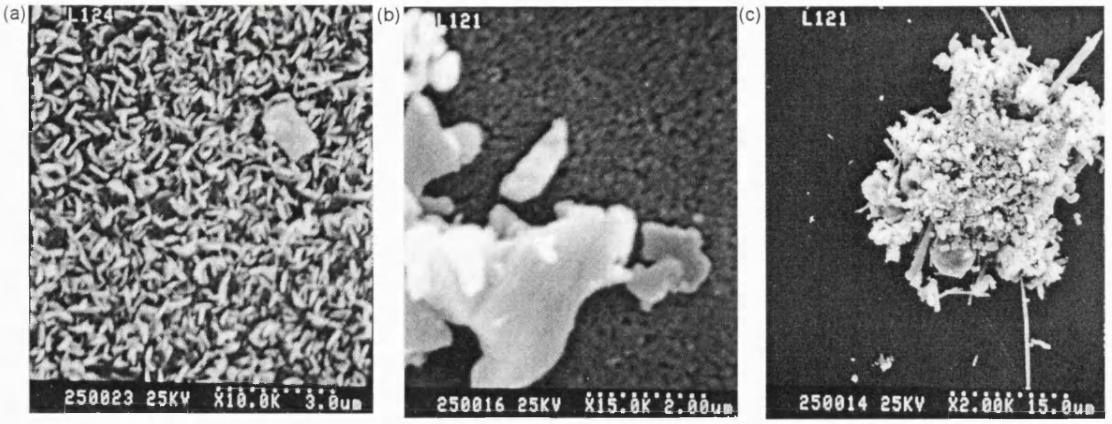


**Figure 5.19 SEM images of films deposited from the reaction of $[Me_3SnS_2CNMe_2]$ at (a) 500 °C and (b), (c) at 550 °C.**

Figure 5.19a shows that at 500 °C very small interlocking plates are deposited. At 550 °C very large clusters (*ca.* 15 μm across) of particles are seen. This is shown in Figure 5.19c. Beneath these wavy structures are observed as depicted in Figure 5.19b. These are very small, but are probably deposited on the surface of the glass, while the larger clusters are more often associated with particles deposited from the gas phase. This indicates that nucleation and growth of particles on the surface is slow compared with the gas phase reaction.

### 5.5.2.6 Conclusions

The films deposited from $[Me_3SnS_2CNMe_2]$ *via* aerosol assisted CVD without hydrogen sulfide showed a mixture of results. Only a small number of reactions were carried out. No film was deposited at 450 °C, while at 550 °C SnS was the only phase observed. At 500 °C a number of reactions were carried out. Sulfur content was undetectable by EDAX, and the Raman spectrum did not show a tin sulfide or tin oxide coating.

## 5.5.3 Reactions of $[Me_3SnS_2CNEt_2]$ *via* aerosol delivery method

### 5.5.3.1 Reactions carried out

In the case of $[Me_3SnS_2CNEt_2]$ using the humidifier, 0.1 g of the precursor was dissolved in 50 ml hexane. A nitrogen flow of 2 $dm^3min^{-1}$ flowed through the round bottomed flask during reaction, and the reaction ran until all the precursor was used up (typically 20 min). The substrate temperature was varied between 450 and 600 °C for all reactions, and a 0.4 $dm^3min^{-1}$ flow of hydrogen sulfide was used in all reactions but the one at 550 °C.

### 5.5.3.2 Visual appearance of films

Using $[Me_3SnS_2CNEt_2]$ in the humidifier led to grey/brown films at all temperatures, regardless of whether hydrogen sulfide was used or not.

### 5.5.3.3 Raman microscopy

Films deposited from $[Me_3SnS_2CNEt_2]$ with the aerosol delivery method showed familiar spectra of tin(II) sulfide for all films deposited with hydrogen sulfide. The film deposited at 450 °C – the lowest temperature attempted in this series – also showed the major band due to mixed valent $Sn_2S_3$ at 307 $cm^{-1}$. Spectra of the films deposited at 450 and 600 °C are given in Figure 5.20. The film deposited at 550 °C from this precursor with no hydrogen sulfide present in the reaction showed the spectrum of tin(II) sulfide.

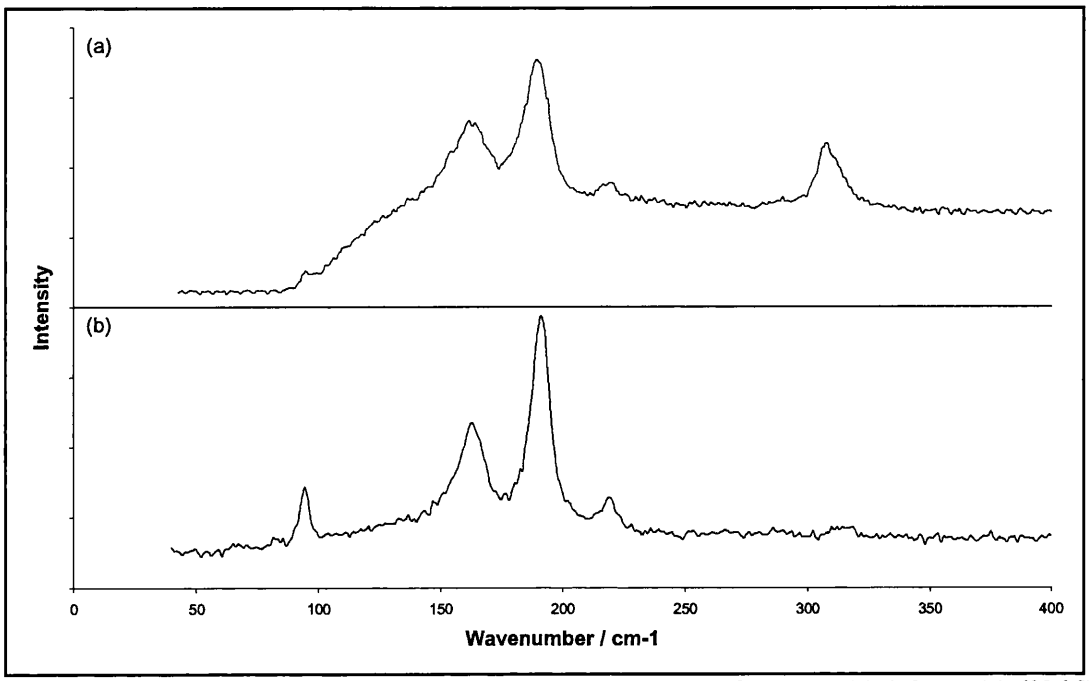


**Figure 5.20 Raman spectra of films deposited from $[Me_3SnS_2CNEt_2]$ at (a) 450 and (b) 600 °C with 0.4 $dm^3min^{-1}$ hydrogen sulfide on tin oxide / silica coated glass using the aerosol delivery method.**

## 5.5.3.4 Energy dispersive analysis by X-rays

Films deposited from this precursor were on tin oxide / silica coated glass, so no useful information could be gathered from EDAX other than that sulfur was present.

## 5.5.3.5 Scanning electron microscopy

Figure 5.21 shows the SEM image of the film deposited from the reaction of $[Me_3SnS_2CNEt_2]$ with hydrogen sulfide at 450 °C.

This shows that the film deposited from this precursor is made up of small particles - *ca.* 2 x 0.5 μm - with large gaps between.

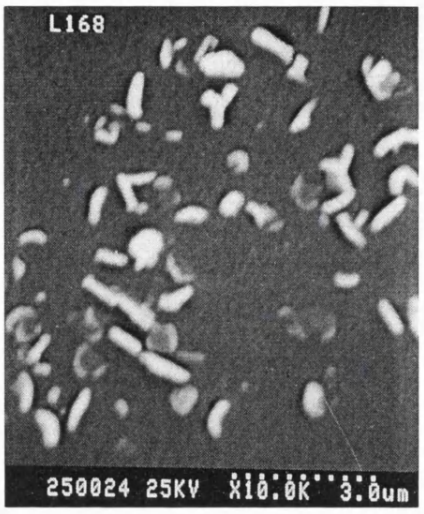


**Figure 5.21 SEM image of the film deposited from the reaction of $[Me_3SnS_2CNEt_2]$ with hydrogen sulfide at 450 °C.**

### 5.5.3.6 Conclusions

The films deposited from $[Me_3SnS_2CNEt_2]$ with hydrogen sulfide using the humidifier were consistent with results from previous systems. At 450 °C, tin(II) sulfide with a small amount of tin(II) tin(IV) trisulfide was deposited. At the higher temperatures of 500 and 600 °C tin(II) sulfide alone was deposited. At 550 °C a film of tin(II) sulfide was produced when no hydrogen sulfide was used.

## 5.5.4 Summary of results of reactions using alkyl tin dithiocarbamates as CVD precursors

In summary, a number of depositions were attempted from $[R_3SnS_2CNR'_2]$ where R=Me, Bu; R'=Me, Et. $[Me_3SnS_2CNMeBu]$ was also used as a precursor.

No films were deposited from $[R_3SnS_2CNR'_2]$ (R=Me, Bu; R'=Me, Et) using the bubbler delivery method.

Using $[Me_3SnS_2CNMe_2]$ without hydrogen sulfide employing the aerosol method of delivery also produced unexpected results. No film could be deposited at 450 °C, while at 550 °C tin(II) sulfide was deposited. At 500 °C the film deposited was shown not to

be tin sulfide or tin oxide by Raman microscopy. In all cases, some sulfur was detected by EDAX, although a large amount of tin was seen in the underlying glass.

The related precursor, $[Me_3SnS_2CNEt_2]$, was used in a number of aerosol assisted reactions with hydrogen sulfide. It was found that tin(II) sulfide was the major component in all films deposited at 450 °C and above, although a small amount of mixed valent $Sn_2S_3$ was seen at 450 °C.

$[Me_3SnS_2CNMeBu]$ was used with the bubbler delivery method, as asymmetric dithiocarbamates are more volatile than their symmetric counterparts. Reactions were carried out with 0.2 $dm^3min^{-1}$ hydrogen sulfide (total gas flow 12.3 $dm^3min^{-1}$). It was found that, at 450 °C, tin(II) tin(IV) trisulfide was the major phase, with a small amount of tin(IV) sulfide. At higher temperatures tin(II) sulfide was the only phase formed. No film could be deposited at 600 °C.

With the exception of films deposited from $[Me_3SnS_2CNMe_2]$, all reactions showed the familiar trend found in previous sections. Reactions were not carried out at temperatures below 450 °C. Mixed valent tin sulfide was generally observed at the lowest deposition temperature of 450 °C, sometimes with tin(II) sulfide. At higher temperatures tin(II) sulfide was the only phase observed. Also, thinner films were deposited at the highest temperature of 600 °C, as has been observed with other systems.

In the case of reactions of $[Me_3SnS_2CNMe_2]$, results were not as expected. The first result that is inconsistent with previous observations is the spectrum of the film deposited at 500 °C from the reaction without hydrogen sulfide using the aerosol delivery method. The Raman spectrum of this film is not indicative of a tin sulfide or tin oxide. As yet, this spectrum has not been identified.

# 5.6 Summary and conclusions

## 5.6.1 Summary

In this Chapter, a variety of precursors was investigated for their potential as single source precursors to tin sulfides. The precursors investigated fell into one of the following categories

- Homoleptic tin(IV) thiolates
- Homoleptic tin(II) thiolates
- Homoleptic tin(IV) dithiocarbamates
- Alkyl tin(IV) dithiocarbamates

It was found that tin(II) thiolates, due to the incomplete coordination sphere around the tin atom, tended to polymerise, thus rendering them insoluble and involatile. The only exception was $[Sn(SCPh_3)_2]$. The bulky ligand prohibited polymeristation, so the compound was soluble. However, investigation by aerosol assisted CVD proved that tin sulfide films could not be deposited.

Tin(IV) thiolates were altogether more successful. Three precursors were extensively investigated, all giving some positive results.

In summary, it was found that tin(IV) thiolates could form films by CVD. In the case of $[Sn(SR)_4]$ (R=Ph, $CH_2CF_3$) if a film could be produced by using the precursor alone, it was tin oxide. With hydrogen sulfide in the system, this was sulfidised to tin sulfide. This was due to loss of ligands (either SR or RSSR) in the initial stages of the reaction. In the case of chelating $[Sn(-SCH_2CH_2S)_2]$ loss of a ligand was less favourable, as the other end was anchored (the chelate effect). The equivalent of losing an RSSR moiety in this case would be to lose an unstable 4-membered ring. TGA indicated that $CH_3CHS$ is lost, following rearrangement and leaving a tin-sulfur bond. All these factors led to the formation of tin(II) sulfide films when no hydrogen sulfide was present in the system.

Tin(IV) dithiocarbamates were also investigated. Only a few reactions were carried out, without hydrogen sulfide. Tin(II) sulfide films could be produced. Again, this result is probably due to the chelate effect, prohibiting loss of ligands.

Alkyl tin(IV) dithiocarbamates investigated followed the established trend of lower temperatures leading to higher oxidation states of tin sulfide formed. Using asymmetric dithiocarbamate ligand allowed bubbler delivery to be used, as melting and boiling points were lower. Using this class of precursor led to one unexpected result. At 500 °C a film was deposited without hydrogen sulfide; this could not be identified as a tin oxide or sulfide by Raman microscopy. At lower temperatures, no film was deposited, which is unusual. Normally, tin(IV) sulfide or tin sesquisulfide could be formed. This unknown phase has yet to be identified.

## 5.6.1 Conclusions

When compounds are designed with a view to forming single source CVD precursors, a tin-sulfur bond is the first prerequisite. If monodentate ligands are used, these are easily lost, either singly or as dimers. This leaves an active tin species, which reacts with the small amount of water present in nitrogen gas cylinders. Bidentate ligands are altogether more effective. This is due to the chelate effect. Ligands cannot be lost easily, so the molecule reaches the surface of the glass intact, before undergoing decomposition.

Of the precursors investigated, $[\overline{Sn(-SCH_2CH_2S)_2}]$, $[Me_3SnS_2CNMe_2]$ and $[Me_3SnS_2CNMeBu]$ all produced films without hydrogen sulfide present in the system. Only $[Me_3SnS_2CNMeBu]$ could be used with the bubbler delivery method. Other similar precursors, with asymmetric dithiocarbamate groups, may also be suitable for formation of tin sulfide films.

# Chapter 6
# Mixed sulfide selenide films

Tin(II) sulfide is widely studied for its semiconducting properties. It has an electronic band gap of 1.3 eV and is a p-type semiconductor. Tin(II) selenide also exhibits semiconducting properties. Its band gap is 1 eV.[30] Tin(IV) selenide has a band gap of 1.03 eV,[56] which is a lot further from that of tin(IV) sulfide.

As advances are made in semiconductor technology, it would be of advantage to create a semiconductor with a predetermined band gap. The similarity in structure of tin(II) sulfide and tin(II) selenide mean that a solid solution of the two phases could be created with any composition. As the composition varies, it is probable that properties of the resulting materials vary between the two extremes of tin sulfide and tin selenide according to some determinable relationship. Hence, the band gap could be tuned by altering the sulfur to selenium ratio in the material.

With these goals in mind, it was decided to attempt to produce a tin sulfide selenide film. Only a preliminary investigation was undertaken. A single source precursor was prepared which contained sulfur and selenium, and CVD reactions were carried out.

## 6.1 Preparation and investigation of the precursor.

The precursor prepared was a tin thiolate selenolate. It was prepared by combining $[Sn(SPh)_4]$ and $[Sn(SePh)_4]$ in toluene. The preparation of tin(IV) phenyl thiolate is described in Section 5.1.1, and tin(IV) phenyl selenolate was prepared by the same method.

The precursor was investigated by NMR. NMR showed that the precursor was not $[Sn(SPh)_2(SePh)_2]$, but a mixture of all compounds $[Sn(SPh)_4]$, $[Sn(SPh)_3(SePh)]$, $[Sn(SPh)_2(SePh)_2]$, $[Sn(SPh)(SePh)_3]$ and $[Sn(SePh)_4]$. Ligand exchange during the final stages of precursor preparation led to all five compounds being formed in the statistical ratio 1:4:6:4:1.

The melting point of the precursor would cover a range as the precursor was a mixture of five compounds. It was thought that, since selenium is heavier than sulfur, the

melting point would be at least as high as that of [$Sn(SPh)_4$], 67°C,[106] and the boiling and vapour pressures correspondingly higher.

# 6.2 CVD investigation of [$Sn(SPh)_n(SePh)_{4-n}$]

## 6.2.1 Reactions carried out

As the precursor was a solid at room temperature and had a high melting point, only the aerosol method of delivery could be used. For full details of this method, refer to Section 2.1.3.

In all reactions, *ca.* 0.1 g of the precursor was dissolved in 50 $cm^3$ acetone. This was poured into the round bottomed flask immediately prior to reaction. A nitrogen flow of 2 $dm^3min^{-1}$ flowed through the round bottomed flask during reaction. Some reactions were carried out with 0.2 $dm^3min^{-1}$ flow of hydrogen sulfide, diluted by 1 $dm^3min^{-1}$ nitrogen, which met the precursor 2 cm before the reaction chamber. Other reactions used no hydrogen sulfide, and the diluting nitrogen was also stopped, hence the overall gas flow to the reactor was 2 $dm^3min^{-1}$. Reactions were carried out with substrate temperatures between 300 and 550 °C. Silica coated glass was used as the substrate.

## 6.2.2 Visual appearance of films

Of the films deposited with 0.2 $dm^3min^{-1}$ hydrogen sulfide in the reaction, the colour of the films varied with deposition temperature. The film deposited at 300 °C was brown, those deposited at 350 and 400 °C were yellow/brown, and films deposited at 450 °C and above were grey in colour. All films were thin and only the first few cm of the substrate was coated.

Films could also be deposited without hydrogen sulfide. The film deposited at 400 °C was yellow, at 450 °C the film was brown, while at 500 °C a grey film was deposited.

Films were too thin to be analysed by X-ray diffraction.

### 6.2.3 Raman microscopy

Raman spectra were recorded for all films. Reference spectra of tin sulfides are given in Figure 2.6. These show that bands appear in tin(II) sulfide at 216-220, 185-189, 159-163 and 94-96 $cm^{-1}$, and at 313 and 214 $cm^{-1}$ in tin(IV) sulfide. As tin selenide has the same structure as tin sulfide, it would be expected that the pattern observed is similar, although bands would move. Selenium is heavier than sulfur, so bands would be expected to appear at lower wavenumber. Figure 6.1 shows Raman spectra recorded for the films deposited from $[Sn(SPh)_n(SePh)_{4-n}]$ (n = 0 – 4), at 300, 400 and 500 °C.

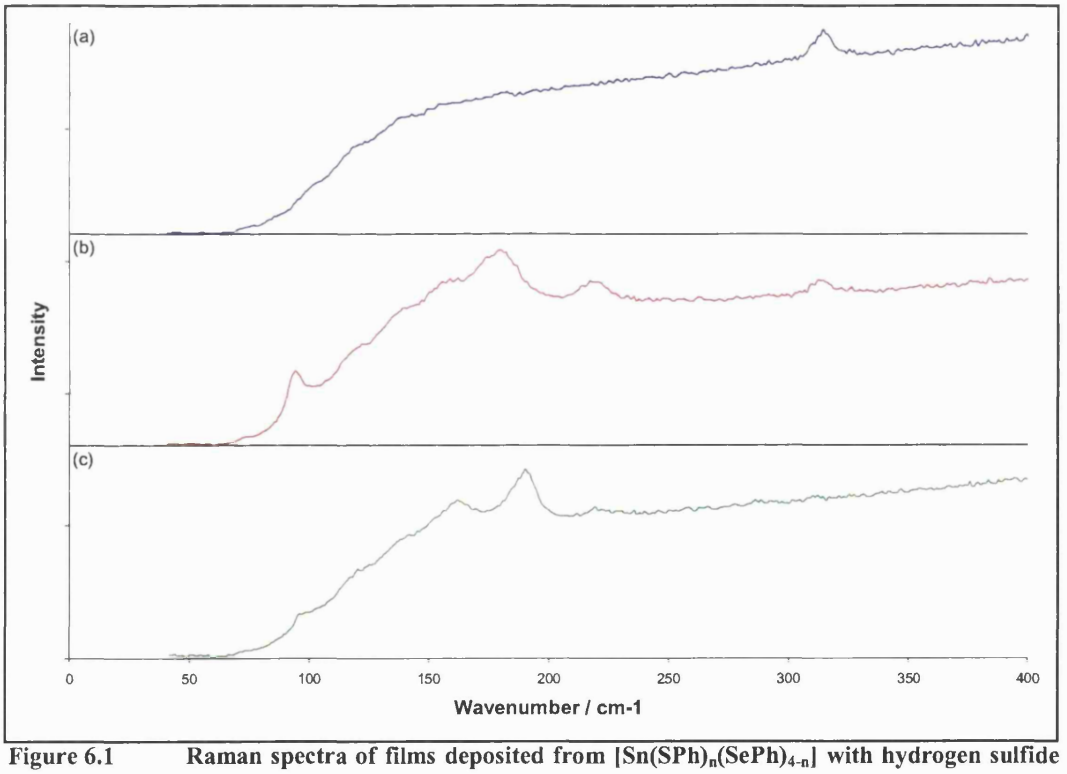


**Figure 6.1 Raman spectra of films deposited from $[Sn(SPh)_n(SePh)_{4-n}]$ with hydrogen sulfide at (a) 300 °C, (b) 400 °C and (c) 500 °C.**

Figure 6.1 shows that at 300 °C tin(IV) sulfide is deposited, at 500 °C tin(II) sulfide is the product and a mixture of the two is achieved at 400 °C. No evidence for mixed valent tin sulfide is seen.

In the Raman spectra of the films deposited at 300 and 400 °C, the $SnS_2$ band occurs at 315 $cm^{-1}$. The bands for SnS are noticed at 221, 182-191, 161-164 and 96-97 $cm^{-1}$ in

the spectra recorded for films deposited at 400 and 500 °C. These bands are all in roughly the same place as in other spectra recorded for tin sulfides.

The spectra of the films deposited without hydrogen sulfide are given in Figure 6.2.

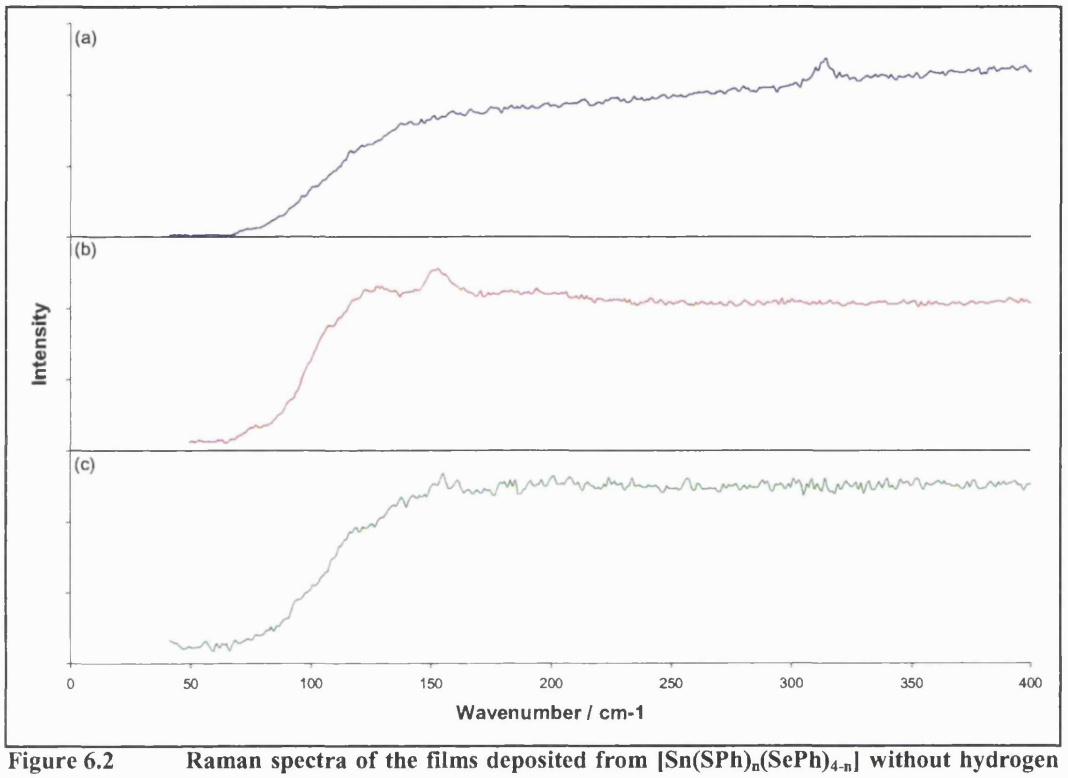


**Figure 6.2 Raman spectra of the films deposited from $[Sn(SPh)_n(SePh)_{4-n}]$ without hydrogen sulfide at (a) 400 °C, (b) 450 °C and (c) 500 °C.**

Figure 6.2 shows that at 400 °C tin(IV) sulfide is deposited, while at 450 °C a film with a Raman spectrum similar to that of tin(II) sulfide is deposited. The position of the $SnS_2$ band in Figure 6.2a is 315 $cm^{-1}$, however the bands for SnS in Figure 6.2b are observed at 154, 130 and 78 $cm^{-1}$. The band at 220 is not observed. The film deposited at 500 °C begins to show the band that should be at 185 $cm^{-1}$.

The shifting of the bands in the spectra of tin(II) sulfide is significant. Spectra are calibrated to within 2 $cm^{-1}$, and shifts of *ca.* 20 $cm^{-1}$ are experienced here. In the films deposited in the presence of hydrogen sulfide, a shift of 7 $cm^{-1}$ occurs in one of the bands, while when no hydrogen sulfide is used shifts of 20 $cm^{-1}$ occur. These shifts may be due to some incorporation of selenium into the films.

### 6.2.4 Energy dispersive analysis by X-rays.

All films were analysed by EDAX. They were found to be thin, with less than 10 % of the excitation volume being made up of tin, sulfur or selenium. The substrate did not contain tin, however calcium found in the glass interferes with the tin signal. At these low amounts of tin, the effect of calcium is significant. Ratios are reported here for comparison with one another, and not as absolute values.

In the films deposited from $[Sn(SPh)_n(SePh)_{4-n}]$ with hydrogen sulfide, tin and sulfur were observed in all films. Some films appeared to contain selenium, while others did not, but in all cases selenium content was so low that it could have been due to error.

Of the films deposited without $H_2S$ in the reaction mixture, the film deposited at 450 °C again showed a selenium content which may be due to error in the instrument. The film deposited at 500 °C, however, showed a selenium content which was above the error of the EDAX machine. Ignoring the tin content, selenium accounted for *ca.* 30 % of the chalcogenide present.

If the tin content in these films is inspected, it is seen to be higher than observed in films deposited under the same conditions without hydrogen sulfide. The total chalcogenide content is, however, similar. This high tin content is far higher than normally observed due to calcium in the underlying glass, so it may be that some tin oxide is present in the films. Oxygen is not detected by the EDAX system used in this work.

Table 6.1 gives the ratio of sulfur and selenium in all films, although some selenium ratios are lower than 2 sigma, as calculated by the EDAX detector.

**Table 6.1 Sulfur and selenium ratios in films deposited from $[Sn(SPh)_n(SePh)_{4-n}]$.**

| Deposition temperature / °C | Hydrogen sulfide flow rate / $dm^3min^{-1}$ | Selenium as percentage of total chalcogenide |
|---|---|---|
| 300 | 0.2 | 10 * |
| 350 | 0.2 | 0 |
| 400 | 0.2 | 9 * |
| 450 | 0.2 | 0 |
| 500 | 0.2 | 10 * |
| 550 | 0.2 | 8 * |
| 450 | 0 | 20 * |
| 500 | 0 | 30 |

* denotes films where selenium content is lower than instrument error.

Although error in measurements on the EDAX machine are high, due to the film being very thin, it is evident from Table 6.1 that presence of $H_2S$ in the reaction mixture leads to lower selenium content in the films. This is to be expected.

## 6.2.5 Scanning electron microscopy

Images of a representative sample of the films are shown in Figure 6.3.

The morphologies observed in Figure 6.3 are not similar to those observed for other films deposited in this thesis. It is to be expected that some similarities would arise in the SEMs, as tin sulfide, tin selenide and all intermediate compounds have the same structure. In addition, as silica coated glass was used in both series of depositions, no difference can arise due to the substrate. In Figure 6.3a the film deposited from $[Sn(SPh)_n(SePh)_{4-n}]$ is shown. This shows similar morphology to films deposited from other precursors, however the particles are much smaller and less well defined. In Figure 6.3b the film deposited from the same precursor at 450 °C is shown. Here, small round particles are observed on the surface of the glass, along with needles over the top. At the higher temperatures of 500 and 550 °C, films are made up of small regular particles. These are larger at the higher temperature indicating that growth rates are higher.

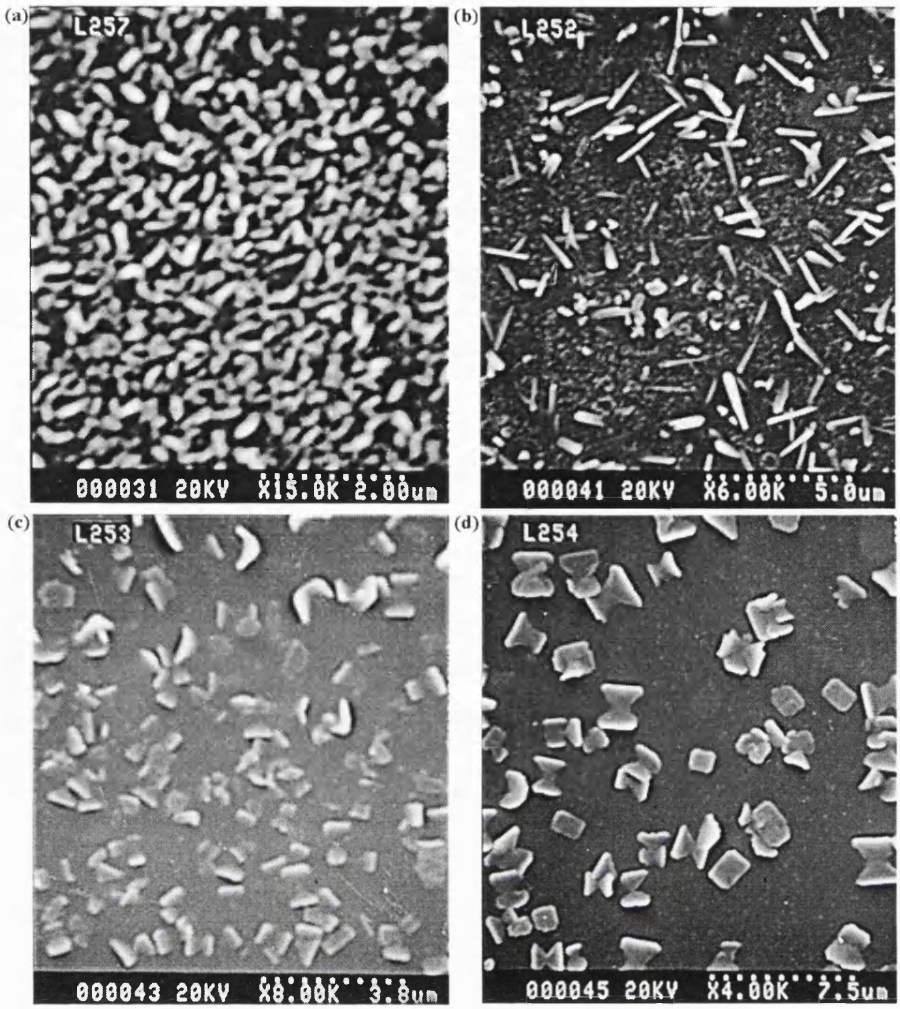


**Figure 6.3 SEM images of films deposited from $[Sn(SPh)_n(SePh)_{4-n}]$ with $H_2S$ at (a) 300, (b) 450, (c) 500 and (d) 550 °C.**

## 6.3 Discussion and conclusions

Films may be deposited from $[Sn(SPh)_n(SePh)_{4-n}]$ with and without hydrogen sulfide. The precursor used is a mixture of all species from n=0 to n=5 and this is likely to contribute to some aspects of the reaction.

EDAX showed that the films were very thin. Selenium content was of the order of the limits of detection. This leads to problems in quantification, however, it may be concluded that films deposited without hydrogen sulfide contained higher levels of selenium that those deposited with hydrogen sulfide.

EDAX data recorded for films deposited without hydrogen sulfide, showed a large amount of tin in excess of that which could be bound to observed chalcogenide. This indicates that tin oxide may have been present in the films.

Raman data followed previously observed trends – lower deposition temperatures lead to higher oxidation states of tin. The patterns were similar in form to those of tin sulfides, however shifts in peak positions were encountered. These shifts could be due to selenium substituting for sulfur on some of the sites. Mixed valent $Sn_2S_3$ is not seen in any of the spectra. Tin oxide bands are not observed in any of the spectra, although the presence of some tin oxide was indicated by the EDAX result. Tin oxide is a much weaker Raman scatterer than tin sulfide, so would probably not be observed along side tin sulfide anyway.

SEM showed that the films were thinner than those deposited from other precursors, and particles were much smaller.

Referring back to observations made in Chapter 5, concerning the reactions of analogous tin(IV) phenyl thiolate, a PhSSPh species was observed in the mass spectrum. Decomposition of tin(IV) phenyl thiolate no doubt includes loss of such a species. This, accompanied by the presence of water in the diluting nitrogen supply, led to deposition of tin oxide films. When the reaction was accompanied by hydrogen sulfide, or when films were subsequently heated in this gas, tin sulfide films were the result.

For reactions of[ $Sn(SPh)_n(SePh)_{4-n}$] similar reaction pathways may be envisaged. Loss of PhSSPh can occur from molecules where $n \geq 2$. Likewise, loss of the analogous species PhSeSePh may also occur in molecules of $n \leq 2$. If $n = 0$ or 4 then two species of the appropriate type would be lost.

Since there is greater overlap of orbitals between atoms of similar size, bonds between atoms of different size are weaker than between those of similar size. Therefore, the central bond in a molecule PhS-SePh would be weaker than either the sulfur-sulfur or selenium-selenium bonds in PhSSPh or PhSeSePh. It is possible that this lower bond energy prohibits loss of such a species. This means that, although all ligands may be

lost from $[Sn(SPh)_n(SePh)_{4-n}]$ where n = 0, 2 or 4, when n is 1 or 3 a species [Sn(SPh)(SePh)] would remain. This may then deposit a tin sulfide selenide film.

In the overall scheme, some tin oxide would be deposited from species where n = 0, 2 or 4 and some tin sulfide selenide from molecules with n = 1 or 3. When hydrogen sulfide is present in the reaction mixture, the tin oxide would be sulfidised, however without hydrogen sulfide tin oxide would remain. This accounts for the high tin content in films deposited without hydrogen sulfide.

If it were the case that PhSeSePh could not be lost from the precursor, the final film would have a higher proportion of selenium. This is not observed – in fact all films contain more sulfur than selenium, although a 1:1 ratio is expected from films deposited without hydrogen sulfide.

# Chapter 7
# Mixed oxide sulfide films

As was observed in the previous chapter, films containing tin, sulfur and selenium may be formed by chemical vapour deposition. These exhibit similar properties to those seen in pure tin sulfide. This is due to tin sulfide, tin selenide and solid solutions of the two phases all having the same structure.

Tin oxide sulfide provides another interesting system. In this case, tin oxide and tin sulfide differ in many ways, so the resulting film may show properties similar to tin sulfide or may be more akin to tin oxide. Alternatively a further new phase may be formed.

Very little is known of a mixed tin oxide sulfide. A structure can be forced to crystallise around organic template molecules, and this is composed of $[Sn_{10}S_{20}O_4]^{8-}$ units lined by sulfide bridges.[111]

In this chapter, formation of tin oxide sulfide films will be attempted. Two approaches will be taken – forming the films from tin tetrachloride, hydrogen sulfide and water, and deposition from single source precursors.

# 7.1 Precursors used

Three systems were studied in the attempt to produce tin oxide sulfide films.

The first, based on previous work in this thesis and by other members of the research group at University College, used tin tetrachloride, hydrogen sulfide and water. In Chapter 3, results showed that tin tetrachloride and hydrogen sulfide, when reacted together under CVD conditions, produced tin sulfide films. Other systems have been studied, such as chromium, vanadium and titanium, whereby appropriate chlorides or oxychlorides react with water to give transition metal oxides. Also noted in Chapter 3, was that tin oxide films, when heated in hydrogen sulfide, could be sulfidised to tin sulfide. With these observations in mind, reaction of tin tetrachloride, hydrogen sulfide and water may lead to a mixed oxide sulfide film, however, presence of hydrogen sulfide is likely to lead to any oxide component being sulfidised.

Two further series of reactions were carried out. These involved use of single source precursors with tin-sulfur and tin-oxygen bonds. All these reactions were carried out with and without hydrogen sulfide. The precursors used were $[Cl_2Sn(SCH_2C(O)OMe)_2]$, where the carbonyl oxygen binds datively to tin and $[^tBu_2\overline{Sn(-OCH_2CH_2S)}]$.

### 7.1.1 Preparation and analysis of $[Cl_2Sn(SCH_2C(O)OMe)_2]$

This was prepared at the University of Bath by Dr. T. Hibbert. $MeOC(O)CH_2CH$ was reacted with BuLi in THF. This gave the lithium salt $MeOC(O)CH_2SLi$ which was reacted with $SnCl_4$ in toluene. Initially, this reaction sequence was thought to have produced $[Sn(SCH_2C(O)OMe)_4]$, however the mass spectrum evidence indicated that $[Cl_2Sn(SCH_2C(O)OMe)_2]$ was the product achieved.

### 7.1.2 Preparation and analysis of $[^tBu_2\overline{Sn(-OCH_2CH_2S)}]$

Dr. T. Hibbert also produced this compound at the University of Bath. $HOCH_2CH_2SH$ was reacted with two equivalent of BuLi in THF. This gave the dilithium salt $LiOCH_2CH_2SLi$. When this was reacted with $[^tBu_2SnCl_2]$ in THF, followed by a $CH_2Cl_2$ work up, $[^tBu_2\overline{Sn(-OCH_2CH_2S)}]$ was produced.

## 7.2 Reactions carried out

### 7.2.1 Reactions of tin tetrachloride, hydrogen sulfide and water

Tin tetrachloride was admitted to the system using a bubbler. The bubbler temperature in all reactions was 70 °C. A nitrogen flow of 0.5 $dm^3min^{-1}$ passed through the bubbler, and was further diluted by 10 $dm^3min^{-1}$ of nitrogen.

Water and hydrogen sulfide were admitted through the same line to the reactor. The total gas flow in this line was 1.5 $dm^3min^{-1}$. Water was admitted using a syringe. The

syringe driver expelled all water in 6 minutes, and 50 $cm^3$ of water was used. The pipe into which water was injected was heated to 280 °C. Hydrogen sulfide flows of 0, 0.1 or 0.2 $dm^3min^{-1}$ were used. This was augmented to a total of 1.5 $dm^3min^{-1}$ with nitrogen. The plain line, which ran directly to the exhaust during reaction, contained a flow of 10 $dm^3min^{-1}$.

Reactions were carried out at 400, 500 and 600 °C. At each temperature 3 reactions were carried out with each of the three hydrogen sulfide flows. Silica coated glass was used as the substrate in all reactions. Reactions were carried out over 30 s. Full reaction conditions are summarised in Table 7.1.

**Table 7.1 Conditions for reactions of tin tetrachloride, hydrogen sulfide and water.**

| | |
|---|---|
| Bubbler temperature | 70 °C |
| Reactor temperature | 400, 500 or 600 °C |
| Temperature of pipe into which water is injected | 280 °C |
| Flow rate through bubbler | 0.5 $dm^3min^{-1}$ |
| Rate of syringe driver | 50 $cm^3$ in 6 min |
| Flow rate of hydrogen sulfide | 0, 0.1 or 0.2 $dm^3min^{-1}$ |
| Flow of nitrogen diluting line from bubbler | 10 $dm^3min^{-1}$ |
| Flow of nitrogen diluting $H_2S$ and $H_2O$ | 1.5, 1.4 or 1.3 $dm^3min^{-1}$ |
| Reaction time | 30 s |
| Substrate | Silica coated glass |
| Flow of nitrogen in plain line | 10 $dm^3min^{-1}$ |

In these reactions, *ca.* 4 $cm^3$ of water is expelled from the syringe during the reaction. This equates to 0.22 moles of water. Either 0, 0.05 or 0.1 $dm^3$ of hydrogen sulfide will flow through the reaction chamber during the reaction. This would equate to 0, 0.002 or 0.004 moles of hydrogen sulfide. It is clear in all cases that water is in vast excess over the hydrogen sulfide. As discovered in Chapter 3, tin has a greater affinity for sulfur than for oxygen, so higher amounts of water would be needed for any oxygen to be incorporated into the films.

### 7.2.2 Reactions of $[Cl_2Sn(SCH_2C(O)OMe)_2]$ with hydrogen sulfide

$[Cl_2Sn(SCH_2C(O)OMe)_2]$ was involatile, so the aerosol delivery method was used. 0.1 g of the precursor was dissolved in of acetone, 50 ml, and poured into the round-bottomed flask immediately prior to reaction. A nitrogen flow of 2 $dm^3min^{-1}$ flowed through the round-bottomed flask. Hydrogen sulfide of 0.2 $dm^3min^{-1}$ was used for some reactions, and a nitrogen flow of 1 $dm^3min^{-1}$ was used to dilute this. The nitrogen was used in all reactions, even where $H_2S$ was not used.

Reactions were carried out until the entire precursor had been used up – typically 25 min. Reactions with hydrogen sulfide were carried out at all temperatures from 350 to 600 °C at intervals of 50 °. Without hydrogen sulfide, substrate temperatures of 350, 450 and 550 °C were used in the attempt to deposit a film. Silica coated glass was used as the substrate for all reactions.

### 7.2.3 Reactions of $[^tBu_2\overline{Sn(-OCH_2CH_2S)}]$ with hydrogen sulfide

This precursor was involatile and air-sensitive. The aerosol delivery method had to be used, and the sample loaded into the modified round-bottomed flask in a glove box. Solvents had to be dry and degassed and added using a Schlenk line. Of all the solvents investigated, $[^tBu_2\overline{Sn(-OCH_2CH_2S)}]$ dissolved only in acetonitrile.

0.1 g of the precursor was dissolved in $CH_3CN$, *ca.* 50 $cm^3$, in the purpose designed round bottomed flask described in Chapter 2. This was attached to the reactor and nitrogen flowed past the flask during heating. During reaction, 2 $dm^3min^{-1}$ of nitrogen flowed through the round-bottomed flask and into the coater. This met with a 0.2 $dm^3min^{-1}$ flow of hydrogen sulfide immediately prior to the coater, which had been diluted by 1 $dm^3min^{-1}$ of nitrogen. In some reactions hydrogen sulfide was not used, but nitrogen of 1 $dm^3min^{-1}$ was used in all cases.

Reactions were carried out with hydrogen sulfide at all temperatures from 350 to 600 °C at intervals of 50 °C. Without hydrogen sulfide, reactions were carried out at 400, 450 and 500 °C only. Reactions ran until all the precursor was expended – typically 30 min. Silica coated glass was used as the substrate.

## 7.3 Results of reactions of tin tetrachloride, hydrogen sulfide and water

### 7.3.1 Visual appearance of films

When deposition reactions were carried out without hydrogen sulfide, no film was deposited. In the case of films deposited at 600 °C, films were grey-black in colour when 0.1 or 0.2 $dm^3min^{-1}$ hydrogen sulfide was used in the reaction. Films deposited at 500 °C were grey when 0.1 $dm^3min^{-1}$ hydrogen sulfide was used, and brown when 0.2 $dm^3min^{-1}$ hydrogen sulfide was used. At 400 °C films deposited were yellow in colour, however the film deposited with the higher hydrogen sulfide flow rate was more brown. All films were brown in reflection.

### 7.3.2 Raman microscopy

In the films deposited with hydrogen sulfide at 400 °C the spectra recorded all exhibit the familiar pattern of tin(IV) sulfide. A spectrum recorded for the film deposited with a 0.2 $dm^3min^{-1}$ flow of hydrogen sulfide is given in Figure 7.1.

Films deposited at 500 and 600 °C showed the familiar spectrum of tin(II) sulfide along with another spectrum consisting of bands at 288, 223, 178 and 91 $cm^{-1}$. For the film deposited at 500 °C with a hydrogen sulfide flow of 0.1 $dm^3min^{-1}$, all spectra recorded showed a mixture of tin(II) sulfide and this second phase. At the same deposition temperature but with a hydrogen sulfide flow of 0.2 $dm^3min^{-1}$ the composition alters along the length of the film. Nearest to the gas inlet a mixture of tin(II) sulfide and the

second phase is observed. Further the film bands due to these phases decrease in intensity and are replaced by bands corresponding to tin(II) tin(IV) trisulfide. In turn, these bands decrease and tin(IV) sulfide is observed. Spectra recorded along the length of this film are shown in Figure 7.2.

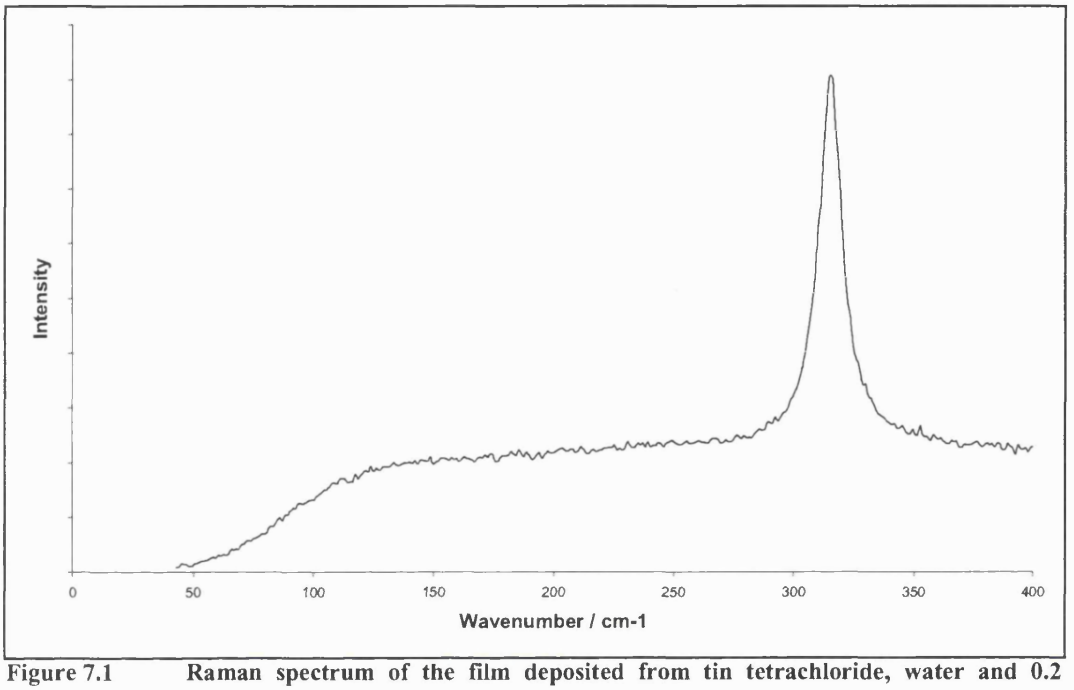


**Figure 7.1 Raman spectrum of the film deposited from tin tetrachloride, water and 0.2 $dm^3min^{-1}$ hydrogen sulfide at 400 °C.**

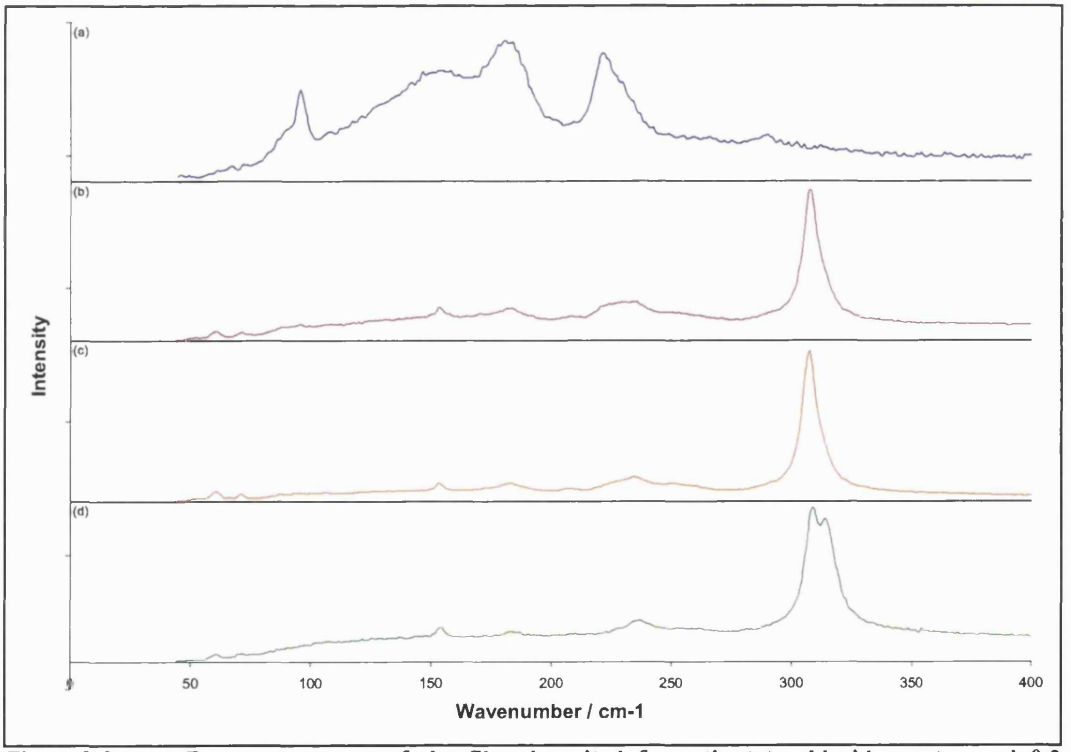


**Figure 7.2 Raman spectrum of the film deposited from tin tetrachloride, water and 0.2 $dm^3min^{-1}$ hydrogen sulfide at 500 °C, (a) closest to gas inlet → (d) furthest from gas inlet.**

The films deposited at 600 °C with 0.1 and 0.2 $dm^3min^{-1}$ both show tin(II) sulfide and the new phase. The film deposited with 0.2 $dm^3min^{-1}$ flow of hydrogen sulfide shows the same relative intensity of bands at all points. When the lower hydrogen sulfide flow of 0.1 $dm^3min^{-1}$ was used, tin(II) sulfide bands decreased in intensity as bands corresponding to the new phase increased along the length of the film. Raman spectra recorded from the two films deposited at 600 °C are shown in Figure 7.3.

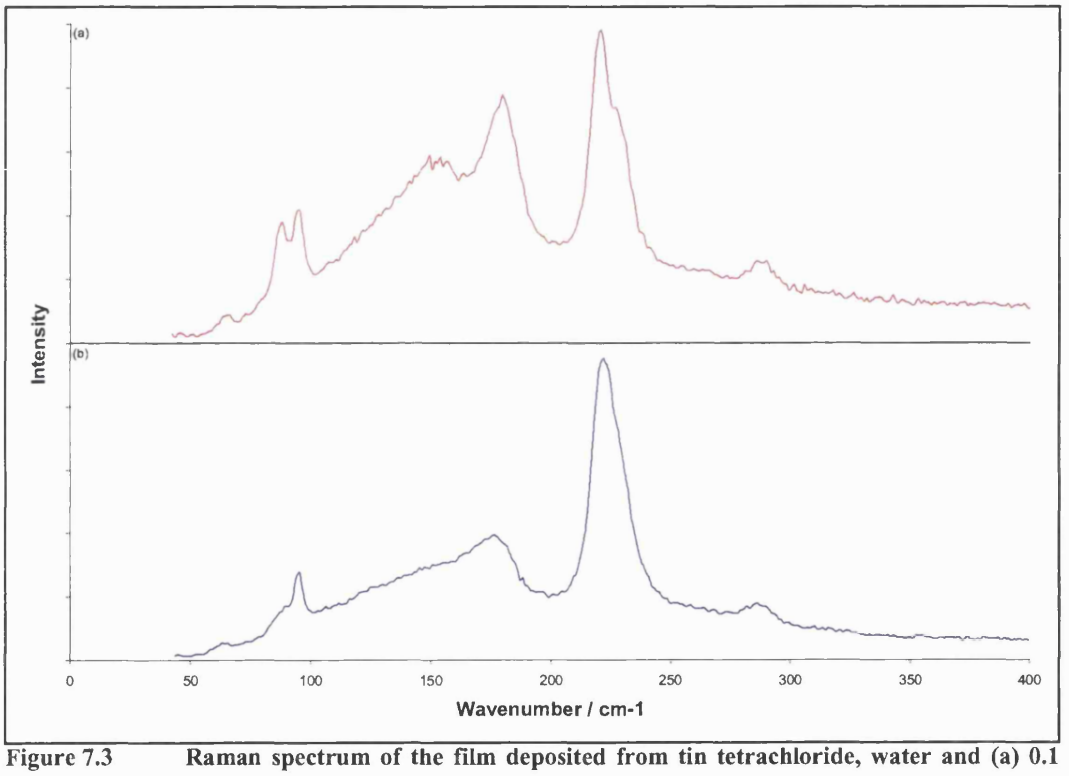


**Figure 7.3 Raman spectrum of the film deposited from tin tetrachloride, water and (a) 0.1 $dm^3min^{-1}$ or (b) 0.2 $dm^3min^{-1}$ hydrogen sulfide at 600 °C.**

## 7.3.3 Energy dispersive analysis by X-rays

EDAX was carried out on all films. Only tin, sulfur and silicon were analysed for. Results by percentage of total volume observed are given in Table 7.2. Excess volume was silicon in all cases.

**Table 7.2 Results of EDAX on films deposited from tin tetrachloride, hydrogen sulfide and water.**

| Coater temperature | 400 °C | | 500 °C | | 600 °C | |
|---|---|---|---|---|---|---|
| Hydrogen sulfide flow | % Sn | % S | % Sn | % S | % Sn | % S |
| 0.1 $dm^3min^{-1}$ | 8 | 4 | 8 | 2 | 30 | 11 |
| 0.2 $dm^3min^{-1}$ | 20 | 10 | 9 | 4 | 41 | 19 |

In all cases, the tin to sulfur ratio is high. Some of this may be due to calcium in the underlying glass, however this has only distorted the tin ratio by 1-2 % of the overall excitation volume. These large excesses indicate that tin is found in its elemental state or bound with something other than sulfur. Oxygen cannot be detected by the EDAX equipment used, so it is impossible to say whether there is any present from this result.

## 7.3.4 Scanning electron microscopy

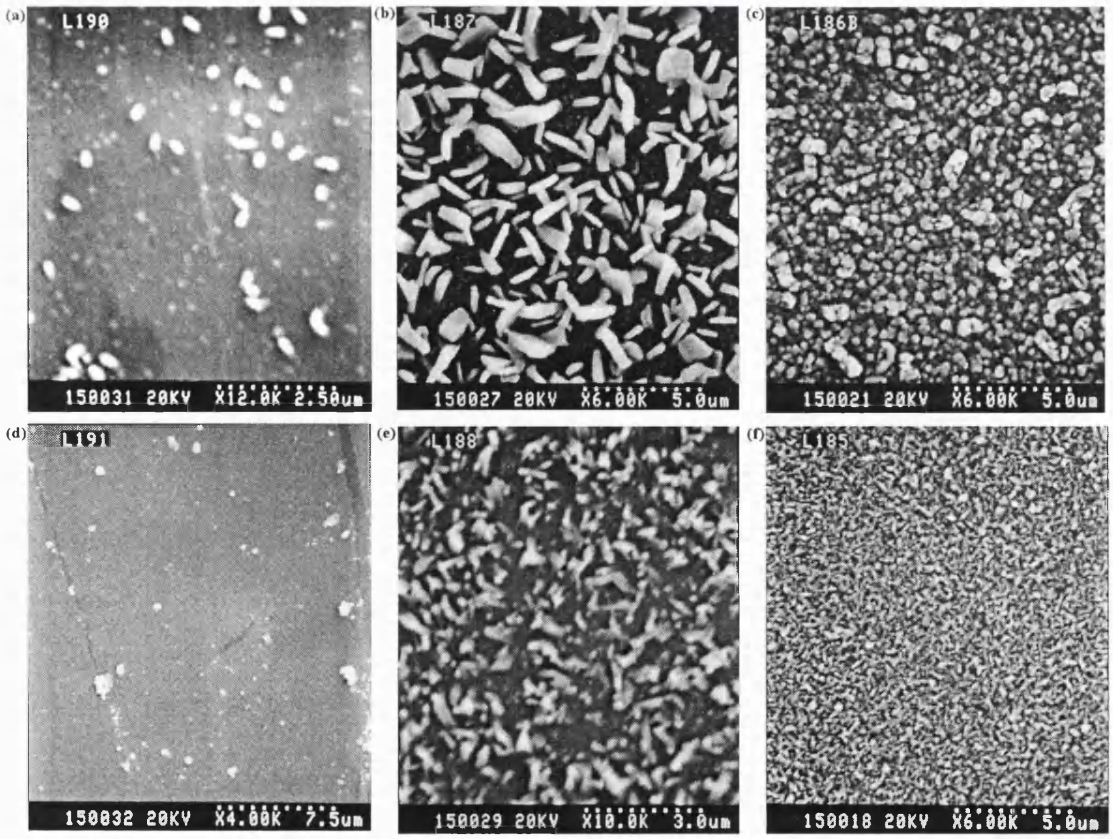


**Figure 7.4 SEM images of films deposited from tin tetrachloride, water and hydrogen sulfide (see next paragraphs for details).**

SEM images of films deposited from tin tetrachloride, hydrogen sulfide and water are shown in Figure 7.4.

Figures 7.4a, 7.4b and 7.4c show films deposited with a 0.1 $dm^3min^{-1}$ flow of hydrogen sulfide at 400, 500 and 600 °C respectively. At 400 °C small particles are observed in the film. These are typically 200 nm across. Larger particles (*ca.* 0.5 x 3 μm) are seen in the film deposited at 500 °C with a 0.1 $dm^3min^{-1}$ flow of hydrogen sulfide. At the highest temperature of 600 °C, particles are smaller (*ca.* 1 μm across). The larger number of particles observed on the surface of the film deposited at 600 °C with a hydrogen sulfide flow rate of 0.1 $dm^3min^{-1}$ is indicative of a higher rate of nucleation under these conditions.

Figures 7.4d, 7.4e and 7.4f show films deposited at 400, 500 and 600 °C respectively with a hydrogen sulfide flow rate of 0.2 $dm^3min^{-1}$. Again, very low surface coverage and small particles are observed at the lowest deposition temperature. At 500 °C, the film exhibits higher surface coverage and larger particles than observed in that deposited at 400 °C. Smaller particles are observed in the film deposited at the highest deposition temperature. This is consistent with the trend observed in films formed with a hydrogen sulfide flow of 0.1 $dm^3min^{-1}$ during deposition.

At all deposition temperatures, the film deposited with a higher hydrogen sulfide flow rate has smaller particles. This indicates that higher hydrogen sulfide flow rate also increases nucleation rate.

## 7.4 Results of reactions of $[Cl_2Sn(SCH_2C(O)OMe)_2]$ with hydrogen sulfide

### 7.4.1 Visual appearance of films

All films were grey in colour. In all cases only the end of the substrate nearer to the gas inlet was coated. *Ca.* 3 cm was coated in all cases. The films were very thin, and

interference was observed in the film deposited at 350 °C with hydrogen sulfide. Here, the film was grey, but yellow and blue interference patterns could be seen in reflection.

### 7.4.2 Raman microscopy

Raman spectra were recorded for all films deposited. Each showed only the familiar spectra of tin sulfide.

Films deposited with hydrogen sulfide showed a mixture of tin(IV) sulfide and mixed valent tin(II) tin(IV) trisulfide at 350 and 400 °C. Tin(II) sulfide was observed at temperatures of 450 °C and above, although the film deposited at 450 °C showed a very weak band due to $Sn_2S_3$.

In the case of films deposited without hydrogen sulfide, $SnS_2$ was deposited at 450 °C and SnS at 550 °C. No spectrum could be recorded from the film deposited at 350 °C as it was very thin. Bands were not shifted and no evidence was found for any phase of tin oxide being present. Tin sulfides are much stronger Raman scatterers than tin oxides, so if the two compounds were present together, only tin sulfide would be observed.

### 7.4.3 Energy dispersive analysis by X-rays

EDAX was carried out on all films. The films were very thin and breakthrough to the underlying glass occurred in all cases.

In the case of films deposited with hydrogen sulfide, whose substrate temperature during deposition was 400 °C or less a 2:3 tin to sulfur ratio was seen. Films deposited at 450 °C or above had a near 1:1 ratio of tin and sulfur.

Films deposited without hydrogen sulfide did not show a similar trend. The film deposited at 350 °C showed that tin and sulfur comprised <10 % of the excitation volume investigated. The observed tin to sulfur ratio was 5:2, however, due to the large volume of glass observed, this high tin content is probably influenced by calcium in the

glass. The film deposited at 450 °C showed a 2:1 ratio of tin to sulfur, while that deposited at 550 °C exhibited a 3:2 ratio. These both show there to be more tin in the film than accountable for by tin sulfides alone.

In light of these results, it appears that tin sulfide films may be deposited when hydrogen sulfide is present in the reaction. Films deposited without hydrogen sulfide have higher tin content, which implies that either elemental tin is present or a tin compound of another element. The tin:sulfur ratio decreases with increasing deposition temperature regardless of whether hydrogen sulfide is present in the reaction or not. Oxygen may be present in the films, and this cannot be detected by the EDAX system used in this work.

### 7.4.4 Scanning electron microscopy

SEM images of films deposited from $[Cl_2Sn(SCH_2C(O)OMe)_2]$ with and without hydrogen sulfide are seen in Fig. 7.5

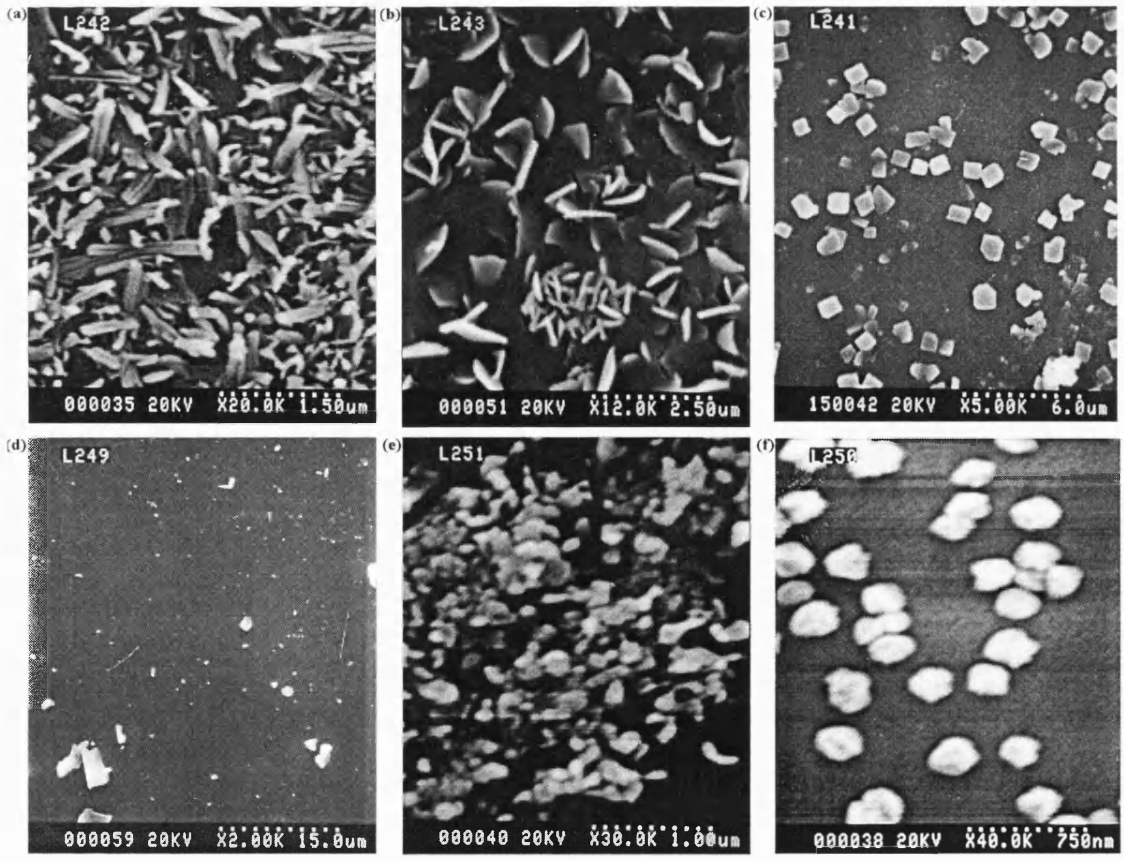


**Figure 7.5 SEM images of films deposited from $[Cl_2Sn(SCH_2C(O)OMe)_2]$ (see next paragraph for details).**

Figure 7.5a shows the SEM image of the film deposited from $[Cl_2Sn(SCH_2C(O)OMe)_2]$ at 400 °C with 0.2 $dm^3min^{-1}$ $H_2S$. Films deposited with $H_2S$ at lower temperatures show similar morphology but smaller particles are observed with decreasing temperature. The film deposited at 450 °C with hydrogen sulfide showed interlocking plates. This is shown in Figure 7.5b. The plates are less than 1 μm across. Clusters appear at regular intervals in the film, where plates are smaller and most appear over a small area. In the film deposited at 500 °C (shown in Figure 7.5c) discreet plates are observed. These are *ca.* 1 μm across. At higher deposition temperatures similar discreet plates are observed. Higher deposition temperatures lead to larger particles.

In the case of films deposited without hydrogen sulfide, virtually no particles are observed in the film deposited at 350 °C (Figure 7.5d). At 450 °C (Figure 7.5e) and 550 °C (Figure 7.5f) small particles are observed. These are similar in size to those observed in films deposited with hydrogen sulfide, and at 450 °C they are deposited close to one another while at 550 °C they are discreet. The main difference from depositions with hydrogen sulfide is that particles are more rounded.

# 7.5 Results of reactions of $[^tBu_2\overline{Sn(-OCH_2CH_2S)}]$ with hydrogen sulfide

## 7.5.1 Visual appearance of films

All films were generally grey in colour. Those deposited at temperatures up to 500 °C with hydrogen sulfide had some brown areas. Of the films deposited with hydrogen sulfide, only those deposited at 400 and 450 °C coated the entire substrate. The film deposited at 350 °C had uncoated glass at the end nearest to the inlet and films deposited at temperatures higher than 500 °C only had the end nearer the inlet coated.

Without hydrogen sulfide in the reaction, no film was deposited at 400 °C. At 450 and 500 °C thin coatings were produced over the first *ca.* 4 cm of the substrate only.

## 7.5.2 Raman microscopy

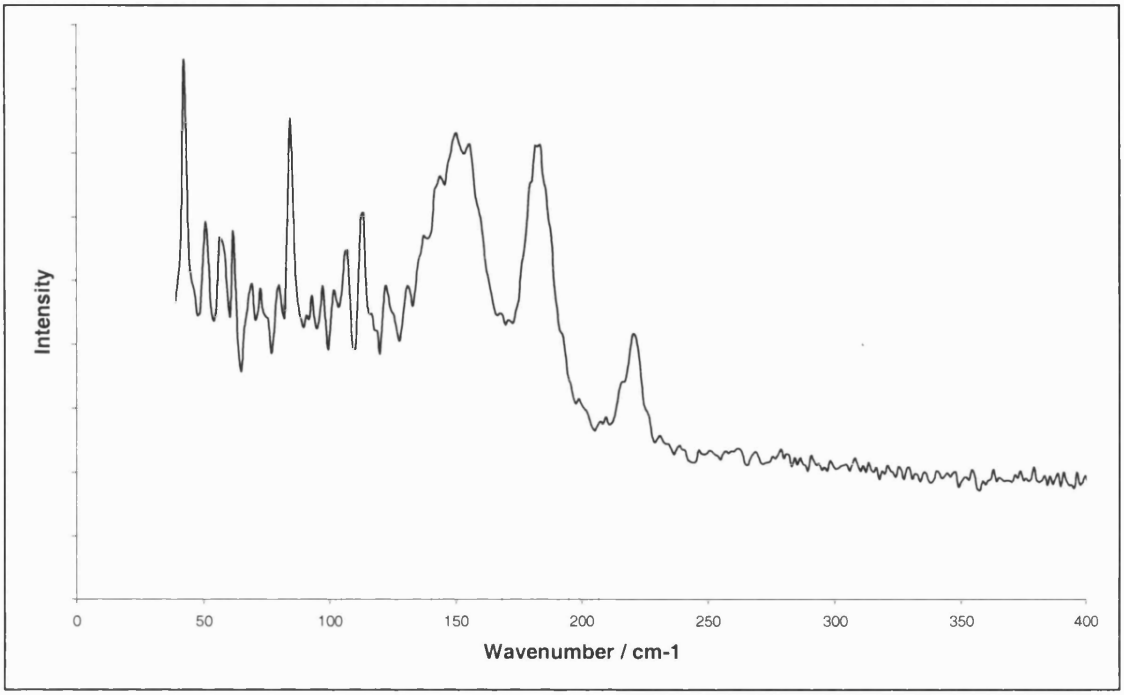


**Figure 7.6 Raman spectrum of the film deposited from [$^t$Bu$_2$Sn(-OCH$_2$CH$_2$S)] with hydrogen sulfide at 600 °C.**

Raman spectra were recorded for all films deposited. All spectra show the characteristic pattern due to tin(II) sulfide. Other bands are also observed.

In all the films deposited with hydrogen sulfide, tin(II) sulfide is seen, along with many sharp bands at low wavenumber. One such typical spectrum is shown in Figure 7.6. This is the pattern recorded from the film deposited at 600 °C.

If the positions of the bands are measured, it is seen that they are 5.18 cm$^{-1}$ apart. This was determined by trial and error as some bands are very weak and others are absent.

The spectrum of the film deposited at 350 °C with hydrogen sulfide is shown in Figure 7.7. This shows the spectrum of tin(II) sulfide more clearly, although the regularly spaced bands are also seen at low wavenumber. Weak bands are seen at 314 and 290 $cm^{-1}$. These correspond to the positions of bands due to tin(IV) sulfide, although they are approximately equal in intensity, a phenomenon that has not previously been observed in this work. These were observed in all films deposited at temperatures up to and including 450 °C.

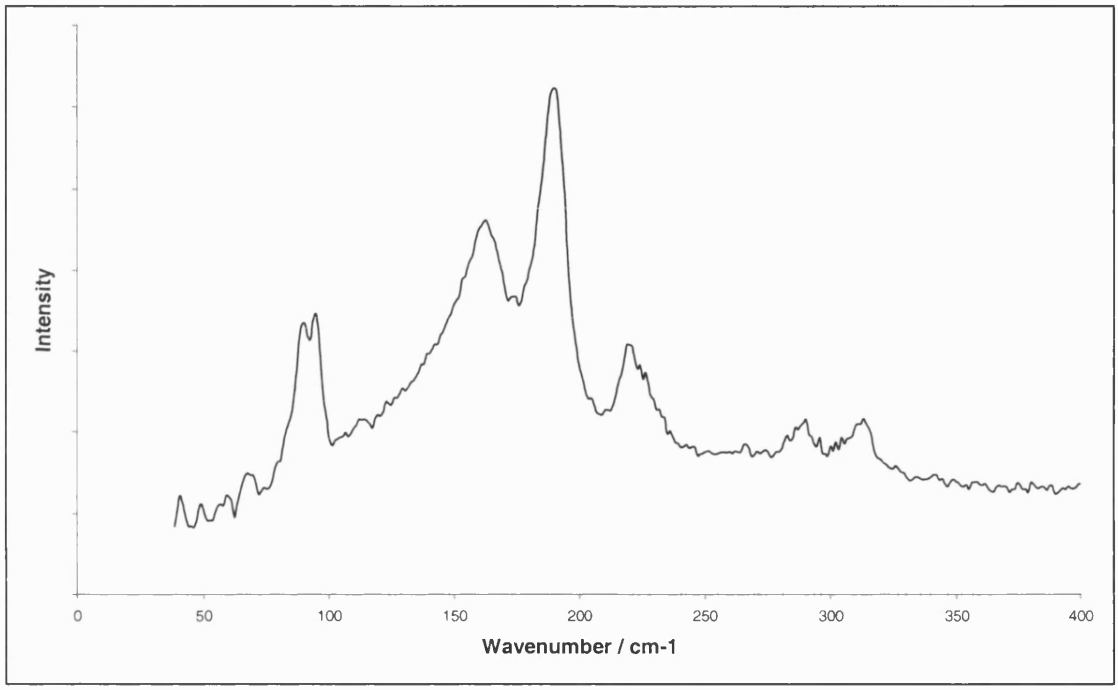


**Figure 7.7 Raman spectrum of the film deposited from [$^t$Bu$_2$Sn(-OCH$_2$CH$_2$S)] with hydrogen sulfide at 350 °C.**

Films deposited without hydrogen sulfide also show these bands, but they are less pronounced than those seen in the films deposited with hydrogen sulfide. This may be partly due to the bands being stronger in films deposited at lower substrate temperatures and, without hydrogen sulfide, films could only be deposited at 450 °C and above.

The appearance of evenly spaced bands in Raman spectroscopy is a characteristic of Resonance Raman Spectroscopy. In this technique, rather than using a laser of arbitrary wavelength, the wavelength is tuned to a particular electronic transition within the sample. This results in fewer transitions being excited, clarifying the spectrum. Also, those transitions observed would be much more intense, and many more quanta will be seen. There is, however, no potential component of the film that may experience

transitions of this frequency. Any organo-tin compounds residual in the film would be so bulky that rotational transitions would be of < 1 $cm^{-1}$.

It is possible that these transitions are a function of the glass substrate. No other films in this thesis were deposited on glass from this batch, while other coatings also show this phenomenon.

### 7.5.3 Energy dispersive analysis by X-rays

EDAX was carried out on all films. All films were very thin and so breakthrough to the underlying glass occurred in all cases.

Regardless of deposition temperature and presence or not of $H_2S$, all films exhibited a near 1:1 ratio of tin to sulfur.

### 7.5.4 Scanning electron microscopy

Figure 7.8 shows a representative sample of SEM images of films deposited from [$^tBu_2Sn(-OCH_2CH_2S)$].

Figure 7.8a shows the film deposited from [$^tBu_2Sn(-OCH_2CH_2S)$] with hydrogen sulfide at 400 °C. This consists of very small particles, which appear to be beginning to coalesce into a film. At 500 °C long needles are observed. These are shown in Figure 7.8b and are *ca.* 5 μm in length. In Figure 7.8c, the film deposited at 600 °C with hydrogen sulfide is shown to comprise flat, regular particles *ca.* 2 μm across.

In the case of films deposited without hydrogen sulfide, at 400 °C (Figure 7.8d) small particles are observed. These are numerous, but irregular. At 500 °C, more regular particles are produced. They are also larger in size, but less prolific than those deposited at 400 °C. At each temperature, there appears to be more surface coverage when hydrogen sulfide is present in the reaction chamber.

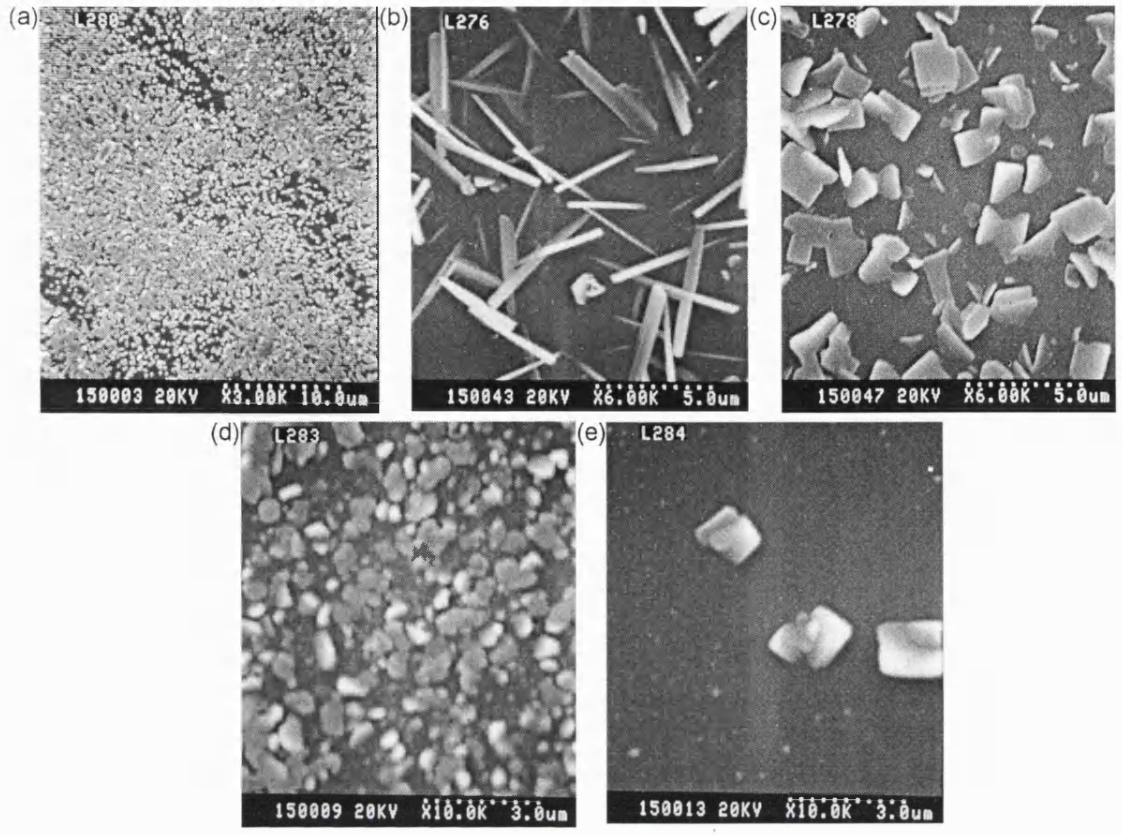


**Figure 7.8 SEM images of films deposited from [$^t$Bu$_2$Sn(-OCH$_2$CH$_2$S)] with hydrogen sulfide at (a) 400, (b) 500 and (c) 600 °C and without hydrogen sulfide at (d) 400 and (e) 500 °C.**

## 7.6 Discussion and conclusions

Three possible methods of producing tin oxide sulfide films were investigated. The principle problem with this work is that the target material is thus far unreported in the literature. A number of structures of these three elements have been produced around organic templates, but there is no record of a single phase. If a tin oxide sulfide were produced, it would be difficult to characterise, as it would be a novel material.

In the case of films deposited from tin tetrachloride, hydrogen sulfide and water, a novel phase was observed in the Raman. Energy dispersive analysis by X-rays showed that the tin to sulfur ratio was high, indicating that tin was found either in its elemental state or with oxygen bound to it. Ratios were approximately 2:1 of tin to sulfur at all reaction conditions, within the limits of the apparatus used.

The new phase observed in the Raman microscopy has bands at 288, 223, 178 and 91 $cm^{-1}$. Three of these are in similar positions to those observed in tin(II) sulfide, namely 221, 161-164 and 96-97 $cm^{-1}$. The tin(II) sulfide band at 182-192 $cm^{-1}$ is not present and an extra band is observed at 288 $cm^{-1}$. It is possible that this new phase is tin(II) sulfide with some oxygen incorporation. The absence of the band at 182-192 $cm^{-1}$ is not significant, as it may be masked by the tin(II) sulfide band. The extra band may be a band which is not Raman active in tin(II) sulfide, but, with oxygen replacing some sulfur, becomes active in the less symmetric system.

This does not account for the large excess of tin encountered in the EDAX. This excess is indicative of a sulfur:oxygen ratio near 1:1, while the above postulation would only hold for very small amounts of oxygen doping. Higher levels of oxygen would alter the structure. It may be that there is also some tin oxide present. This would not be observed in the Raman, as tin sulfides are so Raman active. The small bands due to tin oxide would be completely overpowered by the tin sulfide bands.

With the two compounds investigated, which contained all the required elements of the final film, the results were not so exciting. Raman spectroscopy showed only tin sulfides, although in the case of films deposited from [$^tBu_2\overline{Sn(-OCH_2CH_2S)}$] some bands due to the glass were observed. EDAX showed more sulfur than tin, consistent with the observed phases in the Raman.

It is possible that, in the reaction of tin tetrachloride, hydrogen sulfide and water, a new phase was produced. This showed a similar Raman spectrum to that of tin(II) sulfide with one extra band. The band not observed may have been masked by the existing tin(II) sulfide band in that region. This new phase could not be formed alone, but only with tin sulfide, and tin oxide was probably present too, as indicated by the EDAX.

# Chapter 8
# Conclusions

As a tool for depositing films of tin sulfide, chemical vapour deposition is a versatile technique. Many precursors may be used, with varying success. Different delivery methods can be applied depending on the properties of the precursor. Many parameters may be varied, with differing effects of the final film.

In this, the final chapter, the results of all reactions carried out in this thesis will be summarised and discussed. Firstly, the phases produced will be discussed. Many different precursors were used in this investigation, with different results intended. Some were successful and others not. Here, all the compounds investigated will be compared, and comparisons made. Also, previous literature results will be included and comparisons made.

The second consideration is the form of the final film. Some films were thicker than others and particle sizes and shapes differed. A number of the differences are likely to be due to the substrate, rather than the reaction conditions, so this section will not compare differences in films on different types of glass.

# 8.1 Phases produced

## 8.1.1 Summary of all results

The results of all reactions carried out in an attempt to form tin sulfides are reproduced in Table 8.1.

The first reactions carried out were those of tin tetrahalides with hydrogen sulfide. These provided the basis for much of the subsequent work carried out. It was shown that all phases of tin sulfides could be produced, higher deposition temperatures leading to lower tin oxidation states.

The reactions of tributyl tin trifluoroacetate followed. As the precursor contained no sulfur, hydrogen sulfide had to be used again. Here, however, only tin(II) sulfide could be produced at all temperatures.

**Table 8.1 Summary of results of all reactions carried out in an attempt to produce tin sulfide films.**

| Precursors | $H_2S$ | Substrate | Temperature range | Products |
|---|---|---|---|---|
| $SnCl_4$ | Yes | Carbon-doped silica coated glass | 300 - 500 °C | $SnS_2$ |
| | | | 525 °C | $Sn_2S_3$ |
| | | | 545 °C | SnS |
| $SnBr_4$ | Yes | Tin oxide/silica coated glass | 300 - 450 °C | $SnS_2$ |
| | | | 500 - 525 °C | $Sn_2S_3$ |
| | | | 550 - 600 °C | SnS |
| $[Bu_3SnOC(O)CF_3]$ | Yes | Carbon-doped silica coated glass or tin oxide/silica coated glass | 350 - 550 °C | SnS |
| $[Sn(SPh)_4]$ | No | Carbon-doped silica coated glass | 300 °C | $Sn_3O_4$ |
| $[Sn(SPh)_4]$ | 0.2 $dm^3min^{-1}$ | Silica coated glass | 450 °C | $SnS_2$ |
| | | | 500 °C | SnS |
| $[Sn(SPh)_4]$ | 0.4 $dm^3min^{-1}$ | Tin oxide/silica coated glass | 400 °C | $SnS_2 + Sn_2S_3$ |
| | | | 450 °C | $Sn_2S_3 + SnS$ |
| $[Sn(SCH_2CF_3)_4]$ | Yes | Silica coated glass | 300 - 400 °C | $SnS_2$ |
| | | | 450 °C | $SnS_2 + Sn_2S_3$ |
| | | | 500 °C | $Sn_2S_3$ |
| | | | 525 - 550 °C | $Sn_2S_3 + SnS$ |
| | | | 600 °C | SnS |
| $[Sn(-SCH_2CH_2S)_2]$ | Yes | Silica coated glass | 300 °C | $SnS_2$ |
| | | | 400 °C | $Sn_2S_3$ |
| | | | 525 - 550 °C | SnS |
| $[Sn(-SCH_2CH_2S)_2]$ | No | Silica coated glass | 400 - 500 °C | SnS |
| $[Sn(SCPh_3)_2]$ | | | | no film |
| $[Sn(S_2CNEt_2)_4]$ | Yes | Tin oxide/silica coated glass | 450 - 520 °C | SnS |
| $[Me_3SnS_2CNMeBu]$ | Yes | Silica coated glass | 450 °C | $Sn_2S_3$ |
| | | | 500 - 550 °C | SnS |
| $[Me_3SnS_2CNMe_2]$ | No | Silica coated glass | 500 °C | not tin sulfide or tin oxide |
| | | | 550 °C | SnS |
| $[Me_3SnS_2CnEt_2]$ | Yes | Silica coated glass | 450 °C | $Sn_2S_3 + SnS$ |
| | | | 600 °C | SnS |
| $[Me_3SnS_2CnEt_2]$ | No | Silica coated glass | 500 °C | SnS |

Following this, the search for a single source precursor began. Many precursors were investigated, with varying success.

Some reactions were carried out with the intention of producing tin sulfide selenides. In this case the precursor was $(SPh)_nSn(SePh)_{4-n}$ (n=0-4). Very little selenium was observed in the EDAX, always less than detection limits. Table 8.2 gives a summary of all reactions carried out in this series.

**Table 8.2 Summary of results of all reactions carried out in an attempt to produce tin sulfide selenide films.**

| Precursors | $H_2S$ | Substrate | Temperature range | Products |
|---|---|---|---|---|
| $[(SPh)_nSn(SePh)_{4-n}]$ | Yes | Silica coated glass | 300 °C | $SnS_2$ |
| | | | 400 °C | $SnS_2$ + SnS |
| | | | 500 °C | SnS |
| $[(SPh)_nSn(SePh)_{4-n}]$ | No | Silica coated glass | 400 °C | $SnS_2$ |
| | | | 450 - 500 °C | SnS |

No mixed valent tin sulfide was observed. All SnS spectra showed shifts in the positions of the Raman bands, especially the ones deposited without hydrogen sulfide.

Further reactions were carried out in an attempt to produce tin oxide sulfide films. This material has not previously been reported in the literature. With such common elements, it is highly likely that synthesis has been attempted in the past, so it is probable that no stable phases at room temperature and pressure exist. The summary of all these reactions is given in Table 8.3.

**Table 8.3 Summary of results of all reactions carried out in an attempt to produce tin oxide sulfide films.**

| Precursors | Substrate | Temperature range | Products |
|---|---|---|---|
| $SnCl_4$, $H_2S$, $H_2O$ | Silica coated glass | 400 °C | $SnS_2$ |
| | | 500 and 600 °C | SnS and oxygen doped SnS |
| $[Cl_2Sn(SCH_2C(O)OMe)_2]$, $H_sS$ | Silica coated glass | 350 - 400 °C | $SnS_2$ + $Sn_2S_3$ |
| | | 450 °C | $Sn_2S_3$ + SnS |
| | | 500 - 600 °C | SnS |
| $[Cl_2Sn(SCH_2C(O)OMe)_2]$ | Silica coated glass | 350 °C | no film |
| | | 450 °C | $SnS_2$ + excess Sn |
| | | 550 °C | SnS + excess Sn |
| $[^tBu_2Sn(-OCH_2CH_2S)]$, $H_2S$ | Silica coated glass | 350 - 600 °C | SnS |
| $[^tBu_2Sn(-OCH_2CH_2S)]$ | Silica coated glass | 450 - 500 °C | SnS |

## 8.1.2 Discussion of all results

From the above summary, it is evident that temperature plays an important role in which phase is deposited. Full discussion of this is given in Section 3.8. The reason is that of all the possible combinations of tin sulfide and excess sulfur $SnS_2$, $Sn_2S_3$ + ½S, or SnS + S, the last is the more thermodynamically favourable. $SnS_2$ is most likely to be formed as the kinetic product of the reaction, and at elevated temperatures or in the

presence of $H_2S$ reduction to SnS occurs, accompanied by oxidation of sulfur. The presence of hydrogen sulfide in the reaction chamber leads to lower oxidation state sulfides being formed at lower temperatures. It also aids reduction of tin sulfide films, when subsequently heated.

In almost all cases the transition from tin(IV) sulfide to tin(II) sulfide occurs at *ca.* 450 °C. Around this temperature mixed valent tin sulfide is observed. In many cases it is found along side one or other of the binary compounds.

Exceptions to the above generalisation are as follows.

Tin tetrahalides undergo the transition from tin(IV) sulfide to tin(II) sulfide at 525 °C.

$[Bu_3SnOC(O)CF_3]$ only forms tin(II) sulfide.

$[\overline{Sn(-SCH_2CH_2S)_2}]$ forms $Sn_2S_3$ at 400 °C when $H_2S$ is present, and forms SnS at 400 °C in the absence of $H_2S$.

The reaction of $[Bu_3SnOC(O)CF_3]$ with hydrogen sulfide evidently has tin(II) sulfide as the kinetic product as well as the thermodynamic product. Some of the possible reactions were given in Chapter 4.

$$[Bu_3SnO_2CCF_3] + 2H_2S \rightarrow SnS + 3BuH + HOC(O)CF_3 + S \qquad \textbf{Equation 4.1}$$

$$[Bu_3SnO_2CCF_3] \rightarrow [Bu_2Sn] + BuOC(O)CF_3$$

$$\downarrow H_2S \qquad \textbf{Equation 4.2}$$

$$SnS + 2BuH$$

Equation 4.1 assumes oxidation of sulfur, as was reported in Chapter 3 for the reaction of tin tetrachloride with hydrogen sulfide. Equation 4.2, which involves reductive elimination to a tin(II) species seems more likely. If the reductive elimination step is sufficiently facile, a tin(II) species remains, which would not be oxidised to a tin(IV) species.

APCVD reactions of tin tetrahalides with hydrogen sulfide and of $[\overline{Sn(-SCH_2CH_2S)_2}]$ with hydrogen sulfide both give all three phases of tin sulfide, but the temperatures at which each is accessible varies from the trend shown by all other compounds investigated. This is indicative that the reaction mechanism does not go *via* the same intermediate in all cases.

Tin tetrahalides are markedly different from other precursors used in this work, so it is unsurprising that they follow a different route. In this case it is possible that the reaction forms tin(IV) sulfide directly and then this is converted to tin(II) sulfide. The temperatures at which conversion occurs to previously deposited films are very similar to those at which the different tin sulfides are deposited directly from tin tetrahalides.

In the cases of other reactions, the precursors are very similar, especially in the direct environment surrounding tin. As confirmed in Chapter 5, reaction of the precursors alone produces tin oxide, so the tin-sulfur bonds appear to be fairly easily broken. Bearing this in mind it is probable that the mechanism of reaction in all these cases involves loss of the ligands followed by reaction of a tin atom with hydrogen sulfide. This is likely to be the cause of the observation that different phases of tin sulfide are formed at different temperatures. Deviation of $[\overline{Sn(\text{-}SCH_2CH_2S)_2}]$ from this generalisation, accompanied by the fact that tin sulfide is accessible despite not using hydrogen sulfide indicates that a different mechanism occurs here. In this case, loss of ligands is prohibited by the chelate effect.

## 8.1.3 Comparison with previous work

All the work described here, has also been reported fully in Chapter 1.

The only previously reported examples of formation of tin sulfide by chemical vapour deposition both involved formation of tin(II) sulfide. Plasma-enhanced CVD using $SnCl_4$ and $H_2S$ at 100 °C produced SnS with $SnCl_2$, $SnCl_4$ and sulfur contaminants.[2] At 200 °C, pure SnS was formed. Variation of plasma power also affected the contamination of the film. Higher plasma power was sufficient to decompose $H_2S$, so sulfur was included in the film. Further increases in power led to decomposition of $SnCl_4$, and pure SnS formed.

Tetraethyl tin and hydrogen sulfide have been used in a CVD reaction to form tin(II) sulfide.[43] In this case, no characterisation was carried out and films were assumed to be tin(II) sulfide based purely on the fact that the atmosphere was reducing. Films were observed to be yellow when thin and black when thick, which was observed for films of tin(IV) sulfide deposited from $SnCl_4$ and $H_2S$ in this thesis.

The work in this thesis contrasts both the existing CVD reports of tin sulfide. In the case of PECVD[2] impure films were formed, yet tin(II) sulfide was deposited at lower temperatures. This thesis showed no contamination by chlorine, and for films analysed by XPS no elemental sulfur was observed. In a few cases oxygen was present, or tin:sulfur ratios indicated this was likely.

Observations made in the work on organometallic CVD are shown to contradict the result postulated.[53] This shows the importance of detailed analysis of products, rather than speculating what may have been produced based solely on colour and what one intended at the outset.

Spray pyrolysis of $SnCl_2$ and N,N-dimethylthiourea[57,58] produced tin sesquisulfide below 370 °C and tin monosulfide between 370 and 390 °C. Higher temperatures were found to produce tin oxide. Temperature observations here agree with those discovered in this thesis, namely higher temperatures leading to lower tin oxidation states in the sulfide. It is, however, significant that tin oxide was not produced when hydrogen sulfide is used in reactions. Sulfur is more accessible in this gas than in N,N-dimethylthiourea.

Many groups used deposition from solution as a viable technique in the formation of tin sulfides. Although the initial setting up of a CVD rig is more costly and time consuming, reactions thereafter are as simple. Also, the CVD reaction does not require the reagents to be soluble or miscible. Complicated combinations of reagents, sometimes involving complexing agents for tin compounds are required, for deposition from solution. With CVD, reagents of any phase may be used, with any solvent for involatile liquids. The solvent does not affect the reaction, as it is evaporated the instant it arrives in the reaction chamber, while in the case of solution depositions, the chosen solvent is critical to the reaction.

## 8.2 Forms of film produced

The physical properties of the final film are important if it is to be considered for

electronic applications. Many factors affect the nature of the final film, although one of the key considerations is the substrate.

## 8.2.1 Description of films

Few reactions were carried out on carbon-doped silica coated glass. The only ones were the reactions of tin tetrachloride with hydrogen sulfide, and the initial reactions of tributyl tin trifluoroacetate. These are recounted in Table 8.4.

**Table 8.4 Summary of morphologies observed in films deposited on carbon-doped silica coated glass.**

| Precursors | Temperature range | Phase | Morphology |
|---|---|---|---|
| $SnCl_4$, $H_2S$ | 300 - 350 °C | $SnS_2$ | Irregular needles |
| | 375 - 475 °C | $SnS_2$ | Interlocking plates |
| | 525 °C | $Sn_2S_3$ | Rounded ill-defined particles with regular overlying needles |
| | 545 °C | SnS | Rounded ill-defined particles |
| [$^n$Bu$_3$SnOC(O)CF$_3$], $H_2S$ | 400 °C | SnS | Small round particles |
| | 450 °C | SnS | Large regular particles |

In general, all films deposited onto carbon-doped silica coated glass were very thick.

A large number of reactions were carried out on tin oxide/silica coated glass. Table 8.5 gives details of these.

**Table 8.5 Summary of morphologies observed in films deposited on tin oxide/silica coated glass.**

| Precursors | Temperature range | Phase | Morphology |
|---|---|---|---|
| $SnBr_4$, $H_2S$ | 300 - 350 °C | $SnS_2$ | Irregular needles |
| | 375-375 °C | $SnS_2$ | Interlocking plates |
| | above 525 °C | $Sn_2S_3$ or SnS | Regular needles |
| [$^n$Bu$_3$SnOC(O)CF$_3$], $H_2S$ | 400 - 500 °C | SnS | Wavy particles with overlying rectangular plates |
| [Sn(SPh)$_4$], $H_2S$ | 500 °C | SnS | Clusters of regular plates |
| [Sn(S$_2$CNEt$_2$)$_4$], $H_2S$ | 450 - 520 °C | SnS | Clusters of plates and needles |
| [Me$_3$SnS$_2$CNMe$_2$], $H_2S$ | 500 °C | not tin sulfide or tin oxide | Interlocking plates |
| | 550 °C | SnS | Wavy particles with large clusters of irregular plates |
| [Me$_3$SnS$_2$CNEt$_2$], $H_2S$ | 450 °C | $Sn_2S_3$ + SnS | Wavy particles with overlying rectangular plates |

Many more films were deposited on silica coated glass. These are detailed in Table 8.6.

**Table 8.6 Summary of morphologies observed in films deposited on silica coated glass.**

| Precursors | Temperature range | Phase | Morphology |
|---|---|---|---|
| $[Sn(SCH_2CF_3)_4]$, $H_2S$ | 400 - 450 °C | $SnS_2$ | Wavey interlocking plates |
| | 450 - 550 °C | $Sn_2S_3$ | Long regular needles |
| | 550 - 600 °C | SnS | Cuboidal particles |
| $[Sn(-SCH_2CH_2S)_2]$, $H_2S$ | 350 °C | $SnS_2$ | Small particles |
| | 400 °C | $Sn_2S_3$ | Interlocking plates |
| | 500 °C | SnS | Square particles twinned to resemble butterflies |
| $[Sn(-SCH_2CH_2S)_2]$ | 400 - 450 °C | SnS | Clusters of small irregular plates |
| | 500 - 550 °C | SnS | Large discreet square plates |
| $[Me_3SnS_2CNMeBu]$, $H_2S$ | 450 - 550 °C | $Sn_2S_3$ or SnS | Small rounded plates |

## 8.2.2 Discussion of morphologies

In almost all cases films of tin(IV) sulfide are found as arrays of interlocking irregular plates. For films deposited from tin tetrahalides with hydrogen sulfide, some irregular needles were observed. These were in no way similar to the needles observed when tin(II) tin(IV) trisulfide was formed, but were much less regular.

Films that were analysed as being tin sesquisulfide exhibited long needle particles in all cases.

Almost all films that were analysed as being tin(II) sulfide showed small square plates. Films deposited from tin tetrachloride with hydrogen sulfide on carbon-doped silica coated glass showed the exception to this. This may have been a function of the substrate, however films deposited from tributyl tin trifluoroacetate on the same substrate showed large flat particles.

For films deposited on tin oxide / silica coated glass, many showed a wavy structured accompanied by overlying particles. This was not observed in coatings on any other glass, so is almost certainly a property of the substrate.

# 8.3 Conclusions

Overall, it may be concluded that it is possible to produce a variety of different tin sulfide coatings on glass by Atmospheric Pressure Chemical Vapour Deposition. A number of factors alter the final film and a number of variations in the product are observed.

The simplest method of producing tin sulfide coatings, was that carried out in the initial reactions. Using tin tetrachloride or tin tetrahalide with hydrogen sulfide forms films of all tin phases in a short period of time. All films were relatively thick, and surface coverage was high.

Many of the reactions to prepare precursors used these reagents, or other equally toxic substances. Also, in most cases hydrogen sulfide was essential in forcing the product to be tin sulfide rather than tin oxide. This negates the use of molecular precursors in most cases.

The two main hindrances to the development of single source precursors were the unavailability of pure nitrogen and the facile loss of ligands about tin. As tin and sulfur are in different rows of the periodic table, the overlap of atomic orbitals is less, so weaker bonds are formed. This assists loss of ligands to leave highly active tin species susceptible to attack by minuscule amounts of water in the nitrogen supply.

The one exception was in the case of tin(IV) $\eta^2$-ethane dithiolate which produced films of tin(II) sulfide without hydrogen sulfide being necessary.

The morphology of films depended on the substrate used. Uniform coverage was not found for tin(II) sulfide except where carbon-doped silica coated glass was used as the substrate. In the case of tin oxide / silica coated glass and pure silica coated glass large square plates were formed.

Forming tin sulfide selenides was attempted. Morphologies of particles were similar to those observed in the case of binary tin sulfides. Selenium was detected in the EDAX,

but at lower levels than sulfur. This was unexpected as sulfur and selenium were introduced into the reaction in equal amounts. Raman spectra were recorded with shifts in the band positions. This is to be expected since corresponding tin sulfides and selenides have the same structure, so a mixture would have an intermediate structure.

Forming tin oxide sulfides was not proven, and the lack of literature reports suggests that this compound is not stable at normal temperature and pressure. A Raman spectrum was recorded, which was similar to that of tin(II) sulfide, however bands were shifted. It may be possible that this was oxygen-doped tin(II) sulfide.

# References


1. Renfrew, M. M., Lewis, E. E., *Ind. Eng. Chem.*, 1946, **38**, 870-877.
2. Ortiz, A., Alonso, J. C., Garcia, M., Toriz, J., *Semicond. Sci. Technol.*, 1996, **11**, 243-247.
3. Thomson, J. J., *Proc. Cambridge Phil. Soc.*, 1901, **11**, 120.
4. Maissel, L. I., Francombe, M. H., *An Introduction to Thin Films*, 1973, New York: Gordon and Breach.
5. Sanon, G., Rup, R., Mansingh, A., *Physica Status Solidi A: Appl. Res.*, 1991, **128**, 109-116.
6. Jiang, T., Ozin, G. A., *J. Mater. Chem.*, 1998, **8**, 1099-1108.
7. Jiang, T., Lough, A. J., Ozin, G. A., Bedard, R. L., Broach, R. W., *J. Mater. Chem.*, 1998, **8**, 721-732.
8. Karakhanova, M. I., Pashinkin, A. S., Novoselova, A. V., *Izv. Akad. Nauk SSSR, Neorgan. Mat.*, 1966, **2**, 991-996.
9. Moh, G. H., *N. Jb. Miner. Abh.*, 1969, **111**, 227-263.
10. Sharma, R. C., Chang, Y. A., *Bull. Alloy Phase Diagrams*, 1986, **7**, 269-273 & 307-308.
11. Gerasimove, J. I., Kruglova, E. V., Rosenblum, N. D. *Zh. Obsch. Khim.*, 1937, **7**, 1520-1524.
12. Bok, L. K., Boeyens, J. C. A., *J. S. Afr. Chem. Inst.*, 1957, **10**, 49-53.
13. Bartenev, G. M., Tsysanov, A. D., Dembovskii, S. A., Mikhailov, V. I., *Inorg. Mater.*, 1971, **7**, 1280-1281.
14. Del Bucchia, S., Jumas, J-C., Maurin, M., *Acta Cryst.*, 1981, **B37**, 1903-1905.
15. Tremel, W., Hoffman, R., *Inorg. Chem.*, 1987, **26**, 118-127; Tremel, W., Hoffman, R., *Z. Krist.*, 1987, **178**, 211-212.
16. Martinez, H., Auriel, C., Loudet, M., Pfister-Guillouzo, G., *Appl. Surf. Sci.*, 1996, **103**, 149-158.
17. Oftedal, I., *Z. Phys. Chem.*, 1928, **134**, 301-310.
18. Palosz, B., Steurer, W., Schulz, H., *Acta Cryst.*, 1990, **B46**, 449-455.
19. Kniep, R., Mootz, D., Severin, U., Wunderlich, H., *Acta Cryst.*, 1982, **B38**, 2022-2023.
20. Budavari, S. (editor), *The Merck Index 12$^{th}$ Edition*, 1996, Whitehouse Station, N. J.: Merck & Co. Inc.

21. Isaacs, A., Daintith, J., Martin, E. (editors), *Concise Science Dictionary 3rd Edition*, 1996, Oxford: Oxford University Press.
22. Grant, J. (editor), *Hackh's Chemical Dictionary 4th Edition*, 1969, USA: McGraw-Hill, Inc.
23. Burgio, L., Ciomartan, D. A., Clark, R. J. H., *J. Raman Spec.*, 1997, **28**, 79-83.
24. Woulfe, P., *Philos. Trans. R. Soc. London*, 1771, **61**, 114-130.
25. Herzenberg, R., *Rev. Mineral.*, 1932, **4**, 33.
26. Kihara, H., Io, K., Kowada, Y., Adachi, H., *Hyogo Kyoiku Daigaku Kenkyu Kiyo, Dai-3-bunsatsu*, 1989, **10**, 53-63.
27. Shaw, G. A., Parkin, I. P., *Main Group Metal Chemistry*, 1996, **19**, 499-502.
28. Parkin, I. P., Rowley, A. T., *Polyhedron*, 1993, **12**, 2961-2964.
29. Elkorashy, A. M., *Physica B*, 1991, **168**, 257-267.
30. Boudjouk, P., Seidler, D. J., Grier, D., McCarthy, G. J., *Chem. Mater.*, 1996, **8**, 1189-1196; Seidler, D. J., Boudjouk, P., McCarthy, G. J., Grier, D., *Abstracts of papers (Am. Chem. Soc.)*, 1995, **210**, 513-inor; Boudjouk, P., Seidler, D. J., Bahr, S. R., McCarthy, G. J., *Chem. Mater.*, 1994, **6**, 2108-2112; Bahr, S. R., Boudjouk, P., McCarthy, G. J., *Chem. Mater.*, 1992, **4**, 383-388.
31. Badachhape, S. B., Goswami, A., *Ind. J. Pure Appl. Phys.*, 1964, **2**, 250-253.
32. Palosz, B., Palosz, W., Gierlotka, S., *Bull. Mineral.*, 1986, **109**, 143-150.
33. Arora, S. K., Patel, D. H., Agarwal, M. K., *Mater. Chem. Phys.*, 1996, **45**, 63-65.
34. Arora, S. K., Patel, D. H., Agarwal, M. K., *J. Mater. Sci.*, 1994, **29**, 3979-3983.
35. Lifshitz, E., Chen, Z., Bykov, L., *J. Phys. Chem.*, 1993, **97**, 238-242.
36. Liu, X., Jiang, L., *Huaxue Shijie*, 1994, **35**, 406-408.
37. Qian, X. F., Zhang, X. M., Wang, C., Wang, W. Z., Xie, Y., Qian, Y. T., *J. Phys. Chem. Solids*, 1999, **60**, 415-417.
38. Kaito, C., Saito, Y, Watanabe, T., Matsumoto, A., Ohtsuka, K., Fangyu, C., *J. Cryst. Growth*, 1993, **129**, 367-370.
39. van Alpen, U., Fenner, J., Gmelin, E., *Mat. Res. Bull.*, 1975, **10**, 175-180.
40. Goswami, A., Mitra, A., *Ind. J. Pure Appl. Phys.*, 1975, **13**, 508-511.
41. Deraman, K., Sakrani, S., Ismail, B. B., Wahab, Y., Gould, R. D., *Int. J. Electronics*, 1994, **76**, 917-922.

42. Kawano, K., Nakata, R., Sumita, M., *J. Phys. D: Appl. Phys.* 1989, **22**, 136-141.

43. Lokhande, C. D., *Mater. Chem. Phys.*, 1991, **28**, 145-149; Lokhande, C. D., *J. Phys. D: Appl. Phys.*, 1990, **23**, 1703-1705.

44. Bhad, V. V., Lokhande, C. D., *Bull. Electrochem.*, 1991, **7**, 571-572.

45. Nair, M. T. S., Nair, P. K., *Semicond. Sci. Technol.*, 1991, **6**, 132-134.

46. Pramanik, P., Basu, P. K., Biswas, S., *Thin Solid Films*, 1987, **150**, 269-276.

47. Ristov, M., Sinadinovski G., Grozdanov, I., Mitreski, M., *Thin Solid Films*, 1989, **173**, 53-58.

48. Varkey, A. J., *Int. J. Mater. Prod. Technol.*, 1997, **12**, 490-495.

49. Zainal, Z., Hussein, M. Z., Kassim, A., Ghazali, A., *J. Mater. Sci. Lett.*, 1997, **16**, 1446-1449.

50. Mishra, K., Rajeshwar, K., Weiss, A., Murley, M., Engelken, R. D., Slayton, M., McCloud, H. E., *J. Electrochem. Soc.*, 1989, **136**, 1915-1923.

51. Engelken, R. D., McCloud, H. E., Lee, C., Slayton, M., Ghoreishi, H., *J. Electrochem. Soc.*, 1987, **134**, 2697-2707; Engelken, R. D., McCloud, H. E., US. US 4,681,777 (Cl. 427-87; B05D5/12), 12 Jul 1987.

52. Bidoia, E. D., Bulhaes, L. O de S., *Corros. Sci.*, 1990, **31**, 703-708.

53. Manasevit, H. M., Simpson, W. I., *J.Electrochem. Soc.*, 1975, **122**, 444-450.

54. Nakamura, H., Yano, H., Aoki, N., Sasaki, Y., Jpn. Kokai Tokkyo Koho JP 07 61,818[95 61,818] (Cl. C01G19/00), 7 Mar 1995.

55. Reddy, N. K., Reddy, K. T. R., Fisher, G., Best, R., Dutta, P. K., *J. Phys. D: Appl. Phys.*, 1999, **32**, 988-990.

56. Schlaf, R., Armstrong, N. R., Parkinson, B. A., Pettenkofer, C., Jaegermann, W., *Surf. Sci.*, 1997, **385**, 1-14; Schlaf, R., Louder, D., Lang, O., Pettenkofer, C., Jaegermann, W., Nebesny, K. W., Lee, P. A., Parkinson, B. A., Armstrong, N. R., *J. Vac. Sci. Technol. A*, 1995, **13**, 1761-1767.

57. López, S., Granados, S., Ortíz, A., *Semicond. Sci. Technol.*, 1996, **11**, 433-436.

58. Lopez, S., Ortiz, A, *Semicond. Sci. Technol.*, 1994, **9**, 2130-2133.

59. Case, E. M., Hopper, C. S., Fr. Demande FR 2,510,035 (Cl. B32B5/12), 28 Jan 1983.

60. Geringer, M., PCT Int. Appl. WO 96 36,681 (Cl. C10M103/06), 21 Nov 1996.

61. Hell, M., Ger. Offen. DE 4,340,017 (Cl. C08J5/14), 1 Jun 1995.

62. Takada, H., Shigeta, S., Jpn. Kokai Tokkyo Koho JP 01 88,936[89 88,936] (Cl.

G11B7/24), 3 Apr 1989.

63. Fister, D., Ger. Offen. DE 19,618,170 (Cl. C01G1/12), 13 Nov 1997.
64. Li, J., Kessler, H., *Microporous Mesoporous Mater.*, 1999, **27**, 57-63
65. Li, J., Kessler, H., Delmotte, L., *J. Chem. Soc. Faraday Trans.*, 1997, **93**, 665-668; Li, J., Kessler, H., *Microporous Mater.*, 1997, **9**, 141-147; Li, J., Delmotte, L., Kessler, H., *Chem. Commun.*, 1996, **9**, 1023-1024.
66. Jiang, T., Ozin, G. A., Bedard, R. L., *Adv. Mater.*, 1994, **6**, 860-865.
67. Seeger, K., *Semiconductor Physics: and introduction, 7th Edition*, 1999, Berlin; London: Springer.
68. Grahn, H. T., *Introduction to Semiconductor Physics*, 1999, Singapore; London: World Scientific.
69. Seeger, K., *Semiconductor Physics: an introduction, 4th Edition*, 1989, Berlin: Springer-Verlag.
70. Neville, R. C., *Solar Energy Conversion: the Solar Cell*, 1978, Amsterdam; Oxford: Elsevier.
71. Loferski, J.J., *J. Appl. Phys.*, 1956, **27**, 777-784.
72. Elkorashy, A. M., *Egypt. J. Phys.*, 1986, , 39-46.
73. Dubrovskii, G. B., Zhdanovich, N. S., *Fiz. Tverd. Tela*, 1996, **38**, 272-276.
74. Golubkov, A. V., Dubrovskii, G. V., Prokof'ev, A. V., *Fiz. Tverd. Tela*, 1994, **36**, 2666-2671.
75. Robin, M. B., Day, P., *Adv. Inorg. Chem. Radiochem.*, 1967, **10**, 247-422.
76. Maissel, L. I., Francombe, M. H., *An Introduction to Thin Films*, 1973, New York: Gordon and Breach, Science Publishers, Inc.
77. Chopra, K. L., *Thin Film Phenomena*, 1969, USA: McGraw-Hill, Inc.
78. Weast, R, C., (editor), *Handbook of Chemistry and Physics*, 1975, 55th Edition, USA: Chemical Rubber Publishing Company.
79. Calvert, L., National Research Council of Canada, Ottawa, Canada, ICDD Grant-in-Aid, 1981.
80. Mosburg, S., Ross, D. R., Bethke, M., Toulmin, P., *U.S.G.S. Prof. Paper*, **424C**, 1961, 347-348.
81. Nekrasov et al, *Dok. Akad. Nauk. SSR*, **200**, 1971, 946-949.
82. Donaldson, J. D., Moser, W., Simpson, W. B., *J. Chem. Soc.*, 1961, 839-841.
83. Gauzzi, F., *Ann. Chim. (Rome)*, 1963, **53**, 1503.
84. Suito, K., *Mater. Res. Bull.*, 1975, **10**, 677-680.
85. Chandrasekhar, H. R., Humphreys, R. G., Zwick, U., Cardona, M., *Phys. Rev.*

*B*, 1977, **15**, 2177-2183.

86. Chandrasekhar, H. R., Mead, D. G., *Phys. Rev. B*, 1979, **19**, 932-937.
87. Geurts, J., Rau, S., Richter, W., Schmitte, F. J., *Thin Solid Films*, 1984, **121**, 217-225.
88. Sangletti, L., Depero, L. E., Allieri, B., Pioselli, F., Comini, E., Sberveglieir, G., Zocchi, M., *J. Mater. Res.*, 1998, **13**, 2457-2460.
89. Katiyar, R. S., Dawson, P., Hargreave, M. M., Wilkinson, G. R., *J. Phys. C: Solid St. Phys.*, 1971, **4**, 2421-2431.
90. Smith, K. L., Black, K. M., *J. Vac. Sci. Technol.*, 1984, **A2**, 744-747.
91. Moses, P. R., Weir, L. M., Lennox, J. C., Finklea, H. O., Lenhard, F. R., Murray, R. W., *Anal. Chem.*, 1978, **50**, 576-585.
92. Wagner, C. D., Zatko, D. A., Raymond, R. H., *Anal. Chem.*, 1980, **52**, 1445-1451.
93. Riga, R., Verbist, J. J., *J. Chem. Soc., Perkin Trans. II*, 1983, 1545-1551.
94. Wagner, C. D., *J. Vac. Sci. Technol.*, 1978, **15**, 518-523.
95. Asplund, L., Kelfve, P., Blomster, S., Siegbahn, H., Siegbahn, K., Lozes, R. L., Wahlgren, U. I., *Phys. Scr.*, 1977, **16**, 273-279.
96. Nyholm, R., Martensson, N., *J. Phys. C*, 1980, **13**, L279-L284.
97. Wagner, C. D., *Faraday Discuss.*, 1975, **60**, 291-300.
98. Willemen, H., van de Vondel, D. F., van der Kelen, G. P., *Inorg. Chim. Acta*, 1979, **34**, 175-180.
99. Gordon, R. G., Hoffman, D. M., Riaz, U., *Chem. Mater.*, 1992, **4**, 68-71.
100. Elwin, G. S., *Ph. D. Thesis, (University of London)*, 1999.
101. Kojima, M., Kato, H., Imai, A., Nishi, Y., *Nagoya-shi Kogyo Kenkyosho Kenkyu Hokoko*, 1986, 18-21.
102. Gaydon A. G., *Dissociation Energies and Spectra of Diatomic Molecules*, 3rd Edition, Chapman and Hall, London, 1968.
103. Edwards, J. G., Franklin, H. F., Gilles, P. W., *J. Chem. Phys.*, 1971, **54**, 545-554.
104. Durant, M., Merienne, G., Valette, D., *Eur. Pat. Appl. EP623,564 (Cl. C03C17/25)*, 09 Nov 1994.
105. Tiekink, E. R. T., *Appl. Organomet. Chem.*, 1991, **5**, 1-23.
106. Backer, H. J., Kramer, J., *Rec. Trav. Chim.*, 1934, **53**, 1101-1112.
107. Poller, R. C., Spillman, J. A., *J. Chem. Soc. A*, 1966, 958-960
108. Bates, P. A., Hursthouse, Davies, A. G., Slater, S. D., *J. Organomet. Chem.*,

1989, 363, 45-60.

109. Lalancette, R. A., Cefola, M., Hamilton, W. C., LaPlaca, S. J., *Inorg. Chem.*, 1967, **6**, 2127-2134.

110. Nomura, R., Konishi, K., Matsuda, H., *J. Electrochem. Soc.*, 1991, **138**, 631-632.

111. Parise, J. B., Ko, Y., Tan, K., Nellis, D. M., Koch, S., *J. Solid State Chem.*, **117**, 1995, 219-228.